

## 1 Introduction

Four-top quark production ( $t\bar{t}t\bar{t}$ ) is a rare process within the Standard Model (SM) that serves as a crucial probe for both SM and beyond-the-Standard-Model (BSM) physics. Figure 1 illustrates representative leading-order Feynman diagrams for  $t\bar{t}t\bar{t}$  production. The latest predicted SM cross section for  $t\bar{t}t\bar{t}$  production at next-to-leading order (NLO) with next-to-leading logarithmic (NLL') correction is 13.37 fb at  $\sqrt{s} = 13$  TeV and 15.82 fb at  $\sqrt{s} = 13.6$  TeV [5]. This process is sensitive to the top quark's Yukawa coupling with the Higgs boson while remaining unaffected by the Higgs boson decay, making it a prime candidate for identifying any deviations from SM predictions regarding the top quark Yukawa coupling. Furthermore, deviations in the four-top production cross section from SM predictions could also signal the presence of undiscovered heavy scalar or pseudo-scalar bosons decaying into top quarks, as proposed in several extensions of the SM, including top-philic resonances as shown by Figure 2.

13

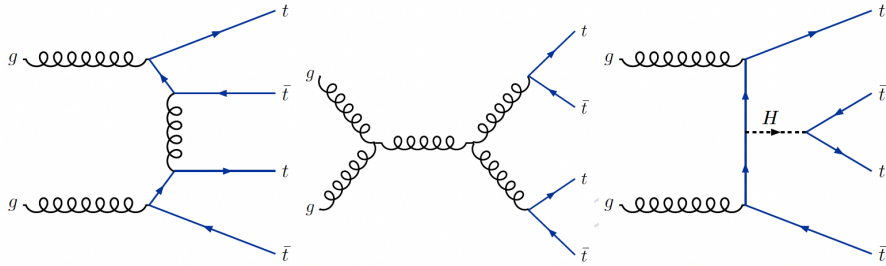


Figure 1: Representative LO Feynman diagrams for SM  $t\bar{t}t\bar{t}$  production.

Each top quark predominantly decays into a bottom quark and a W boson. The W boson then decays either hadronically, producing quarks, or leptonically, yielding a lepton and a neutrino. In this analysis, the fully hadronic final state, where all four top quarks decay entirely into hadrons, is being investigated for the first time, representing about 20% of all four-top quark events.

18

This analysis follows a previous CMS analysis [3] on all-hadronic four-top production with Run2 pre-legacy dataset described in AN2020\_021. The observed significance of the  $t\bar{t}t\bar{t}$  signal in this channel was 2.5 standard deviations (with 0.4 expected). When combined with other channels (Single Lepton, opposite-sign dilepton), the observed significance of the  $t\bar{t}t\bar{t}$  signal was 3.9 standard deviations (with 1.5 expected). In this analysis, we improve upon the previous all-hadronic channel analysis by switching to ultra-legacy Run2 data and by including 2022, 2023 Run3 data. While most of the methodology follows, everything (ML training, scale factor derivations etc.) is redone on the new ultra-legacy dataset. We will also include an interpretation against the top-philic resonance BSM model[4].

28

The search for four-top quark production in the fully hadronic final state faces significant challenges due to substantial backgrounds from top quark pair ( $t\bar{t}$ ) and QCD multijet production. To address these challenges, specialized machine learning tools for hadronic top quark tagging are utilized. In the "boosted" regime, where top quarks have high transverse momentum ( $p_T$ ) and their decay products produce collimated jets, the Particlenet boosted object tagger is employed for identification. For top quarks in the "resolved" regime, characterized by moderate  $p_T$  and distinct jets resulting from the hadronization of decay products, a dedicated BDT-based resolved top tagger has been developed specifically for this analysis.

37

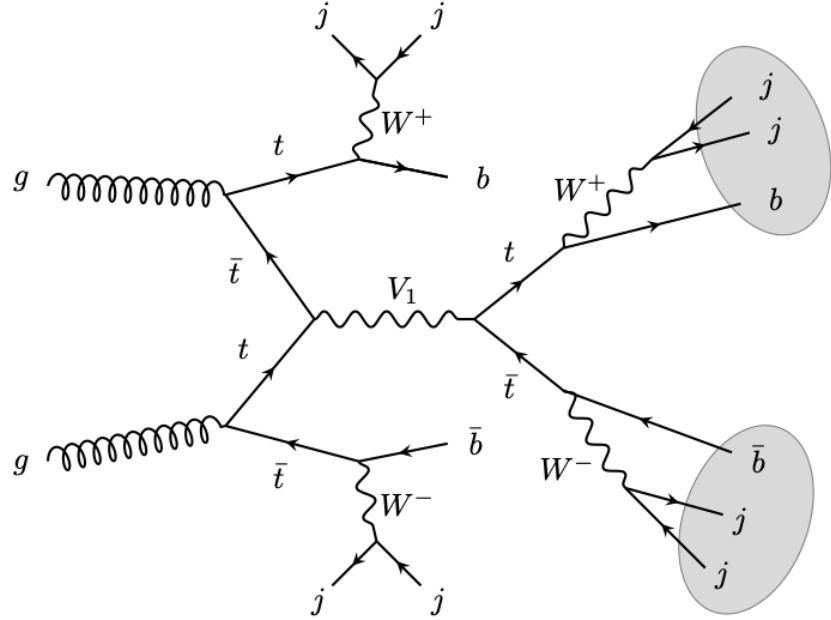


Figure 2: Representative LO Feynman diagrams for tree-level single production of the  $V_1$  decaying into the fully-hadronic channel in the BSM top-philic resonance model.

<sup>38</sup> The search strategy classifies events into distinct categories based on the number of reconstructed  
<sup>39</sup> top quarks and the scalar sum of jet transverse momenta ( $H_T$ ). An event-level BDT, trained  
<sup>40</sup> on kinematic variables, is then employed to distinguish the  $t\bar{t}t\bar{t}$  signal from the background. To  
<sup>41</sup> estimate the dominant backgrounds, originating from  $t\bar{t}$  and QCD multijet production, data-driven  
<sup>42</sup> techniques are applied, ensuring accurate background modeling and robust signal extraction.

## 2 Triggers and Dataset

---

### 2 Triggers and Dataset

The data for this search are recorded using a suite of cross-triggers requiring the presence of  $\geq 6$  jets,  $\geq 1$  or  $\geq 2$  b-tagged jets, and large  $H_T$ . The HLT paths of the triggers used for the 2016, 2017, and 2018 data-taking periods are listed in Table 1. The HLT paths of the triggers used for the 2022 and 2023 data-taking periods are listed in Table 2.

Table 1: HLT paths corresponding to the triggers used for the search in 2016, 2017, and 2018.

Year	Era	Trigger path
2016	B, C, D, E, F, G, H	HLT_PFHT400_SixJet30_DoubleBTagCSV_p056 HLT_PFHT450_SixJet40_BTagCSV_p056
2017	B	HLT_PFHT380_SixJet32_DoubleBTagCSV_p075 HLT_PFHT430_SixJet40_BTagCSV_p080
	C, D, E, F	HLT_PFHT380_SixPFJet32_DoublePFBTagCSV_2p2 HLT_PFHT430_SixPFJet40_PFBTagCSV_1p5
2018	A	HLT_PFHT380_SixPFJet32_DoublePFBTagDeepCSV_2p2 HLT_PFHT430_SixPFJet40_PFBTagDeepCSV_1p5
	B, C, D	HLT_PFHT400_SixPFJet32_DoublePFBTagDeepCSV_2p94 HLT_PFHT450_SixPFJet36_PFBTagDeepCSV_1p59

The efficiency of these triggers is measured in an independent sample selected with a single muon trigger (HLT\_IsoMu24 or HLT\_IsoMu27). The efficiency is measured as a function of  $N_{b-jet}$  and  $N_{jet}$ . The efficiency is measured in the region where  $H_T > 900$  GeV, as the trigger efficiency is expected to be independent of  $H_T$  in this region. In order to ensure that the events passing the single muon trigger are triggered by genuine muons rather than jets, one or more offline muons as defined in 3.2 are required. The efficiency is computed as follows:

$$\epsilon(N_j, N_b) = \frac{\text{Number of events passed OR of triggers and denominator selection}}{\text{Number of events that passed HLT_IsoMu24 or HLT_IsoMu27}}. \quad (1)$$

The datasets used for measuring trigger efficiency, as listed in Tables 3 and 4, include events that have passed the isolated muon trigger. Figure 1 and 2 show the measured efficiency in the  $N_{jet}$  and  $N_{b-jet}$  plane for each year. There is a clear dependence on  $N_{jet}$  and  $N_{b-jet}$ , which justifies the necessity of corrections depending on  $N_{jet}$  and  $N_{b-jet}$ . The bottom row corresponds to  $N_{jet} = 6$  and shows low efficiencies due to the requirement of  $N_{jet} \geq 6$  in trigger paths. This region is used only for the validation of the background estimation methods. Details will be discussed in Section 5.

The trigger paths include selection criteria based on  $N_{jet}$ ,  $N_{b-jet}$ , and  $H_T$ . Ideally, the trigger efficiency should be measured as a function of all three variables. However, due to limited statistical precision, the efficiency is measured as a function of  $N_{jet}$  and  $N_{b-jet}$ . To validate that

Table 2: HLT paths corresponding to the triggers used for the search in 2022 and 2023

Year	Era	Trigger path
2022	C, D, E, F, G	HLT_PFHT400_SixPFJet32_DoublePFBTagDeepJet_2p94 HLT_PFHT450_SixPFJet36_PFBTagDeepJet_1p59
2023	C	HLT_PFHT400_SixPFJet32_DoublePFBTagDeepJet_2p94 HLT_PFHT450_SixPFJet36_PFBTagDeepJet_1p59
	D	HLT_PFHT400_SixPFJet32_PNet2BTagMean0p50 HLT_PFHT450_SixPFJet36_PNetBTag0p35

Table 3: Dataset used for run2 trigger efficiency measurement

Year	Dataset
2016 pre VFP	/SingleMuon/Run2016B-ver1_HIPM_UL2016_MiniAODv2_NanoAODv9-v2/NANOAOD
	/SingleMuon/Run2016C-HIPM_UL2016_MiniAODv2_NanoAODv9-v2/NANOAOD
	/SingleMuon/Run2016D-HIPM_UL2016_MiniAODv2_NanoAODv9-v2/NANOAOD
	/SingleMuon/Run2016E-HIPM_UL2016_MiniAODv2_NanoAODv9-v2/NANOAOD
	/SingleMuon/Run2016F-HIPM_UL2016_MiniAODv2_NanoAODv9-v2/NANOAOD
2016 post VFP	/SingleMuon/Run2016F-UL2016_MiniAODv2_NanoAODv9-v1/NANOAOD
	/SingleMuon/Run2016G-UL2016_MiniAODv2_NanoAODv9-v1/NANOAOD
	/SingleMuon/Run2016H-UL2016_MiniAODv2_NanoAODv9-v1/NANOAOD
2017	/SingleMuon/Run2017B-UL2017_MiniAODv2_NanoAODv9-v1/NANOAOD
	/SingleMuon/Run2017C-UL2017_MiniAODv2_NanoAODv9-v1/NANOAOD
	/SingleMuon/Run2017D-UL2017_MiniAODv2_NanoAODv9-v1/NANOAOD
	/SingleMuon/Run2017E-UL2017_MiniAODv2_NanoAODv9-v1/NANOAOD
	/SingleMuon/Run2017F-UL2017_MiniAODv2_NanoAODv9-v1/NANOAOD
2018	/SingleMuon/Run2018A-UL2018_MiniAODv2_NanoAODv9-v2/NANOAOD
	/SingleMuon/Run2018B-UL2018_MiniAODv2_NanoAODv9-v2/NANOAOD
	/SingleMuon/Run2018C-UL2018_MiniAODv2_NanoAODv9-v2/NANOAOD
	/SingleMuon/Run2018D-UL2018_MiniAODv2_NanoAODv9-v1/NANOAOD

Table 4: Dataset used for early run3 trigger efficiency measurement

Year	Trigger path
2022	/Muon/Run2022C-22Sep2023-v1/NANOAOD
	/Muon/Run2022D-22Sep2023-v1/NANOAOD
2022EE	/Muon/Run2022E-22Sep2023-v1/NANOAOD
	/Muon/Run2022F-22Sep2023-v2/NANOAOD
	/Muon/Run2022G-22Sep2023-v1/NANOAOD
2023	/Muon0/Run2023C-22Sep2023_v1-v1/NANOAOD
	/Muon0/Run2023C-22Sep2023_v2-v1/NANOAOD
	/Muon0/Run2023C-22Sep2023_v3-v1/NANOAOD
	/Muon0/Run2023C-22Sep2023_v4-v1/NANOAOD
	/Muon1/Run2023C-22Sep2023_v1-v1/NANOAOD
	/Muon1/Run2023C-22Sep2023_v2-v1/NANOAOD
	/Muon1/Run2023C-22Sep2023_v3-v1/NANOAOD
	/Muon1/Run2023C-22Sep2023_v4-v1/NANOAOD
2023BPix	/Muon0/Run2023D-22Sep2023_v1-v1/NANOAOD
	/Muon0/Run2023D-22Sep2023_v2-v1/NANOAOD
	/Muon1/Run2023D-22Sep2023_v1-v1/NANOAOD
	/Muon1/Run2023D-22Sep2023_v2-v1/NANOAOD

## 2 Triggers and Dataset

---

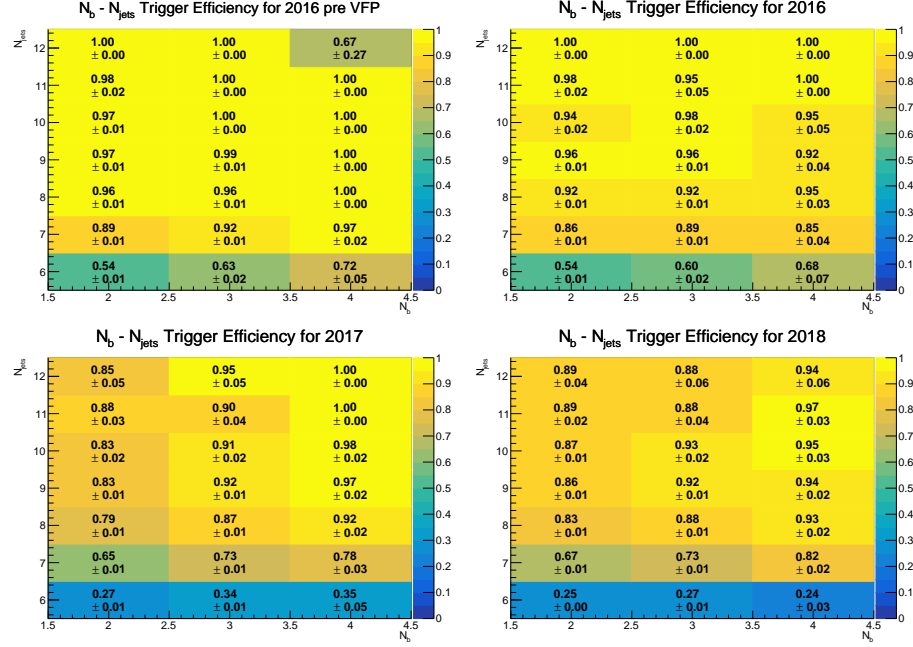


Figure 3: Efficiency measured for search triggers as a function of  $N_{jet}$  and  $N_{b-jet}$  for 2016 pre VFP, 2016 post VFP, 2017 and 2018 data. The  $N_{jet} = 6$  region used for the validation test is shown as well.

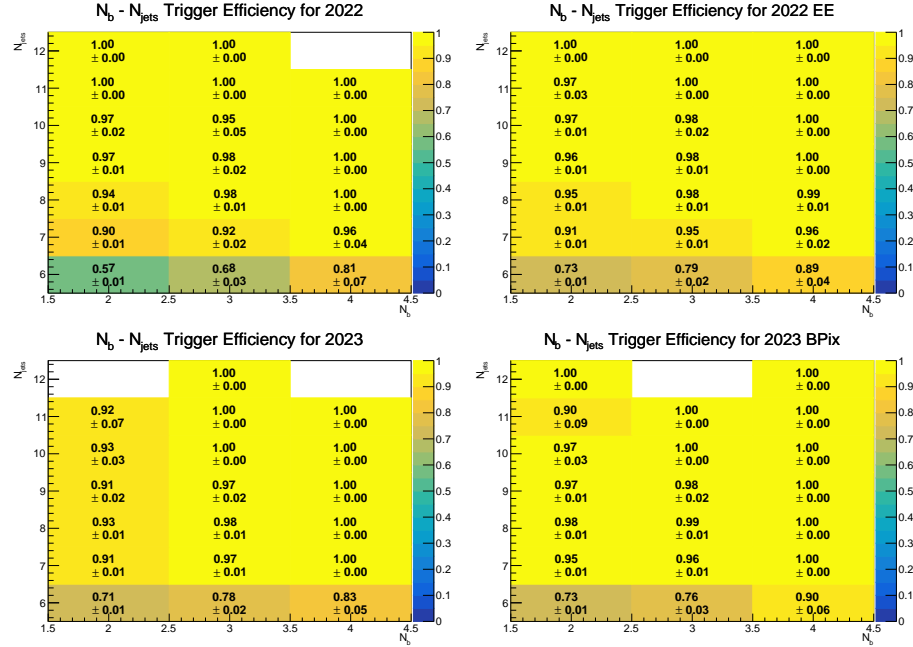


Figure 4: Efficiency measured for search triggers as a function of  $N_{jet}$  and  $N_{b-jet}$  for 2016 pre VFP, 2016 post VFP, 2017 and 2018 data. The  $N_{jet} = 6$  region used for the validation test is shown as well.

## 2 Triggers and Dataset

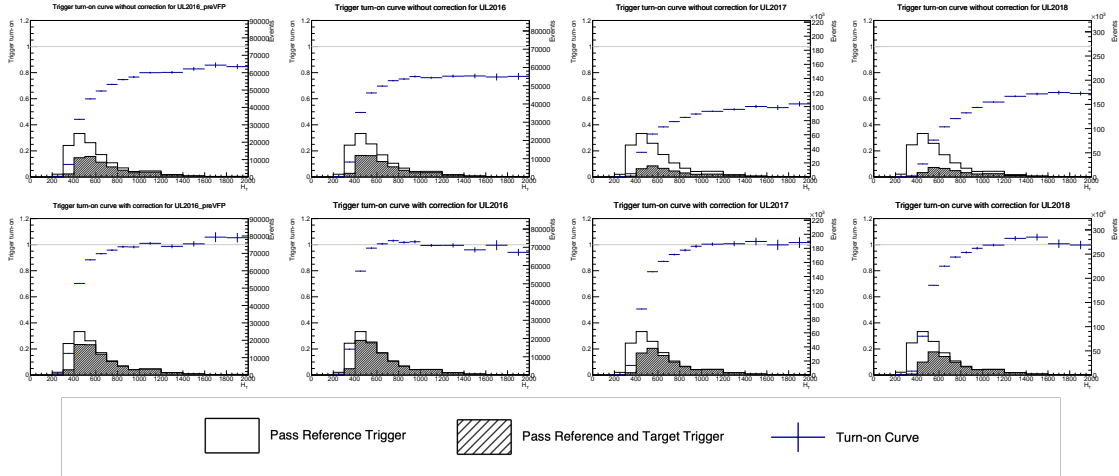


Figure 5: Trigger turn-on vs  $H_T$  before (top) and after (bottom) correcting for efficiencies measured as a function of  $N_{jet}$  and  $N_{b-jet}$  for 2016 pre VFP, 2016 post VFP, 2017 and 2018 data. The target trigger refers to the OR of the trigger paths listed in Table 1 for the respective era, while the reference trigger refers to the OR of IsoMU triggers

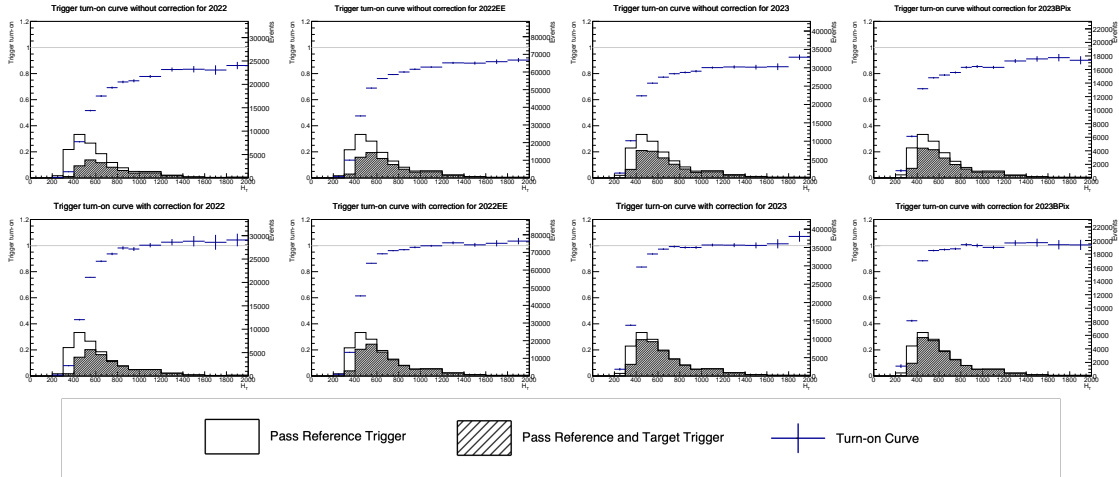


Figure 6: Trigger turn-on vs  $H_T$  before (top) and after (bottom) correcting for efficiencies measured as a function of  $N_{jet}$  and  $N_{b-jet}$  for 2022 and 2023 data. The target trigger refers to the OR of the trigger paths listed in Table 2 for the respective era, while the reference trigger refers to the OR of IsoMU triggers

this approach is sufficient, the trigger turn-on curve is used. Figure 3 and 4 show the  $H_T$  turn-on for each year before and after applying the  $N_{jet}$  and  $N_{b-jet}$  dependent corrections. Before the corrections, the efficiency in the plateau region ( $H_T \geq 900$

70

71 The datasets and Golden JSON files used in this analysis are listed in table 5 and table 6. The

## 2 Triggers and Dataset

---

<sup>72</sup> MC samples used in this analysis are listed in table 7, 8, 9, 10, 11, 12, 13, and 14.

Table 5: Main Dataset used in this analysis

Year	Dataset
2016 preVFP	/JetHT/Run2016B-ver1_HIPM_UL2016_MiniAODv2_NanoAODv9-v2/NANOAOD /JetHT/Run2016D-HIPM_UL2016_MiniAODv2_NanoAODv9-v2/NANOAOD /JetHT/Run2016B-ver2_HIPM_UL2016_MiniAODv2_NanoAODv9-v2/NANOAOD /JetHT/Run2016E-HIPM_UL2016_MiniAODv2_NanoAODv9-v2/NANOAOD /JetHT/Run2016C-HIPM_UL2016_MiniAODv2_NanoAODv9-v2/NANOAOD /JetHT/Run2016F-HIPM_UL2016_MiniAODv2_NanoAODv9-v2/NANOAOD
2016	/JetHT/Run2016F-UL2016_MiniAODv2_NanoAODv9-v1/NANOAOD /JetHT/Run2016G-UL2016_MiniAODv2_NanoAODv9-v1/NANOAOD /JetHT/Run2016H-UL2016_MiniAODv2_NanoAODv9-v1/NANOAOD
2017	/JetHT/Run2017B-UL2017_MiniAODv2_NanoAODv9-v1/NANOAOD /JetHT/Run2017C-UL2017_MiniAODv2_NanoAODv9-v1/NANOAOD /JetHT/Run2017D-UL2017_MiniAODv2_NanoAODv9-v1/NANOAOD /JetHT/Run2017E-UL2017_MiniAODv2_NanoAODv9-v1/NANOAOD /JetHT/Run2017F-UL2017_MiniAODv2_NanoAODv9-v1/NANOAOD
2018	/JetHT/Run2018A-UL2018_MiniAODv2_NanoAODv9_GT36-v1/NANOAOD /JetHT/Run2018B-UL2018_MiniAODv2_NanoAODv9_GT36-v1/NANOAOD /JetHT/Run2018C-UL2018_MiniAODv2_NanoAODv9_GT36-v1/NANOAOD /JetHT/Run2018D-UL2018_MiniAODv2_NanoAODv9_GT36-v1/NANOAOD
2022	/JetMET/Run2022C-22Sep2023-v1/NANOAOD /JetMET/Run2022D-22Sep2023-v1/NANOAOD
2022EE	/JetMET/Run2022E-22Sep2023-v1/NANOAOD /JetMET/Run2022F-22Sep2023-v2/NANOAOD /JetMET/Run2022G-22Sep2023-v2/NANOAOD
2023	/JetMET0/Run2023C-19Dec2023-v1/NANOAOD /JetMET1/Run2023C-19Dec2023-v1/NANOAOD
2023BPix	/ParkingHH/Run2023D-22Sep2023_v1-v1/NANOAOD

Table 6: List of certification JSON files for different years.

Year	Golden JSON File
2016preVFP/2016 ( $36.31 \text{ fb}^{-1}$ )	<a href="https://cms-service-dqmdc.web.cern.ch/CAF/certification/Collisions16/13TeV/Legacy_2016/Cert_271036-284044_13TeV_Legacy2016_Collisions16_JSON.txt">https://cms-service-dqmdc.web.cern.ch/CAF/certification/Collisions16/13TeV/Legacy_2016/Cert_271036-284044_13TeV_Legacy2016_Collisions16_JSON.txt</a>
2017 ( $41.48 \text{ fb}^{-1}$ )	<a href="https://cms-service-dqmdc.web.cern.ch/CAF/certification/Collisions17/13TeV/Legacy_2017/Cert_294927-306462_13TeV_UL2017_Collisions17_GoldenJSON.txt">https://cms-service-dqmdc.web.cern.ch/CAF/certification/Collisions17/13TeV/Legacy_2017/Cert_294927-306462_13TeV_UL2017_Collisions17_GoldenJSON.txt</a>
2018 ( $59.83 \text{ fb}^{-1}$ )	<a href="https://cms-service-dqmdc.web.cern.ch/CAF/certification/Collisions18/13TeV/Legacy_2018/Cert_314472-325175_13TeV_Legacy2018_Collisions18_JSON.txt">https://cms-service-dqmdc.web.cern.ch/CAF/certification/Collisions18/13TeV/Legacy_2018/Cert_314472-325175_13TeV_Legacy2018_Collisions18_JSON.txt</a>
2022/2022EE ( $34.65 \text{ fb}^{-1}$ )	<a href="https://cms-service-dqmdc.web.cern.ch/CAF/certification/Collisions22/Cert_Collisions2022_355100_362760_Golden.json">https://cms-service-dqmdc.web.cern.ch/CAF/certification/Collisions22/Cert_Collisions2022_355100_362760_Golden.json</a>

(Continued on next page)

(Continued from previous page)

Year	Golden JSON File
2023/2023BPix ( $27.24 \text{ fb}^{-1}$ )	<a href="https://cms-service-dqmdc.web.cern.ch/CAF/certification/Collisions23/Cert_Collisions2023_366442_370790_Golden.json">https://cms-service-dqmdc.web.cern.ch/CAF/certification/Collisions23/Cert_Collisions2023_366442_370790_Golden.json</a>

Table 7: List of MC samples for year 2016preVFP.

Category	MC Sample	Cross Section (pb)
TTTT	/TTTT_TuneCP5_13TeV-amcatnlo-pythia8/RunIISummer20UL16NanoAODAPVv9-106X_mcRun2_asymptotic_preVFP_v11-v2/NANOAODSIM	0.01337
TT	/TTToHadronic_TuneCP5_13TeV-powheg-pythia8/RunIISummer20UL16NanoAODAPVv9-106X_mcRun2_asymptotic_preVFP_v11-v1/NANOAODSIM	378.93
	/TTToSemiLeptonic_TuneCP5_13TeV-powheg-pythia8/RunIISummer20UL16NanoAODAPVv9-106X_mcRun2_asymptotic_preVFP_v11-v1/NANOAODSIM	366.29
	/TTTo2L2Nu_TuneCP5_13TeV-powheg-pythia8/RunIISummer20UL16NanoAODAPVv9-106X_mcRun2_asymptotic_preVFP_v11-v1/NANOAODSIM	88.51
QCD	/QCD_HT200to300_TuneCP5_PSWeights_13TeV-madgraphMLM-pythia8/RunIISummer20UL16NanoAODAPVv9-106X_mcRun2_asymptotic_preVFP_v11-v2/NANOAODSIM	1554000.0
	/QCD_HT300to500_TuneCP5_PSWeights_13TeV-madgraphMLM-pythia8/RunIISummer20UL16NanoAODAPVv9-106X_mcRun2_asymptotic_preVFP_v11-v2/NANOAODSIM	323800.0
	/QCD_HT500to700_TuneCP5_PSWeights_13TeV-madgraphMLM-pythia8/RunIISummer20UL16NanoAODAPVv9-106X_mcRun2_asymptotic_preVFP_v11-v1/NANOAODSIM	30280.0
	/QCD_HT700to1000_TuneCP5_PSWeights_13TeV-madgraphMLM-pythia8/RunIISummer20UL16NanoAODAPVv9-106X_mcRun2_asymptotic_preVFP_v11-v1/NANOAODSIM	6392.0
	/QCD_HT1000to1500_TuneCP5_PSWeights_13TeV-madgraphMLM-pythia8/RunIISummer20UL16NanoAODAPVv9-106X_mcRun2_asymptotic_preVFP_v11-v1/NANOAODSIM	1118.0
	/QCD_HT1500to2000_TuneCP5_PSWeights_13TeV-madgraphMLM-pythia8/RunIISummer20UL16NanoAODAPVv9-106X_mcRun2_asymptotic_preVFP_v11-v1/NANOAODSIM	108.9
	/QCD_HT2000toInf_TuneCP5_PSWeights_13TeV-madgraphMLM-pythia8/RunIISummer20UL16NanoAODAPVv9-106X_mcRun2_asymptotic_preVFP_v11-v1/NANOAODSIM	21.93
ttX	/TTWJetsToLNu_TuneCP5_13TeV-amcatnloFXFX-madspin-pythia8/RunIISummer20UL16NanoAODAPVv9-106X_mcRun2_asymptotic_preVFP_v11-v2/NANOAODSIM	0.2161
	/TTWJetsToQQ_TuneCP5_13TeV-amcatnloFXFX-madspin-pythia8/RunIISummer20UL16NanoAODAPVv9-106X_mcRun2_asymptotic_preVFP_v11-v2/NANOAODSIM	0.4377
	/TTZToLLNuNu_M-10_TuneCP5_13TeV-amcatnlo-pythia8/RunIISummer20UL16NanoAODAPVv9-106X_mcRun2_asymptotic_preVFP_v11-v1/NANOAODSIM	0.2439
	/TTZToQQ_TuneCP5_13TeV-amcatnlo-pythia8/RunIISummer20UL16NanoAODAPVv9-106X_mcRun2_asymptotic_preVFP_v11-v1/NANOAODSIM	0.5113
	/ttHTobb_M125_TuneCP5_13TeV-powheg-pythia8/RunIISummer20UL16NanoAODAPVv9-106X_mcRun2_asymptotic_preVFP_v11-v2/NANOAODSIM	0.2934

(Continued on next page)

## 2 Triggers and Dataset

---

(Continued from previous page)

Category	MC Sample	Cross Section (pb)
	/ttHToNonbb_M125_TuneCP5_13TeV-powheg-pythia8/RunIISummer20UL16NanoAODAPVv9-106X_mcRun2_asymptotic_preVFP_v11-v2/NANOAODSIM	0.2151
	/TTGJets_TuneCP5_13TeV-amcatnloFXFX-madspin-pythia8/RunIISummer20UL16NanoAODAPVv9-106X_mcRun2_asymptotic_preVFP_v11-v2/NANOAODSIM	3.757
tZq	/tZq_ll_4f_ckm_NLO_TuneCP5_13TeV-amcatnlo-pythia8/RunIISummer20UL16NanoAODAPVv9-106X_mcRun2_asymptotic_preVFP_v11-v1/NANOAODSIM	0.07561
Single-top	/ST_s-channel_4f_hadronicDecays_TuneCP5_13TeV-amcatnlo-pythia8/RunIISummer20UL16NanoAODAPVv9-106X_mcRun2_asymptotic_preVFP_v11-v1/NANOAODSIM	7.104
	/ST_s-channel_4f_leptonDecays_TuneCP5_13TeV-amcatnlo-pythia8/RunIISummer20UL16NanoAODAPVv9-106X_mcRun2_asymptotic_preVFP_v11-v1/NANOAODSIM	3.549
	/ST_tW_antitop_5f_inclusiveDecays_TuneCP5_13TeV-powheg-pythia8/RunIISummer20UL16NanoAODAPVv9-106X_mcRun2_asymptotic_preVFP_v11-v1/NANOAODSIM	32.51
	/ST_tW_top_5f_inclusiveDecays_TuneCP5_13TeV-powheg-pythia8/RunIISummer20UL16NanoAODAPVv9-106X_mcRun2_asymptotic_preVFP_v11-v1/NANOAODSIM	32.45
	/ST_t-channel_top_4f_InclusiveDecays_TuneCP5_13TeV-powheg-madspin-pythia8/RunIISummer20UL16NanoAODAPVv9-106X_mcRun2_asymptotic_preVFP_v11-v1/NANOAODSIM	113.4
	/ST_t-channel_antitop_4f_InclusiveDecays_TuneCP5_13TeV-powheg-madspin-pythia8/RunIISummer20UL16NanoAODAPVv9-106X_mcRun2_asymptotic_preVFP_v11-v1/NANOAODSIM	67.93
WJets	/WJetsToQQ_HT-400to600_TuneCP5_13TeV-madgraphMLM-pythia8/RunIISummer20UL16NanoAODAPVv9-106X_mcRun2_asymptotic_preVFP_v11-v2/NANOAODSIM	276.5
	/WJetsToQQ_HT-600to800_TuneCP5_13TeV-madgraphMLM-pythia8/RunIISummer20UL16NanoAODAPVv9-106X_mcRun2_asymptotic_preVFP_v11-v2/NANOAODSIM	59.25
	/WJetsToQQ_HT-800toInf_TuneCP5_13TeV-madgraphMLM-pythia8/RunIISummer20UL16NanoAODAPVv9-106X_mcRun2_asymptotic_preVFP_v11-v2/NANOAODSIM	28.75
	/WJetsToLNu_HT-400To600_TuneCP5_13TeV-madgraphMLM-pythia8/RunIISummer20UL16NanoAODAPVv9-106X_mcRun2_asymptotic_preVFP_v11-v1/NANOAODSIM	45.25
	/WJetsToLNu_HT-600To800_TuneCP5_13TeV-madgraphMLM-pythia8/RunIISummer20UL16NanoAODAPVv9-106X_mcRun2_asymptotic_preVFP_v11-v1/NANOAODSIM	10.97
	/WJetsToLNu_HT-800To1200_TuneCP5_13TeV-madgraphMLM-pythia8/RunIISummer20UL16NanoAODAPVv9-106X_mcRun2_asymptotic_preVFP_v11-v1/NANOAODSIM	4.933
	/WJetsToLNu_HT-1200To2500_TuneCP5_13TeV-madgraphMLM-pythia8/RunIISummer20UL16NanoAODAPVv9-106X_mcRun2_asymptotic_preVFP_v11-v1/NANOAODSIM	1.16
	/WJetsToLNu_HT-2500ToInf_TuneCP5_13TeV-madgraphMLM-pythia8/RunIISummer20UL16NanoAODAPVv9-106X_mcRun2_asymptotic_preVFP_v11-v2/NANOAODSIM	0.02646
ZJets	/ZJetsToQQ_HT-400to600_TuneCP5_13TeV-madgraphMLM-pythia8/RunIISummer20UL16NanoAODAPVv9-106X_mcRun2_asymptotic_preVFP_v11-v2/NANOAODSIM	114.2

(Continued on next page)

(Continued from previous page)

Category	MC Sample	Cross Section (pb)
	/ZJetsToQQ_HT-600to800_TuneCP5_13TeV-madgraphMLM-pythia8/RunIISummer20UL16NanoAODAPVv9-106X_mcRun2_asymptotic_preVFP_v11-v2/NANOAODSIM	25.34
	/ZJetsToQQ_HT-800toInf.TuneCP5_13TeV-madgraphMLM-pythia8/RunIISummer20UL16NanoAODAPVv9-106X_mcRun2_asymptotic_preVFP_v11-v2/NANOAODSIM	13.1
	/ZJetsToNuNu_HT-400To600_TuneCP5_13TeV-madgraphMLM-pythia8/RunIISummer20UL16NanoAODAPVv9-106X_mcRun2_asymptotic_preVFP_v11-v2/NANOAODSIM	9.904
	/ZJetsToNuNu_HT-600To800_TuneCP5_13TeV-madgraphMLM-pythia8/RunIISummer20UL16NanoAODAPVv9-106X_mcRun2_asymptotic_preVFP_v11-v2/NANOAODSIM	2.413
	/ZJetsToNuNu_HT-800To1200_TuneCP5_13TeV-madgraphMLM-pythia8/RunIISummer20UL16NanoAODAPVv9-106X_mcRun2_asymptotic_preVFP_v11-v2/NANOAODSIM	1.071
	/ZJetsToNuNu_HT-1200To2500_TuneCP5_13TeV-madgraphMLM-pythia8/RunIISummer20UL16NanoAODAPVv9-106X_mcRun2_asymptotic_preVFP_v11-v2/NANOAODSIM	0.2497
	/ZJetsToNuNu_HT-2500ToInf.TuneCP5_13TeV-madgraphMLM-pythia8/RunIISummer20UL16NanoAODAPVv9-106X_mcRun2_asymptotic_preVFP_v11-v2/NANOAODSIM	0.005618
other	/WW_TuneCP5_13TeV-pythia8/RunIISummer20UL16NanoAODAPVv9-106X_mcRun2_asymptotic_preVFP_v11-v1/NANOAODSIM	75.95
	/WZ_TuneCP5_13TeV-pythia8/RunIISummer20UL16NanoAODAPVv9-106X_mcRun2_asymptotic_preVFP_v11-v1/NANOAODSIM	27.59
	/ZZ_TuneCP5_13TeV-pythia8/RunIISummer20UL16NanoAODAPVv9-106X_mcRun2_asymptotic_preVFP_v11-v1/NANOAODSIM	12.17
	/DYJetsToLL_M-50_TuneCP5_13TeV-amcatnloFXFX-pythia8/RunIISummer20UL16NanoAODAPVv9-106X_mcRun2_asymptotic_preVFP_v11-v1/NANOAODSIM	6404.0
	/DYJetsToLL_M-10to50_TuneCP5_13TeV-amcatnloFXFX-pythia8/RunIISummer20UL16NanoAODAPVv9-106X_mcRun2_asymptotic_preVFP_v11-v1/NANOAODSIM	20460.0

Table 8: List of MC samples for year 2016.

Category	MC Sample	Cross Section (pb)
TTTT	/TTTT_TuneCP5_13TeV-amcatnlo-pythia8/RunIISummer20UL16NanoAODv9-106X_mcRun2_asymptotic_v17-v2/NANOAODSIM	0.01337
TT	/TTToHadronic_TuneCP5_13TeV-powheg-pythia8/RunIISummer20UL16NanoAODv9-106X_mcRun2_asymptotic_v17-v1/NANOAODSIM	378.93
	/TTToSemiLeptonic_TuneCP5_13TeV-powheg-pythia8/RunIISummer20UL16NanoAODv9-106X_mcRun2_asymptotic_v17-v1/NANOAODSIM	366.29
	/TTTo2L2Nu_TuneCP5_13TeV-powheg-pythia8/RunIISummer20UL16NanoAODv9-106X_mcRun2_asymptotic_v17-v1/NANOAODSIM	88.51
	/QCD_HT200to300_TuneCP5_PSWeights_13TeV-madgraphMLM-pythia8/RunIISummer20UL16NanoAODv9-106X_mcRun2_asymptotic_v17-v1/NANOAODSIM	1554000.0

QCD

(Continued on next page)

## 2 Triggers and Dataset

---

(Continued from previous page)

Category	MC Sample	Cross Section (pb)
	/QCD_HT300to500_TuneCP5_PSWeights_13TeV-madgraphMLM-pythia8/RunIISummer20UL16NanoAODv9-106X_mcRun2_asymptotic_v17-v1/NANOAODSIM	323800.0
	/QCD_HT500to700_TuneCP5_PSWeights_13TeV-madgraphMLM-pythia8/RunIISummer20UL16NanoAODv9-106X_mcRun2_asymptotic_v17-v1/NANOAODSIM	30280.0
	/QCD_HT700to1000_TuneCP5_PSWeights_13TeV-madgraphMLM-pythia8/RunIISummer20UL16NanoAODv9-106X_mcRun2_asymptotic_v17-v1/NANOAODSIM	6392.0
	/QCD_HT1000to1500_TuneCP5_PSWeights_13TeV-madgraphMLM-pythia8/RunIISummer20UL16NanoAODv9-106X_mcRun2_asymptotic_v17-v1/NANOAODSIM	1118.0
	/QCD_HT1500to2000_TuneCP5_PSWeights_13TeV-madgraphMLM-pythia8/RunIISummer20UL16NanoAODv9-106X_mcRun2_asymptotic_v17-v1/NANOAODSIM	108.9
	/QCD_HT2000toInf_TuneCP5_PSWeights_13TeV-madgraphMLM-pythia8/RunIISummer20UL16NanoAODv9-106X_mcRun2_asymptotic_v17-v1/NANOAODSIM	21.93
ttX	/TTWJetsToLNu_TuneCP5_13TeV-amcatnloFXFX-madspin-pythia8/RunIISummer20UL16NanoAODv9-106X_mcRun2_asymptotic_v17-v1/NANOAODSIM	0.2161
	/TTWJetsToQQ_TuneCP5_13TeV-amcatnloFXFX-madspin-pythia8/RunIISummer20UL16NanoAODv9-106X_mcRun2_asymptotic_v17-v1/NANOAODSIM	0.4377
	/TTZToLLNuNu_M-10_TuneCP5_13TeV-amcatnlo-pythia8/RunIISummer20UL16NanoAODv9-106X_mcRun2_asymptotic_v17-v1/NANOAODSIM	0.2439
	/TTZToQQ_TuneCP5_13TeV-amcatnlo-pythia8/RunIISummer20UL16NanoAODv9-106X_mcRun2_asymptotic_v17-v1/NANOAODSIM	0.5113
	/ttHTobb_M125_TuneCP5_13TeV-powheg-pythia8/RunIISummer20UL16NanoAODv9-106X_mcRun2_asymptotic_v17-v2/NANOAODSIM	0.2934
	/ttHToNonbb_M125_TuneCP5_13TeV-powheg-pythia8/RunIISummer20UL16NanoAODv9-106X_mcRun2_asymptotic_v17-v2/NANOAODSIM	0.2151
	/TTGJets_TuneCP5_13TeV-amcatnloFXFX-madspin-pythia8/RunIISummer20UL16NanoAODv9-106X_mcRun2_asymptotic_v17-v1/NANOAODSIM	3.757
	/tZq_ll_4f_ckm_NLO_TuneCP5_13TeV-amcatnlo-pythia8/RunIISummer20UL16NanoAODv9-106X_mcRun2_asymptotic_v17-v1/NANOAODSIM	0.07561
Single-top	/ST_s-channel_4f_leptonDecays_TuneCP5_13TeV-amcatnlo-pythia8/RunIISummer20UL16NanoAODv9-106X_mcRun2_asymptotic_v17-v1/NANOAODSIM	3.549
	/ST_s-channel_4f_hadronicDecays_TuneCP5_13TeV-amcatnlo-pythia8/RunIISummer20UL16NanoAODv9-106X_mcRun2_asymptotic_v17-v1/NANOAODSIM	7.104
	/ST_tW_antitop_5f_inclusiveDecays_TuneCP5_13TeV-powheg-pythia8/RunIISummer20UL16NanoAODv9-106X_mcRun2_asymptotic_v17-v2/NANOAODSIM	32.51
	/ST_tW_top_5f_inclusiveDecays_TuneCP5_13TeV-powheg-pythia8/RunIISummer20UL16NanoAODv9-106X_mcRun2_asymptotic_v17-v2/NANOAODSIM	32.45
	/ST_t-channel_top_4f_InclusiveDecays_TuneCP5_13TeV-powheg-madspin-pythia8/RunIISummer20UL16NanoAODv9-106X_mcRun2_asymptotic_v17-v1/NANOAODSIM	113.4

(Continued on next page)

(Continued from previous page)

Category	MC Sample	Cross Section (pb)
	/ST_t-channel_antitop_4f_InclusiveDecays_TuneCP5_13TeV-powheg-madspin-pythia8/RunIISummer20UL16NanoAODv9-106X_mcRun2_asymptotic_v17-v1/NANOAODSIM	67.93
WJets	/WJetsToQQ_HT-400to600_TuneCP5_13TeV-madgraphMLM-pythia8/RunIISummer20UL16NanoAODv9-106X_mcRun2_asymptotic_v17-v2/NANOAODSIM	276.5
	/WJetsToQQ_HT-600to800_TuneCP5_13TeV-madgraphMLM-pythia8/RunIISummer20UL16NanoAODv9-106X_mcRun2_asymptotic_v17-v2/NANOAODSIM	59.25
	/WJetsToQQ_HT-800toInf_TuneCP5_13TeV-madgraphMLM-pythia8/RunIISummer20UL16NanoAODv9-106X_mcRun2_asymptotic_v17-v2/NANOAODSIM	28.75
	/WJetsToLNu_HT-400To600_TuneCP5_13TeV-madgraphMLM-pythia8/RunIISummer20UL16NanoAODv9-106X_mcRun2_asymptotic_v17-v1/NANOAODSIM	45.25
	/WJetsToLNu_HT-600To800_TuneCP5_13TeV-madgraphMLM-pythia8/RunIISummer20UL16NanoAODv9-106X_mcRun2_asymptotic_v17-v1/NANOAODSIM	10.97
	/WJetsToLNu_HT-800To1200_TuneCP5_13TeV-madgraphMLM-pythia8/RunIISummer20UL16NanoAODv9-106X_mcRun2_asymptotic_v17-v1/NANOAODSIM	4.933
	/WJetsToLNu_HT-1200To2500_TuneCP5_13TeV-madgraphMLM-pythia8/RunIISummer20UL16NanoAODv9-106X_mcRun2_asymptotic_v17-v1/NANOAODSIM	1.16
	/WJetsToLNu_HT-2500ToInf_TuneCP5_13TeV-madgraphMLM-pythia8/RunIISummer20UL16NanoAODv9-106X_mcRun2_asymptotic_v17-v2/NANOAODSIM	0.02646
ZJets	/ZJetsToQQ_HT-400to600_TuneCP5_13TeV-madgraphMLM-pythia8/RunIISummer20UL16NanoAODv9-106X_mcRun2_asymptotic_v17-v2/NANOAODSIM	114.2
	/ZJetsToQQ_HT-600to800_TuneCP5_13TeV-madgraphMLM-pythia8/RunIISummer20UL16NanoAODv9-106X_mcRun2_asymptotic_v17-v2/NANOAODSIM	25.34
	/ZJetsToQQ_HT-800toInf_TuneCP5_13TeV-madgraphMLM-pythia8/RunIISummer20UL16NanoAODv9-106X_mcRun2_asymptotic_v17-v2/NANOAODSIM	13.1
	/ZJetsToNuNu_HT-400To600_TuneCP5_13TeV-madgraphMLM-pythia8/RunIISummer20UL16NanoAODv9-106X_mcRun2_asymptotic_v17-v2/NANOAODSIM	9.904
	/ZJetsToNuNu_HT-600To800_TuneCP5_13TeV-madgraphMLM-pythia8/RunIISummer20UL16NanoAODv9-106X_mcRun2_asymptotic_v17-v2/NANOAODSIM	2.413
	/ZJetsToNuNu_HT-800To1200_TuneCP5_13TeV-madgraphMLM-pythia8/RunIISummer20UL16NanoAODv9-106X_mcRun2_asymptotic_v17-v2/NANOAODSIM	1.071
	/ZJetsToNuNu_HT-1200To2500_TuneCP5_13TeV-madgraphMLM-pythia8/RunIISummer20UL16NanoAODv9-106X_mcRun2_asymptotic_v17-v2/NANOAODSIM	0.2497
	/ZJetsToNuNu_HT-2500ToInf_TuneCP5_13TeV-madgraphMLM-pythia8/RunIISummer20UL16NanoAODv9-106X_mcRun2_asymptotic_v17-v2/NANOAODSIM	0.005618
	/WW_TuneCP5_13TeV-pythia8/RunIISummer20UL16NanoAODv9-106X_mcRun2_asymptotic_v17-v1/NANOAODSIM	75.95
other	(Continued on next page)	

## 2 Triggers and Dataset

---

(Continued from previous page)

Category	MC Sample	Cross Section (pb)
	/WZ_TuneCP5_13TeV-pythia8/RunIISummer20UL16NanoAODv9-106X_mcRun2_asymptotic_v17-v1/NANOAODSIM	27.59
	/ZZ_TuneCP5_13TeV-pythia8/RunIISummer20UL16NanoAODv9-106X_mcRun2_asymptotic_v17-v1/NANOAODSIM	12.17
	/DYJetsToLL_M-50_TuneCP5_13TeV-amcatnloFXFX-pythia8/RunIISummer20UL16NanoAODv9-106X_mcRun2_asymptotic_v17-v1/NANOAODSIM	6404.0
	/DYJetsToLL_M-10to50_TuneCP5_13TeV-amcatnloFXFX-pythia8/RunIISummer20UL16NanoAODv9-106X_mcRun2_asymptotic_v17-v1/NANOAODSIM	20460.0

Table 9: List of MC samples for year 2017.

Category	MC Sample	Cross Section (pb)
TTTT	/TTTT_TuneCP5_13TeV-amcatnlo-pythia8/RunIISummer20UL17NanoAODv9-106X_mc2017_realistic_v9-v2/NANOAODSIM	0.01337
TT	/TTToHadronic_TuneCP5_13TeV-powheg-pythia8/RunIISummer20UL17NanoAODv9-106X_mc2017_realistic_v9-v1/NANOAODSIM	378.93
	/TTToSemiLeptonic_TuneCP5_13TeV-powheg-pythia8/RunIISummer20UL17NanoAODv9-106X_mc2017_realistic_v9-v1/NANOAODSIM	366.29
	/TTTo2L2Nu_TuneCP5_13TeV-powheg-pythia8/RunIISummer20UL17NanoAODv9-106X_mc2017_realistic_v9-v1/NANOAODSIM	88.51
QCD	/QCD_HT200to300_TuneCP5_13TeV-madgraphMLM-pythia8/RunIISummer20UL17NanoAODv9-106X_mc2017_realistic_v9-v1/NANOAODSIM	1552000.0
	/QCD_HT300to500_TuneCP5_13TeV-madgraphMLM-pythia8/RunIISummer20UL17NanoAODv9-106X_mc2017_realistic_v9-v1/NANOAODSIM	321100.0
	/QCD_HT500to700_TuneCP5_13TeV-madgraphMLM-pythia8/RunIISummer20UL17NanoAODv9-106X_mc2017_realistic_v9-v1/NANOAODSIM	30250.0
	/QCD_HT700to1000_TuneCP5_13TeV-madgraphMLM-pythia8/RunIISummer20UL17NanoAODv9-106X_mc2017_realistic_v9-v1/NANOAODSIM	6398.0
	/QCD_HT1000to1500_TuneCP5_13TeV-madgraphMLM-pythia8/RunIISummer20UL17NanoAODv9-106X_mc2017_realistic_v9-v1/NANOAODSIM	1122.0
	/QCD_HT1500to2000_TuneCP5_13TeV-madgraphMLM-pythia8/RunIISummer20UL17NanoAODv9-106X_mc2017_realistic_v9-v1/NANOAODSIM	109.4
	/QCD_HT2000toInf_TuneCP5_13TeV-madgraphMLM-pythia8/RunIISummer20UL17NanoAODv9-106X_mc2017_realistic_v9-v1/NANOAODSIM	21.74
ttX	/TTWJetsToLNu_TuneCP5_13TeV-amcatnloFXFX-madspin-pythia8/RunIISummer20UL17NanoAODv9-106X_mc2017_realistic_v9-v1/NANOAODSIM	0.2163
	/TTWJetsToQQ_TuneCP5_13TeV-amcatnloFXFX-madspin-pythia8/RunIISummer20UL17NanoAODv9-106X_mc2017_realistic_v9-v1/NANOAODSIM	0.4432
	/TTZToLLNuNu_M-10_TuneCP5_13TeV-amcatnlo-pythia8/RunIISummer20UL17NanoAODv9-106X_mc2017_realistic_v9-v1/NANOAODSIM	0.2439
	/TTZToQQ_TuneCP5_13TeV-amcatnlo-pythia8/RunIISummer20UL17NanoAODv9-106X_mc2017_realistic_v9-v1/NANOAODSIM	0.5113
	/ttHTobb_M125_TuneCP5_13TeV-powheg-pythia8/RunIISummer20UL17NanoAODv9-106X_mc2017_realistic_v9-v2/NANOAODSIM	0.2934
	/ttHToNonbb_M125_TuneCP5_13TeV-powheg-pythia8/RunIISummer20UL17NanoAODv9-106X_mc2017_realistic_v9-v2/NANOAODSIM	0.2151

(Continued on next page)

(Continued from previous page)

Category	MC Sample	Cross Section (pb)
	/TTGJets_TuneCP5_13TeV-amcatnloFXFX-madspin-pythia8/RunIISummer20UL17NanoAODv9-106X_mc2017_realistic_v9-v1/NANOAODSIM	3.774
Single-top	/ST_s-channel_4f_leptonDecays_TuneCP5_13TeV-amcatnlo-pythia8/RunIISummer20UL17NanoAODv9-106X_mc2017_realistic_v9-v1/NANOAODSIM	3.549
	/ST_s-channel_4f_hadronicDecays_TuneCP5_13TeV-amcatnlo-pythia8/RunIISummer20UL17NanoAODv9-106X_mc2017_realistic_v9-v1/NANOAODSIM	7.104
	/ST_tW_antitop_5f_inclusiveDecays_TuneCP5_13TeV-powheg-pythia8/RunIISummer20UL17NanoAODv9-106X_mc2017_realistic_v9-v2/NANOAODSIM	32.51
	/ST_tW_top_5f_inclusiveDecays_TuneCP5_13TeV-powheg-pythia8/RunIISummer20UL17NanoAODv9-106X_mc2017_realistic_v9-v2/NANOAODSIM	32.45
	/ST_t-channel_top_4f_InclusiveDecays_TuneCP5_13TeV-powheg-madspin-pythia8/RunIISummer20UL17NanoAODv9-106X_mc2017_realistic_v9-v1/NANOAODSIM	113.4
	/ST_t-channel_antitop_4f_InclusiveDecays_TuneCP5_13TeV-powheg-madspin-pythia8/RunIISummer20UL17NanoAODv9-106X_mc2017_realistic_v9-v1/NANOAODSIM	67.93
WJets	/WJetsToQQ_HT-400to600_TuneCP5_13TeV-madgraphMLM-pythia8/RunIISummer20UL17NanoAODv9-106X_mc2017_realistic_v9-v2/NANOAODSIM	275.4
	/WJetsToQQ_HT-600to800_TuneCP5_13TeV-madgraphMLM-pythia8/RunIISummer20UL17NanoAODv9-106X_mc2017_realistic_v9-v2/NANOAODSIM	59.55
	/WJetsToQQ_HT-800toInf_TuneCP5_13TeV-madgraphMLM-pythia8/RunIISummer20UL17NanoAODv9-106X_mc2017_realistic_v9-v2/NANOAODSIM	29.1
	/WJetsToLNu_HT-400To600_TuneCP5_13TeV-madgraphMLM-pythia8/RunIISummer20UL17NanoAODv9-106X_mc2017_realistic_v9-v1/NANOAODSIM	44.93
	/WJetsToLNu_HT-600To800_TuneCP5_13TeV-madgraphMLM-pythia8/RunIISummer20UL17NanoAODv9-106X_mc2017_realistic_v9-v1/NANOAODSIM	11.19
	/WJetsToLNu_HT-800To1200_TuneCP5_13TeV-madgraphMLM-pythia8/RunIISummer20UL17NanoAODv9-106X_mc2017_realistic_v9-v3/NANOAODSIM	4.926
	/WJetsToLNu_HT-1200To2500_TuneCP5_13TeV-madgraphMLM-pythia8/RunIISummer20UL17NanoAODv9-106X_mc2017_realistic_v9-v1/NANOAODSIM	1.152
	/WJetsToLNu_HT-2500ToInf_TuneCP5_13TeV-madgraphMLM-pythia8/RunIISummer20UL17NanoAODv9-106X_mc2017_realistic_v9-v2/NANOAODSIM	0.02646
ZJets	/ZJetsToQQ_HT-400to600_TuneCP5_13TeV-madgraphMLM-pythia8/RunIISummer20UL17NanoAODv9-106X_mc2017_realistic_v9-v2/NANOAODSIM	116.4
	/ZJetsToQQ_HT-600to800_TuneCP5_13TeV-madgraphMLM-pythia8/RunIISummer20UL17NanoAODv9-106X_mc2017_realistic_v9-v2/NANOAODSIM	25.47
	/ZJetsToQQ_HT-800toInf_TuneCP5_13TeV-madgraphMLM-pythia8/RunIISummer20UL17NanoAODv9-106X_mc2017_realistic_v9-v2/NANOAODSIM	13.1
	/ZJetsToNuNu_HT-400To600_TuneCP5_13TeV-madgraphMLM-pythia8/RunIISummer20UL17NanoAODv9-106X_mc2017_realistic_v9-v1/NANOAODSIM	9.961
	/ZJetsToNuNu_HT-600To800_TuneCP5_13TeV-madgraphMLM-pythia8/RunIISummer20UL17NanoAODv9-106X_mc2017_realistic_v9-v1/NANOAODSIM	2.425
	/ZJetsToNuNu_HT-800To1200_TuneCP5_13TeV-madgraphMLM-pythia8/RunIISummer20UL17NanoAODv9-106X_mc2017_realistic_v9-v1/NANOAODSIM	1.076
	/ZJetsToNuNu_HT-1200To2500_TuneCP5_13TeV-madgraphMLM-pythia8/RunIISummer20UL17NanoAODv9-106X_mc2017_realistic_v9-v1/NANOAODSIM	0.2474
	/ZJetsToNuNu_HT-2500ToInf_TuneCP5_13TeV-madgraphMLM-pythia8/RunIISummer20UL17NanoAODv9-106X_mc2017_realistic_v9-v1/NANOAODSIM	0.005609
other	/WW_TuneCP5_13TeV-pythia8/RunIISummer20UL17NanoAODv9-106X_mc2017_realistic_v9-v1/NANOAODSIM	76.25
	/WZ_TuneCP5_13TeV-pythia8/RunIISummer20UL17NanoAODv9-106X_mc2017_realistic_v9-v1/NANOAODSIM	27.55
	/ZZ_TuneCP5_13TeV-pythia8/RunIISummer20UL17NanoAODv9-106X_mc2017_realistic_v9-v1/NANOAODSIM	12.23

(Continued on next page)

## 2 Triggers and Dataset

---

(Continued from previous page)

Category	MC Sample	Cross Section (pb)
	/DYJetsToLL_M-50_TuneCP5_13TeV-amcatnloFXFX-pythia8/RunIISummer20UL17NanoAODv9-106X_mc2017_realistic_v9-v2/NANOAODSIM	6424.0
	/DYJetsToLL_M-10to50_TuneCP5_13TeV-madgraphMLM-pythia8/RunIISummer20UL17NanoAODv9-106X_mc2017_realistic_v9-v1/NANOAODSIM	15910.0

Table 10: List of MC samples for year 2018.

Category	MC Sample	Cross Section (pb)
TTTT	/TTTT_TuneCP5_13TeV-amcatnlo-pythia8/RunIISummer20UL18NanoAODv9-106X_upgrade2018_realistic_v16_L1v1-v2/NANOAODSIM	0.01337
TT	/TTToHadronic_TuneCP5_13TeV-powheg-pythia8/RunIISummer20UL18NanoAODv9-106X_upgrade2018_realistic_v16_L1v1-v1/NANOAODSIM	378.93
	/TTToSemiLeptonic_TuneCP5_13TeV-powheg-pythia8/RunIISummer20UL18NanoAODv9-106X_upgrade2018_realistic_v16_L1v1-v1/NANOAODSIM	366.29
	/TTTo2L2Nu_TuneCP5_13TeV-powheg-pythia8/RunIISummer20UL18NanoAODv9-106X_upgrade2018_realistic_v16_L1v1-v1/NANOAODSIM	88.51
	/QCD_HT200to300_TuneCP5_13TeV-madgraphMLM-pythia8/RunIISummer20UL18NanoAODv9-106X_upgrade2018_realistic_v16_L1v1-v1/NANOAODSIM	1554000.0
QCD	/QCD_HT300to500_TuneCP5_13TeV-madgraphMLM-pythia8/RunIISummer20UL18NanoAODv9-106X_upgrade2018_realistic_v16_L1v1-v1/NANOAODSIM	323800.0
	/QCD_HT500to700_TuneCP5_13TeV-madgraphMLM-pythia8/RunIISummer20UL18NanoAODv9-106X_upgrade2018_realistic_v16_L1v1-v1/NANOAODSIM	30280.0
	/QCD_HT700to1000_TuneCP5_13TeV-madgraphMLM-pythia8/RunIISummer20UL18NanoAODv9-106X_upgrade2018_realistic_v16_L1v1-v1/NANOAODSIM	6392.0
	/QCD_HT1000to1500_TuneCP5_13TeV-madgraphMLM-pythia8/RunIISummer20UL18NanoAODv9-106X_upgrade2018_realistic_v16_L1v1-v1/NANOAODSIM	1118.0
	/QCD_HT1500to2000_TuneCP5_13TeV-madgraphMLM-pythia8/RunIISummer20UL18NanoAODv9-106X_upgrade2018_realistic_v16_L1v1-v1/NANOAODSIM	108.9
	/QCD_HT2000toInf_TuneCP5_13TeV-madgraphMLM-pythia8/RunIISummer20UL18NanoAODv9-106X_upgrade2018_realistic_v16_L1v1-v1/NANOAODSIM	21.93
	/TTWJetsToLNu_TuneCP5_13TeV-amcatnloFXFX-madspin-pythia8/RunIISummer20UL18NanoAODv9-106X_upgrade2018_realistic_v16_L1v1-v1/NANOAODSIM	0.2161
ttX	/TTWJetsToQQ_TuneCP5_13TeV-amcatnloFXFX-madspin-pythia8/RunIISummer20UL18NanoAODv9-106X_upgrade2018_realistic_v16_L1v1-v1/NANOAODSIM	0.4377
	/TTZToLLNuNu_M-10_TuneCP5_13TeV-amcatnlo-pythia8/RunIISummer20UL18NanoAODv9-106X_upgrade2018_realistic_v16_L1v1-v1/NANOAODSIM	0.2439
	/TTZToQQ_TuneCP5_13TeV-amcatnlo-pythia8/RunIISummer20UL18NanoAODv9-106X_upgrade2018_realistic_v16_L1v1-v1/NANOAODSIM	0.5113

(Continued on next page)

(Continued from previous page)

Category	MC Sample	Cross Section (pb)
	/ttHTobb_M125_TuneCP5_13TeV-powheg-pythia8/RunIISummer20UL18NanoAODv9-106X_upgrade2018_realistic_v16_L1v1-v2/NANOAODSIM	0.2934
	/ttHToNonbb_M125_TuneCP5_13TeV-powheg-pythia8/RunIISummer20UL18NanoAODv9-106X_upgrade2018_realistic_v16_L1v1-v2/NANOAODSIM	0.2151
	/TTGJets_TuneCP5_13TeV-amcatnloFXFX-madspin-pythia8/RunIISummer20UL18NanoAODv9-106X_upgrade2018_realistic_v16_L1v1-v1/NANOAODSIM	3.757
Single-top	/ST_s-channel_4f_leptonDecays_TuneCP5_13TeV-amcatnlo-pythia8/RunIISummer20UL18NanoAODv9-106X_upgrade2018_realistic_v16_L1v1-v1/NANOAODSIM	3.549
	/ST_s-channel_4f_hadronicDecays_TuneCP5_13TeV-amcatnlo-pythia8/RunIISummer20UL18NanoAODv9-106X_upgrade2018_realistic_v16_L1v1-v1/NANOAODSIM	7.104
	/ST_tW_antitop_5f_inclusiveDecays_TuneCP5_13TeV-powheg-pythia8/RunIISummer20UL18NanoAODv9-106X_upgrade2018_realistic_v16_L1v1-v2/NANOAODSIM	32.51
	/ST_tW_top_5f_inclusiveDecays_TuneCP5_13TeV-powheg-pythia8/RunIISummer20UL18NanoAODv9-106X_upgrade2018_realistic_v16_L1v1-v2/NANOAODSIM	32.45
	/ST_t-channel_top_4f_InclusiveDecays_TuneCP5_13TeV-powheg-madspin-pythia8/RunIISummer20UL18NanoAODv9-106X_upgrade2018_realistic_v16_L1v1-v1/NANOAODSIM	113.4
	/ST_t-channel_antitop_4f_InclusiveDecays_TuneCP5_13TeV-powheg-madspin-pythia8/RunIISummer20UL18NanoAODv9-106X_upgrade2018_realistic_v16_L1v1-v1/NANOAODSIM	67.93
WJets	/WJetsToQQ_HT-400to600_TuneCP5_13TeV-madgraphMLM-pythia8/RunIISummer20UL18NanoAODv9-106X_upgrade2018_realistic_v16_L1v1-v2/NANOAODSIM	276.5
	/WJetsToQQ_HT-600to800_TuneCP5_13TeV-madgraphMLM-pythia8/RunIISummer20UL18NanoAODv9-106X_upgrade2018_realistic_v16_L1v1-v2/NANOAODSIM	59.25
	/WJetsToQQ_HT-800toInf_TuneCP5_13TeV-madgraphMLM-pythia8/RunIISummer20UL18NanoAODv9-106X_upgrade2018_realistic_v16_L1v1-v2/NANOAODSIM	28.75
	/WJetsToLNu_HT-400To600_TuneCP5_13TeV-madgraphMLM-pythia8/RunIISummer20UL18NanoAODv9-106X_upgrade2018_realistic_v16_L1v1-v1/NANOAODSIM	45.25
	/WJetsToLNu_HT-600To800_TuneCP5_13TeV-madgraphMLM-pythia8/RunIISummer20UL18NanoAODv9-106X_upgrade2018_realistic_v16_L1v1-v1/NANOAODSIM	10.97
	/WJetsToLNu_HT-800To1200_TuneCP5_13TeV-madgraphMLM-pythia8/RunIISummer20UL18NanoAODv9-106X_upgrade2018_realistic_v16_L1v1-v1/NANOAODSIM	4.933
	/WJetsToLNu_HT-1200To2500_TuneCP5_13TeV-madgraphMLM-pythia8/RunIISummer20UL18NanoAODv9-106X_upgrade2018_realistic_v16_L1v1-v1/NANOAODSIM	1.16
	/WJetsToLNu_HT-2500ToInf_TuneCP5_13TeV-madgraphMLM-pythia8/RunIISummer20UL18NanoAODv9-106X_upgrade2018_realistic_v16_L1v1-v2/NANOAODSIM	0.02646
ZJets	/ZJetsToQQ_HT-400to600_TuneCP5_13TeV-madgraphMLM-pythia8/RunIISummer20UL18NanoAODv9-106X_upgrade2018_realistic_v16_L1v1-v2/NANOAODSIM	114.2

(Continued on next page)

## 2 Triggers and Dataset

---

(Continued from previous page)

Category	MC Sample	Cross Section (pb)
	/ZJetsToQQ_HT-600to800_TuneCP5_13TeV-madgraphMLM-pythia8/RunIISummer20UL18NanoAODv9-106X_upgrade2018_realistic_v16_L1v1-v2/NANOAODSIM	25.34
	/ZJetsToQQ_HT-800toInf.TuneCP5_13TeV-madgraphMLM-pythia8/RunIISummer20UL18NanoAODv9-106X_upgrade2018_realistic_v16_L1v1-v2/NANOAODSIM	13.1
	/ZJetsToNuNu_HT-400To600_TuneCP5_13TeV-madgraphMLM-pythia8/RunIISummer20UL18NanoAODv9-106X_upgrade2018_realistic_v16_L1v1-v1/NANOAODSIM	9.904
	/ZJetsToNuNu_HT-600To800_TuneCP5_13TeV-madgraphMLM-pythia8/RunIISummer20UL18NanoAODv9-106X_upgrade2018_realistic_v16_L1v1-v1/NANOAODSIM	2.413
	/ZJetsToNuNu_HT-800To1200_TuneCP5_13TeV-madgraphMLM-pythia8/RunIISummer20UL18NanoAODv9-106X_upgrade2018_realistic_v16_L1v1-v1/NANOAODSIM	1.071
	/ZJetsToNuNu_HT-1200To2500_TuneCP5_13TeV-madgraphMLM-pythia8/RunIISummer20UL18NanoAODv9-106X_upgrade2018_realistic_v16_L1v1-v1/NANOAODSIM	0.2497
	/ZJetsToNuNu_HT-2500ToInf.TuneCP5_13TeV-madgraphMLM-pythia8/RunIISummer20UL18NanoAODv9-106X_upgrade2018_realistic_v16_L1v1-v1/NANOAODSIM	0.005618
other	/WW_TuneCP5_13TeV-pythia8/RunIISummer20UL18NanoAODv9-106X_upgrade2018_realistic_v16_L1v1-v1/NANOAODSIM	75.95
	/WZ_TuneCP5_13TeV-pythia8/RunIISummer20UL18NanoAODv9-106X_upgrade2018_realistic_v16_L1v1-v1/NANOAODSIM	27.59
	/ZZ_TuneCP5_13TeV-pythia8/RunIISummer20UL18NanoAODv9-106X_upgrade2018_realistic_v16_L1v1-v1/NANOAODSIM	12.17
	/DYJetsToLL_M-50_TuneCP5_13TeV-amcatnloFXFX-pythia8/RunIISummer20UL18NanoAODv9-106X_upgrade2018_realistic_v16_L1v1-v2/NANOAODSIM	6404.0
	/DYJetsToLL_M-10to50_TuneCP5_13TeV-madgraphMLM-pythia8/RunIISummer20UL18NanoAODv9-106X_upgrade2018_realistic_v16_L1v1-v1/NANOAODSIM	20460.0

Table 11: List of MC samples for year 2022.

Category	MC Sample	Cross Section (pb)
TTTT	/TTTT_TuneCP5_13p6TeV_amcatnlo_pythia8/Run3Summer22NanoAODv12-130X_mcRun3_2022_realistic_v5-v2/NANOAODSIM	0.01582
TT	/TTto4Q_TuneCP5_13p6TeV_powheg_pythia8/Run3Summer22NanoAODv12-130X_mcRun3_2022_realistic_v5-v2/NANOAODSIM	419.69
	/TTtoLNu2Q_TuneCP5_13p6TeV_powheg_pythia8/Run3Summer22NanoAODv12-130X_mcRun3_2022_realistic_v5-v2/NANOAODSIM	404.64
	/TTto2LNu_TuneCP5_13p6TeV_powheg_pythia8/Run3Summer22NanoAODv12-130X_mcRun3_2022_realistic_v5-v2/NANOAODSIM	98.03
QCD	/QCD-4Jets_HT-1000to1200_TuneCP5_13p6TeV_madgraphMLM-pythia8/Run3Summer22NanoAODv12-130X_mcRun3_2022_realistic_v5-v2/NANOAODSIM	883.7
	/QCD-4Jets_HT-1200to1500_TuneCP5_13p6TeV_madgraphMLM-pythia8/Run3Summer22NanoAODv12-130X_mcRun3_2022_realistic_v5-v2/NANOAODSIM	383.5

QCD

(Continued on next page)

(Continued from previous page)

Category	MC Sample	Cross Section (pb)
ttX	/QCD-4Jets_HT-1500to2000_TuneCP5_13p6TeV_madgraphMLM-pythia8/Run3Summer22NanoAODv12-130X_mcRun3_2022_realistic_v5-v2/NANOAODSIM	125.2
	/QCD-4Jets_HT-2000_TuneCP5_13p6TeV_madgraphMLM-pythia8/Run3Summer22NanoAODv12-130X_mcRun3_2022_realistic_v5-v2/NANOAODSIM	26.49
	/QCD-4Jets_HT-200to400_TuneCP5_13p6TeV_madgraphMLM-pythia8/Run3Summer22NanoAODv12-130X_mcRun3_2022_realistic_v5-v2/NANOAODSIM	1961000.0
	/QCD-4Jets_HT-400to600_TuneCP5_13p6TeV_madgraphMLM-pythia8/Run3Summer22NanoAODv12-130X_mcRun3_2022_realistic_v5-v2/NANOAODSIM	95620.0
	/QCD-4Jets_HT-600to800_TuneCP5_13p6TeV_madgraphMLM-pythia8/Run3Summer22NanoAODv12-130X_mcRun3_2022_realistic_v5-v2/NANOAODSIM	13540.0
	/QCD-4Jets_HT-70to100_TuneCP5_13p6TeV_madgraphMLM-pythia8/Run3Summer22NanoAODv12-130X_mcRun3_2022_realistic_v5-v2/NANOAODSIM	58500000.0
	/QCD-4Jets_HT-800to1000_TuneCP5_13p6TeV_madgraphMLM-pythia8/Run3Summer22NanoAODv12-130X_mcRun3_2022_realistic_v5-v2/NANOAODSIM	3033.0
	/TTNu-1Jets_TuneCP5_13p6TeV_amcatnloFXFX-pythia8/Run3Summer22NanoAODv12-130X_mcRun3_2022_realistic_v5-v1/NANOAODSIM	0.2505
Single-top	/TTLL_MLL-4to50_TuneCP5_13p6TeV_amcatnlo-pythia8/Run3Summer22NanoAODv12-130X_mcRun3_2022_realistic_v5-v2/NANOAODSIM	0.03949
	/TTLL_MLL-50_TuneCP5_13p6TeV_amcatnlo-pythia8/Run3Summer22NanoAODv12-130X_mcRun3_2022_realistic_v5-v2/NANOAODSIM	0.08646
	/TTNuNu_TuneCP5_13p6TeV_amcatnlo-pythia8/Run3Summer22NanoAODv12-130X_mcRun3_2022_realistic_v5-v2/NANOAODSIM	0.1638
	/TTZ-ZtoQQ-1Jets_TuneCP5_13p6TeV_amcatnloFXFX-pythia8/Run3Summer22NanoAODv12-130X_mcRun3_2022_realistic_v5-v2/NANOAODSIM	0.6603
	/TTH_Hto2B_M-125_TuneCP5_13p6TeV_powheg-pythia8/Run3Summer22NanoAODv12-130X_mcRun3_2022_realistic_v5-v3/NANOAODSIM	0.3257
	/TTHtoNon2B_M-125_TuneCP5_13p6TeV_powheg-pythia8/Run3Summer22NanoAODv12-130X_mcRun3_2022_realistic_v5-v4/NANOAODSIM	0.2381
	/TTG-1Jets_PTG-10to100_TuneCP5_13p6TeV_amcatnloFXFXold-pythia8/Run3Summer22NanoAODv12-130X_mcRun3_2022_realistic_v5-v1/NANOAODSIM	4.216
	/TTG-1Jets_PTG-100to200_TuneCP5_13p6TeV_amcatnloFXFXold-pythia8/Run3Summer22NanoAODv12-130X_mcRun3_2022_realistic_v5-v3/NANOAODSIM	0.4114
	/TTG-1Jets_PTG-200_TuneCP5_13p6TeV_amcatnloFXFXold-pythia8/Run3Summer22NanoAODv12-130X_mcRun3_2022_realistic_v5-v3/NANOAODSIM	0.1284
	/TbarBQ_t-channel_4FS_TuneCP5_13p6TeV_powheg-madspin-pythia8/Run3Summer22NanoAODv12-130X_mcRun3_2022_realistic_v5-v2/NANOAODSIM	75.47
	/TBbarQ_t-channel_4FS_TuneCP5_13p6TeV_powheg-madspin-pythia8/Run3Summer22NanoAODv12-130X_mcRun3_2022_realistic_v5-v2/NANOAODSIM	123.8
	/TbarWplusto2L2Nu_TuneCP5_13p6TeV_powheg-pythia8/Run3Summer22NanoAODv12-130X_mcRun3_2022_realistic_v5-v2/NANOAODSIM	4.663
	/TbarWplusto4Q_TuneCP5_13p6TeV_powheg-pythia8/Run3Summer22NanoAODv12-130X_mcRun3_2022_realistic_v5-v2/NANOAODSIM	19.971
	/TbarWplustoLNu2Q_TuneCP5_13p6TeV_powheg-pythia8/Run3Summer22NanoAODv12-130X_mcRun3_2022_realistic_v5-v2/NANOAODSIM	19.303
	/TWminusto2L2Nu_TuneCP5_13p6TeV_powheg-pythia8/Run3Summer22NanoAODv12-130X_mcRun3_2022_realistic_v5-v2/NANOAODSIM	4.663
	/TWminusto4Q_TuneCP5_13p6TeV_powheg-pythia8/Run3Summer22NanoAODv12-130X_mcRun3_2022_realistic_v5-v2/NANOAODSIM	19.971
	/TWminustoLNu2Q_TuneCP5_13p6TeV_powheg-pythia8/Run3Summer22NanoAODv12-130X_mcRun3_2022_realistic_v5-v2/NANOAODSIM	19.303
	/TBbarLplusNuBbar-s-channel-4FS_TuneCP5_13p6TeV_amcatnlo-pythia8/Run3Summer22NanoAODv12-130X_mcRun3_2022_realistic_v5-v2/NANOAODSIM	2.278

(Continued on next page)

## 2 Triggers and Dataset

---

(Continued from previous page)

Category	MC Sample	Cross Section (pb)
	/TbarBtoLminusNuB-s-channel-4FS_TuneCP5_13p6TeV_amcatnlo-pythia8/Run3Summer22NanoAODv12-130X_mcRun3_2022_realistic_v5-v2/NANOAODSIM	1.43
WJets	/Wto2Q-3Jets_HT-200to400_TuneCP5_13p6TeV_madgraphMLM-pythia8/Run3Summer22NanoAODv12-130X_mcRun3_2022_realistic_v5-v2/NANOAODSIM	2723.0
	/Wto2Q-3Jets_HT-400to600_TuneCP5_13p6TeV_madgraphMLM-pythia8/Run3Summer22NanoAODv12-130X_mcRun3_2022_realistic_v5-v2/NANOAODSIM	299.8
	/Wto2Q-3Jets_HT-600to800_TuneCP5_13p6TeV_madgraphMLM-pythia8/Run3Summer22NanoAODv12-130X_mcRun3_2022_realistic_v5-v2/NANOAODSIM	63.9
	/Wto2Q-3Jets_HT-800_TuneCP5_13p6TeV_madgraphMLM-pythia8/Run3Summer22NanoAODv12-130X_mcRun3_2022_realistic_v5-v2/NANOAODSIM	31.9
	/WtoLNu-4Jets_TuneCP5_13p6TeV_madgraphMLM-pythia8/Run3Summer22NanoAODv12-130X_mcRun3_2022_realistic_v5-v2/NANOAODSIM	55390.0
	/Zto2Nu-4Jets_HT-100to200_TuneCP5_13p6TeV_madgraphMLM-pythia8/Run3Summer22NanoAODv12-130X_mcRun3_2022_realistic_v5-v2/NANOAODSIM	273.7
ZJets	/Zto2Nu-4Jets_HT-200to400_TuneCP5_13p6TeV_madgraphMLM-pythia8/Run3Summer22NanoAODv12-130X_mcRun3_2022_realistic_v5-v2/NANOAODSIM	75.96
	/Zto2Nu-4Jets_HT-400to800_TuneCP5_13p6TeV_madgraphMLM-pythia8/Run3Summer22NanoAODv12-130X_mcRun3_2022_realistic_v5-v2/NANOAODSIM	13.19
	/Zto2Nu-4Jets_HT-800to1500_TuneCP5_13p6TeV_madgraphMLM-pythia8/Run3Summer22NanoAODv12-130X_mcRun3_2022_realistic_v5-v2/NANOAODSIM	1.364
	/Zto2Nu-4Jets_HT-1500to2500_TuneCP5_13p6TeV_madgraphMLM-pythia8/Run3Summer22NanoAODv12-130X_mcRun3_2022_realistic_v5-v2/NANOAODSIM	0.09865
	/Zto2Nu-4Jets_HT-2500_TuneCP5_13p6TeV_madgraphMLM-pythia8/Run3Summer22NanoAODv12-130X_mcRun3_2022_realistic_v5-v2/NANOAODSIM	0.006699
	/Zto2Q-4Jets_HT-200to400_TuneCP5_13p6TeV_madgraphMLM-pythia8/Run3Summer22NanoAODv12-130X_mcRun3_2022_realistic_v5-v2/NANOAODSIM	1082.0
	/Zto2Q-4Jets_HT-400to600_TuneCP5_13p6TeV_madgraphMLM-pythia8/Run3Summer22NanoAODv12-130X_mcRun3_2022_realistic_v5-v2/NANOAODSIM	124.1
	/Zto2Q-4Jets_HT-600to800_TuneCP5_13p6TeV_madgraphMLM-pythia8/Run3Summer22NanoAODv12-130X_mcRun3_2022_realistic_v5-v2/NANOAODSIM	27.28
	/Zto2Q-4Jets_HT-800_TuneCP5_13p6TeV_madgraphMLM-pythia8/Run3Summer22NanoAODv12-130X_mcRun3_2022_realistic_v5-v2/NANOAODSIM	14.57
	/WW_TuneCP5_13p6TeV_pythia8/Run3Summer22NanoAODv12-130X_mcRun3_2022_realistic_v5-v2/NANOAODSIM	80.23
other	/WZ_TuneCP5_13p6TeV_pythia8/Run3Summer22NanoAODv12-130X_mcRun3_2022_realistic_v5-v2/NANOAODSIM	29.1
	/ZZ_TuneCP5_13p6TeV_pythia8/Run3Summer22NanoAODv12-130X_mcRun3_2022_realistic_v5-v2/NANOAODSIM	12.75
	/DYto2L-4Jets_MLL-10to50_TuneCP5_13p6TeV_madgraphMLM-pythia8/Run3Summer22NanoAODv12-130X_mcRun3_2022_realistic_v5-v1/NANOAODSIM	17380.0
	/DYto2L-4Jets_MLL-50_TuneCP5_13p6TeV_madgraphMLM-pythia8/Run3Summer22NanoAODv12-130X_mcRun3_2022_realistic_v5-v2/NANOAODSIM	5467.0

Table 12: List of MC samples for year 2022EE.

Category	MC Sample	Cross Section (pb)
TTTT	/TTTT_TuneCP5_13p6TeV_amcatnlo_pythia8/Run3Summer22EENanoAODv12-130X_mcRun3_2022_realistic_postEE_v6-v1/NANOAODSIM	0.01582
TT	/TTto4Q_TuneCP5_13p6TeV_powheg_pythia8/Run3Summer22EENanoAODv12-130X_mcRun3_2022_realistic_postEE_v6-v2/NANOAODSIM	419.69
	/TTtoLNu2Q_TuneCP5_13p6TeV_powheg_pythia8/Run3Summer22EENanoAODv12-130X_mcRun3_2022_realistic_postEE_v6-v2/NANOAODSIM	404.64
	/TTto2L2Nu_TuneCP5_13p6TeV_powheg_pythia8/Run3Summer22EENanoAODv12-130X_mcRun3_2022_realistic_postEE_v6-v2/NANOAODSIM	98.03
QCD	/QCD-4Jets_HT-1000to1200_TuneCP5_13p6TeV_madgraphMLM-pythia8/Run3Summer22EENanoAODv12-130X_mcRun3_2022_realistic_postEE_v6-v2/NANOAODSIM	883.7
	/QCD-4Jets_HT-1200to1500_TuneCP5_13p6TeV_madgraphMLM-pythia8/Run3Summer22EENanoAODv12-130X_mcRun3_2022_realistic_postEE_v6-v2/NANOAODSIM	383.5
	/QCD-4Jets_HT-1500to2000_TuneCP5_13p6TeV_madgraphMLM-pythia8/Run3Summer22EENanoAODv12-130X_mcRun3_2022_realistic_postEE_v6-v2/NANOAODSIM	125.2
	/QCD-4Jets_HT-2000_TuneCP5_13p6TeV_madgraphMLM-pythia8/Run3Summer22EENanoAODv12-130X_mcRun3_2022_realistic_postEE_v6-v2/NANOAODSIM	26.49
	/QCD-4Jets_HT-200to400_TuneCP5_13p6TeV_madgraphMLM-pythia8/Run3Summer22EENanoAODv12-130X_mcRun3_2022_realistic_postEE_v6-v2/NANOAODSIM	1961000.0
	/QCD-4Jets_HT-400to600_TuneCP5_13p6TeV_madgraphMLM-pythia8/Run3Summer22EENanoAODv12-130X_mcRun3_2022_realistic_postEE_v6-v2/NANOAODSIM	95620.0
	/QCD-4Jets_HT-600to800_TuneCP5_13p6TeV_madgraphMLM-pythia8/Run3Summer22EENanoAODv12-130X_mcRun3_2022_realistic_postEE_v6-v2/NANOAODSIM	13540.0
	/QCD-4Jets_HT-800to1000_TuneCP5_13p6TeV_madgraphMLM-pythia8/Run3Summer22EENanoAODv12-130X_mcRun3_2022_realistic_postEE_v6-v2/NANOAODSIM	3033.0
	/TTLNu-1Jets_TuneCP5_13p6TeV_amcatnloFXFX-pythia8/Run3Summer22EENanoAODv12-130X_mcRun3_2022_realistic_postEE_v6-v4/NANOAODSIM	0.2505
ttX	/TTLL_MLL-4to50_TuneCP5_13p6TeV_amcatnlo-pythia8/Run3Summer22EENanoAODv12-130X_mcRun3_2022_realistic_postEE_v6-v2/NANOAODSIM	0.03949
	/TTLL_MLL-50_TuneCP5_13p6TeV_amcatnlo-pythia8/Run3Summer22EENanoAODv12-130X_mcRun3_2022_realistic_postEE_v6-v2/NANOAODSIM	0.08646
	/TTNuNu_TuneCP5_13p6TeV_amcatnlo-pythia8/Run3Summer22EENanoAODv12-130X_mcRun3_2022_realistic_postEE_v6-v2/NANOAODSIM	0.1638
	/TTZ_ZtoQQ-1Jets_TuneCP5_13p6TeV_amcatnloFXFX-pythia8/Run3Summer22EENanoAODv12-130X_mcRun3_2022_realistic_postEE_v6-v2/NANOAODSIM	0.6603
	/TTH_Hto2B_M-125_TuneCP5_13p6TeV_powheg-pythia8/Run3Summer22EENanoAODv12-130X_mcRun3_2022_realistic_postEE_v6-v3/NANOAODSIM	0.3257
	/TTHtoNon2B_M-125_TuneCP5_13p6TeV_powheg-pythia8/Run3Summer22EENanoAODv12-130X_mcRun3_2022_realistic_postEE_v6-v2/NANOAODSIM	0.2381

(Continued on next page)

## 2 Triggers and Dataset

---

(Continued from previous page)

Category	MC Sample	Cross Section (pb)
	/TTG-1Jets_PTG-10to100_TuneCP5_13p6TeV_amcatnloFXFXold-pythia8/Run3Summer22ENanoAODv12-130X_mcRun3_2022_realistic_postEE_v6-v4/NANOAODSIM	4.216
	/TTG-1Jets_PTG-100to200_TuneCP5_13p6TeV_amcatnloFXFXold-pythia8/Run3Summer22ENanoAODv12-130X_mcRun3_2022_realistic_postEE_v6-v3/NANOAODSIM	0.4114
	/TTG-1Jets_PTG-200_TuneCP5_13p6TeV_amcatnloFXFXold-pythia8/Run3Summer22ENanoAODv12-130X_mcRun3_2022_realistic_postEE_v6-v3/NANOAODSIM	0.1284
Single-top	/TbarBQ_t-channel_4FS_TuneCP5_13p6TeV_powheg-madspin-pythia8/Run3Summer22ENanoAODv12-130X_mcRun3_2022_realistic_postEE_v6-v2/NANOAODSIM	75.47
	/TBbarQ_t-channel_4FS_TuneCP5_13p6TeV_powheg-madspin-pythia8/Run3Summer22ENanoAODv12-130X_mcRun3_2022_realistic_postEE_v6-v2/NANOAODSIM	123.8
	/TbarWplusto2L2Nu_TuneCP5_13p6TeV_powheg-pythia8/Run3Summer22ENanoAODv12-130X_mcRun3_2022_realistic_postEE_v6-v2/NANOAODSIM	4.663
	/TbarWplusto4Q_TuneCP5_13p6TeV_powheg-pythia8/Run3Summer22ENanoAODv12-130X_mcRun3_2022_realistic_postEE_v6-v2/NANOAODSIM	19.971
	/TbarWplustoLNu2Q_TuneCP5_13p6TeV_powheg-pythia8/Run3Summer22ENanoAODv12-130X_mcRun3_2022_realistic_postEE_v6-v2/NANOAODSIM	19.303
	/TWminusto2L2Nu_TuneCP5_13p6TeV_powheg-pythia8/Run3Summer22ENanoAODv12-130X_mcRun3_2022_realistic_postEE_v6-v2/NANOAODSIM	4.663
	/TWminusto4Q_TuneCP5_13p6TeV_powheg-pythia8/Run3Summer22ENanoAODv12-130X_mcRun3_2022_realistic_postEE_v6-v2/NANOAODSIM	19.971
	/TWminustoLNu2Q_TuneCP5_13p6TeV_powheg-pythia8/Run3Summer22ENanoAODv12-130X_mcRun3_2022_realistic_postEE_v6-v2/NANOAODSIM	19.303
	/TBbaroLplusNuBbar-s-channel-4FS_TuneCP5_13p6TeV_amcatnlo-pythia8/Run3Summer22ENanoAODv12-130X_mcRun3_2022_realistic_postEE_v6-v2/NANOAODSIM	2.278
	/TbarBtoLminusNuB-s-channel-4FS_TuneCP5_13p6TeV_amcatnlo-pythia8/Run3Summer22ENanoAODv12-130X_mcRun3_2022_realistic_postEE_v6-v2/NANOAODSIM	1.43
WJets	/WtoQ-3Jets_HT-200to400_TuneCP5_13p6TeV_madgraphMLM-pythia8/Run3Summer22ENanoAODv12-130X_mcRun3_2022_realistic_postEE_v6-v2/NANOAODSIM	2723.0
	/WtoQ-3Jets_HT-400to600_TuneCP5_13p6TeV_madgraphMLM-pythia8/Run3Summer22ENanoAODv12-130X_mcRun3_2022_realistic_postEE_v6-v2/NANOAODSIM	299.8
	/WtoQ-3Jets_HT-600to800_TuneCP5_13p6TeV_madgraphMLM-pythia8/Run3Summer22ENanoAODv12-130X_mcRun3_2022_realistic_postEE_v6-v2/NANOAODSIM	63.9
	/WtoQ-3Jets_HT-800_TuneCP5_13p6TeV_madgraphMLM-pythia8/Run3Summer22ENanoAODv12-130X_mcRun3_2022_realistic_postEE_v6-v2/NANOAODSIM	31.9
	/WtoLNu-4Jets_TuneCP5_13p6TeV_madgraphMLM-pythia8/Run3Summer22ENanoAODv12-130X_mcRun3_2022_realistic_postEE_v6-v2/NANOAODSIM	55390.0
	/Zto2Nu-4Jets_HT-100to200_TuneCP5_13p6TeV_madgraphMLM-pythia8/Run3Summer22ENanoAODv12-130X_mcRun3_2022_realistic_postEE_v6-v2/NANOAODSIM	273.7

(Continued on next page)

ZJets

(Continued from previous page)

Category	MC Sample	Cross Section (pb)
other	/Zto2Nu-4Jets_HT-200to400_TuneCP5_13p6TeV_madgraphMLM-pythia8/Run3Summer22ENanoAODv12-130X_mcRun3_2022_realistic_postEE_v6-v2/NANOAODSIM	75.96
	/Zto2Nu-4Jets_HT-400to800_TuneCP5_13p6TeV_madgraphMLM-pythia8/Run3Summer22ENanoAODv12-130X_mcRun3_2022_realistic_postEE_v6-v2/NANOAODSIM	13.19
	/Zto2Nu-4Jets_HT-800to1500_TuneCP5_13p6TeV_madgraphMLM-pythia8/Run3Summer22ENanoAODv12-130X_mcRun3_2022_realistic_postEE_v6-v1/NANOAODSIM	1.364
	/Zto2Nu-4Jets_HT-1500to2500_TuneCP5_13p6TeV_madgraphMLM-pythia8/Run3Summer22ENanoAODv12-130X_mcRun3_2022_realistic_postEE_v6-v2/NANOAODSIM	0.09865
	/Zto2Nu-4Jets_HT-2500_TuneCP5_13p6TeV_madgraphMLM-pythia8/Run3Summer22ENanoAODv12-130X_mcRun3_2022_realistic_postEE_v6-v2/NANOAODSIM	0.006699
	/Zto2Q-4Jets_HT-200to400_TuneCP5_13p6TeV_madgraphMLM-pythia8/Run3Summer22ENanoAODv12-130X_mcRun3_2022_realistic_postEE_v6-v2/NANOAODSIM	1082.0
	/Zto2Q-4Jets_HT-400to600_TuneCP5_13p6TeV_madgraphMLM-pythia8/Run3Summer22ENanoAODv12-130X_mcRun3_2022_realistic_postEE_v6-v2/NANOAODSIM	124.1
	/Zto2Q-4Jets_HT-600to800_TuneCP5_13p6TeV_madgraphMLM-pythia8/Run3Summer22ENanoAODv12-130X_mcRun3_2022_realistic_postEE_v6-v2/NANOAODSIM	27.28
	/Zto2Q-4Jets_HT-800_TuneCP5_13p6TeV_madgraphMLM-pythia8/Run3Summer22ENanoAODv12-130X_mcRun3_2022_realistic_postEE_v6-v2/NANOAODSIM	14.57
	/WW_TuneCP5_13p6TeV_pythia8/Run3Summer22ENanoAODv12-130X_mcRun3_2022_realistic_postEE_v6-v2/NANOAODSIM	80.23
other	/WZ_TuneCP5_13p6TeV_pythia8/Run3Summer22ENanoAODv12-130X_mcRun3_2022_realistic_postEE_v6-v2/NANOAODSIM	29.1
	/ZZ_TuneCP5_13p6TeV_pythia8/Run3Summer22ENanoAODv12-130X_mcRun3_2022_realistic_postEE_v6-v2/NANOAODSIM	12.75
	/DYto2L-4Jets_MLL-50_TuneCP5_13p6TeV_madgraphMLM-pythia8/Run3Summer22ENanoAODv12-130X_mcRun3_2022_realistic_postEE_v6-v2/NANOAODSIM	5467.0
	/DYto2L-4Jets_MLL-10to50_TuneCP5_13p6TeV_madgraphMLM-pythia8/Run3Summer22ENanoAODv12-130X_mcRun3_2022_realistic_postEE_v6-v3/NANOAODSIM	17380.0

Table 13: List of MC samples for year 2023.

Category	MC Sample	Cross Section (pb)
TTTT	/TTTT_TuneCP5_13p6TeV_amcatnlo_pythia8/Run3Summer23NanoAODv12-130X_mcRun3_2023_realistic_v15-v2/NANOAODSIM	0.01582
TT	/TTto4Q_TuneCP5_13p6TeV_powheg_pythia8/Run3Summer23NanoAODv12-130X_mcRun3_2023_realistic_v14-v2/NANOAODSIM	419.69
	/TTtoLNu2Q_TuneCP5_13p6TeV_powheg_pythia8/Run3Summer23NanoAODv12-130X_mcRun3_2023_realistic_v14-v2/NANOAODSIM	404.64

(Continued on next page)

## 2 Triggers and Dataset

---

(Continued from previous page)

Category	MC Sample	Cross Section (pb)
	/TTto2L2Nu_TuneCP5_13p6TeV_powheg-pythia8/Run3Summer23NanoAODv12-130X_mcRun3_2023_realistic_v14-v2/NANOAODSIM	98.03
QCD	/QCD-4Jets_HT-1000to1200_TuneCP5_13p6TeV_madgraphMLM-pythia8/Run3Summer23NanoAODv12-130X_mcRun3_2023_realistic_v14-v2/NANOAODSIM	883.7
	/QCD-4Jets_HT-1200to1500_TuneCP5_13p6TeV_madgraphMLM-pythia8/Run3Summer23NanoAODv12-130X_mcRun3_2023_realistic_v14-v2/NANOAODSIM	383.5
	/QCD-4Jets_HT-1500to2000_TuneCP5_13p6TeV_madgraphMLM-pythia8/Run3Summer23NanoAODv12-130X_mcRun3_2023_realistic_v14-v3/NANOAODSIM	125.2
	/QCD-4Jets_HT-2000_TuneCP5_13p6TeV_madgraphMLM-pythia8/Run3Summer23NanoAODv12-130X_mcRun3_2023_realistic_v14-v2/NANOAODSIM	26.49
	/QCD-4Jets_HT-400to600_TuneCP5_13p6TeV_madgraphMLM-pythia8/Run3Summer23NanoAODv12-130X_mcRun3_2023_realistic_v14-v3/NANOAODSIM	95620
	/QCD-4Jets_HT-600to800_TuneCP5_13p6TeV_madgraphMLM-pythia8/Run3Summer23NanoAODv12-130X_mcRun3_2023_realistic_v14-v2/NANOAODSIM	13540
	/QCD-4Jets_HT-800to1000_TuneCP5_13p6TeV_madgraphMLM-pythia8/Run3Summer23NanoAODv12-130X_mcRun3_2023_realistic_v14-v2/NANOAODSIM	3033
ttX	/TTLL_MLL-4to50_TuneCP5_13p6TeV_amcatnlo-pythia8/Run3Summer23NanoAODv12-130X_mcRun3_2023_realistic_v15-v2/NANOAODSIM	0.03949
	/TTLL_MLL-50_TuneCP5_13p6TeV_amcatnlo-pythia8/Run3Summer23NanoAODv12-130X_mcRun3_2023_realistic_v15-v2/NANOAODSIM	0.08646
	/TTZ_ZtoQQ-1Jets_TuneCP5_13p6TeV_amcatnloFXFX-pythia8/Run3Summer23NanoAODv12-130X_mcRun3_2023_realistic_v15-v3/NANOAODSIM	0.6603
	/TTNuNu_TuneCP5_13p6TeV_amcatnlo-pythia8/Run3Summer23NanoAODv12-130X_mcRun3_2023_realistic_v15-v3/NANOAODSIM	0.1638
	/TTLNu-1Jets_TuneCP5_13p6TeV_amcatnloFXFX-pythia8/Run3Summer23NanoAODv12-130X_mcRun3_2023_realistic_v15-v2/NANOAODSIM	0.2505
	/TTHto2B_M-125_TuneCP5_13p6TeV_powheg-pythia8/Run3Summer23NanoAODv12-130X_mcRun3_2023_realistic_v14-v3/NANOAODSIM	0.3257
	/TTHtoNon2B_M-125_TuneCP5_13p6TeV_powheg-pythia8/Run3Summer23NanoAODv12-130X_mcRun3_2023_realistic_v14-v2/NANOAODSIM	0.2381
	/TTG-1Jets_PTG-10to100_TuneCP5_13p6TeV_amcatnloFXFXold-pythia8/Run3Summer23NanoAODv12-130X_mcRun3_2023_realistic_v15-v2/NANOAODSIM	4.216
	/TTG-1Jets_PTG-100to200_TuneCP5_13p6TeV_amcatnloFXFXold-pythia8/Run3Summer23NanoAODv12-130X_mcRun3_2023_realistic_v15-v2/NANOAODSIM	0.4114
	/TTG-1Jets_PTG-200_TuneCP5_13p6TeV_amcatnloFXFXold-pythia8/Run3Summer23NanoAODv12-130X_mcRun3_2023_realistic_v15-v2/NANOAODSIM	0.1284
Single-top	/TbarBQ_t-channel_4FS_TuneCP5_13p6TeV_powheg-madspin-pythia8/Run3Summer23NanoAODv12-130X_mcRun3_2023_realistic_v15-v2/NANOAODSIM	75.47
	/TBbarQ_t-channel_4FS_TuneCP5_13p6TeV_powheg-madspin-pythia8/Run3Summer23NanoAODv12-130X_mcRun3_2023_realistic_v15-v2/NANOAODSIM	123.8

(Continued on next page)

(Continued from previous page)

Category	MC Sample	Cross Section (pb)
WJets	/TbarWplusto2L2Nu_TuneCP5_13p6TeV_powheg-pythia8/Run3Summer23NanoAODv12-130X_mcRun3_2023_realistic_v15-v4/NANOAODSIM	4.663
	/TbarWplusto4Q_TuneCP5_13p6TeV_powheg-pythia8/Run3Summer23NanoAODv12-130X_mcRun3_2023_realistic_v15-v4/NANOAODSIM	19.971
	/TbarWplustoLNu2Q_TuneCP5_13p6TeV_powheg-pythia8/Run3Summer23NanoAODv12-130X_mcRun3_2023_realistic_v15-v6/NANOAODSIM	19.303
	/TWminusto2L2Nu_TuneCP5_13p6TeV_powheg-pythia8/Run3Summer23NanoAODv12-130X_mcRun3_2023_realistic_v14-v2/NANOAODSIM	4.663
	/TWminusto4Q_TuneCP5_13p6TeV_powheg-pythia8/Run3Summer23NanoAODv12-130X_mcRun3_2023_realistic_v14-v2/NANOAODSIM	19.971
	/TWminustoLNu2Q_TuneCP5_13p6TeV_powheg-pythia8/Run3Summer23NanoAODv12-130X_mcRun3_2023_realistic_v14-v2/NANOAODSIM	19.303
	/TBbartoLplusNuBbar-s-channel-4FS_TuneCP5_13p6TeV_amcatnlo-pythia8/Run3Summer23NanoAODv12-130X_mcRun3_2023_realistic_v15-v2/NANOAODSIM	2.278
	/TbarBtoLminusNuB-s-channel-4FS_TuneCP5_13p6TeV_amcatnlo-pythia8/Run3Summer23NanoAODv12-130X_mcRun3_2023_realistic_v15-v2/NANOAODSIM	1.43
ZJets	/Wto2Q-3Jets_HT-200to400_TuneCP5_13p6TeV_madgraphMLM-pythia8/Run3Summer23NanoAODv12-130X_mcRun3_2023_realistic_v14-v2/NANOAODSIM	2723.0
	/Wto2Q-3Jets_HT-400to600_TuneCP5_13p6TeV_madgraphMLM-pythia8/Run3Summer23NanoAODv12-130X_mcRun3_2023_realistic_v14-v2/NANOAODSIM	299.8
	/Wto2Q-3Jets_HT-600to800_TuneCP5_13p6TeV_madgraphMLM-pythia8/Run3Summer23NanoAODv12-130X_mcRun3_2023_realistic_v14-v2/NANOAODSIM	63.9
	/Wto2Q-3Jets_HT-800_TuneCP5_13p6TeV_madgraphMLM-pythia8/Run3Summer23NanoAODv12-130X_mcRun3_2023_realistic_v14-v2/NANOAODSIM	31.9
	/WtoLNu-4Jets_TuneCP5_13p6TeV_madgraphMLM-pythia8/Run3Summer23NanoAODv12-130X_mcRun3_2023_realistic_v14-v3/NANOAODSIM	55390
	/Zto2Nu-4Jets_HT-100to200_TuneCP5_13p6TeV_madgraphMLM-pythia8/Run3Summer23NanoAODv12-130X_mcRun3_2023_realistic_v14-v2/NANOAODSIM	273.7
Other	/Zto2Nu-4Jets_HT-200to400_TuneCP5_13p6TeV_madgraphMLM-pythia8/Run3Summer23NanoAODv12-130X_mcRun3_2023_realistic_v14-v2/NANOAODSIM	75.96
	/Zto2Nu-4Jets_HT-400to800_TuneCP5_13p6TeV_madgraphMLM-pythia8/Run3Summer23NanoAODv12-130X_mcRun3_2023_realistic_v14-v2/NANOAODSIM	13.19
	/Zto2Nu-4Jets_HT-800to1500_TuneCP5_13p6TeV_madgraphMLM-pythia8/Run3Summer23NanoAODv12-130X_mcRun3_2023_realistic_v14-v2/NANOAODSIM	1.364
	/Zto2Nu-4Jets_HT-1500to2500_TuneCP5_13p6TeV_madgraphMLM-pythia8/Run3Summer23NanoAODv12-130X_mcRun3_2023_realistic_v14-v2/NANOAODSIM	0.09865
	/Zto2Nu-4Jets_HT-2500_TuneCP5_13p6TeV_madgraphMLM-pythia8/Run3Summer23NanoAODv12-130X_mcRun3_2023_realistic_v14-v3/NANOAODSIM	0.006699
	/Zto2Q-4Jets_HT-200to400_TuneCP5_13p6TeV_madgraphMLM-pythia8/Run3Summer23NanoAODv12-130X_mcRun3_2023_realistic_v14-v1/NANOAODSIM	1082.0

(Continued on next page)

## 2 Triggers and Dataset

---

(Continued from previous page)

Category	MC Sample	Cross Section (pb)
other	/Zto2Q-4Jets-HT-400to600.TuneCP5_13p6TeV_madgraphMLM-pythia8/Run3Summer23NanoAODv12-130X_mcRun3_2023_realistic_v14-v1/NANOAODSIM	124.1
	/Zto2Q-4Jets-HT-600to800.TuneCP5_13p6TeV_madgraphMLM-pythia8/Run3Summer23NanoAODv12-130X_mcRun3_2023_realistic_v14-v1/NANOAODSIM	27.28
	/Zto2Q-4Jets-HT-800.TuneCP5_13p6TeV_madgraphMLM-pythia8/Run3Summer23NanoAODv12-130X_mcRun3_2023_realistic_v14-v1/NANOAODSIM	14.57
	/WW_TuneCP5_13p6TeV_pythia8/Run3Summer23NanoAODv12-130X_mcRun3_2023_realistic_v14-v2/NANOAODSIM	80.23
	/WZ_TuneCP5_13p6TeV_pythia8/Run3Summer23NanoAODv12-130X_mcRun3_2023_realistic_v14-v2/NANOAODSIM	29.1
	/ZZ_TuneCP5_13p6TeV_pythia8/Run3Summer23NanoAODv12-130X_mcRun3_2023_realistic_v14-v2/NANOAODSIM	12.75
	/DYto2L-4Jets_MLL-10to50_TuneCP5_13p6TeV_madgraphMLM-pythia8/Run3Summer23NanoAODv12-130X_mcRun3_2023_realistic_v14-v3/NANOAODSIM	17380
	/DYto2L-4Jets_MLL-50_TuneCP5_13p6TeV_madgraphMLM-pythia8/Run3Summer23NanoAODv12-130X_mcRun3_2023_realistic_v14-v1/NANOAODSIM	5467

Table 14: List of MC samples for year 2023BPix.

Category	MC Sample	Cross Section (pb)
TTTT	/TTTT_TuneCP5_13p6TeV_amcatnlo_pythia8/Run3Summer23BPixNanoAODv12-130X_mcRun3_2023_realistic_postBPix_v6-v2/NANOAODSIM	0.01582
TT	/TTto4Q_TuneCP5_13p6TeV_powheg_pythia8/Run3Summer23BPixNanoAODv12-130X_mcRun3_2023_realistic_postBPix_v2-v3/NANOAODSIM	419.69
	/TTto2LNu_TuneCP5_13p6TeV_powheg_pythia8/Run3Summer23BPixNanoAODv12-130X_mcRun3_2023_realistic_postBPix_v2-v3/NANOAODSIM	98.03
	/TTtoLNu2Q_TuneCP5_13p6TeV_powheg_pythia8/Run3Summer23BPixNanoAODv12-130X_mcRun3_2023_realistic_postBPix_v2-v3/NANOAODSIM	404.64
QCD	/QCD-4Jets_HT-1000to1200.TuneCP5_13p6TeV_madgraphMLM-pythia8/Run3Summer23BPixNanoAODv12-130X_mcRun3_2023_realistic_postBPix_v2-v4/NANOAODSIM	883.7
	/QCD-4Jets_HT-1200to1500.TuneCP5_13p6TeV_madgraphMLM-pythia8/Run3Summer23BPixNanoAODv12-130X_mcRun3_2023_realistic_postBPix_v2-v4/NANOAODSIM	383.5
	/QCD-4Jets_HT-1500to2000.TuneCP5_13p6TeV_madgraphMLM-pythia8/Run3Summer23BPixNanoAODv12-130X_mcRun3_2023_realistic_postBPix_v2-v3/NANOAODSIM	125.2
	/QCD-4Jets_HT-2000.TuneCP5_13p6TeV_madgraphMLM-pythia8/Run3Summer23BPixNanoAODv12-130X_mcRun3_2023_realistic_postBPix_v2-v4/NANOAODSIM	26.49
	/QCD-4Jets_HT-400to600.TuneCP5_13p6TeV_madgraphMLM-pythia8/Run3Summer23BPixNanoAODv12-130X_mcRun3_2023_realistic_postBPix_v2-v4/NANOAODSIM	95620

(Continued on next page)

(Continued from previous page)

Category	MC Sample	Cross Section (pb)
	/QCD-4Jets_HT-600to800_TuneCP5_13p6TeV_madgraphMLM-pythia8/Run3Summer23BPixNanoAODv12-130X_mcRun3_2023_realistic_postBPix_v2-v3/NANOAODSIM	13540
	/QCD-4Jets_HT-800to1000_TuneCP5_13p6TeV_madgraphMLM-pythia8/Run3Summer23BPixNanoAODv12-130X_mcRun3_2023_realistic_postBPix_v2-v4/NANOAODSIM	3033
ttX	/TTLL_MLL-4to50_TuneCP5_13p6TeV_amcatnlo-pythia8/Run3Summer23BPixNanoAODv12-130X_mcRun3_2023_realistic_postBPix_v6-v2/NANOAODSIM	0.03949
	/TTLL_MLL-50_TuneCP5_13p6TeV_amcatnlo-pythia8/Run3Summer23BPixNanoAODv12-130X_mcRun3_2023_realistic_postBPix_v6-v2/NANOAODSIM	0.08646
	/TTZ_ZtoQQ-1Jets_TuneCP5_13p6TeV_amcatnloFXFX-pythia8/Run3Summer23BPixNanoAODv12-130X_mcRun3_2023_realistic_postBPix_v6-v2/NANOAODSIM	0.6603
	/TTLNuNu_TuneCP5_13p6TeV_amcatnloFXFX-pythia8/Run3Summer23BPixNanoAODv12-130X_mcRun3_2023_realistic_postBPix_v6-v2/NANOAODSIM	0.2505
	/TTHto2B_M-125_TuneCP5_13p6TeV_powheg-pythia8/Run3Summer23BPixNanoAODv12-130X_mcRun3_2023_realistic_postBPix_v2-v3/NANOAODSIM	0.1638
	/TTHtoNon2B_M-125_TuneCP5_13p6TeV_powheg-pythia8/Run3Summer23BPixNanoAODv12-130X_mcRun3_2023_realistic_postBPix_v2-v2/NANOAODSIM	0.3257
	/TTG-1Jets_PTG-10to100_TuneCP5_13p6TeV_amcatnloFXFXold-pythia8/Run3Summer23BPixNanoAODv12-130X_mcRun3_2023_realistic_postBPix_v6-v2/NANOAODSIM	0.2381
	/TTG-1Jets_PTG-100to200_TuneCP5_13p6TeV_amcatnloFXFXold-pythia8/Run3Summer23BPixNanoAODv12-130X_mcRun3_2023_realistic_postBPix_v6-v2/NANOAODSIM	4.216
	/TTG-1Jets_PTG-200_TuneCP5_13p6TeV_amcatnloFXFXold-pythia8/Run3Summer23BPixNanoAODv12-130X_mcRun3_2023_realistic_postBPix_v6-v2/NANOAODSIM	0.4114
		0.1284
Single-top	/TbarBQ_t-channel_4FS_TuneCP5_13p6TeV_powheg-madspin-pythia8/Run3Summer23BPixNanoAODv12-130X_mcRun3_2023_realistic_postBPix_v6-v2/NANOAODSIM	75.47
	/TBbarQ_t-channel_4FS_TuneCP5_13p6TeV_powheg-madspin-pythia8/Run3Summer23BPixNanoAODv12-130X_mcRun3_2023_realistic_postBPix_v6-v2/NANOAODSIM	123.8
	/TbarWplusto2L2Nu_TuneCP5_13p6TeV_powheg-pythia8/Run3Summer23BPixNanoAODv12-130X_mcRun3_2023_realistic_postBPix_v6-v2/NANOAODSIM	4.663
	/TbarWplusto4Q_TuneCP5_13p6TeV_powheg-pythia8/Run3Summer23BPixNanoAODv12-130X_mcRun3_2023_realistic_postBPix_v6-v2/NANOAODSIM	19.971
	/TbarWplustoLNu2Q_TuneCP5_13p6TeV_powheg-pythia8/Run3Summer23BPixNanoAODv12-130X_mcRun3_2023_realistic_postBPix_v6-v2/NANOAODSIM	19.303
	/TWminusto2L2Nu_TuneCP5_13p6TeV_powheg-pythia8/Run3Summer23BPixNanoAODv12-130X_mcRun3_2023_realistic_postBPix_v2-v3/NANOAODSIM	4.663
	/TWminusto4Q_TuneCP5_13p6TeV_powheg-pythia8/Run3Summer23BPixNanoAODv12-130X_mcRun3_2023_realistic_postBPix_v2-v3/NANOAODSIM	19.971

(Continued on next page)

## 2 Triggers and Dataset

---

(Continued from previous page)

Category	MC Sample	Cross Section (pb)
	/TWminustoLNu2Q_TuneCP5_13p6TeV_powheg-pythia8/Run3Summer23BPixNanoAODv12-130X_mcRun3_2023_realistic_postBPix_v2-v3/NANOAODSIM	19.303
	/TBbaroLplusNuBbar-s-channel-4FS_TuneCP5_13p6TeV_amcatnlo-pythia8/Run3Summer23BPixNanoAODv12-130X_mcRun3_2023_realistic_postBPix_v6-v2/NANOAODSIM	2.278
	/TbarBtoLminusNuB-s-channel-4FS_TuneCP5_13p6TeV_amcatnlo-pythia8/Run3Summer23BPixNanoAODv12-130X_mcRun3_2023_realistic_postBPix_v6-v2/NANOAODSIM	1.43
WJets	/Wto2Q-3Jets_HT-200to400_TuneCP5_13p6TeV_madgraphMLM-pythia8/Run3Summer23BPixNanoAODv12-130X_mcRun3_2023_realistic_postBPix_v2-v2/NANOAODSIM	2723.0
	/Wto2Q-3Jets_HT-400to600_TuneCP5_13p6TeV_madgraphMLM-pythia8/Run3Summer23BPixNanoAODv12-130X_mcRun3_2023_realistic_postBPix_v2-v2/NANOAODSIM	299.8
	/Wto2Q-3Jets_HT-600to800_TuneCP5_13p6TeV_madgraphMLM-pythia8/Run3Summer23BPixNanoAODv12-130X_mcRun3_2023_realistic_postBPix_v2-v2/NANOAODSIM	63.9
	/Wto2Q-3Jets_HT-800_TuneCP5_13p6TeV_madgraphMLM-pythia8/Run3Summer23BPixNanoAODv12-130X_mcRun3_2023_realistic_postBPix_v2-v2/NANOAODSIM	31.9
	/WtoLNu-4Jets_TuneCP5_13p6TeV_madgraphMLM-pythia8/Run3Summer23BPixNanoAODv12-130X_mcRun3_2023_realistic_postBPix_v2-v3/NANOAODSIM	55390
ZJets	/Zto2Nu-4Jets_HT-100to200_TuneCP5_13p6TeV_madgraphMLM-pythia8/Run3Summer23BPixNanoAODv12-130X_mcRun3_2023_realistic_postBPix_v2-v2/NANOAODSIM	273.7
	/Zto2Nu-4Jets_HT-200to400_TuneCP5_13p6TeV_madgraphMLM-pythia8/Run3Summer23BPixNanoAODv12-130X_mcRun3_2023_realistic_postBPix_v2-v2/NANOAODSIM	75.96
	/Zto2Nu-4Jets_HT-400to800_TuneCP5_13p6TeV_madgraphMLM-pythia8/Run3Summer23BPixNanoAODv12-130X_mcRun3_2023_realistic_postBPix_v2-v2/NANOAODSIM	13.19
	/Zto2Nu-4Jets_HT-800to1500_TuneCP5_13p6TeV_madgraphMLM-pythia8/Run3Summer23BPixNanoAODv12-130X_mcRun3_2023_realistic_postBPix_v2-v2/NANOAODSIM	1.364
	/Zto2Nu-4Jets_HT-1500to2500_TuneCP5_13p6TeV_madgraphMLM-pythia8/Run3Summer23BPixNanoAODv12-130X_mcRun3_2023_realistic_postBPix_v2-v2/NANOAODSIM	0.09865
	/Zto2Nu-4Jets_HT-2500_TuneCP5_13p6TeV_madgraphMLM-pythia8/Run3Summer23BPixNanoAODv12-130X_mcRun3_2023_realistic_postBPix_v2-v3/NANOAODSIM	0.006699
	/Zto2Q-4Jets_HT-200to400_TuneCP5_13p6TeV_madgraphMLM-pythia8/Run3Summer23BPixNanoAODv12-130X_mcRun3_2023_realistic_postBPix_v2-v1/NANOAODSIM	1082.0
	/Zto2Q-4Jets_HT-400to600_TuneCP5_13p6TeV_madgraphMLM-pythia8/Run3Summer23BPixNanoAODv12-130X_mcRun3_2023_realistic_postBPix_v2-v2/NANOAODSIM	124.1
	/Zto2Q-4Jets_HT-600to800_TuneCP5_13p6TeV_madgraphMLM-pythia8/Run3Summer23BPixNanoAODv12-130X_mcRun3_2023_realistic_postBPix_v2-v1/NANOAODSIM	27.28
	/Zto2Q-4Jets_HT-800_TuneCP5_13p6TeV_madgraphMLM-pythia8/Run3Summer23BPixNanoAODv12-130X_mcRun3_2023_realistic_postBPix_v2-v1/NANOAODSIM	14.57

(Continued on next page)

*(Continued from previous page)*

Category	MC Sample	Cross Section (pb)
other	/WW_TuneCP5_13p6TeV_pythia8/Run3Summer23BPixNanoAODv12-130X_mcRun3_2023_realistic_postBPix_v2-v2/NANOAODSIM	80.23
	/WZ_TuneCP5_13p6TeV_pythia8/Run3Summer23BPixNanoAODv12-130X_mcRun3_2023_realistic_postBPix_v2-v2/NANOAODSIM	29.1
	/ZZ_TuneCP5_13p6TeV_pythia8/Run3Summer23BPixNanoAODv12-130X_mcRun3_2023_realistic_postBPix_v2-v2/NANOAODSIM	12.75
	/DYto2L-4Jets_MLL-50_TuneCP5_13p6TeV_madgraphMLM-pythia8/Run3Summer23BPixNanoAODv12-130X_mcRun3_2023_realistic_postBPix_v2-v3/NANOAODSIM	5467
	/DYto2L-4Jets_MLL-10to50_TuneCP5_13p6TeV_madgraphMLM-pythia8/Run3Summer23BPixNanoAODv12-130X_mcRun3_2023_realistic_postBPix_v2-v3/NANOAODSIM	17380

## 73 3 Object Selection

### 74 3.1 Vertex Selection

75 Standard CMS vertex selection criteria corresponding to the “goodVertices” flag in NanoAOD is  
76 applied. Specifically, each event is required to have at least one primary vertex that satisfies the  
77 following criteria:

- 78 • The vertex must contain trajectories of reconstructed particle tracks with positive  $\chi^2$  values.
- 79 • There are at least 5 degrees of freedom in the vertex fit.
- 80 • The distance,  $|z|$ , along the beam line from the nominal center of the detector is less than  
81 24 cm.
- 82 • The transverse displacement,  $r$ , from the beam line is less than 2 cm.

### 83 3.2 Leptons

84 Events with electron or muon candidates identified with the following criteria are vetoed from the  
85 analysis. For the selection of electrons, the EGamma POG “Fall17-noIso-v2” MVA with a “loose”  
86 working point is used for Run 2. The EGamma “Winter22V1” MVA noIso score is used for Run  
87 3, with a working point that gives similar signal and background efficiencies as Run 2. We further  
88 require that the electrons have  $p_T > 15\text{GeV}$  and  $|\eta| < 2.5$ , excluding those in the barrel-endcap  
89 transition region. The “loose” muon ID recommended by the Muon POG is used to select muon  
90 candidates with  $p_T > 15\text{GeV}$  and  $|\eta| < 2.5$ . To isolate lepton candidates from hadronic activity,  
91 we require the “mini-isolation” of electrons to be less than 0.4 and “miniIsoId” for muons to be  
92 “loose”.

### 93 3.3 Jets

94 ParticleFlow jets clustered with the anti- $k_T$  algorithm with distance parameter  $R = 0.4$ . To correct  
95 for pileup, charged hadron subtraction procedure is used for Run 2, where as PUPPI jets are used  
96 for Run 3. Latest jet energy corrections as recommended by the JetMET POG is reapplied to  
97 recalibrate from the NanoAoD values. These corrections are applied using the correctionlib tool  
98 with the JSON files provided by JetMET POG here. JEC corrections already applied in the  
99 NanoAoD are always removed and recalibrated using the latest JSON files available to make  
100 sure up-to-date correction is applied. JER Smearing is with the recommended “hybrid” method,  
101 similarly with correctionlib and the latest JSON provided by JetMET POG. Since JER scale  
102 factors are not available for AK8 jets, we use the smearing for AK4chs/AK4Puppi jets instead  
103 as recommended by JetMET POG expert. The jets are further required to have  $p_T > 35\text{GeV}$   
104 and  $|\eta| < 2.4$ . Additionally, selected jets are required to pass “tight” working point of Jet ID as  
105 recommended by the JetMET POG.

#### 106 3.3.1 B-tagging

107 B jets are identified with the DeepJet algorithm with the “M” working point as recommended by  
108 the BTV POG, which corresponds to a b jet efficiency of about 80%. B-tag SF Shape corrections  
109 is applied according to BTV POG recommendation, using JSON files provided by BTV POG here  
110 and correctionlib.

#### 111 3.3.2 W and Boosted Top tagging

112 For boosted top quarks with  $p_T > 400\text{GeV}$ , or W bosons with  $p_T > 200\text{GeV}$ , the decay products  
113 are expected to be contained within a  $\Delta R$  of 0.8. We apply Particlenet algorithm to jets clustered

114 with anti- $k_T$  algorithm with a distance parameter of 0.8 to identify these W and boosted top  
 115 quarks. Working point corresponding to a 1% mistag rate as recommended by the JetMET POG  
 116 is used. Corrections are applied WITH SFs recommended by the JetMET POG for Run2 and  
 117 Run3 2022. Run3 2023 SFs are not yet available.

118 **3.3.3 Resolved Top tagging**

119 For moderately boosted top quarks, the decay products can be resolved into separate AK4 jets. A  
 120 dedicated XGBoost BDT trigger is developed for tagging these resolved tops, following the same  
 121 methodology as the Run2 all-hadronic TTTT analysis [3]. From the AK4 jets collection, up to four  
 122 jets with the highest Deepjet b-tag scores are selected. For each b jet candidate, we identify all the  
 123 unique two-jet combinations in the AK4 jets collection (excluding the b jet candidate) as W subjet  
 124 candidates, with the condition that the combined mass of the two W subjet candidate is within 40  
 125 GeV of the true W boson mass, and that the mass of the combined three-jet candidate is within  
 126 80 GeV of the true top quark mass. These selected three-jet combinations are the candidates for  
 127 resolved tops.

128 The following variables form the inputs to the BDT:

- 129 • Mass of the b jet candidate
- 130 • Pairwise invariant mass of the b jet candidate with the W subjet candidate
- 131 • Mass of the resolved top candidate, from combining the four-vectors of the constituent jets
- 132 • Combined mass of the two W subjet candidates, from combining the four-vectors of the two  
   W subjet candidates
- 133 • The product of the top candidate  $p_T$  and  $\Delta R$  between the b jet and the W candidate.
- 134 • The product of the W candidate  $p_T$  and  $\Delta R$  between the W subjet candidates.
- 135 • The “soft-drop condition” from the soft-drop declustering algorithm reinterpreted as a vari-  
   able over the two W subjets:  $\frac{\min(p_{T1}, p_{T2})}{p_{T1} + p_{T2}} \Delta R_{j_1, j_2}^{-2}$ , which tends to reject relatively soft collinear  
   jets.
- 136 • The DeepJet b-tag scores of all three constituent jets.
- 137 • The DeepJet c-tag scores of the W subjets.
- 138 • The quark-gluon likelihood scores of the W subjets. (Run2 Only)
- 139 • The DeepJet g vs uds discriminator scores of the W subjets. (Run3 Only)
- 140 • The jet constituent multiplicities of the W subjets.

144 For training, genuine hadronic top candidates are taken from single-lepton  $t\bar{t}$  simulation samples,  
 145 and fake hadronic top candidates from di-lepton  $t\bar{t}$  simulation samples, with the requirement of  
 146  $MET > 100$ ,  $N_{jets} \geq 5$  and  $N_{bjets} \geq 1$ . 2018 samples are used for Run2 model and 2022  
 147 samples for Run3. The BDT is trained with the XGBoost library on 500000 candidates for gen-  
 148 uine and fake samples each. Before training, to decorrelate from  $p_T$  of the top candidate, the  
 149 candidates are reweighted according to the  $p_T$  of the top candidate in bins of 25 GeV width from  
 150 0 GeV to 900 GeV, 50 GeV width from 900 GeV to 1000 GeV, and 100 GeV width from 1000  
 151 GeV to 5000 GeV, such that the sum of weights of candidates in each bin is equal. If the resolved  
 152 top candidates overlap with one another within a  $\Delta R$  of 0.4, the lower scoring candidate is rejected.

153  
 154 The working point for this resolved top tagger is selected at 2% False Positive Rate and given in  
 155 Table 15.

Year	topWP
2016preVFP	0.961
2016	0.954
2017	0.961
2018	0.961
2022	0.966
2022EE	0.968
2023	0.963
2023BPix	0.969

Table 15: Resolved TopWP values for different years

156 Scales factors for tagging efficiencies and misidentification rates are derived for this resolved top  
 157 tagger. These scale factors are parameterized in the resolved top candidate  $p_T$ , and the uncertain-  
 158 ties thereof are propagated as part of the systematic uncertainties. For scale factor derivations,  
 159 b-tag SF corrections, pileup weight and latest JERC corrections is applied to MC samples in the  
 160 following procedure and reported to JeTMET POG.

161

162 For the derivation of the misidentification rates, we use a 0-lepton,  $N_b = 1$  region, selected with  
 163 pure  $H_T$  triggers and requiring  $H_T > 1200\text{GeV}$ . This region was selected to be enriched in  
 164 QCD multi-jet events and is orthogonal to the signal region via the  $N_b = 1$  requirement. In this  
 165 region, simulation is normalized to data. To correct the contamination of genuine tops in the  
 166 data, we estimate the number of genuine tops in data by the number of candidates matched to top  
 167 quarks at the generator level in simulation, and then subtract it from the data. In simulation, the  
 168 misidentification rates are measured to be the fraction of fake resolved top candidates that pass the  
 169 working point. In data, the misidentification rates are measured to be the fraction of candidates  
 170 (after subtraction of the estimated genuine tops) that pass the working point. In the end, the scale  
 171 factor is calculated as the ratio of the misidentification rates in data to those in simulation.

172 For the derivation of the tagging efficiency scale factor, we used single muon triggers to define  
 173 a control region selected to be enriched in semi-leptonic  $t\bar{t}$  events with similar kinematics to the  
 174 Signal Region. This region is orthogonal to the Signal Region via the requirement on the muon.  
 175 We further require that the events to be  $N_b \geq 2$ ,  $N_j \geq 4$ ,  $p_T^{\text{miss}} > 75\text{ GeV}$ , and muon  $p_T > 50\text{ GeV}$ .  
 176 In each event, jets are first cleaned against leptons, and resolved top candidates cleaned against  
 177 muons with a  $\Delta R$  of 0.4. We first normalize simulation to data. The misidentification scale factor is  
 178 applied to candidates in simulation that pass the working point but fail to be matched to top quarks  
 179 at generator level. Candidates are then split into three  $p_T$  categories: low ( $100 - 300\text{GeV}$ ), medium  
 180 ( $300 - 500\text{GeV}$ ) and high ( $\geq 500\text{GeV}$ ). We then perform a simultaneous template fit, where two  
 181 templates of candidates in simulation matched and unmatched to top quarks at generator level  
 182 respectively are used. The templates are binned in top candidate mass, since it is independent of  
 183 candidate  $p_T$ . The fit from simulation to data is performed simultaneously for candidates passing  
 184 and failing the working point. In each  $p_T$  category, the tagging efficiency scale factor is calculated  
 185 as  $\frac{\epsilon_{\text{post-fit}}}{\epsilon_{\text{pre-fit}}}$ , where tagging efficiency  $\epsilon$  is defined as the ratio of number of matched (genuine) top  
 186 candidates passing the working point to the total number of matched top candidates, and  $\epsilon_{\text{post-fit}}$   
 187 is the tagging efficiency in data estimated from fitting simulation to data.

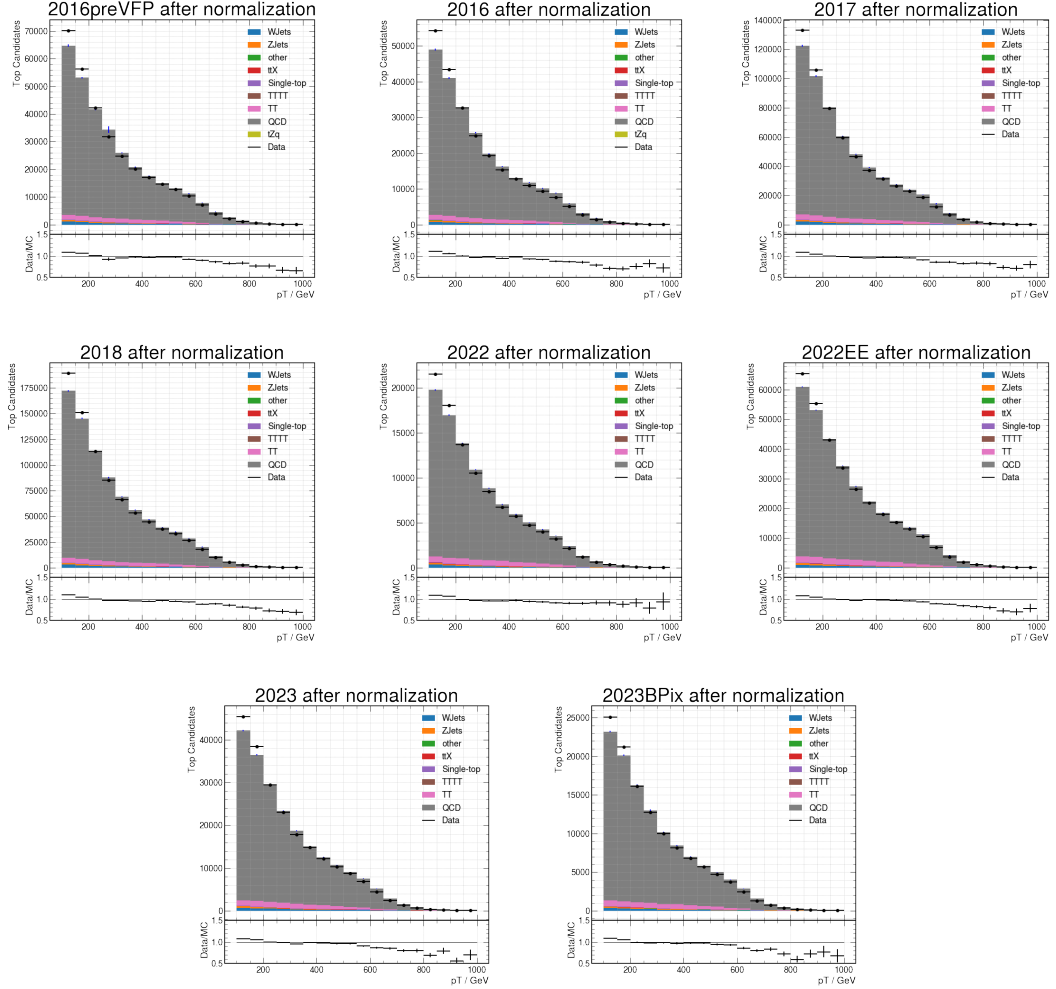


Figure 7: Distributions of resolved top candidate  $p_T$  in data and simulation for all candidates in the region used to derive the misidentification rate scale factor. Contributions from different processes as estimated from simulation are shown in the stacked histograms. The event yield in simulation is scaled to match data inclusively in this region, prior to the application of the top tagger working point.

### 3 Object Selection

#### 3.3 Jets

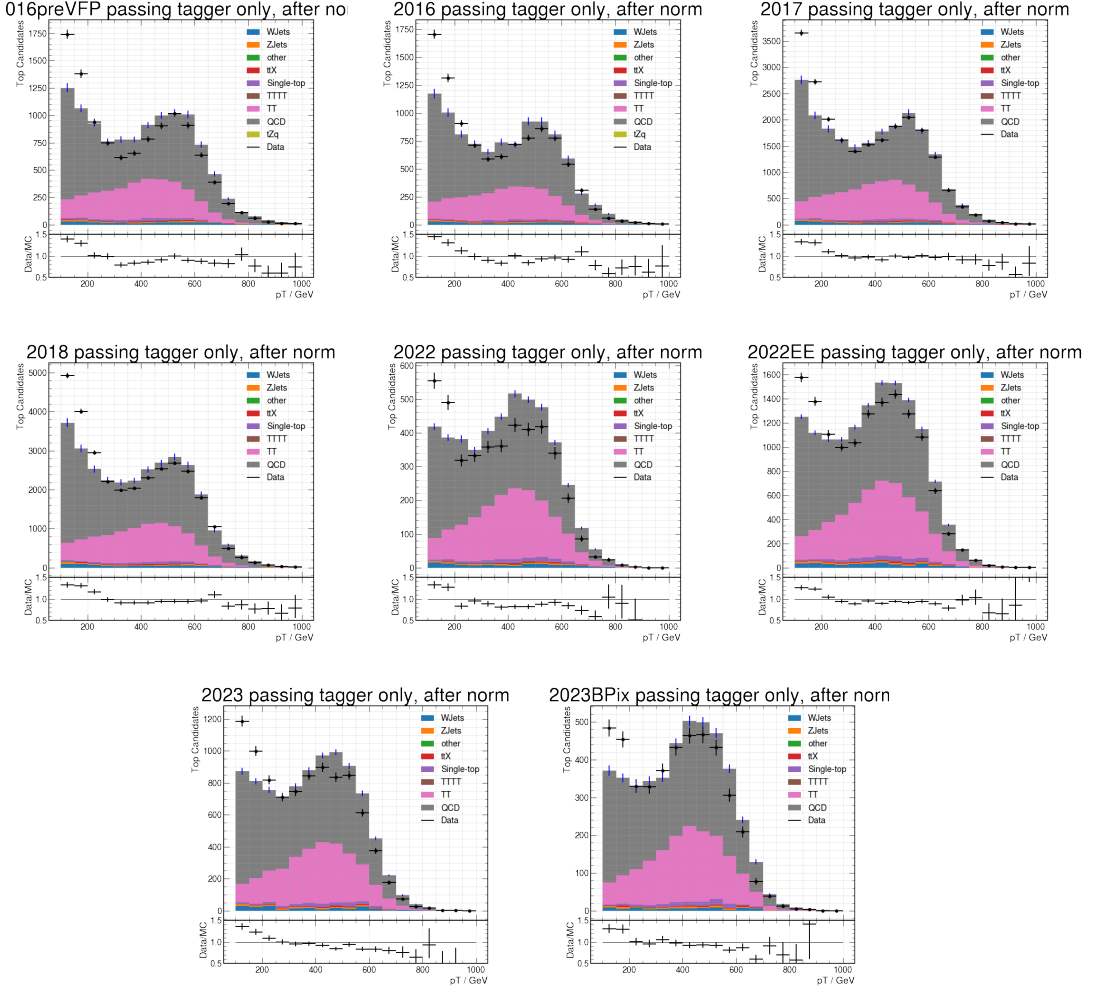


Figure 8: Distributions of resolved top candidate  $p_T$  in data and simulation for candidates passing the working point in the region used to derive the misidentification rate scale factor. Contributions from different processes as estimated from simulation are shown in the stacked histograms. The event yield in simulation is normalized to data by the scale obtained from the same distributions for all candidates in Figure 7

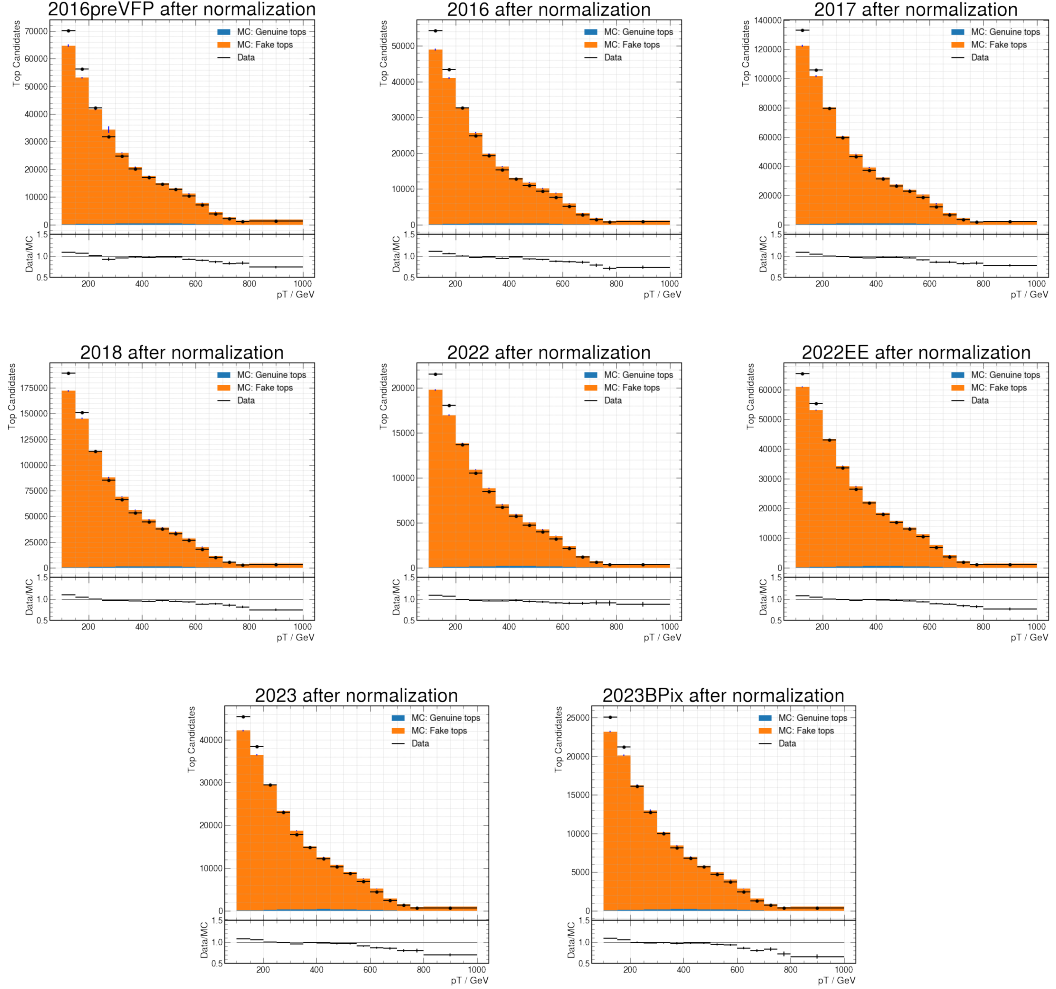


Figure 9: Distributions of resolved top candidate  $p_T$  in data and simulation for all candidates in the region used to derive the misidentification rate scale factor. Contributions from candidates matched and not matched to top quarks at the generator level in simulation are shown in the stacked histograms. The event yield in simulation is scaled to match data inclusively in this region, prior to the application of the top tagger working point.

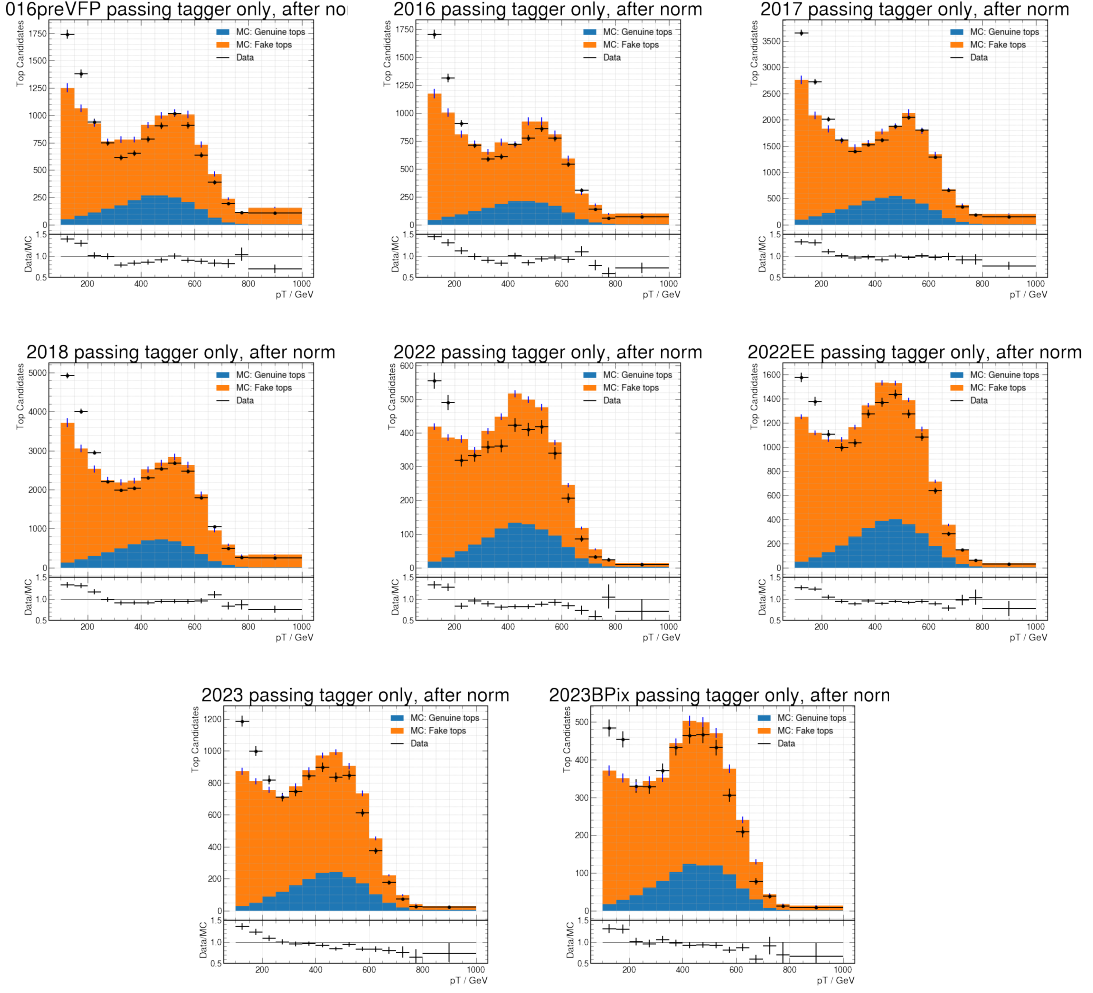


Figure 10: Distributions of resolved top candidate  $p_T$  in data and simulation for candidates passing the working point in the region used to derive the misidentification rate scale factor. Contributions from candidates matched and not matched to top quarks at the generator level in simulation are shown in the stacked histograms. The event yield in simulation is normalized to data by the scale obtained from the same distributions for all candidates in Figure 7

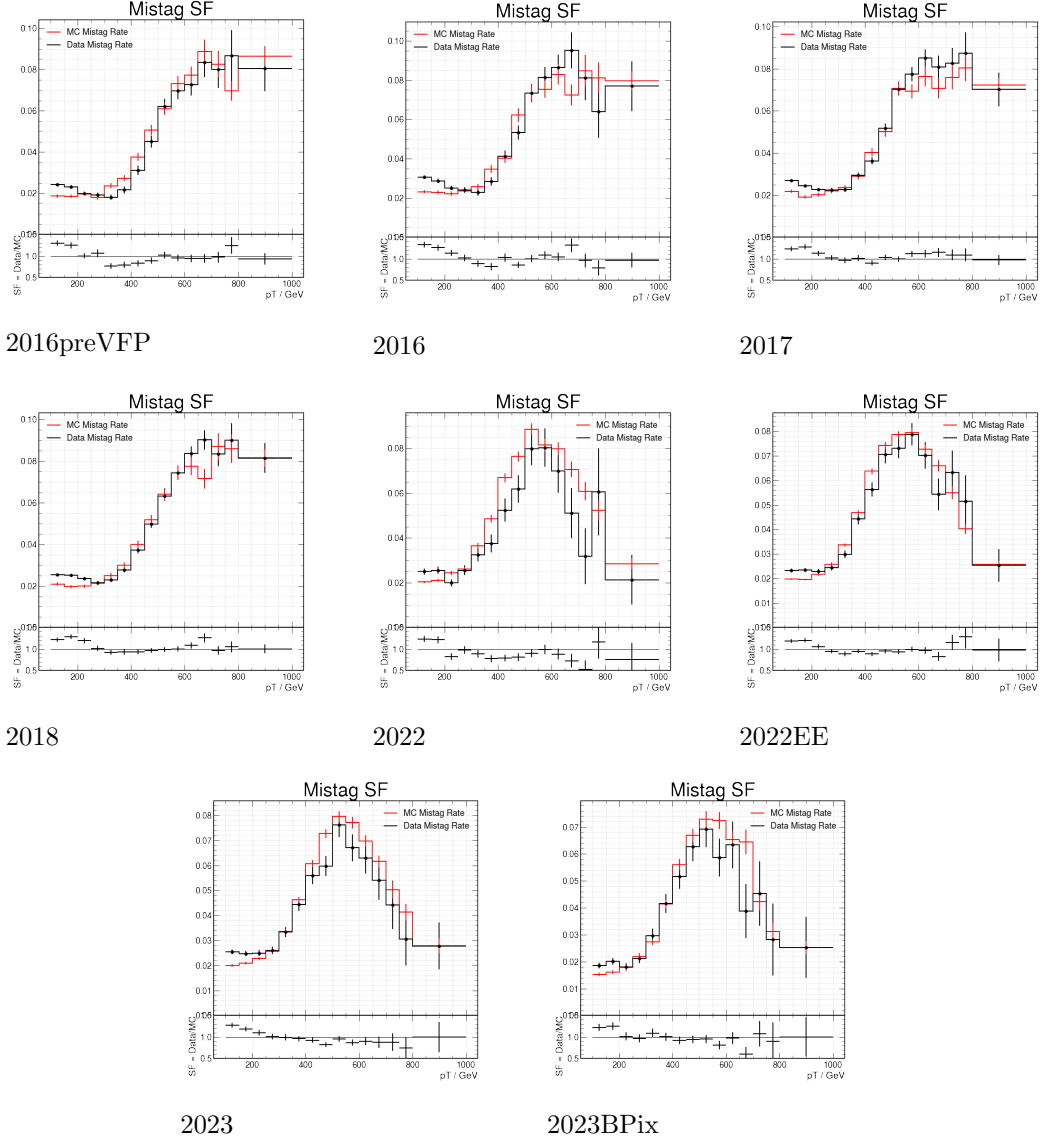


Figure 11: Misidentification rates measured in data and simulation after subtracting the estimated contribution from genuine tops. Misidentification rate scale factors are defined as the ratio of misidentification rate of data over simulation.

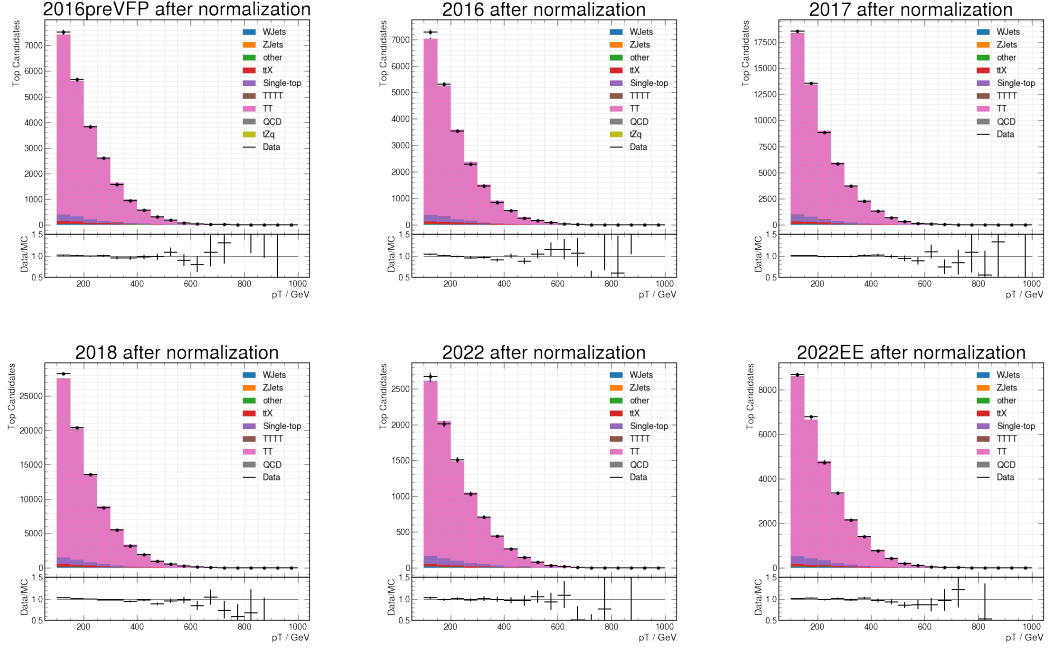


Figure 12: Distributions of resolved top candidate  $p_T$  in data and simulation for all candidates in the region used to derive the tagging efficiency scale factor. Contributions from different processes as estimated from simulation are shown in the stacked histograms. The event yield in simulation is scaled to match data inclusively in this region, prior to the application of the top tagger working point.

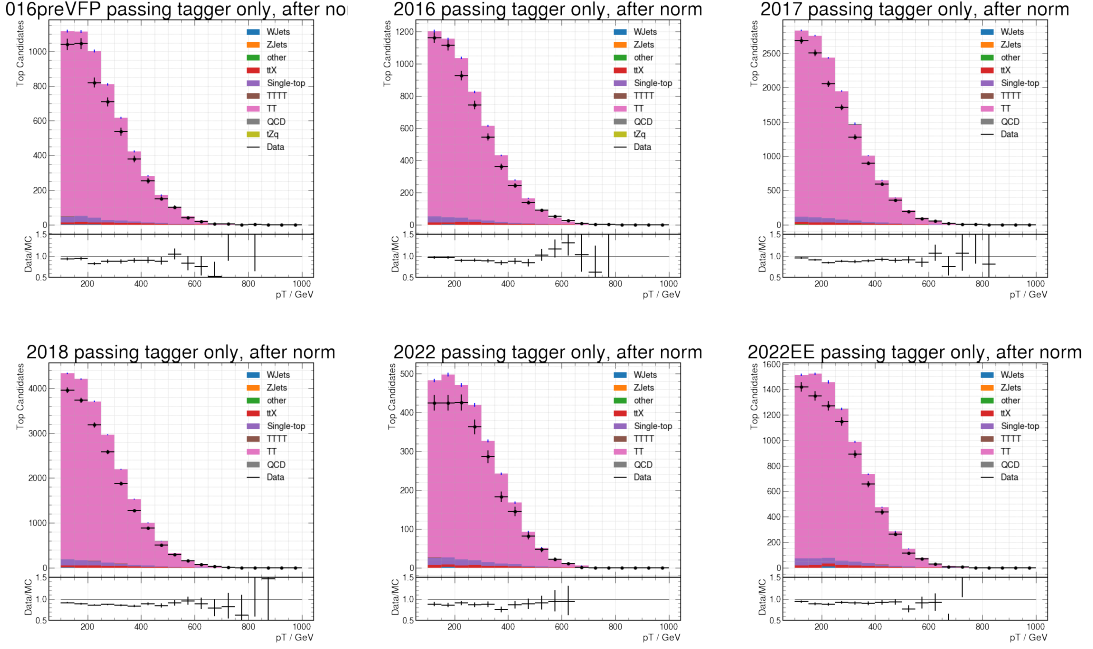


Figure 13: Distributions of resolved top candidate  $p_T$  in data and simulation for candidates passing the working point in the region used to derive the tagging efficiency scale factor. Contributions from different processes as estimated from simulation are shown in the stacked histograms. The event yield in simulation is normalized to data by the scale obtained from the same distributions for all candidates in Figure 12

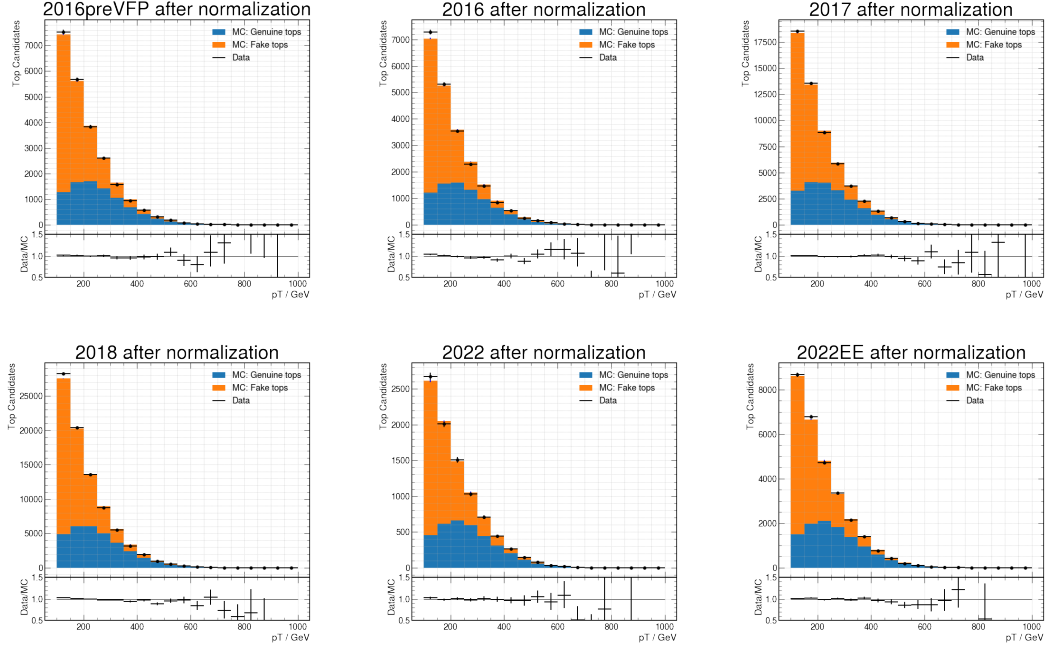


Figure 14: Distributions of resolved top candidate  $p_T$  in data and simulation for all candidates in the region used to derive the tagging efficiency scale factor. Contributions from candidates matched and not matched to top quarks at the generator level in simulation are shown in the stacked histograms. The event yield in simulation is scaled to match data inclusively in this region, prior to the application of the top tagger working point.

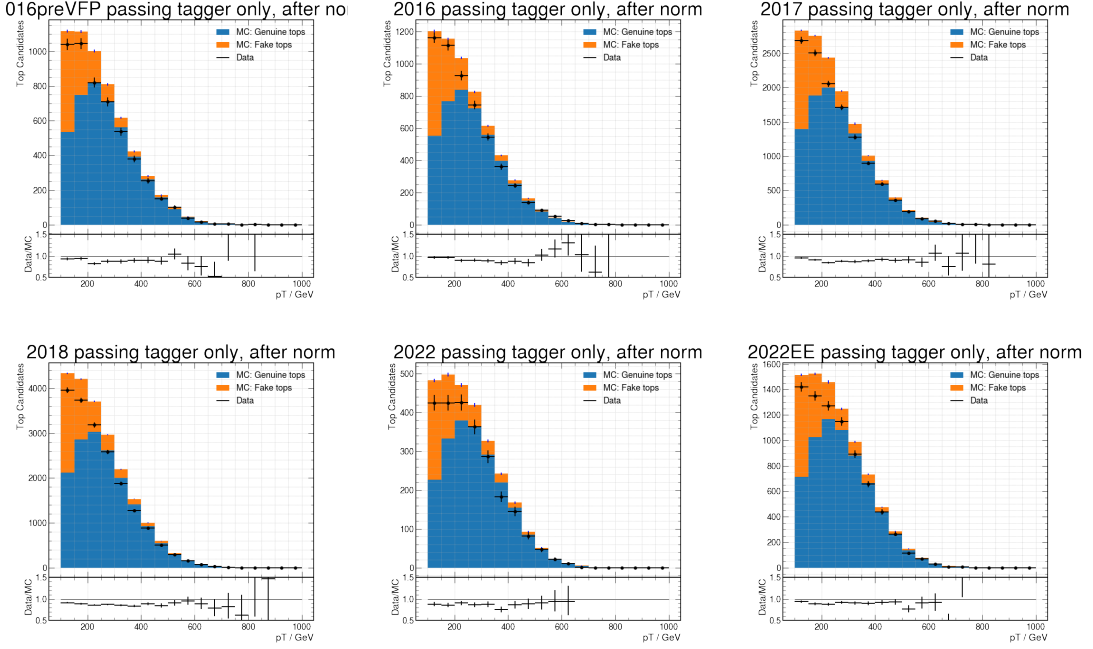
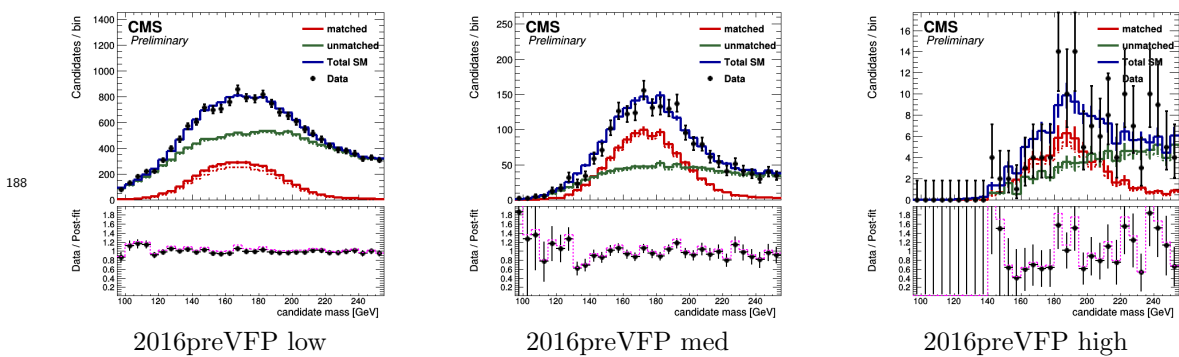
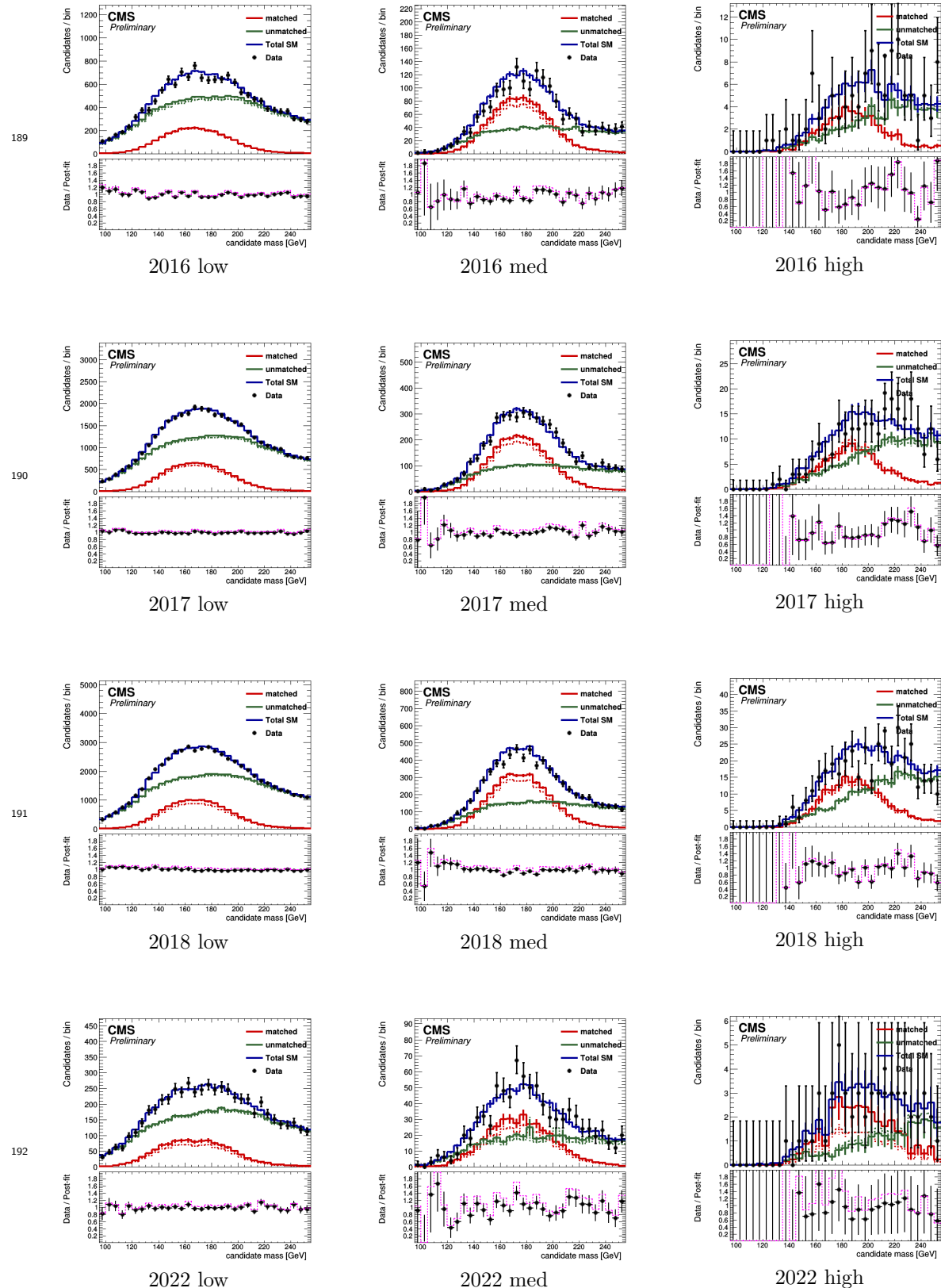


Figure 15: Distributions of resolved top candidate  $p_T$  in data and simulation for candidates passing the working point in the region used to derive the tagging efficiency scale factor. Contributions from candidates matched and not matched to top quarks at the generator level in simulation are shown in the stacked histograms. The event yield in simulation is normalized to data by the scale obtained from the same distributions for all candidates in Figure 12



### 3 Object Selection

#### 3.3 Jets



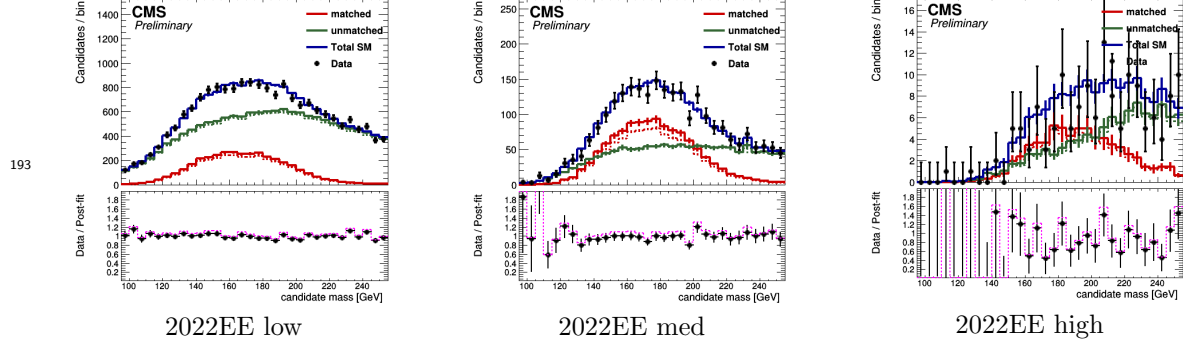
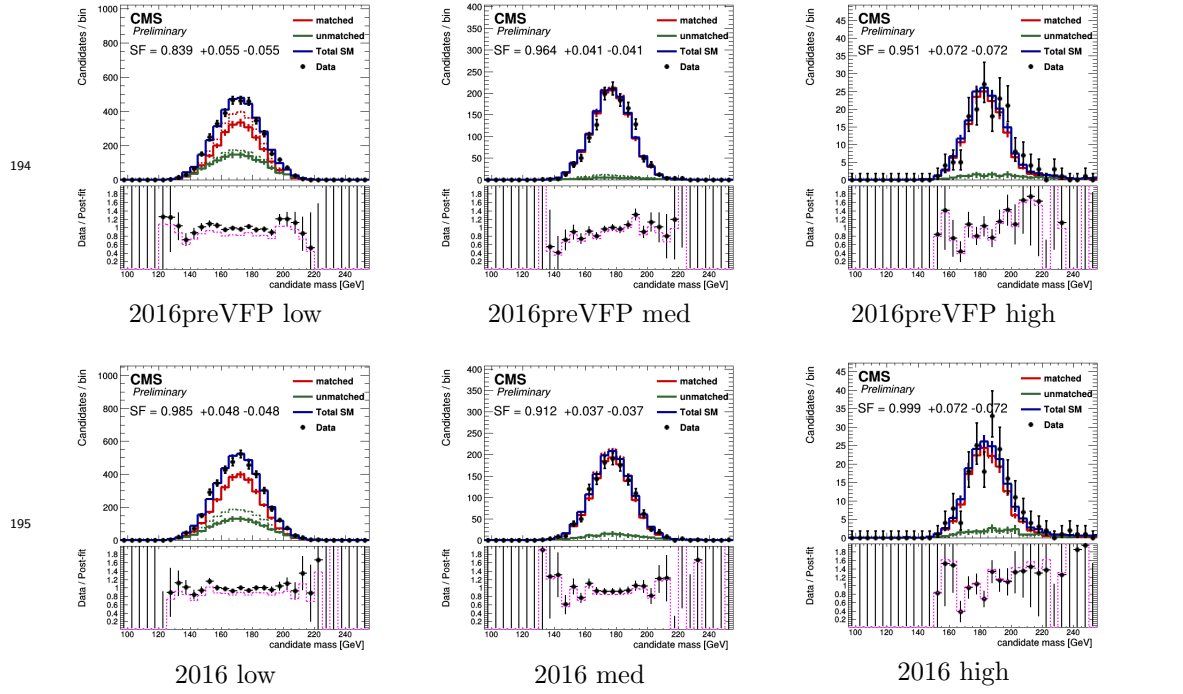


Figure 16: Data vs pre- and post-fit distributions in candidate mass for top candidates failing the working point in years for low (left column), medium (middle column), and high (right column)  $p_T$  categories. Solid lines correspond to post-fit distributions and dashed lines to pre-fit distributions. Candidates matched to generator-level tops are shown in red. Candidates unmatched to generator-level tops and total candidates are shown in green and blue respectively. The ratio of data to the total pre- and post-fit simulation is shown in the ratio panels.



### 3 Object Selection

#### 3.3 Jets

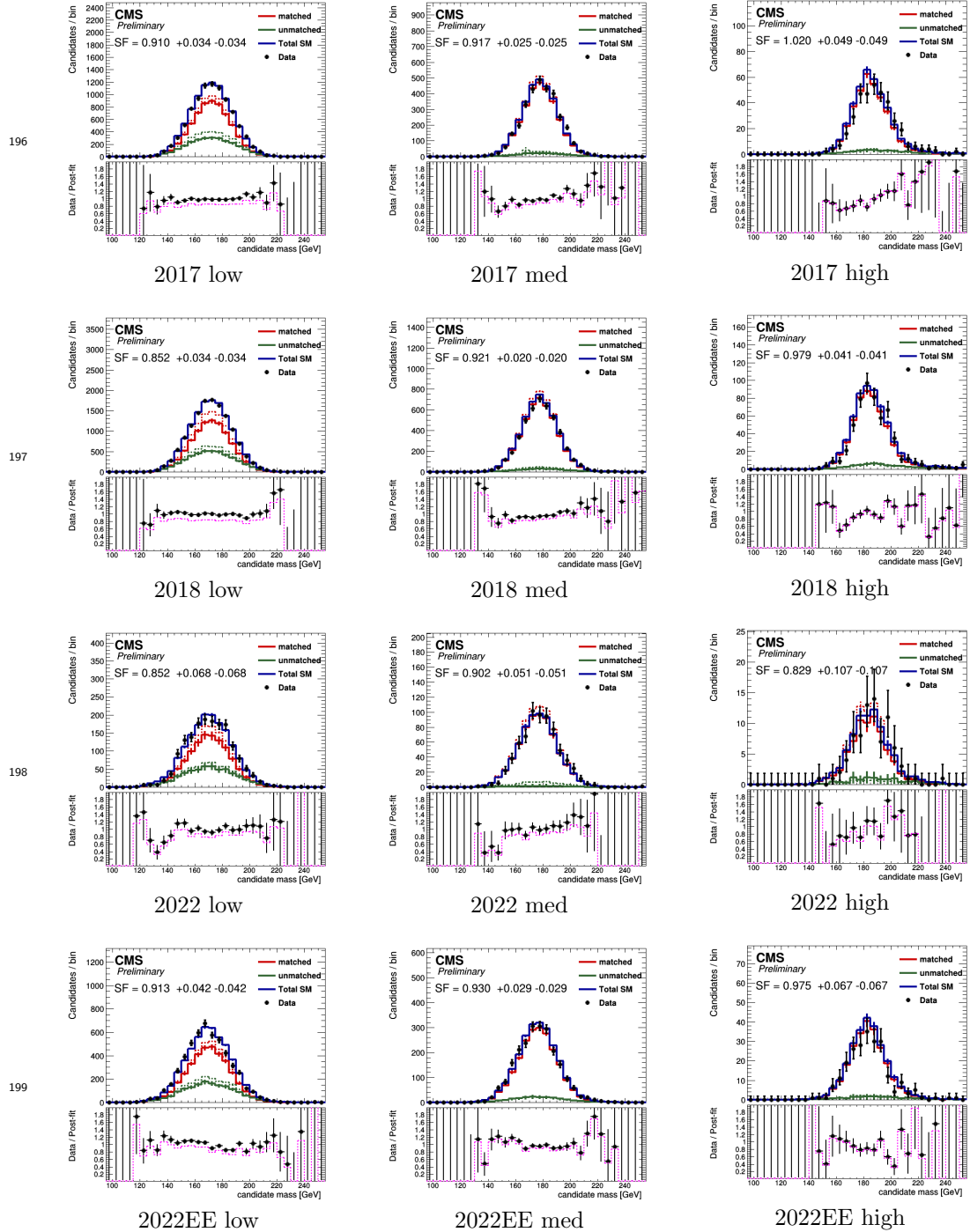


Figure 17: Data vs pre- and post-fit distributions in candidate mass for top candidates passing the working point in years for low (left column), medium (middle column), and high (right column)  $p_T$  categories. Solid lines correspond to post-fit distributions and dashed lines to pre-fit distributions. Candidates matched to generator-level tops are shown in red. Candidates unmatched to generator-level tops and total candidates are shown in green and blue respectively. The ratio of data to the total pre- and post-fit simulation is shown in the ratio panels. The scale factor extracted from the fit as shown by this figure and figure 16 is shown.

## 200 4 Event Selection

### 201 4.1 Baseline Selection and Signal Region

202 We apply to the events passing the triggers described in section 2 the following baseline selection:  
203  $N_{jet} \geq 9$ ,  $N_{bjet} \geq 3$ ,  $H_T > 700$  GeV, and no leptons. The objects are defined according to the  
204 criteria in section 3

205 The signal region (SR) is defined with the additional requirement of at least one tagged resolved  
206 top. Events in the SR are then subdivided into 12 categories based on the number of tagged resolved  
207 tops ( $N_{RT}$ ), the number of tagged boosted tops ( $N_{BT}$ ), and  $H_T$ . Table 16 defines these  
208 categories.

Top tags	$H_T$ [GeV]						
$N_{RT} = 1, N_{BT} = 0$	700–800	800–900	900–1000	1000–1100	1100–1200	1200–1300	>1500
$N_{RT} = 1, N_{BT} \geq 1$	700–1400					1200–1300	>1400
$N_{RT} \geq 2$	700–1100					>1100	

209 Table 16: Definitions of the SR categories based on the number of resolved tops ( $N_{RT}$ ), number  
of boosted tops ( $N_{BT}$ ), and  $H_T$ .

### 210 4.2 Event-level BDT

211 To further discriminate between signal and background, we implement an event-level BDT with  
212 the "CatBoost" library. This library is selected because it is found to perform better as compared  
213 to XGBoost BDT and neural networks. We use simulated  $t\bar{t}t\bar{t}$  events as signal and a mixture  
214 of simulated  $t\bar{t}$  and QCD multijet events as background. We require the events to pass the  
215 baseline selection of the signal region. Across the different background processes, events are  
216 first reweighted proportionally according to the cross section of their respective processes, and  
217 then reweighted so that  $t\bar{t}$  events take 80% of the total weights in background. For each year  
218 (separate training for preVFP for 2016, EE for 2022 and BPix for 2023), we use around 20,000  
219  $t\bar{t}t\bar{t}$  and 15,000  $t\bar{t}$  events. The use of statistics is limited here since we need to exclude these used  
220 events from downstream ML training and statistical analysis. However, for QCD events, we use  
221 all events available since it is not used downstream. Around 500 QCD events are available per  
222 year. We used CrossEntropy loss function, a growth policy of "Lossguide" and a learning rate of  
223 0.003. We apply further regularization to the training by setting "depth" to 2, "l2\_leaf\_reg" to 300,  
224 "min\_data\_in\_leaf" to 500 and "max\_leaves" to 10. These parameters are found by a grid search,  
225 and are found to combat overtraining under our constrained statistics effectively. Training against  
226 a mixture of background processes as such are found to perform better than training against  $t\bar{t}$   
227 alone. The BDT is trained and applied to each year separately. Figure 19 and 20 are example  
228 BDT discriminant distribution and ROC curve (with comparison against prelegacy training) for  
229 2018.

230  
231 Following the pre legacy iteration of this analysis, we choose the kinematics of jets, b-jets and  
232 the associated variables thereof as inputs for the even-level BDT. The number of boosted W  
233 candidates, the  $p_T$  of the leading resolved top candidate and b-jet are also used. Event shape  
234 variables that reflect event topology information are also included as inputs to the BDT. On the  
235 other hand, the number of resolved tops and boosted tops are deliberately excluded from the  
236 inputs to the BDT so that they can be used as independent variables for binning in SR. Resolved  
237 and boosted top discriminants are also excluded to prevent the potential dependence on the shape  
238 of these discriminants. Figure ?? shows the distribution of the input variables for signal and

background processes on 2018UL dataset. The following is the optimized set of variables input to the event-level BDT:

- The number of jets present in the event,  $N_j$
- The number of b-tagged jets present in the event,  $N_b$
- The number of boosted  $W$  candidates
- The sum of the masses of  $R = 0.8$  jets
- The missing transverse energy,  $P_T^{\text{miss}}$
- The scalar sum of  $p_T$  of jets,  $H_T$
- The scalar sum of  $p_T$  of b-tagged jets
- The  $P_T^{\text{miss}}$  divided by square root of  $H_T$
- The  $p_T$  of the leading b jet
- The  $p_T$  of the leading resolved top candidate
- The  $\eta$  difference between the leading and sub-leading jets
- The  $\eta$  difference between the leading and sub-leading b-tagged jets
- The absolute  $\phi$  difference between the leading and sub-leading jets
- The absolute  $\phi$  difference between the leading and sub-leading b-tagged jets
- The mean of the DeepJet b-tag scores of the b jets in the event
- The  $H_T$  of the six highest- $p_T$  jets divided by the total  $H_T$  in the event
- The transverse momenta of the jet with the seventh-largest  $p_T$  in the event
- Hadronic centrality ( $C$ ), defined as the value of  $H_T$  divided by the sum of the energies of all jets in the event
- Event sphericity ( $S$ ), calculated from all of the jets in the event in terms of the tensor

$$S^{\alpha\beta} = \sum_i p_i^\alpha p_i^\beta / \sum_i |\vec{p}_i|^2,$$

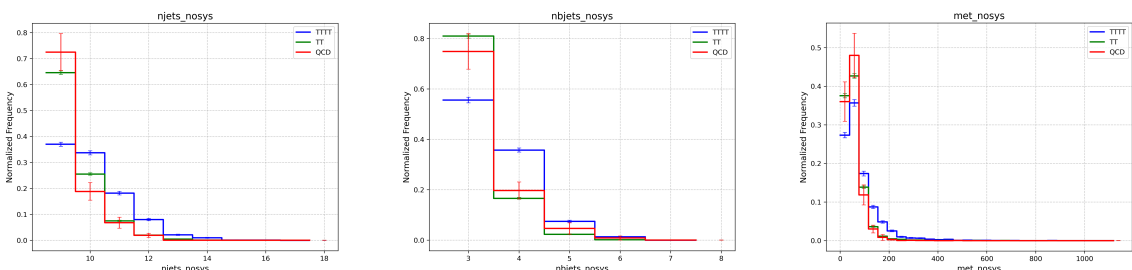
where  $\alpha$  and  $\beta$  refer to the three-components of the momentum of the  $i$ -th jet. The sphericity is then

$$S = (3/2)(\lambda_2 + \lambda_3),$$

where  $\lambda_2$  and  $\lambda_3$  are the two smallest eigenvalues of  $S^{\alpha\beta}$ .

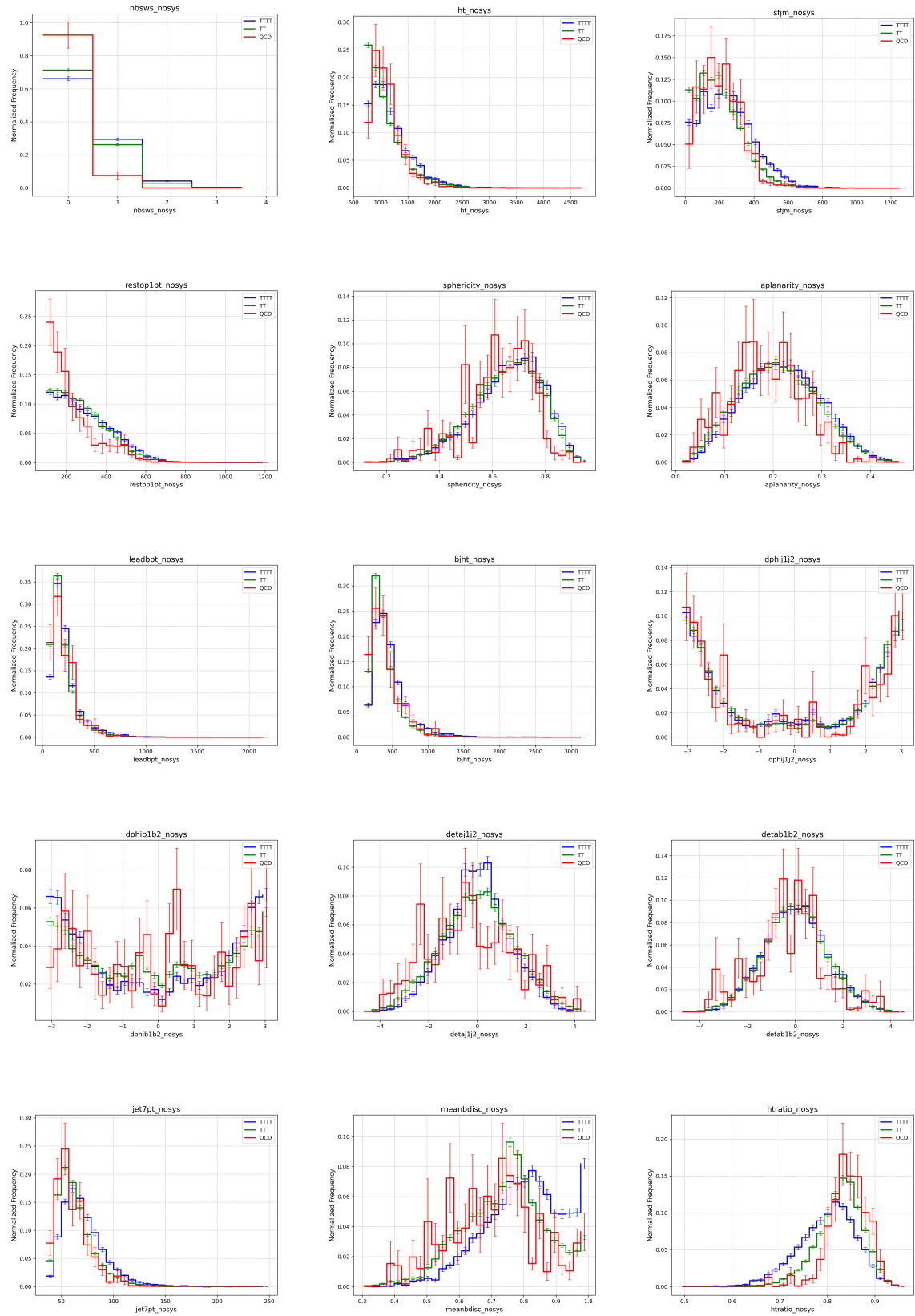
- Event aplanarity ( $A$ ), defined as

$$A = (3/2)(\lambda_3)$$



## 4 Event Selection

### 4.2 Event-level BDT



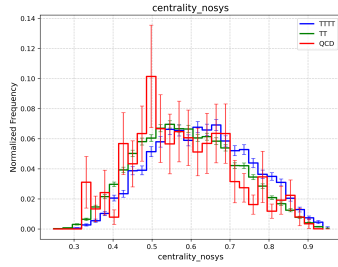


Figure 18: Input variable distribution for 2018UL for the event-level BDT. Error bar shows statistical uncertainty of each bin.

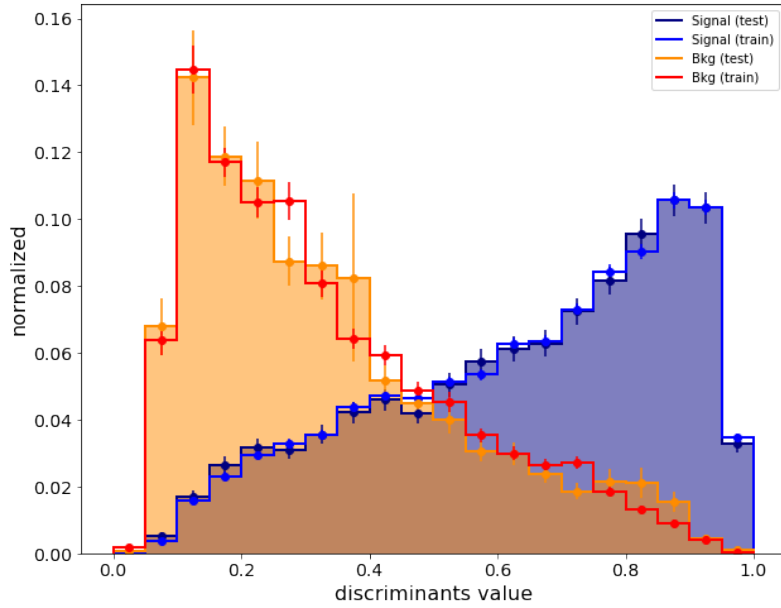


Figure 19: As an example, the discriminant distributions for the event-level BDT for signal and background samples for 2018.

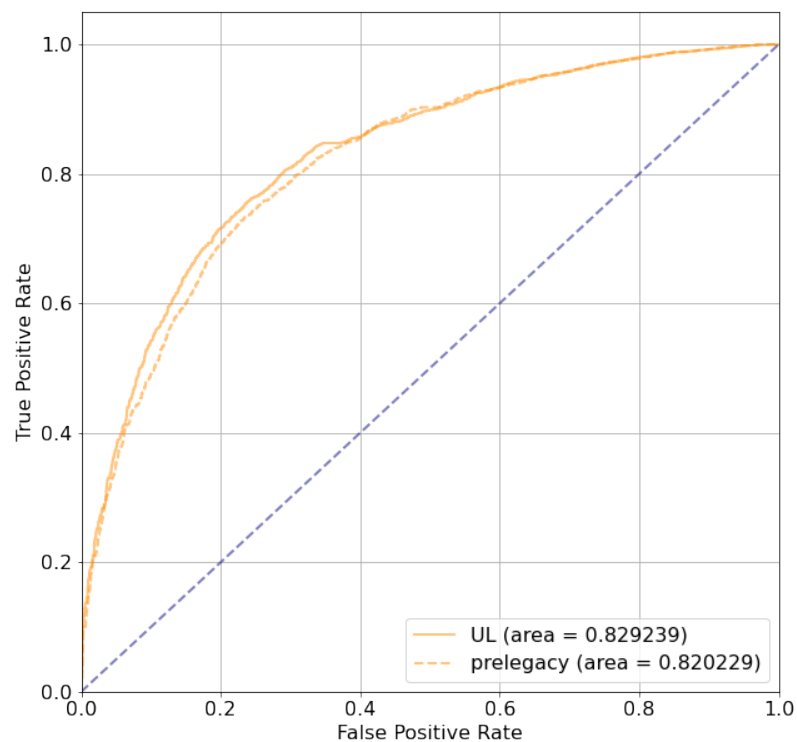


Figure 20: ROC curves of the event-level BDT for 2018, as compared against the prelegacy model.

## 266 5 Background Estimation

267 QCD multijet and hadronic  $t\bar{t}$  processes are the dominant background of this analysis. Next-  
 268 to-leading order (NLO) calculations in strong interactions and limited statistics lead to large  
 269 uncertainties in the simulation of the very high jet and b-jet multiplicity regions of these  
 270 processes used in this analysis. Therefore, we cannot rely on the simulation-based approach to  
 271 predict the QCD multijet and  $t\bar{t}$  + jets background. To overcome this, we adopt two data-driven  
 272 methods: the “extended ABCD” method for data-driven estimation of the absolute rate of the  
 273 background, and the “ABCDnn” method for data-driven estimation of the shape of the background.

274

### 275 5.1 Extended ABCD method

276 We divide the phase space into two dimensions using  $N_j$ , the number of jets, and  $N_b$ , the number  
 277 of b-jets. In the vanilla ABCD method, the phase space is divided into four regions along the two  
 278 dimensions, one of which is the Signal Region (SR) D and the other three are Control Regions  
 279 (CR) A, B and C. The yield in the Signal region D is estimated as  $\hat{F}_D = \frac{F_B}{F_A} \times F_C$ , where  $\hat{F}_D$   
 280 is the estimated yield in Signal Region D and  $F_A$ ,  $F_B$  and  $F_C$  are the observed yield in Control  
 281 Regions A, B and C respectively. This method assumes joint distributions in  $N_j$  and  $N_b$  are  
 282 mostly factorizable.

283

284 To improve the accuracy of the estimation, we extend the CRs to lower multiplicity in  $N_j$  as seen  
 285 in fig 21. Then, yield in the SR can be estimated as  $\hat{F}_D = \left(\frac{F_B F_C}{F_A}\right)^2 \left(\frac{F_X}{F_B F_Y}\right)$ .

286 Here,  $F$  is the estimated  $t\bar{t}$  + QCD multijet yield in each Control Region. This is estimated by  
 287 subtracting the  $t\bar{t}t\bar{t}$  MC yield and minor background processes MC yield from the observed yield  
 288 in data in each Control Region.

289

290 The extended ABCD method is applied to each  $h_T$  bin as specified in table 16 for each year  
 291 separately (separate training for preVFP for 2016, EE for 2022 and BPix for 2023).

292

293 Closure test conducted on prelegacy 2016  $t\bar{t}$  events requiring 0 lepton and same regions defined on  
 294  $N_j$  and  $N_b$  shows that yield predicted by vanilla ABCD method is off by 18%. The disagreement  
 295 between the estimated and true yield improves to 7% for the extended ABCD method. A closure  
 296 test with the same selection conducted on 2022  $t\bar{t}$  dataset shows a similar result: vanilla ABCD  
 297 method is off by 19.5% whereas extended ABCD method is only off by less than 1% as seen in  
 298 table 17.

299

Extended ABCD	ABCD	True
$6112 \pm 145.8$	$4943 \pm 58.95$	$6139 \pm 38.49$

Table 17: The absolute normalization predicted by the extended ABCD method and ABCD method in 2022 TT simulation, in a region satisfying the baseline selection with 0 leptons,  $N_j \geq 9$ ,  $N_b \geq 3$ , and  $H_T > 700$  GeV. The 3rd column shows the true absolute normalization. Only statistical uncertainties are presented.

300 Appendix C includes yields for control regions and estimated yield for the signal region for each  
 301  $H_T$  bin and for each year.

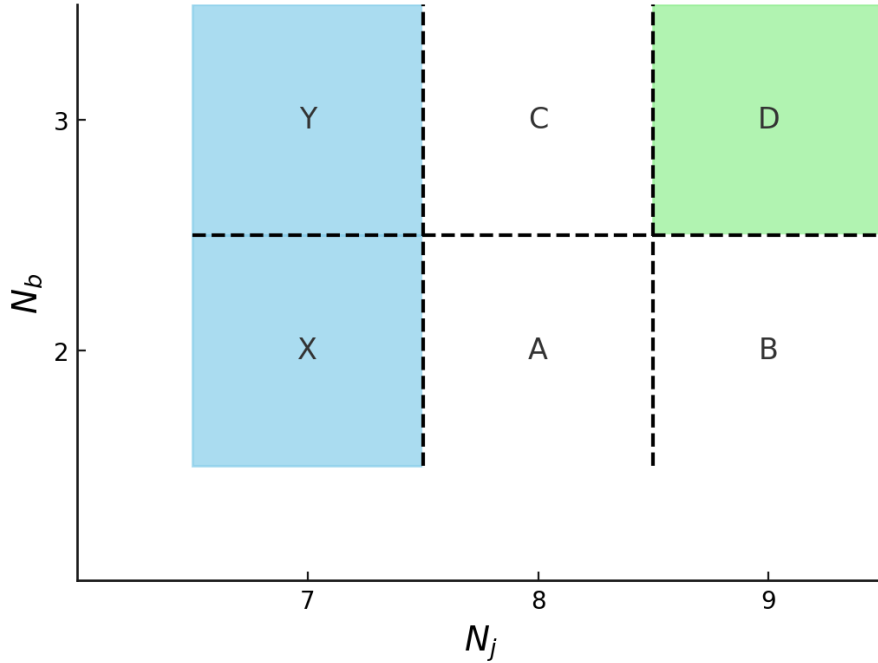


Figure 21: A, B and C are the Control Regions for the vanilla ABCD method and Y and X are the added adjacent Control Regions for the extended ABCD method. D is the Signal Region

## 5.2 ABCDnn method

We use the “ABCDnn” method [1] to estimate the shape of the event-level BDT discriminant for the  $t\bar{t} + \text{QCD}$  multijet background in the Signal Region. Specifically, “ABCDnn” method utilizes a Machine Learning technique named Neural Autoregressive Flow, which creates transformations between distributions of the feature variables under different conditions. These transformations are constructed as invertible bijective functions implemented as DNNs and learnt during training. In addition, the method automatically take into account the complex correlations between feature variables, so that multi-dimensional distributions can also be estimated.

Specifically, for this analysis, we use the same definition of Control Regions and Signal Regions as the ones defined for extended ABCD. That is, the neural networks are trained on Control Regions and applied to the Signal Region. For each Control Region, the neural network takes two distributions for training: the normalized distribution of  $t\bar{t}$  MC as the input distribution, and the normalized data-driven estimated  $t\bar{t} + \text{QCD}$  multijet distribution as the target distribution. The target distribution is created by taking the actual observed data distribution and subtract it by the  $t\bar{t}\bar{t}$  MC distribution and other minor background MC distributions. The neural network learns the transformation from the input distribution to the target distribution in each Control Region, as well as the condition, i.e. the label of the Control Region in the phase space, so that it learns how the transformation should change across the phase space defined by  $N_j$  and  $N_b$ . It does this by minimizing the maximum-mean-discrepancy between the output predicted distribution and the target distribution. Finally, the neural network is applied to the input distribution of  $t\bar{t}$  MC in the Signal Region to obtain the desired shape of data-driven estimated  $t\bar{t} + \text{QCD}$  multijet distribution in the Signal Region.

326 The learned models in this analysis not only transforms from MC distribution to data-driven  
 327 distribution to compensate for potential data-MC disagreement, but also transforms from a  
 328 single process distribution ( $t\bar{t}$ ) to dual process ( $t\bar{t} + \text{QCD multijet distribution}$ ). We do not use  
 329 the MC QCD multijet distribution as input due to limited statistics, especially in the Signal Region.

330  
 331 This training is done for each top-tag instead of each  $H_T$  bin because of the limited statistics  
 332 in each  $H_T$  bin. Therefore, for this analysis the feature variables underlying the transformed  
 333 distributions are event-level BDT discriminant and  $H_T$ . The predicted  $H_T$  of each event in the  
 334 input distribution is used to place them in the corresponding  $H_T$  bin, and the BDT discriminant  
 335 is used in each  $H_T$  bin to create the predicted shape. A separate “ABCDnn” model is trained  
 336 for each year (merged for 2016/2016preVFP, 2022/2022EE and 2023/2023BPix).

337  
 338 We used all remaining statistics for  $t\bar{t}$  events (excluding those used in the event-level BDT  
 339 training). We optimized the network hyperparameters with a combination of manual tuning and  
 340 grid search, and set the width of our dense layer to 256 and use 4096 minibatch size. The dense  
 341 layers here are used to condition on the CR labels during training and output the weights and  
 342 biases of the main network through which feature variables pass through and become morphed.  
 343 The nafdim, which controls the width of the main network which morphs the feature variables, is  
 344 set to 60. The depth is set to 3, which means that the entire model is made of 3 consecutive NAF  
 345 blocks.

346  
 347 A closure test for the method has been done by the previous iteration of this analysis morphing  
 348  $t\bar{t}$  MC distribution into  $t\bar{t}X$  MC distributions, with the same event selection and Control/Signal  
 349 Region definition as the main analysis. We merged 2016, 2017 and 2018 ultralegacy dataset to  
 350 improve the statistics for this test. The results of the test is in Appendix F. The method was  
 351 found to predict the target shape well.

352

### 353 5.3 Validation of the background estimation methods

354 The two background estimation methods are validated in a validation region (VR) requiring lower  
 355  $N_j$  than the previously defined SR. Specifically, we use  $N_j = 8, N_b >= 3$  as the VR, and define the  
 356 Control Regions for this VR correspondingly. We then perform the same procedures as defined  
 357 previously for “extendedABCD” and “ABCDnn”, and compare the predicted yield and shape  
 358 with the truth.

359

360 We find that the estimated yield in the Validation Region in each  $H_T$  bin agrees with the true  
 361 yield after accounting for statistical error from MC propagated through the extended ABCD  
 362 formula and statistical error in the true yield. The result is in Appendix D. We account for the  
 363 disagreement as a systematic uncertainty detailed in section 6.1.1.

364

365 We find that the predicted shape in the Validation Region largely agrees well with the true shape,  
 366 especially for  $H_T$  bins with higher statistics. The result is in Appendix ???. We account for the  
 367 disagreement as a systematic uncertainty detailed in section 6.1.2.

## 368 6 Systematic Uncertainties

### 369 6.1 Systematics from background estimation

370 We derive the systematic uncertainties for our background estimation methods from the Validation  
 371 Region defined in section 5.3, where we compare the output (yield/shape) of the specific background  
 372 estimation method against the truth. We then apply the derived systematics to the Signal Region.  
 373 These uncertainties are calculated separately for each  $H_T$  bin defined in table 16. A summary of  
 374 different sources of systematic uncertainties are in table 18.

Table 18: Summary of systematic uncertainties and the ranges of their effects on signal and background yields. The uncertainty type (shape vs normalization only), affected processes, correlations (between processes and/or years), and effects on signal and background yields as % are shown. Systematic uncertainties are considered for all years unless otherwise indicated. Statistics of extendedABCD is the statistical uncertainties of the QCD+ $t\bar{t}$  samples in the Control Regions, propagated via extendedABCD.

Name	Type	Processes	Correlations	$t\bar{t}t\bar{t}$ Signal Uncertainty (%)	Background Uncertainty (%)
Statistics of extendedABCD	shape	QCD+ $t\bar{t}$	-	-	5-30
Statistics of transformed samples	shape	QCD+ $t\bar{t}$	-	-	5
Statistics of simulated samples	shape	$t\bar{t}t\bar{t}$ , $t\bar{t}X$ , other	-	0-5	0-30
Data-prediction normalization	lnN	QCD+ $t\bar{t}$	-	-	6-41
Data-prediction shape uncertainty	shape	QCD+ $t\bar{t}$	-	-	n/a
DeepJet b-tag SF (HF, LF, cferr)	shape	$t\bar{t}t\bar{t}$ , $t\bar{t}X$ , other	processes+years	0-40	0-40
DeepJet b-tag SF (stats)	shape	$t\bar{t}t\bar{t}$ , $t\bar{t}X$ , other	processes	0-10	0-10
Resolved top efficiency SF	shape	$t\bar{t}t\bar{t}$ , $t\bar{t}X$ , other	processes	0-5	0-5
Resolved top mistag SF	shape	$t\bar{t}t\bar{t}$ , $t\bar{t}X$ , other	processes	0-10	0-10
PNet boosted top SF	shape	$t\bar{t}t\bar{t}$ , $t\bar{t}X$ , other	processes	0-15	0-20
PNet boosted W SF	shape	$t\bar{t}t\bar{t}$ , $t\bar{t}X$ , other	processes	0-20	0-30
JER	shape	$t\bar{t}t\bar{t}$ , $t\bar{t}X$ , other	processes	0-3	0-15
JES	shape	$t\bar{t}t\bar{t}$ , $t\bar{t}X$ , other	processes	0-15	0-25
Pileup	shape	$t\bar{t}t\bar{t}$ , $t\bar{t}X$ , other	processes	0-2	0-10
Trigger efficiency	shape	$t\bar{t}t\bar{t}$ , $t\bar{t}X$ , other	processes	0-10	0-5
Luminosity	lnN	$t\bar{t}t\bar{t}$ , $t\bar{t}X$ , other	processes	2.3-2.5	2.3-2.5
Cross section	lnN	$t\bar{t}X$	processes+years	-	26

#### 375 6.1.1 ExtendedABCD

376 We derive a normalization uncertainty from the Validation Region based on the disagreement  
 377 between the data and predicted background in the VRs. This uncertainty is calculated in each VR  
 378  $H_T$  bin as the sum in quadrature of two quantities: the deviation of the weighted mean (average)  
 379 of events in that VR  $H_T$  bin from 1, and the weighted RMS of events in that VR  $H_T$  bin. The  
 380 weighted mean  $\langle f \rangle$  is defined as

$$\langle f \rangle = \frac{\sum_i f_i w_i}{\sum_i w_i},$$

381 for each discriminant histogram bin  $i$  in the VR  $H_T$  bin of interest, where the weight  $w_i$  is the  
 382 number of events in that histogram bin and  $f_i$  is the ratio of observed events to predicted events  
 383 ( $N_{\text{data}}/N_{\text{pred}}$ ) in that histogram bin. The mean is weighted to reflect the distribution of events in  
 384 the histogram, and the deviation of this weighted mean from 1, i.e.  $(1 - \langle f \rangle)$  reflects the overall  
 385 offset in normalization between the prediction and the data. Similarly, the weighted RMS is defined  
 386 as

$$\sqrt{\langle f^2 \rangle - \langle f \rangle^2},$$

387 where

$$\langle f^2 \rangle = \frac{\sum_i f_i^2 w_i}{\sum_i w_i},$$

388 and reflects the spread of the disagreement between the prediction and the data in the histogram  
 389 bins. This method of quantifying the data-prediction discrepancy is based on recommendations

390 from the CMS Statistics Committee. These uncertainties are taken to be uncorrelated across  $H_T$   
 391 bins and years.

### 392 6.1.2 ABCDnn

393 We derive an uncertainty for the shape of ABCDnn output from the Validation Region, based  
 394 on observed disagreement between the shape of data and predicted background in the VRs. This  
 395 uncertainty is calculated in each VR  $H_T$  bin as a linear shift, both up and down, of the BDT  
 396 discriminant value of each event. For example, a shift up of 2% ( $s = +0.02$ ) for a particular VR  
 397  $H_T$  bin means that the BDT discriminant value of every event in that VR  $H_T$  bin is multiplied  
 398 by 1.02. Qualitatively, in both up and down directions, we shift the BDT discriminants such that  
 399 the disagreement between the shape of the normalized BDT discriminant distribution of the data  
 400 and the predicted background is as small as possible. Quantitatively, the extent of the shift is  
 401 determined by minimizing the following metric:

$$s = \arg \min_s \sum_i \max \left( \frac{|f_i(s) - 1|}{\sigma_i(s)}, \frac{|f_i(0.0) - 1|}{\sigma_i(0.0)} \right)$$

402 where  $s$  is a particular shift up (positive) and down (negative),  $f_i = \frac{N_{\text{pred},i}}{N_{\text{truth},i}}$ , the ratio of predicted  
 403 events over observed events in BDT discriminant bin  $i$ , and  $\sigma_i$  is the statistical uncertainty in  
 404 bin  $i$ .  $\frac{|f_i(s) - 1|}{\sigma_i(s)}$  measures the deviation of ratio in bin  $i$  from 1 under shift  $s$ , inversely scaled by  
 405 the statistical uncertainty in that bin. In most cases, the deviation increases for some bins and  
 406 decreases for the others under a particular shift, therefore a naive minimization of this term across  
 407 the bins results in bad coverage in the bins whose deviation decreases. These bins are the bins  
 408 that are supposed to be covered by the shift, since the bins whose deviation increases would be  
 409 covered by the shift in the opposite direction.

410 To overcome this, we include a maximization against the second term  $\frac{|f_i(0.0) - 1|}{\sigma_i(0.0)}$ , which is the same  
 411 scaled deviation of ratio before shifting. The maximization of the first term against the unshifted  
 412 scaled deviation of ratio removes the effect of bins whose deviation worsened under a particular  
 413 shift direction, so that by minimizing this metric, the shifting method can obtain good coverage  
 414 of disagreement in all bins.

416 A minimum shift of 1% is imposed in either direction.

418 Currently, we consider this shape uncertainty as uncorrelated across  $H_T$  bins and across years.  
 419 Comparison of pre-fit binned BDT discriminant distribution between MC and data in the validation  
 420 regions, where MC includes the data-driven yield and shape estimation, can be seen in Appendix  
 421 A.

### 423 6.1.3 Closure Test on systematic uncertainty estimation for background estimation

425 We perform closure tests to make sure that the methods used to estimate the systematic  
 426 uncertainties of the two background estimation are reasonable. We use ultralegacy 2018 data,  
 427 using exactly the same requirement as our event selection and inputs to extended ABCD formula,  
 428 and using the same  $H_T$  bin definition as  $N_{RT}=1$ ,  $N_{BT}=0$  top-tag, but requiring 0 resolved top  
 429 instead of at least 1 so that the regions are orthogonal from the main analysis. We define this  
 430 as the "Closure Test Region". In this region, we estimate the systematic uncertainties of the  
 431 two background estimation methods in the VR ( $N_{RT}=1$ ,  $N_{BT}=0$ ,  $N_{jets} = 8$ ,  $N_{bjets} \geq 3$ ), and  
 432 apply them to the SR ( $N_{RT}=1$ ,  $N_{BT}=0$ ,  $N_{jets} \geq 9$ ,  $N_{bjets} \geq 3$ ), and finally compare the  
 433 predicted yield and shape with the truth in SR while taking into account the estimated systematic

434 uncertainties. Note that this region is used for the closure test for the systematic uncertainty  
435 estimation methods, and is different from the closure tests for extendedABCD shown in Table 17  
436 and for ABCDnn shown in Appendix F.

437 For “extendedABCD”, the result shows that the estimated yield in the Signal Region in each  $H_T$   
438 bin agrees with the true yield after accounting for statistical error from MC propagated through  
439 the extended ABCD formula and statistical error in the true yield, as well as the systematic  
440 uncertainty as defined in sec 6.1.1. The result is in Appendix E.

442 For “ABCDnn”, the result shows that the systematic uncertainty as defined in sec 6.1.2 mostly  
443 covers the disagreement between the predicted and the true shape in each  $H_T$  bin in the Closure  
444 Test region. The result is in Appendix ??.

446

## 447 6.2 Other sources of systematic uncertainties

- 448 • The statistical uncertainties of SM/top philic  $t\bar{t}t\bar{t}$  signal samples and background processes  
449 modeled with MC samples.
- 450 • The statistical uncertainties of the estimated QCD +  $t\bar{t}$  yields in each CR, propagated through  
451 the extendedABCD formula.
- 452 • The statistical uncertainties of the simulated  $t\bar{t}$  events transformed by ABCDnn to form the  
453 predicted discriminant distribution of BDT.
- 454 • The statistical uncertainties from the trigger efficiency corrections, parameterized in  $N_b$  and  
455  $N_j$ .
- 456 • Uncertainties related to the boosted top and W tagging correction factors used to correct  
457 the performance of the Particlenet algorithm in simulation to match data. Two uncertainties  
458 are included: boosted top and boosted W uncertainties related to the non-mass-decorrelated  
459 scale factors. These uncertainties are correlated between processes but uncorrelated between  
460 years.
- 461 • Tagging and misidentification uncertainties related to resolved top tagging correction factors  
462 used to correct the performance of the resolved top tagging algorithm in simulation to match  
463 data, as described in Section 3.3.3. Two uncertainties for both tagging efficiency and mistag  
464 rate scale factors are considered, and uncertainties in these stem from statistical uncertain-  
465 ties that arise in calculating the scale factors. These are correlated between processes and  
466 uncorrelated between years.
- 467 • Uncertainties related to correction factors used to correct for the performance of the DeepJet  
468 b-tagging algorithm in simulation with respect to data. The DeepJet iterative fit/shape scale  
469 factors are used. Scale factors per event are calculated as the product of the scale factors for  
470 all jets in a given event passing pre-selection. The uncertainties are split into several sources,  
471 including those affecting HF (heavy-flavor) or LF (light-flavor) jets, uncertainties from charm  
472 jets (cferr1 and cferr2), and linear and quadratic statistical fluctuations (LFstats1, LFstats2,  
473 HFstats1, HFstats2). These are all considered as separate systematic variations, with sta-  
474 tistical variations correlated between processes and uncorrelated between years (LFstats1,  
475 LFstats2, HFstats1, HFstats2) and others correlated between both processes and years (HF,  
476 LF, cferr1 and cferr2).
- 477 • Uncertainties associated to the pileup reweighting correction factor.
- 478 • Jet energy scale (JES) and resolution (JER) uncertainties impacting the reconstruction of  
479 jets, including  $R = 0.4$  and  $R = 0.8$  jets,  $p_T^{miss}$ , and tagged top, W, and b candidates  
480 and their correction factors. The JES systematic uncertainty is currently applied using the  
481 combined JES uncertainty. We vary the JES and JER up and down by their systematic  
482 uncertainties and propagate the effects through all analysis objects and selections, including

483       in selecting jets and boosted objects and re-propagating the varied jets through our resolved  
484       top algorithm. JER and JES variations are correlated between processes but not between  
485       years.

- 486     ● Uncertainties assigned to the integrated luminosity measured by the CMS experiment. Ac-  
487       cording to LUM recommendations for Run2 and Run3, the uncorrelated uncertainties are  
488       1.0%, 2.0%, 1.5% respectively for 2016, 2017 and 2018 for run2. Across run2, the correlated  
489       uncertainties are 0.6%, 0.9% and 2.0% for 2016, 2017 and 2018. Between 2017 and 2018,  
490       there is a further correlated uncertainty of 0.6% and 0.2%. The uncertainties are 1.4% and  
491       1.3% respectively for 2022 and 2023 for run3.
- 492     ● Uncertainties in the theoretical cross sections used to normalize ttX backgrounds are consid-  
493       ered. These impact the number of ttX events in each SR bin. For ttX processes (X=W,Z,H),  
494       we assign an uncertainty of 26% based on the largest deviation of the signal strength observed  
495       by CMS for any of these processes (relative to the SM prediction), which is the observation  
496       of ttH in this case [2].

## 497 7 Results and interpretation

498 A binned likelihood analysis is carried out in the SR categories split by resolved and boosted  
 499 top multiplicities and  $H_T$ , as defined in Table 16. As input to each SR category, the shape and  
 500 yields of the event-level BDT discriminant of  $t\bar{t}t\bar{t}$ ,  $t\bar{t}X$  and other minor background processes are  
 501 provided to CMSCombine from Monte Carlo, and those of  $t\bar{t}$  and QCD processes are provided  
 502 from data-driven background estimation methods extendedABCD (Section 6.1.1) and ABCDnn  
 503 (Section 6.1.2). The event yields for each process in each SR channel are listed in the tables 19,  
 504 20, 21, 22.

505  
 506 The systematic uncertainties described in Section 6 are included in the analysis as nuisance  
 507 parameters. Up and down variations of the BDT discriminant shapes are provided as inputs for  
 508 each nuisance parameter corresponding to shape-based systematic variations, while uncertainties  
 509 affecting only the normalizations of processes are implemented using log-normally distributed  
 510 constraints on the simulation rates in each data-taking period. Pre-fit binned BDT discriminant  
 511 distribution of MC, including the data-driven estimate of shape and yield and their variances, can  
 512 be seen in Appendix B.

513  
 514 Currently at the blinded stage, we have the following preliminary result. The median expected  
 515 limit is obtained asymptotically, while the significance is obtained via 500 trials of toy (Asimov  
 516 dataset shows bias).

517

		<b>ttt</b>	<b>ttx</b>	<b>other</b>	<b>QCD+tt</b>
$N_{RT} = 1, N_{BT} = 0$	$700 \leq H_T < 800$	$2.79 \pm 0.04$	$35.07 \pm 2.48$	$26.22 \pm 2.68$	$1763.50 \pm 72.37$
	$800 \leq H_T < 900$	$3.19 \pm 0.04$	$30.54 \pm 2.21$	$36.42 \pm 3.47$	$1438.50 \pm 69.82$
	$900 \leq H_T < 1000$	$3.08 \pm 0.04$	$27.87 \pm 2.14$	$25.46 \pm 2.57$	$1348.86 \pm 79.41$
	$1000 \leq H_T < 1100$	$2.63 \pm 0.04$	$24.66 \pm 2.11$	$27.69 \pm 3.20$	$806.24 \pm 59.18$
	$1100 \leq H_T < 1200$	$1.98 \pm 0.04$	$16.43 \pm 2.02$	$24.41 \pm 3.31$	$606.99 \pm 56.13$
	$1200 \leq H_T < 1300$	$1.50 \pm 0.03$	$9.97 \pm 1.91$	$16.31 \pm 1.99$	$569.46 \pm 65.10$
	$1300 \leq H_T < 1500$	$1.62 \pm 0.04$	$20.32 \pm 2.24$	$27.36 \pm 3.22$	$508.92 \pm 56.53$
$N_{RT} = 1, N_{BT} = 1$	$H_T \geq 1500$	$1.42 \pm 0.04$	$25.64 \pm 2.90$	$36.69 \pm 3.60$	$507.57 \pm 65.56$
	$700 \leq H_T < 1400$	$2.69 \pm 0.04$	$12.87 \pm 1.61$	$6.56 \pm 1.38$	$378.31 \pm 44.48$
	$H_T \geq 1400$	$4.44 \pm 0.07$	$18.90 \pm 3.16$	$18.36 \pm 3.00$	$376.07 \pm 73.49$
$N_{RT} = 2$	$700 \leq H_T < 1100$	$2.96 \pm 0.04$	$19.12 \pm 1.53$	$4.81 \pm 1.31$	$408.11 \pm 42.71$
	$H_T \geq 1100$	$3.25 \pm 0.05$	$15.77 \pm 1.99$	$4.99 \pm 1.42$	$135.28 \pm 33.46$

Table 19: Yields of tttt, ttX, other bakcgound and data-driven estimated QCD+tt processes in the Signal Region of 2016.

		<b>tttt</b>	<b>ttX</b>	<b>other</b>	<b>QCD+tt</b>
$N_{RT} = 1, N_{BT} = 0$	$700 \leq Ht < 800$	$2.87 \pm 0.03$	$28.57 \pm 1.89$	$31.27 \pm 4.19$	$1732.06 \pm 76.57$
	$800 \leq Ht < 900$	$3.40 \pm 0.04$	$36.08 \pm 1.95$	$25.14 \pm 2.20$	$1594.95 \pm 82.52$
	$900 \leq Ht < 1000$	$3.17 \pm 0.04$	$24.01 \pm 1.65$	$19.60 \pm 1.74$	$1106.32 \pm 106.67$
	$1000 \leq Ht < 1100$	$2.50 \pm 0.03$	$18.29 \pm 1.28$	$16.17 \pm 1.52$	$812.48 \pm 62.89$
	$1100 \leq Ht < 1200$	$1.84 \pm 0.03$	$13.55 \pm 1.12$	$16.52 \pm 1.69$	$581.11 \pm 55.87$
	$1200 \leq Ht < 1300$	$1.16 \pm 0.02$	$9.44 \pm 1.05$	$14.31 \pm 1.55$	$566.33 \pm 66.77$
	$1300 \leq Ht < 1500$	$1.20 \pm 0.02$	$10.48 \pm 1.20$	$12.68 \pm 1.20$	$538.62 \pm 60.02$
	$Ht \geq 1500$	$0.78 \pm 0.02$	$9.64 \pm 1.17$	$15.99 \pm 1.27$	$464.71 \pm 57.93$
$N_{RT} = 1, N_{BT} = 1$	$700 \leq Ht < 1400$	$1.75 \pm 0.02$	$9.63 \pm 0.98$	$4.15 \pm 0.86$	$289.36 \pm 34.27$
	$Ht \geq 1400$	$1.94 \pm 0.02$	$7.25 \pm 0.76$	$4.00 \pm 0.65$	$347.34 \pm 67.38$
$N_{RT} \geq 2$	$700 \leq Ht < 1100$	$2.90 \pm 0.03$	$16.67 \pm 1.37$	$6.77 \pm 1.31$	$413.93 \pm 44.52$
	$Ht \geq 1100$	$2.20 \pm 0.03$	$9.41 \pm 0.81$	$2.77 \pm 0.65$	$191.45 \pm 45.09$

Table 20: Yields of tttt, ttX, other background and data-driven estimated QCD+tt processes in the Signal Region of 2017.

		<b>tttt</b>	<b>ttX</b>	<b>other</b>	<b>QCD+tt</b>
$N_{RT} = 1, N_{BT} = 0$	$700 \leq Ht < 800$	$4.24 \pm 0.04$	$46.65 \pm 2.67$	$42.05 \pm 3.34$	$2755.76 \pm 96.26$
	$800 \leq Ht < 900$	$4.93 \pm 0.05$	$47.82 \pm 2.75$	$49.07 \pm 4.47$	$2397.37 \pm 96.79$
	$900 \leq Ht < 1000$	$4.67 \pm 0.05$	$37.03 \pm 2.26$	$36.91 \pm 3.01$	$1926.95 \pm 93.86$
	$1000 \leq Ht < 1100$	$3.81 \pm 0.04$	$33.50 \pm 2.42$	$30.69 \pm 2.60$	$1492.59 \pm 89.64$
	$1100 \leq Ht < 1200$	$2.82 \pm 0.04$	$23.24 \pm 1.95$	$27.78 \pm 2.97$	$1028.50 \pm 76.64$
	$1200 \leq Ht < 1300$	$1.99 \pm 0.03$	$17.28 \pm 1.85$	$20.71 \pm 2.21$	$919.48 \pm 84.45$
	$1300 \leq Ht < 1500$	$2.24 \pm 0.04$	$22.44 \pm 2.22$	$25.72 \pm 2.20$	$779.95 \pm 71.94$
	$Ht \geq 1500$	$1.63 \pm 0.03$	$21.11 \pm 1.91$	$38.71 \pm 2.87$	$1076.03 \pm 108.71$
$N_{RT} = 1, N_{BT} = 1$	$700 \leq Ht < 1400$	$3.37 \pm 0.04$	$17.86 \pm 1.85$	$10.95 \pm 2.39$	$383.82 \pm 39.46$
	$Ht \geq 1400$	$4.58 \pm 0.05$	$17.85 \pm 2.12$	$15.07 \pm 1.85$	$431.24 \pm 69.58$
$N_{RT} = 2$	$700 \leq Ht < 1100$	$4.29 \pm 0.04$	$29.78 \pm 2.05$	$12.62 \pm 2.68$	$638.34 \pm 55.12$
	$Ht \geq 1100$	$4.04 \pm 0.04$	$18.20 \pm 1.91$	$5.58 \pm 1.36$	$267.33 \pm 48.23$

Table 21: Yields of tttt, ttX, other background and data-driven estimated QCD+tt processes in the Signal Region of 2018.

		<b>tttt</b>	<b>ttX</b>	<b>other</b>	<b>QCD+tt</b>
$N_{RT} = 1, N_{BT} = 0$	$700 \leq Ht < 800$	$1.32 \pm 0.03$	$15.25 \pm 1.46$	$17.04 \pm 2.17$	$771.57 \pm 45.17$
	$800 \leq Ht < 900$	$1.70 \pm 0.03$	$19.20 \pm 1.54$	$24.63 \pm 7.77$	$772.71 \pm 50.14$
	$900 \leq Ht < 1000$	$1.61 \pm 0.04$	$15.58 \pm 1.53$	$18.66 \pm 2.20$	$592.81 \pm 45.15$
	$1000 \leq Ht < 1100$	$1.45 \pm 0.03$	$14.46 \pm 1.35$	$16.87 \pm 2.97$	$513.32 \pm 47.09$
	$1100 \leq Ht < 1200$	$1.10 \pm 0.03$	$8.95 \pm 1.16$	$13.83 \pm 2.26$	$442.53 \pm 49.53$
	$1200 \leq Ht < 1300$	$0.81 \pm 0.03$	$10.64 \pm 1.15$	$9.14 \pm 2.07$	$283.01 \pm 38.38$
	$1300 \leq Ht < 1500$	$0.89 \pm 0.03$	$11.99 \pm 1.34$	$13.30 \pm 1.55$	$270.64 \pm 37.71$
	$Ht \geq 1500$	$0.66 \pm 0.03$	$13.58 \pm 1.36$	$21.51 \pm 3.96$	$323.68 \pm 51.58$
$N_{RT} = 1, N_{BT} = 1$	$700 \leq Ht < 1400$	$1.38 \pm 0.03$	$7.66 \pm 1.12$	$3.38 \pm 0.75$	$196.61 \pm 29.13$
	$Ht \geq 1400$	$1.99 \pm 0.04$	$8.80 \pm 1.18$	$5.88 \pm 0.83$	$164.39 \pm 37.38$
$N_{RT} \geq 2$	$700 \leq Ht < 1100$	$1.58 \pm 0.03$	$13.15 \pm 1.37$	$4.60 \pm 0.99$	$209.70 \pm 26.24$
	$Ht \geq 1100$	$1.71 \pm 0.04$	$8.76 \pm 1.15$	$2.52 \pm 0.40$	$148.26 \pm 37.76$

Table 22: Yields of tttt, ttX, other background and data-driven estimated QCD+tt processes in the Signal Region of 2022.

	Expected significance	Median expected limit
2016 + 2016preVFP	0.340	6.500
2017	0.594	5.094
2018	0.402	5.625
2022 + 2022EE	0.298	7.375
<b>Total</b>	<b>0.614</b>	<b>2.289</b>

Table 23: Expected significance and median expected limits for SM  $T\bar{T}T\bar{T}$ .

518 **A Pre-fit binned BDT distribution for Validation Re-**  
519 **gion**

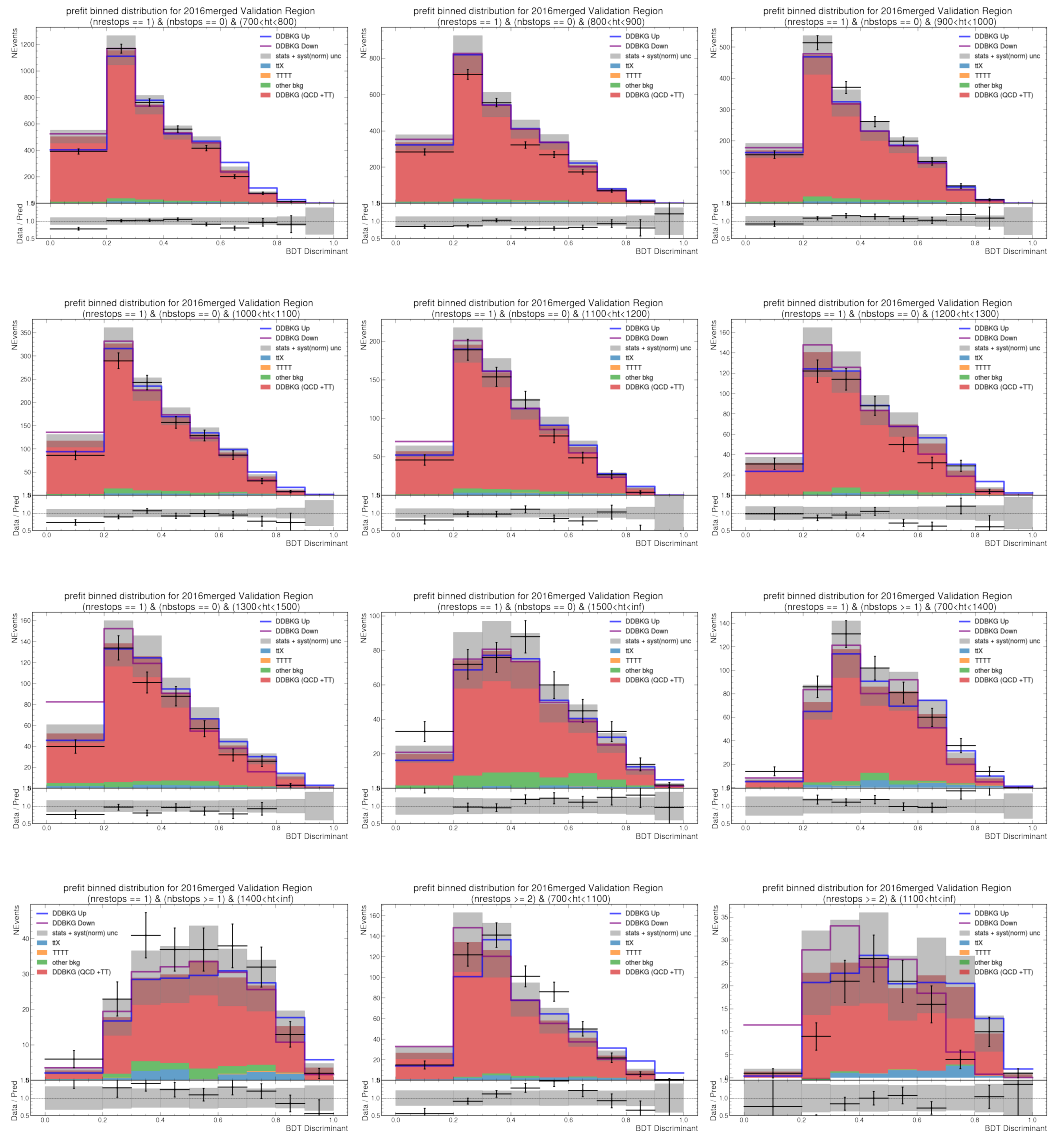


Figure 22: Pre-fit binned BDT distribution for Validation Region for 2016. DDBKG (data-driven background) is the predicted TT+QCD distribution from extendedABCD and ABCDnn. DDBKG Up/Down is the shift in distribution from systematic uncertainty estimation of ABCDnn. Shaded region represented statistical + normalization systematic uncertainty from extendedABCD.

## A Pre-fit binned BDT distribution for Validation Region

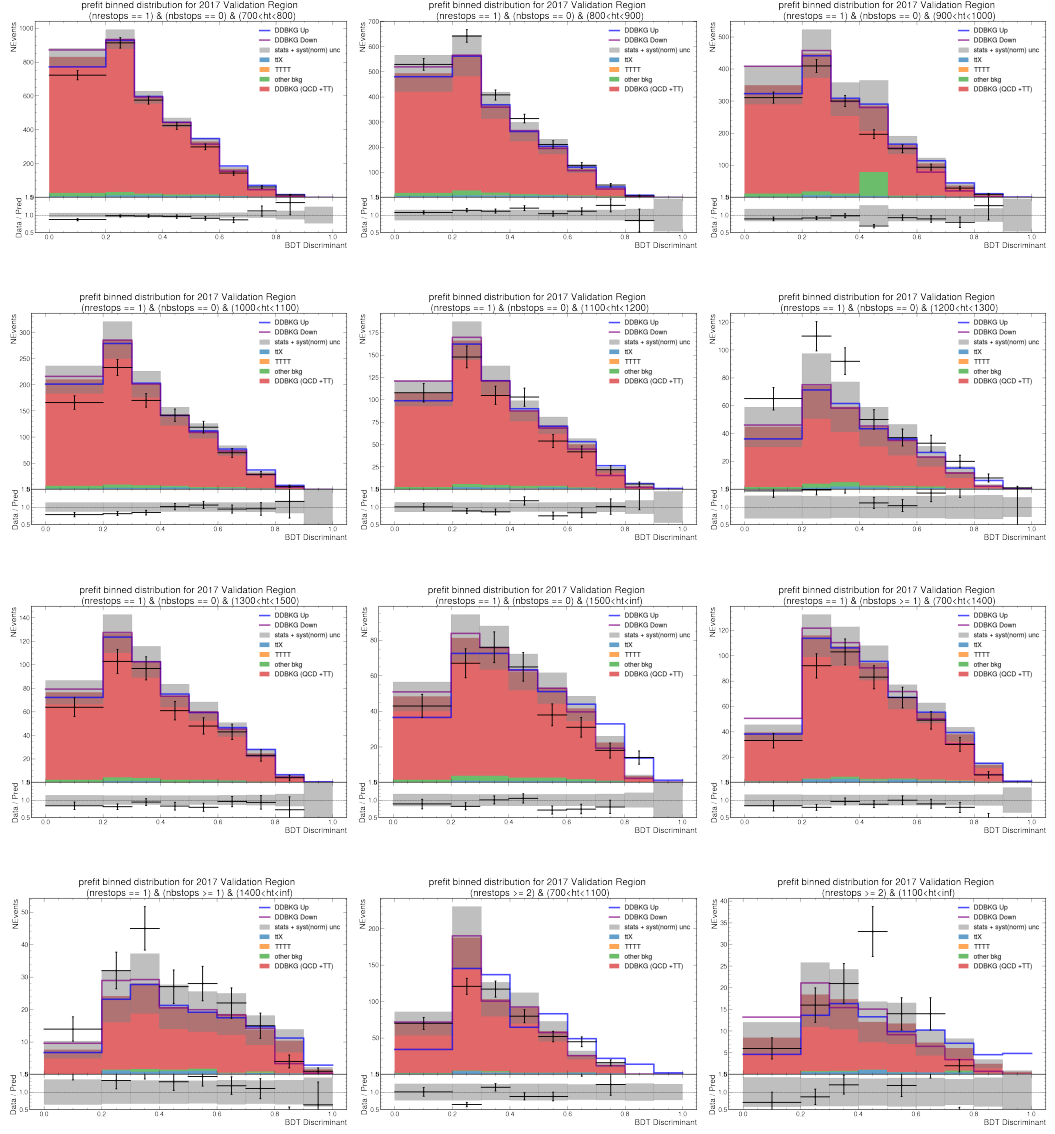


Figure 23: Pre-fit binned BDT distribution for Validation Region for 2017. DDBKG (data-driven background) is the predicted TT+QCD distribution from extendedABCD and ABCDnn. DDBKG Up/Down is the shift in distribution from systematic uncertainty estimation of ABCDnn. Shaded region represented statistical + normalization systematic uncertainty from extendedABCD.

## A Pre-fit binned BDT distribution for Validation Region

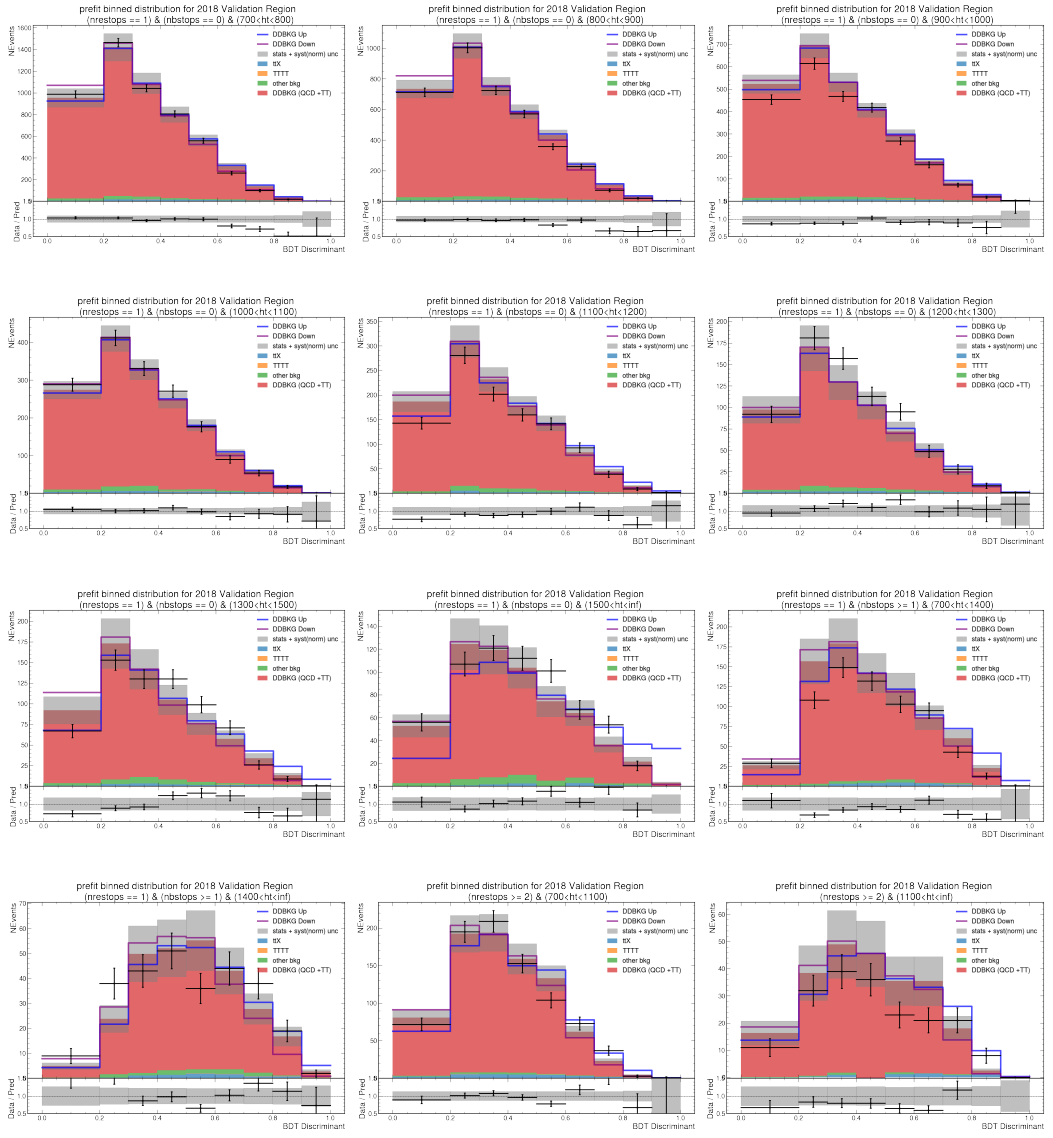


Figure 24: Pre-fit binned BDT distribution for Validation Region for 2018. DDBKG (data-driven background) is the predicted TT+QCD distribution from extendedABCD and ABCDnn. DDBKG Up/Down is the shift in distribution from systematic uncertainty estimation of ABCDnn. Shaded region represented statistical + normalization systematic uncertainty from extendedABCD.

## A Pre-fit binned BDT distribution for Validation Region

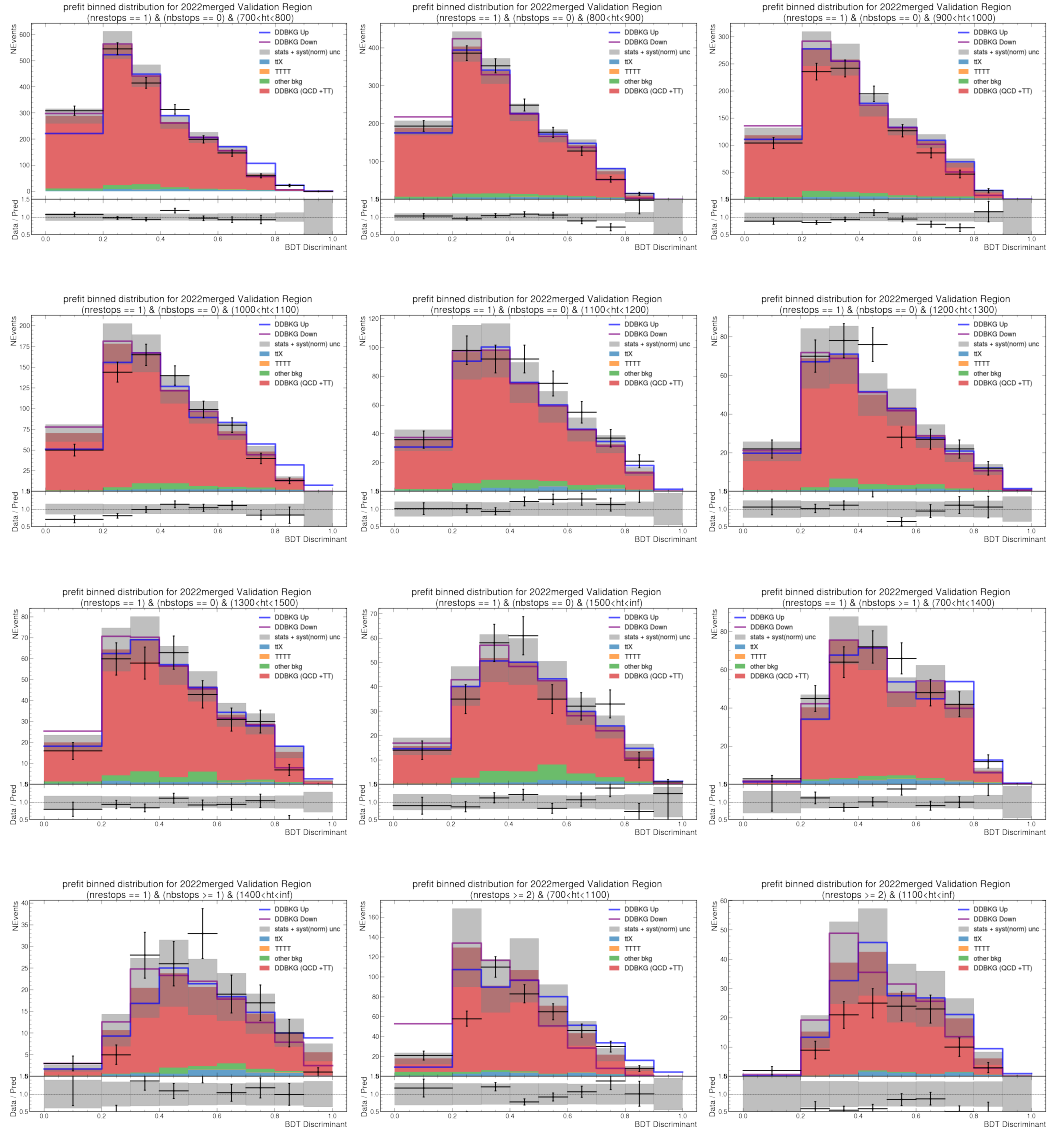


Figure 25: Pre-fit binned BDT distribution for Validation Region for 2022. DDBKG (data-driven background) is the predicted TT+QCD distribution from extendedABCD and ABCDnn. DDBKG Up/Down is the shift in distribution from systematic uncertainty estimation of ABCDnn. Shaded region represented statistical + normalization systematic uncertainty from extendedABCD.

## 520 B Pre-fit binned BDT distribution for Signal Region

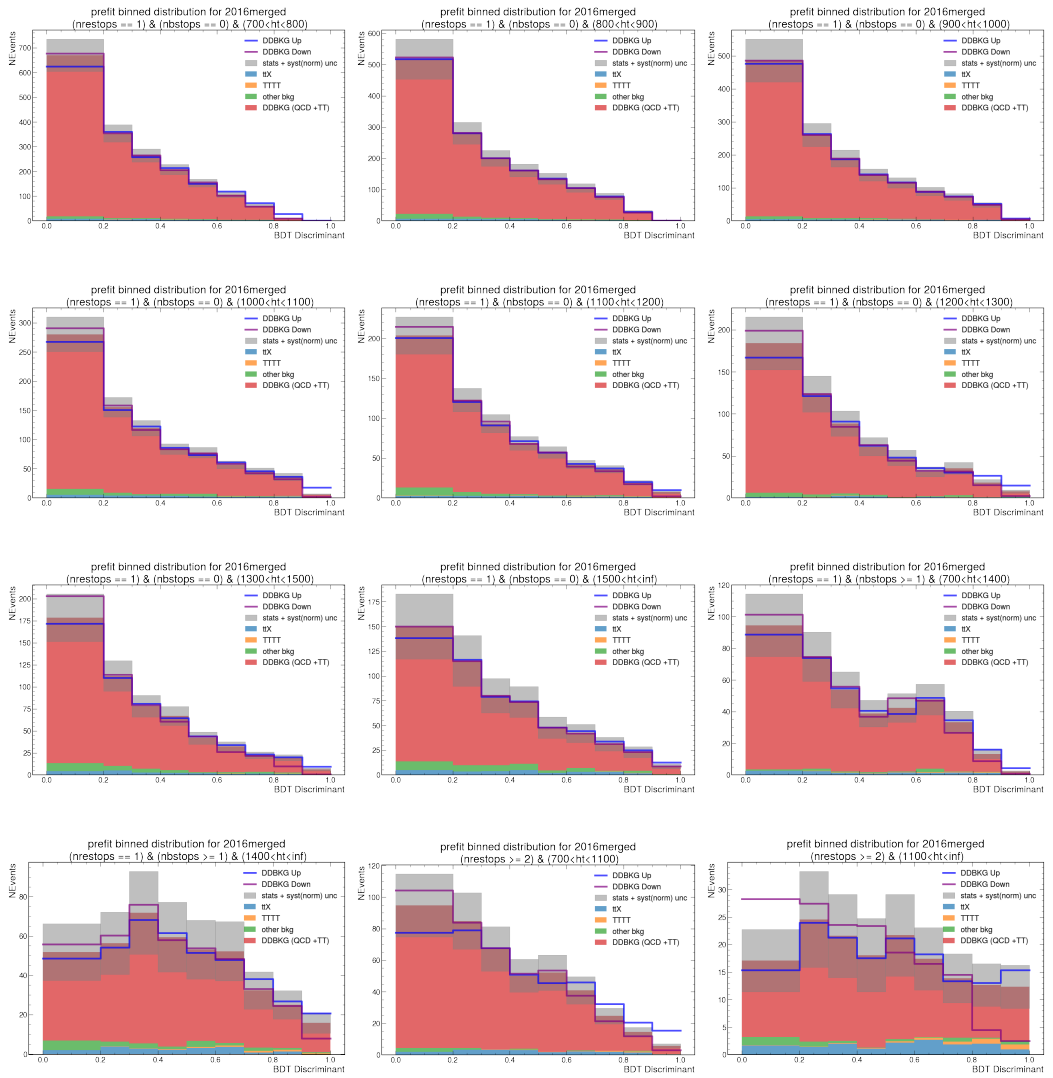


Figure 26: Pre-fit binned BDT distribution for Signal Region for 2016. DDBKG (data-driven background) is the predicted TT+QCD distribution from extendedABCD and ABCDnn. DDBKG Up/Down is the shift in distribution from systematic uncertainty estimation of ABCDnn. Shaded region represented statistical + normalization systematic uncertainty from extendedABCD.

## B Pre-fit binned BDT distribution for Signal Region

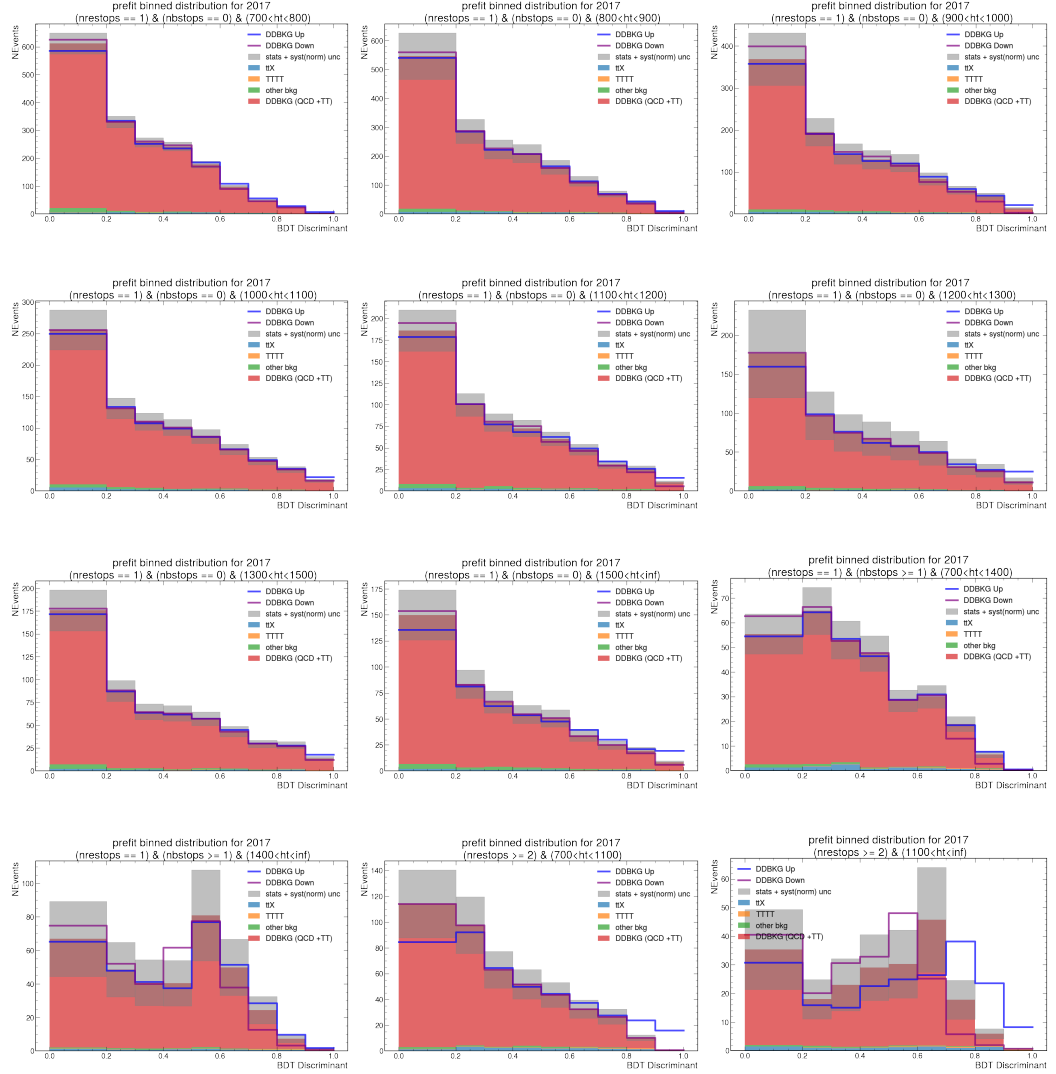


Figure 27: Pre-fit binned BDT distribution for Signal Region for 2017. DDBKG (data-driven background) is the predicted TT+QCD distribution from extendedABCD and ABCDnn. DDBKG Up/Down is the shift in distribution from systematic uncertainty estimation of ABCDnn. Shaded region represented statistical + normalization systematic uncertainty from extendedABCD.

## B Pre-fit binned BDT distribution for Signal Region

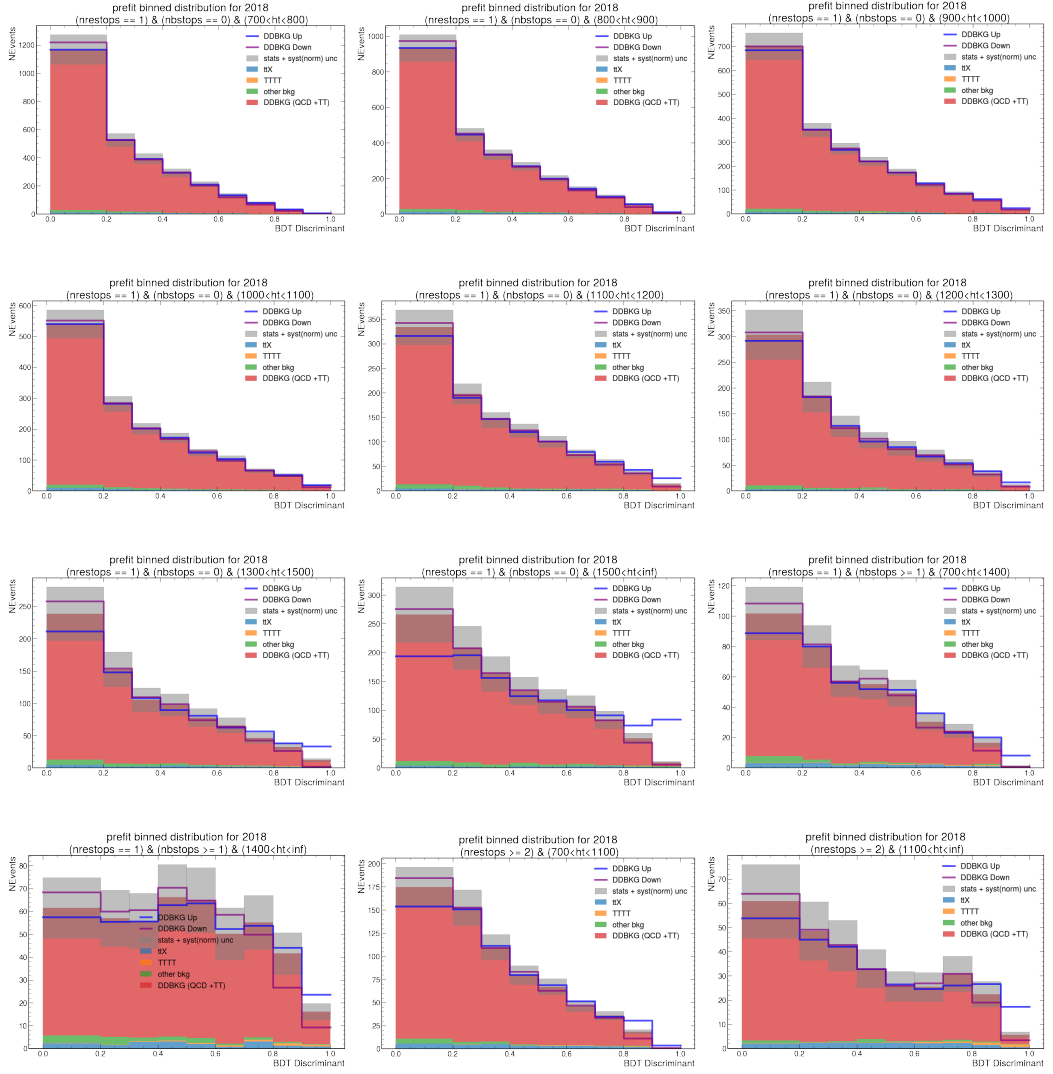


Figure 28: Pre-fit binned BDT distribution for Signal Region for 2018. DDBKG (data-driven background) is the predicted TT+QCD distribution from extendedABCD and ABCDnn. DDBKG Up/Down is the shift in distribution from systematic uncertainty estimation of ABCDnn. Shaded region represented statistical + normalization systematic uncertainty from extendedABCD.

## B Pre-fit binned BDT distribution for Signal Region

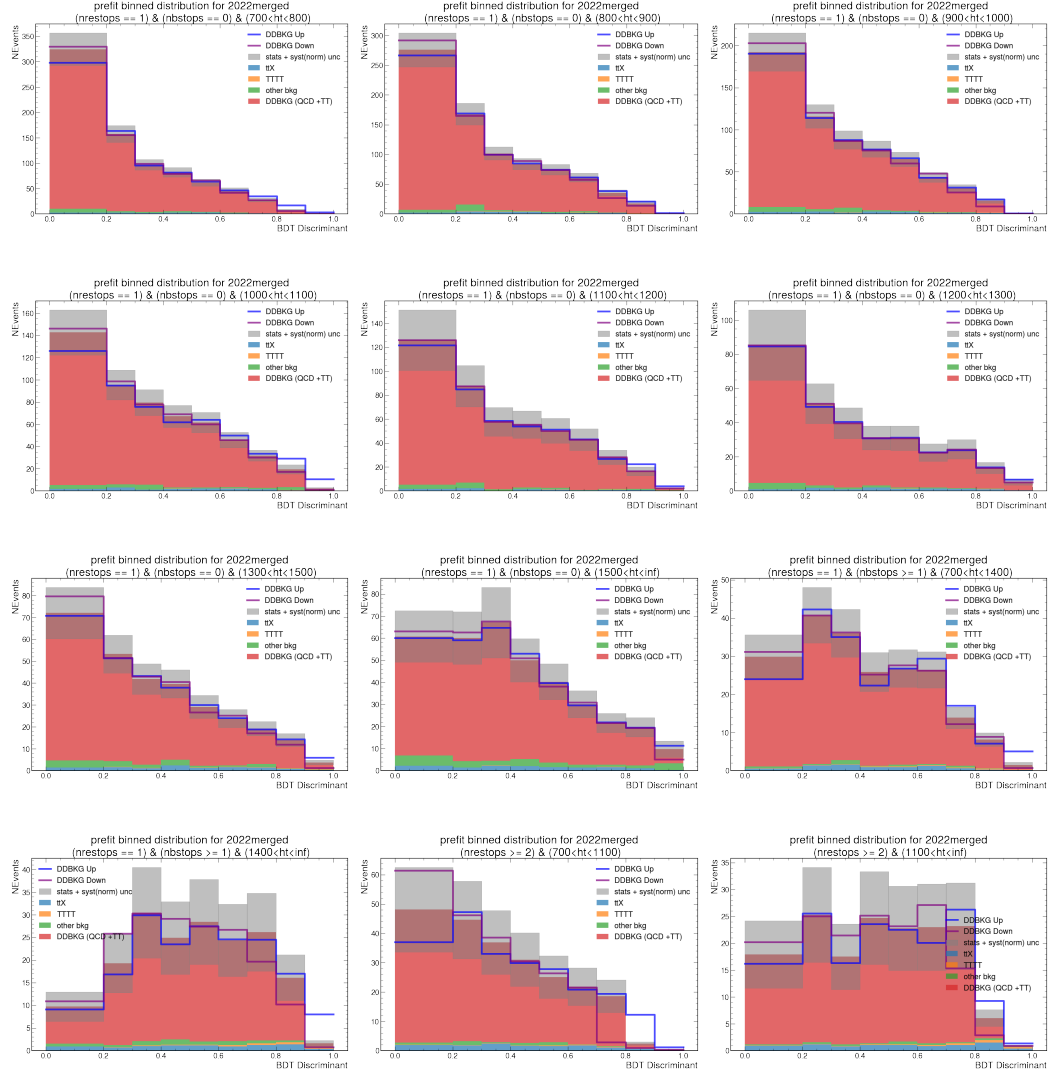


Figure 29: Pre-fit binned BDT distribution for Signal Region for 2022. DDBKG (data-driven background) is the predicted TT+QCD distribution from extendedABCD and ABCDnn. DDBKG Up/Down is the shift in distribution from systematic uncertainty estimation of ABCDnn. Shaded region represented statistical + normalization systematic unceetainty from extendedABCD.

## 521 C Extended ABCD yields in signal region

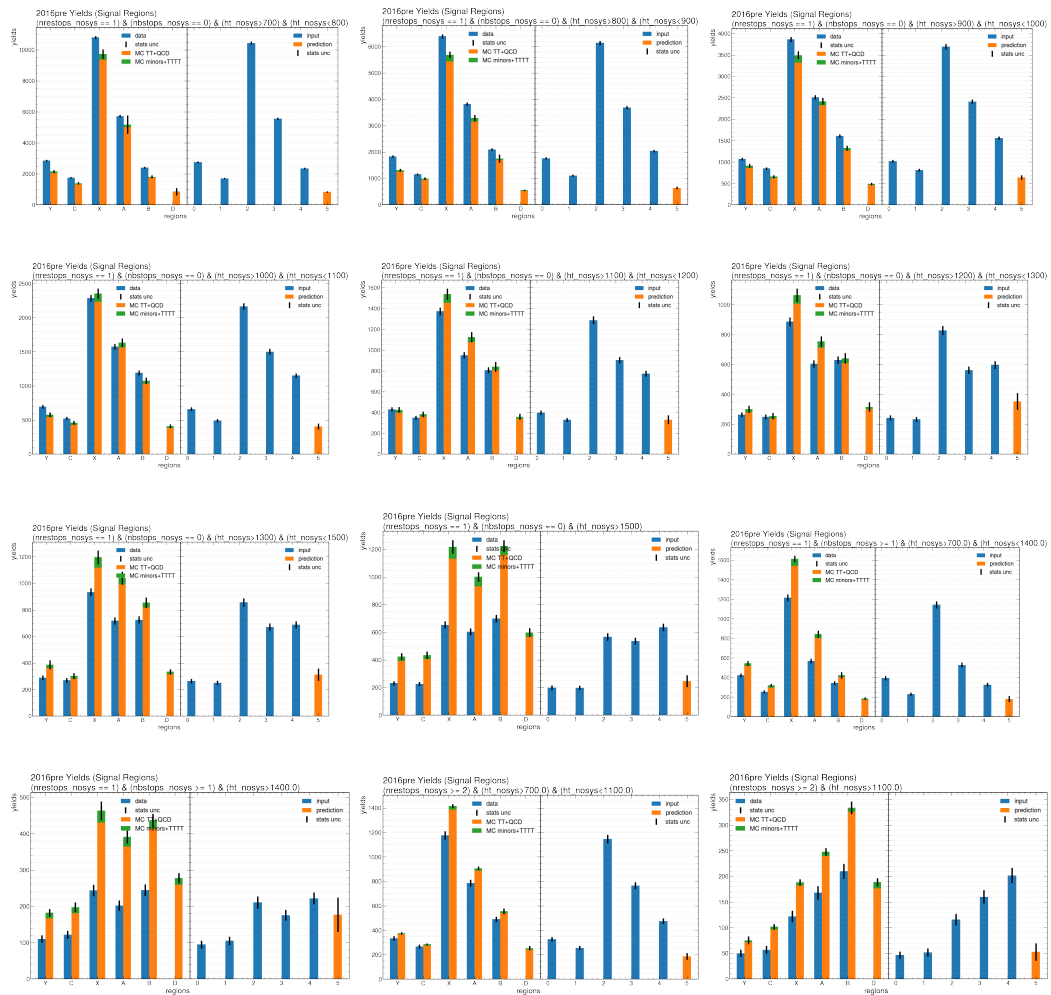


Figure 30: Left: Yields of data and MC in signal region for 2016preVFP. Right: Inputs to the extendedABCD algorithm are the (Data - MC minor backgrounds - MC TTTT) yields in the five control regions Y, C, X, A, and B. Predicted yield of TT+QCD is in region D. Uncertainty shown are statistical uncertainty of the CR inputs propagated.

### C Extended ABCD yields in signal region

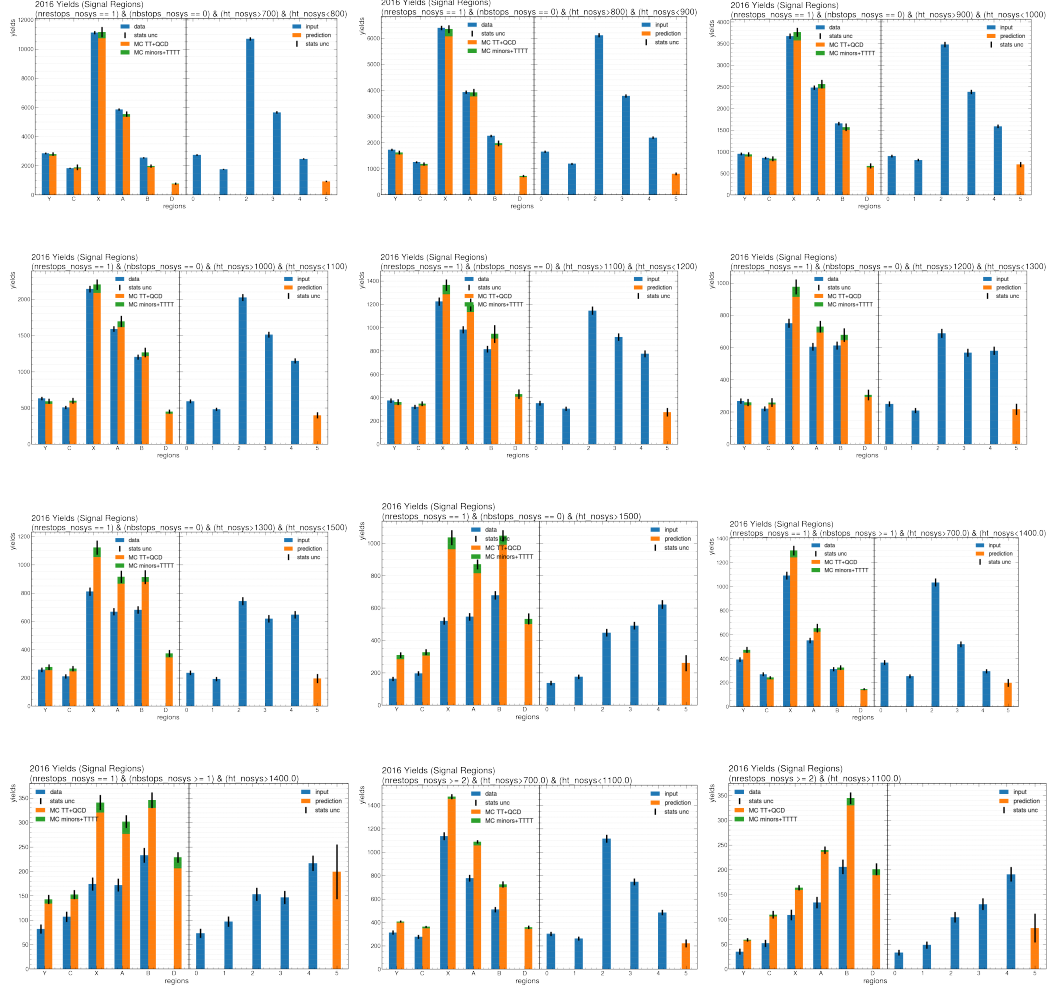


Figure 31: Left: Yields of data and MC in signal region for 2016. Right: Inputs to the extended ABCD algorithm are the (Data - MC minor backgrounds - MC TTT) yields in the five control regions Y, C, X, A, and B. Predicted yield of TT+QCD is in region D. Uncertainty shown are statistical uncertainty of the CR inputs propagated.

### C Extended ABCD yields in signal region

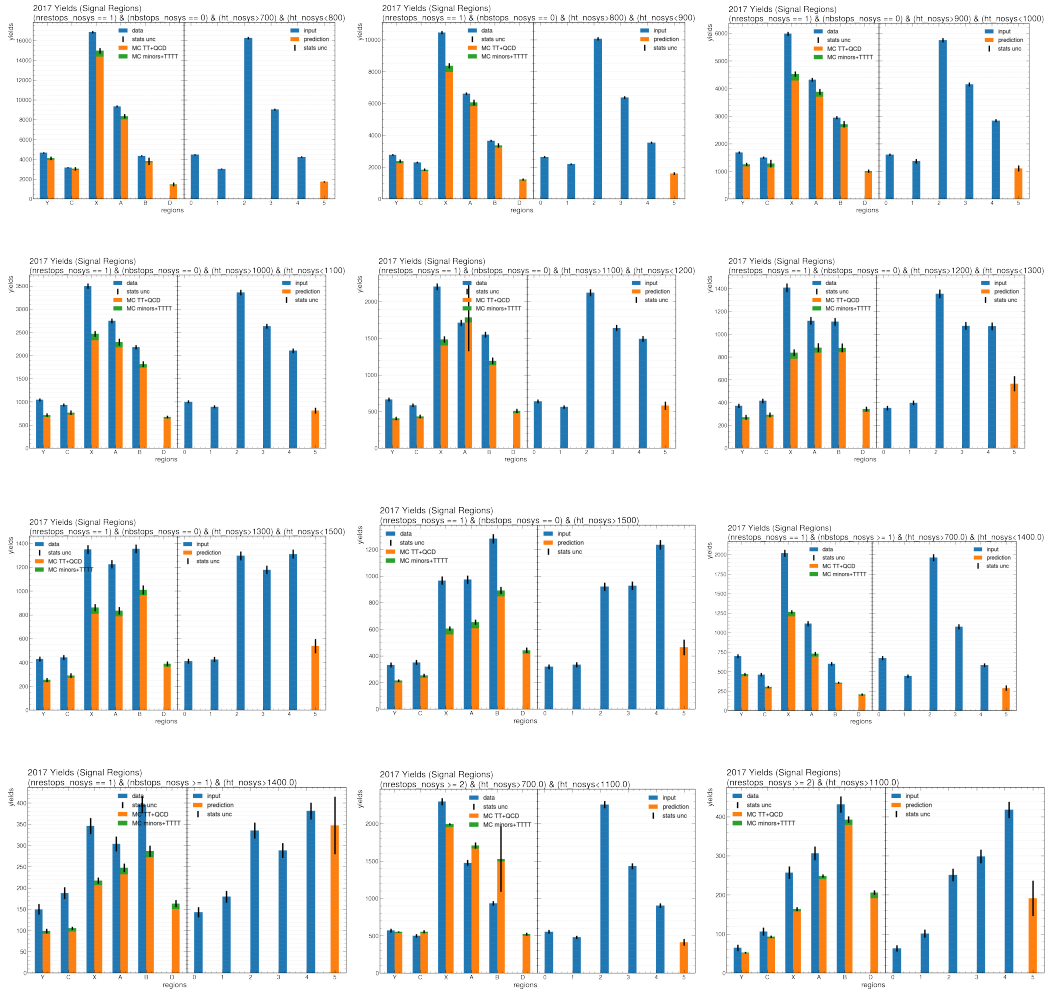


Figure 32: Left: Yields of data and MC in signal region for 2017. Right: Inputs to the extended ABCD algorithm are the (Data - MC minor backgrounds - MC TTT) yields in the five control regions Y, C, X, A, and B. Predicted yield of TT+QCD is in region D. Uncertainty shown are statistical uncertainty of the CR inputs propagated.

### C Extended ABCD yields in signal region

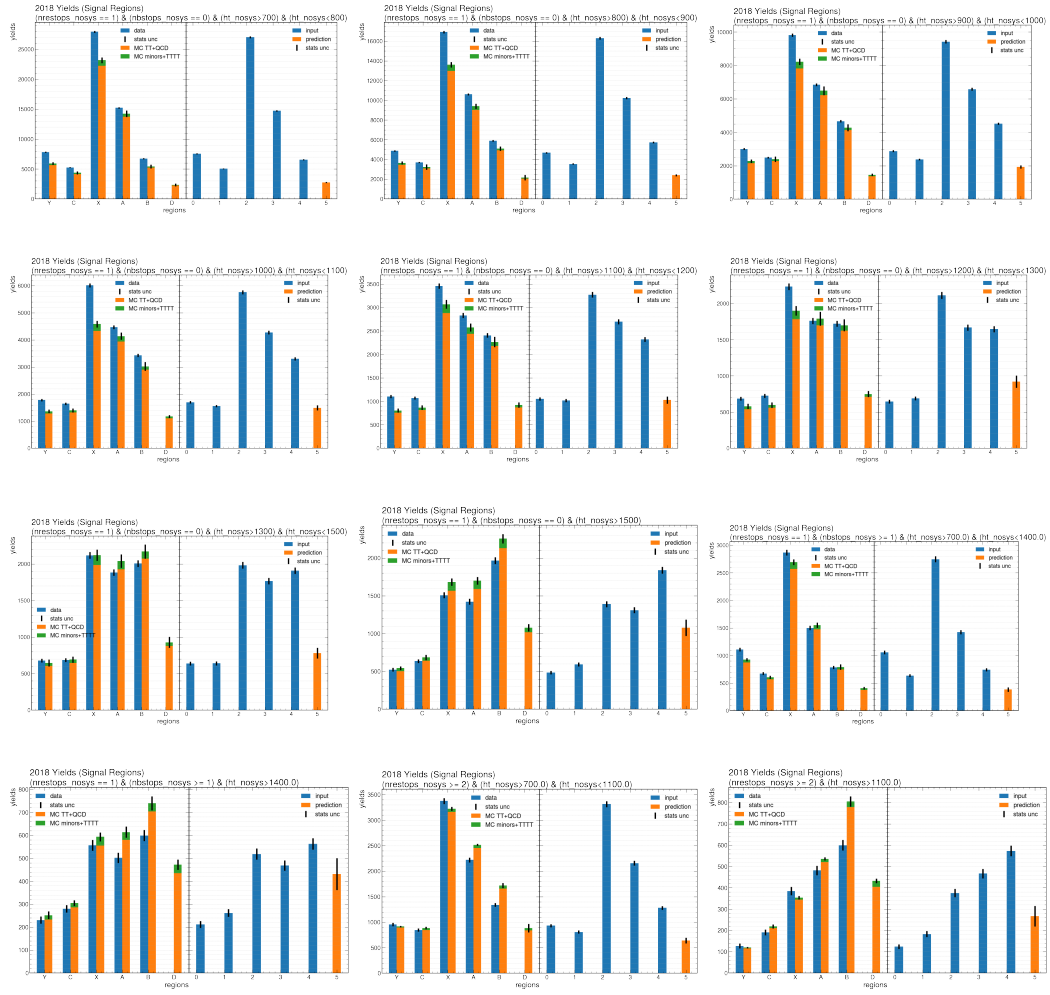


Figure 33: Left: Yields of data and MC in signal region for 2018. Right: Inputs to the extended-ABCD algorithm are the (Data - MC minor backgrounds - MC TTT) yields in the five control regions Y, C, X, A, and B. Predicted yield of TT+QCD is in region D. Uncertainty shown are statistical uncertainty of the CR inputs propagated.

### C Extended ABCD yields in signal region

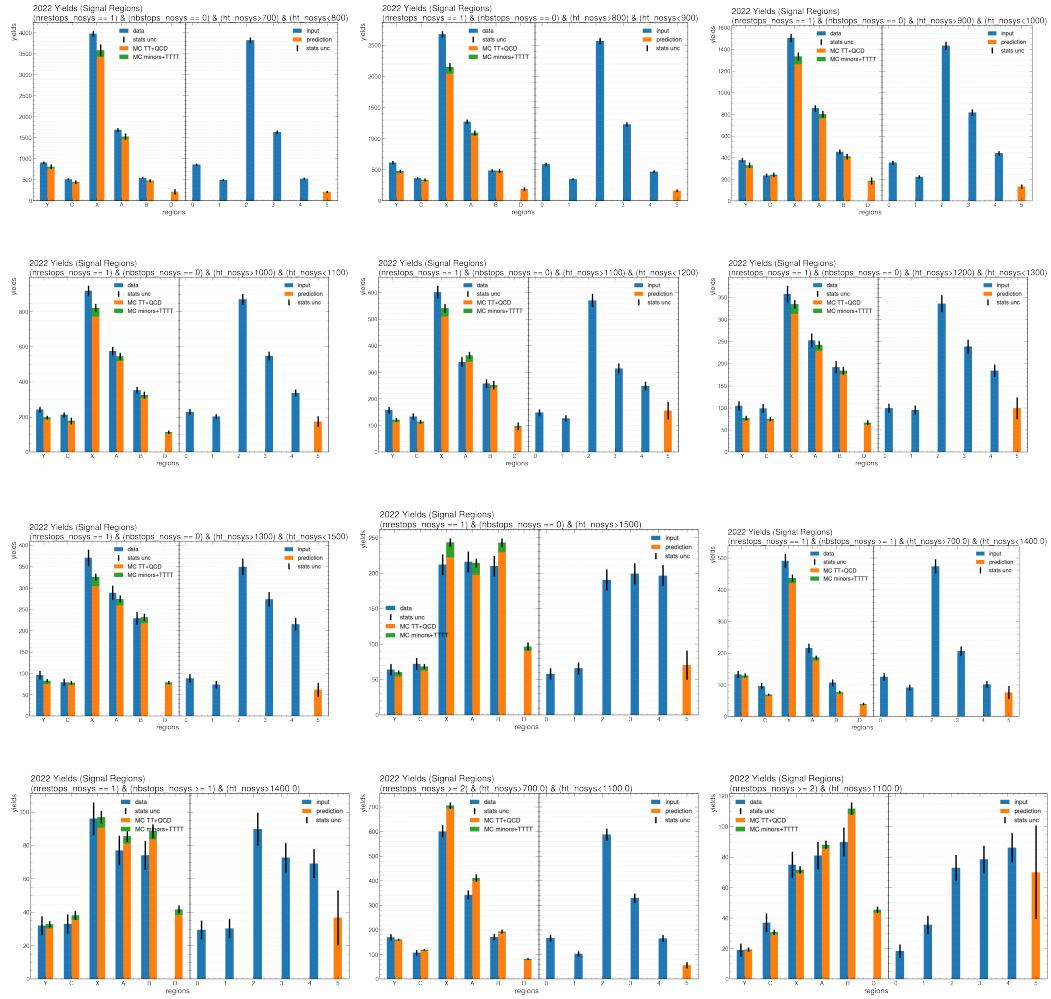


Figure 34: Left: Yields of data and MC in signal region for 2022. Right: Inputs to the extended-ABCD algorithm are the (Data - MC minor backgrounds - MC TTT) yields in the five control regions Y, C, X, A, and B. Predicted yield of TT+QCD is in region D. Uncertainty shown are statistical uncertainty of the CR inputs propagated.

### C Extended ABCD yields in signal region

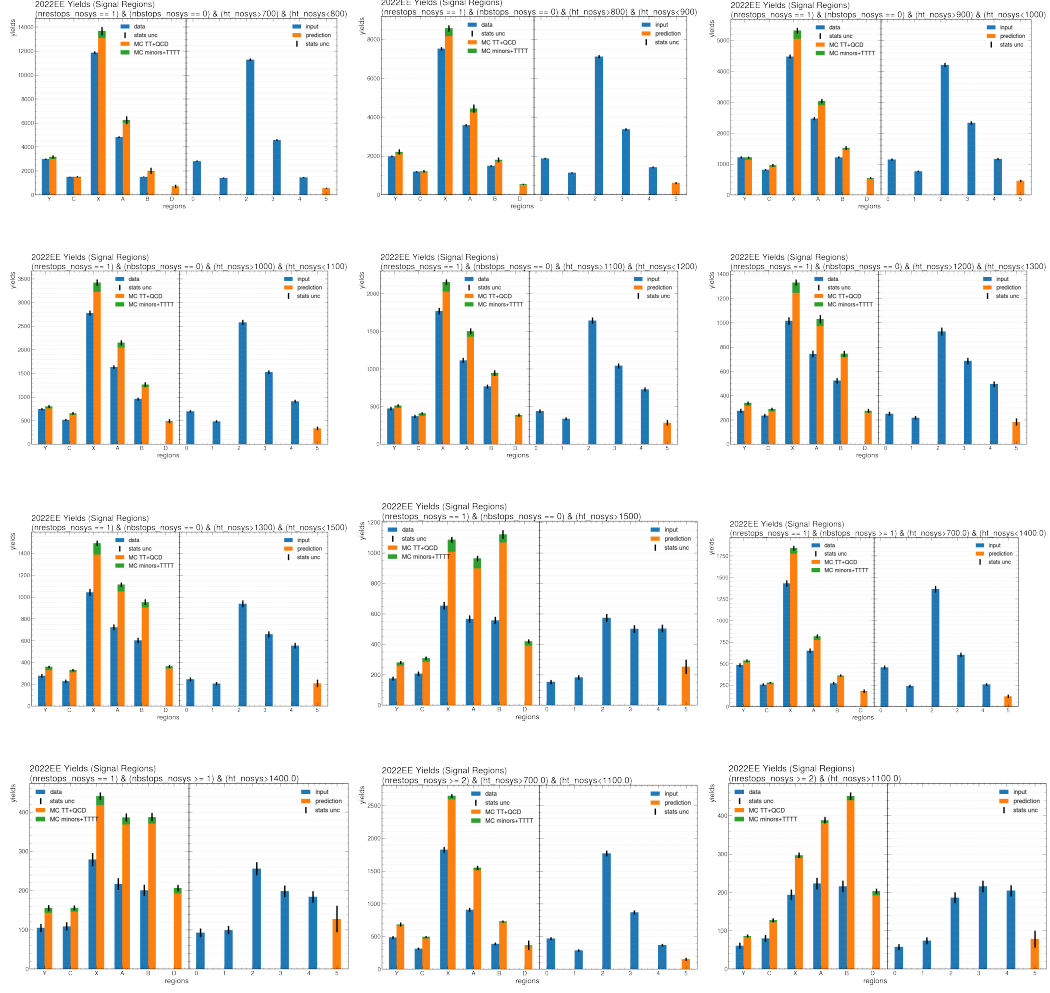


Figure 35: Left: Yields of data and MC in signal region for 2022EE. Right: Inputs to the extendedABCD algorithm are the (Data - MC minor backgrounds - MC TTTT) yields in the five control regions Y, C, X, A, and B. Predicted yield of TT+QCD is in region D. Uncertainty shown are statistical uncertainty of the CR inputs propagated.

## 522 D Extended ABCD yields in validation region



Figure 36: Left: Yields of data and MC in validation region for 2016preVFP. Right: Inputs to the extendedABCD algorithm are the (Data - MC minor backgrounds - MC TTTT) yields in the five control regions Y, C, X, A, and B. Truth is the (Data - MC minor backgrounds - MC TTTT) yield in region D, as compared against predicted yield of TT+QCD in region D. Uncertainty shown are statistical uncertainty of the CR inputs propagated.

## D Extended ABCD yields in validation region



Figure 37: Left: Yields of data and MC in validation region for 2016. Right: Inputs to the extendedABCD algorithm are the (Data - MC minor backgrounds - MC TTTT) yields in the five control regions Y, C, X, A, and B. Truth is the (Data - MC minor backgrounds - MC TTTT) yield in region D, as compared against predicted yield of TT+QCD in region D. Uncertainty shown are statistical uncertainty of the CR inputs propagated.

## D Extended ABCD yields in validation region

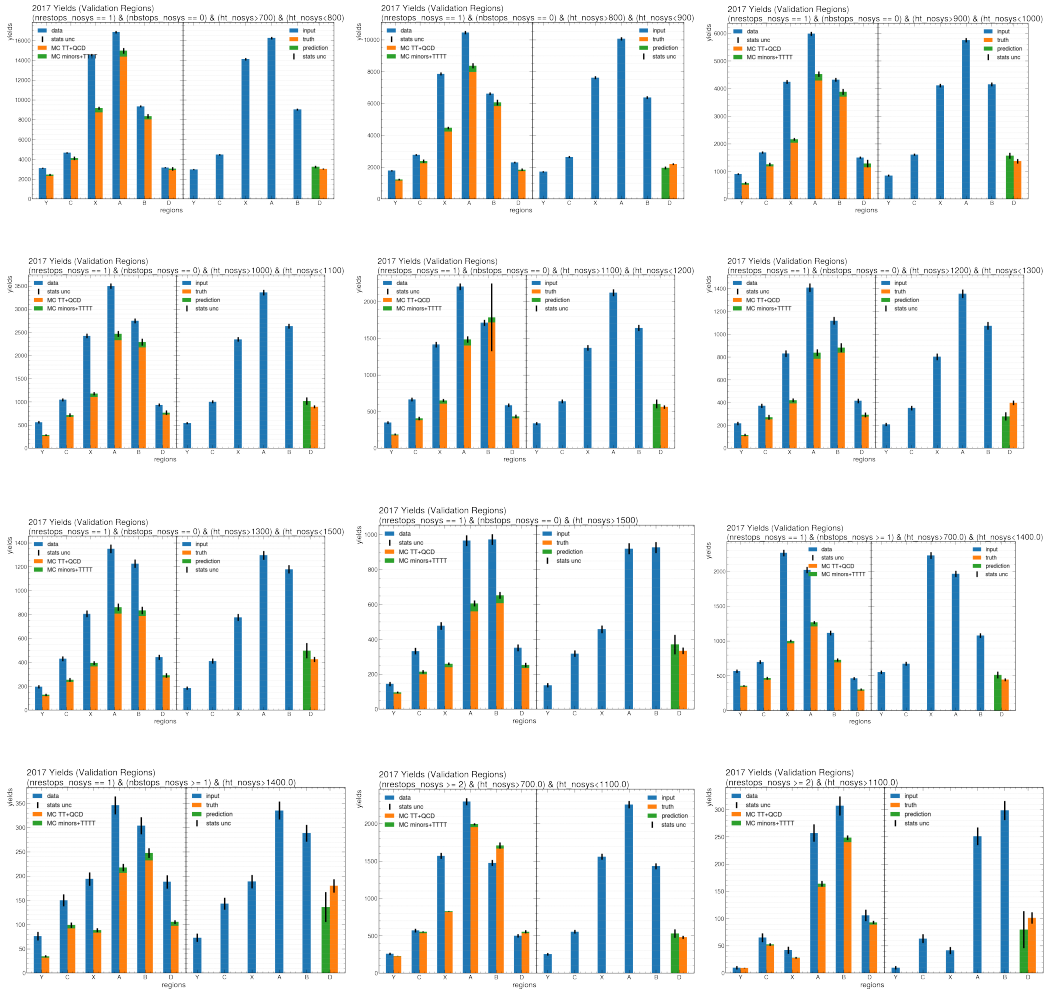


Figure 38: Left: Yields of data and MC in validation region for 2017. Right: Inputs to the extendedABCD algorithm are the (Data - MC minor backgrounds - MC TTTT) yields in the five control regions Y, C, X, A, and B. Truth is the (Data - MC minor backgrounds - MC TTTT) yield in region D, as compared against predicted yield of TT+QCD in region D. Uncertainty shown are statistical uncertainty of the CR inputs propagated.

## D Extended ABCD yields in validation region

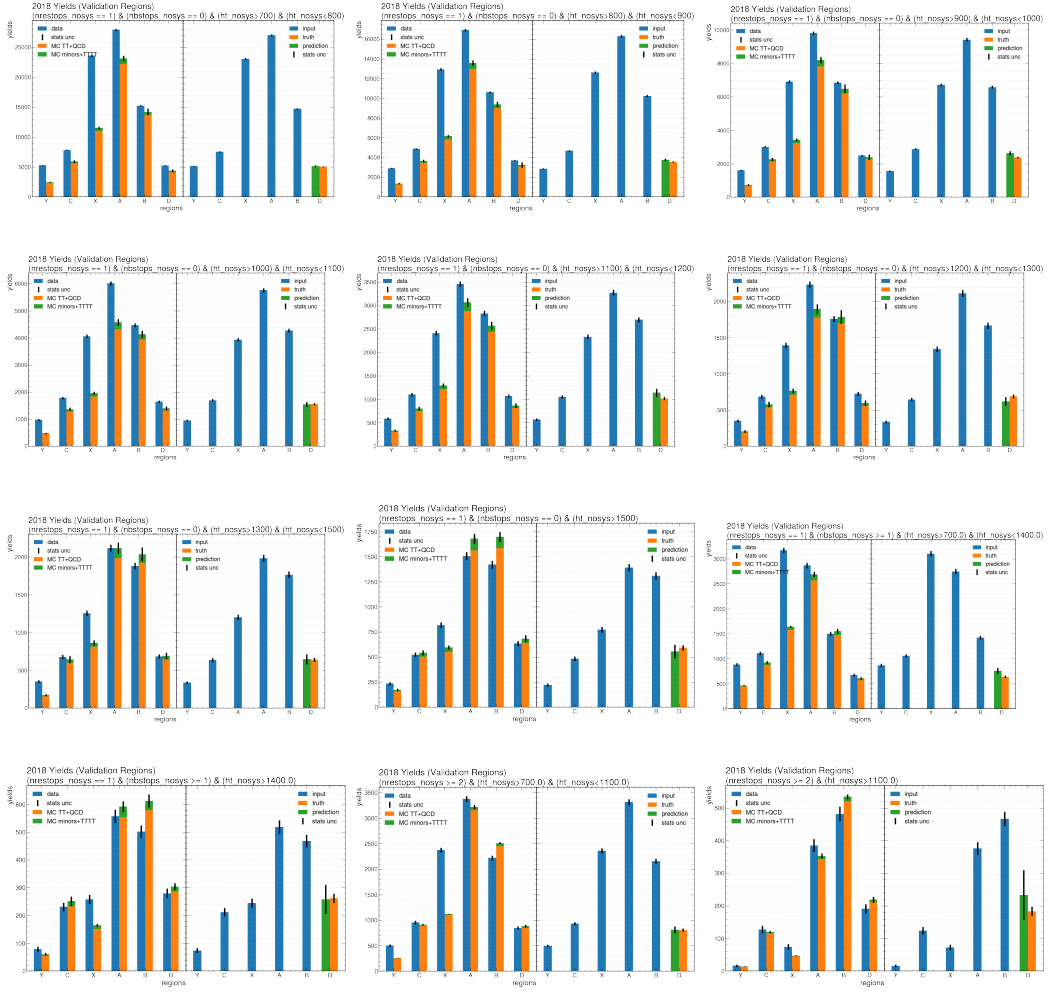


Figure 39: Left: Yields of data and MC in validation region for 2018. Right: Inputs to the extendedABCD algorithm are the (Data - MC minor backgrounds - MC TTTT) yields in the five control regions Y, C, X, A, and B. Truth is the (Data - MC minor backgrounds - MC TTTT) yield in region D, as compared against predicted yield of TT+QCD in region D. Uncertainty shown are statistical uncertainty of the CR inputs propagated.

## D Extended ABCD yields in validation region

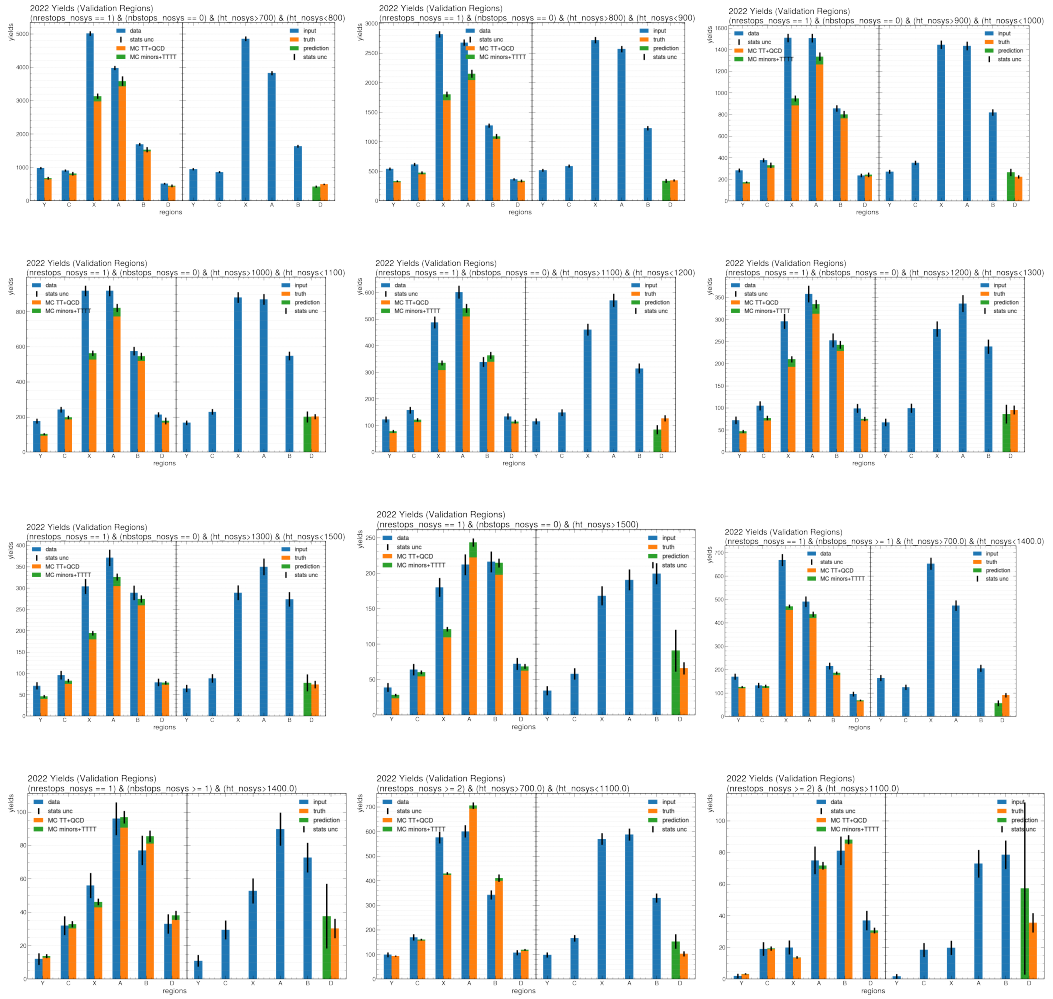


Figure 40: Left: Yields of data and MC in validation region for 2022. Right: Inputs to the extendedABCD algorithm are the (Data - MC minor backgrounds - MC TTTT) yields in the five control regions Y, C, X, A, and B. Truth is the (Data - MC minor backgrounds - MC TTTT) yield in region D, as compared against predicted yield of TT+QCD in region D. Uncertainty shown are statistical uncertainty of the CR inputs propagated.

## D Extended ABCD yields in validation region

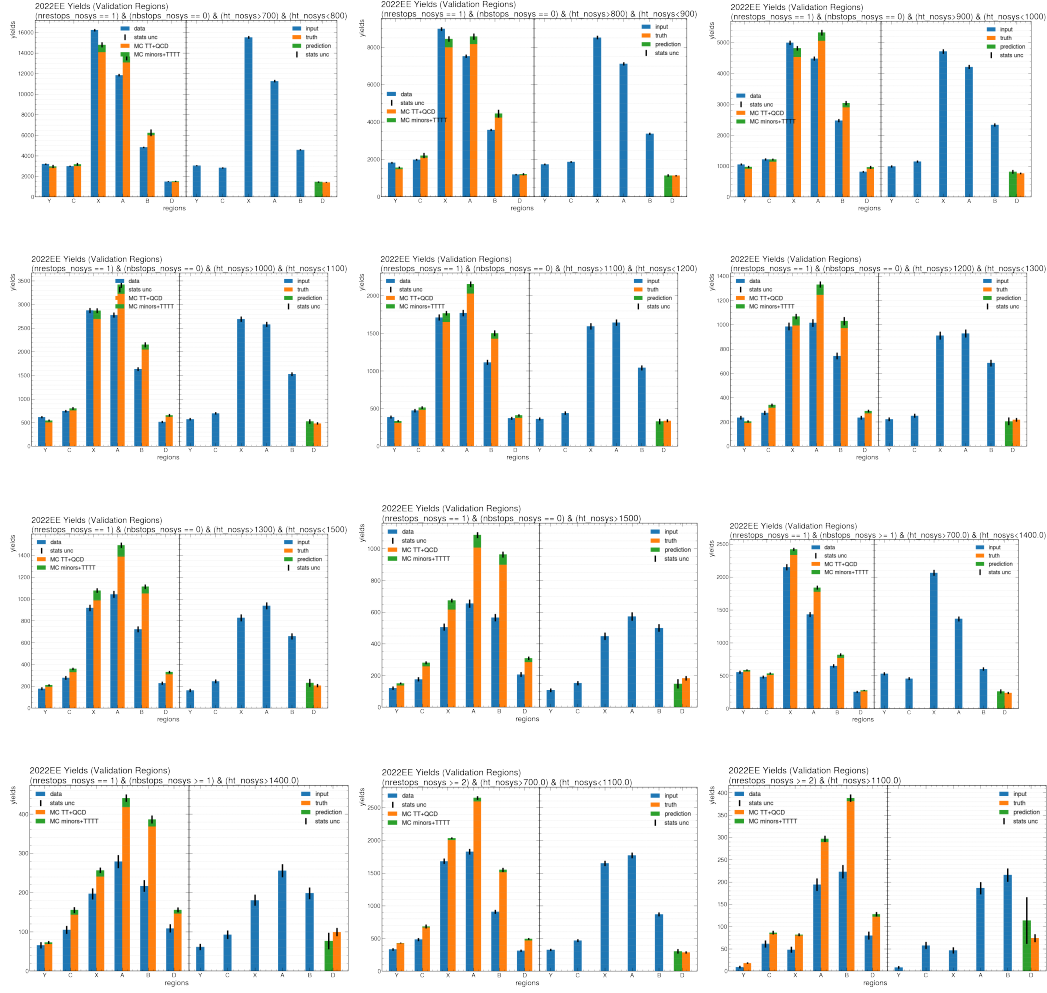
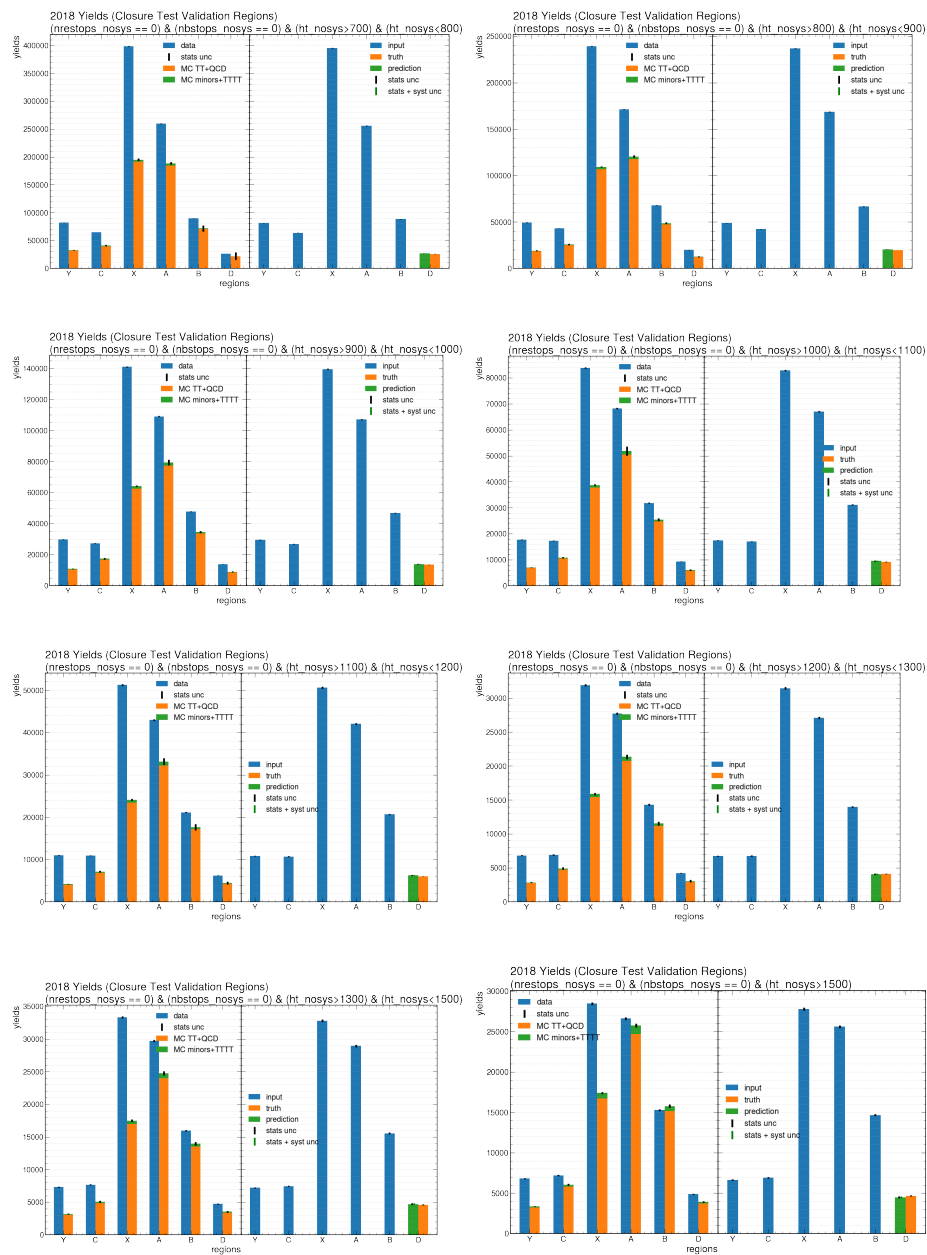


Figure 41: Left: Yields of data and MC in validation region for 2022EE. Right: Inputs to the extendedABCD algorithm are the (Data - MC minor backgrounds - MC TTTT) yields in the five control regions Y, C, X, A, and B. Truth is the (Data - MC minor backgrounds - MC TTTT) yield in region D, as compared against predicted yield of TT+QCD in region D. Uncertainty shown are statistical uncertainty of the CR inputs propagated.

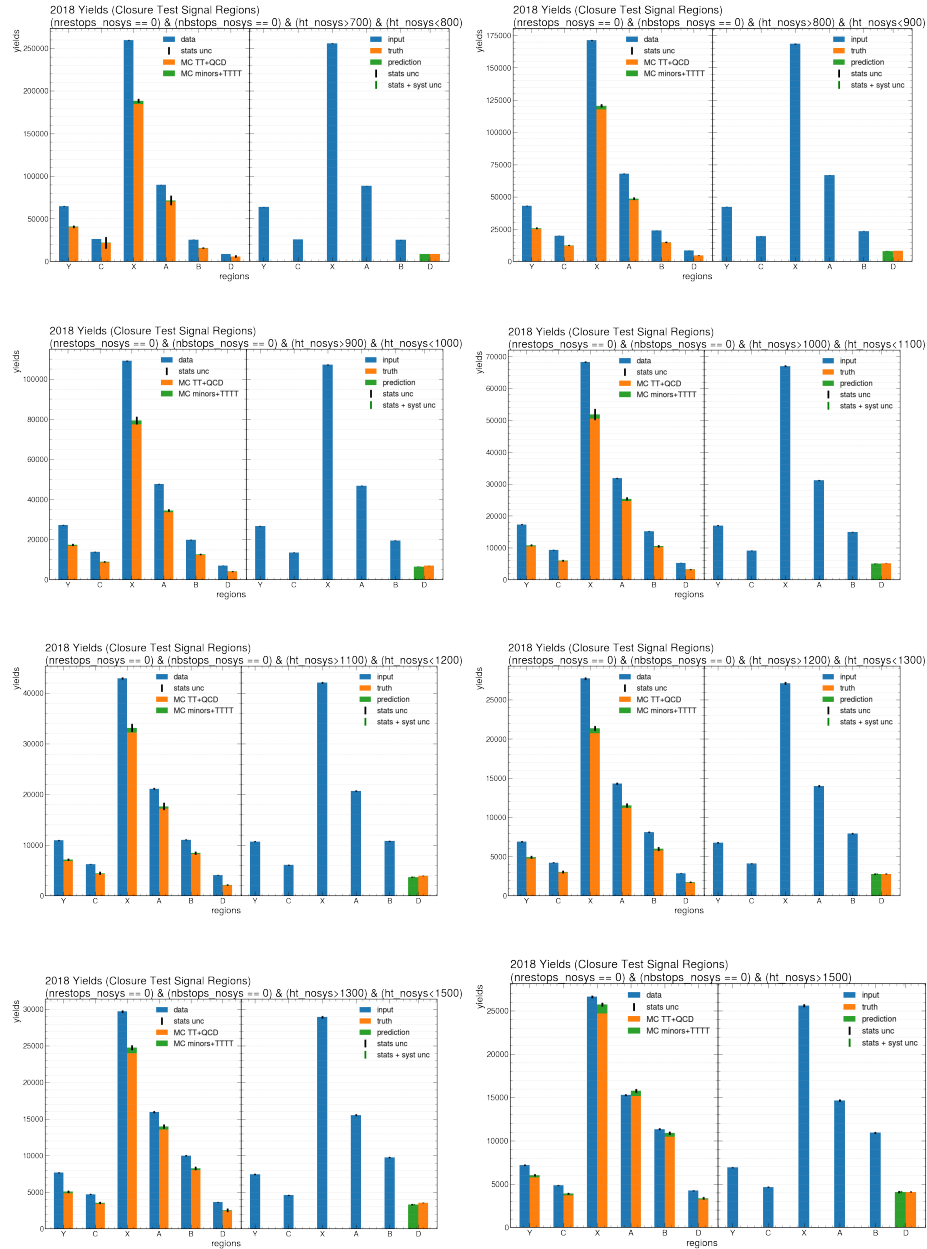
## 523 E Closure Test for Systematic Uncertainty of Extended ABCD

524



## E Closure Test for Systematic Uncertainty of Extended ABCD

Figure 42: Left: Yields of data and MC in closure test validation region for 2018, which is defined as  $N_{RT}=0$ ,  $N_{BT}=0$ ,  $N_{jet} == 8$  and  $N_{bjet} \geq 3$ , orthogonal to both Validation and Signal Region. To test our method for estimating systematic uncertainty for extendedABCD, normalization uncertainty is derived from this region to apply to the closure test signal region. Right: Inputs to the extendedABCD algorithm are the (Data - MC minor backgrounds - MC TTTT) yields in the five control regions Y, C, X, A, and B. Truth is the (Data - MC minor backgrounds - MC TTTT) yield in region D, as compared against predicted yield of TT+QCD in region D. Uncertainty shown are  $\pm$  statistical  $\pm$  systematic (normalization).



---

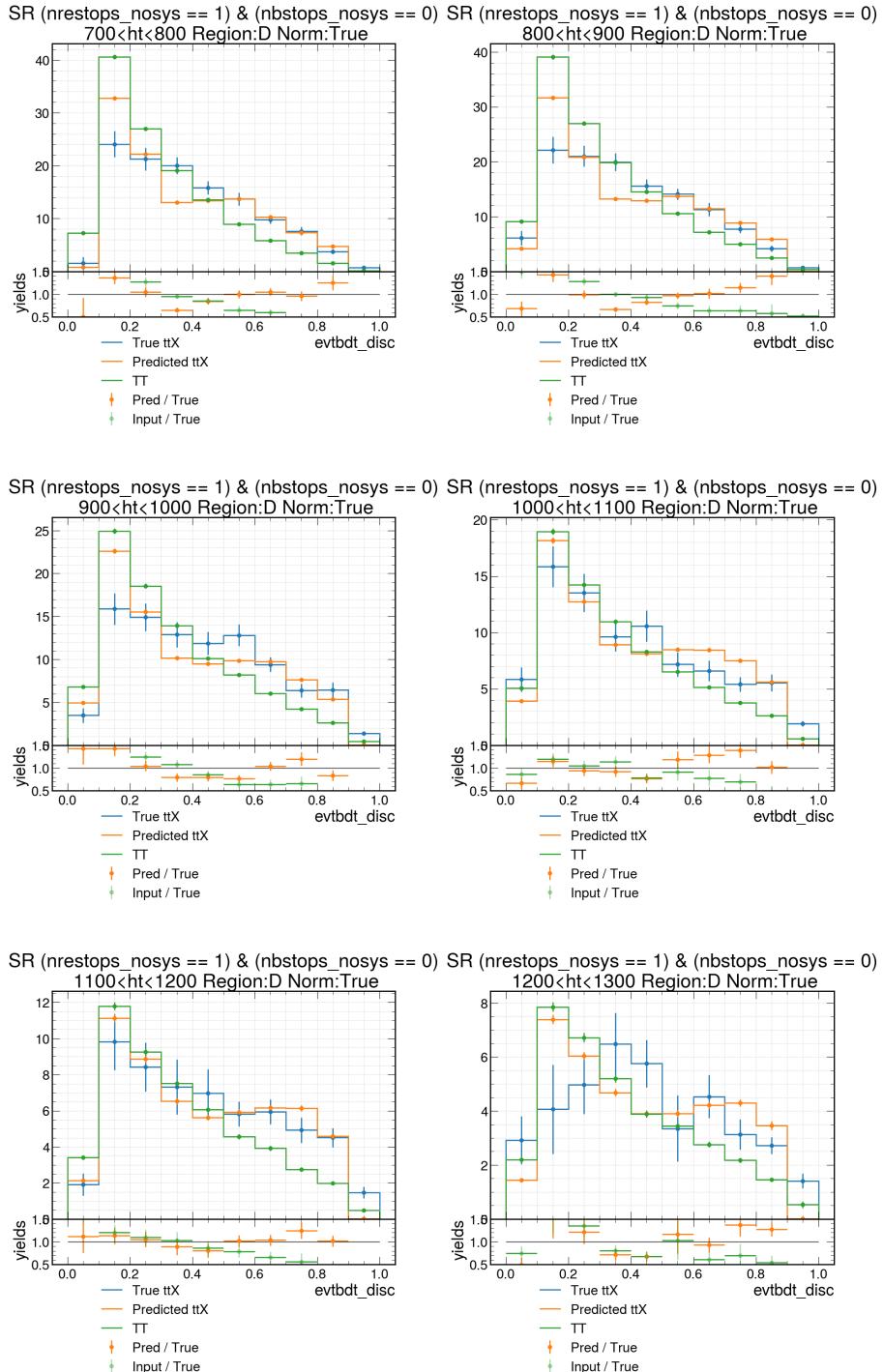
## E Closure Test for Systematic Uncertainty of Extended ABCD

Figure 43: Left: Yields of data and MC in closure test signal region for 2018, which is defined as  $N_{RT}=0$ ,  $N_{BT}=0$ ,  $N_{jet} \geq 9$  and  $N_{bjet} \geq 3$ , orthogonal to both Validation and Signal Region. To test our method for estimating systematic uncertainty for extendedABCD, normalization uncertainty is derived from the closure test validation region to apply to this region. Right: Inputs to the extendedABCD algorithm are the (Data - MC minor backgrounds - MC TTTT) yields in the five control regions Y, C, X, A, and B. Truth is the (Data - MC minor backgrounds - MC TTTT) yield in region D, as compared against predicted yield of TT+QCD in region D. Uncertainty shown are  $\pm$  statistical  $\pm$  systematic (normalization). These tables show that the method for estimating normalization systematic uncertainty of the extendedABCD as described in section 6.1.1 provides good coverage for the disagreement between truth and predicted.

## F ABCDnn closure test

---

### 525 F ABCDnn closure test



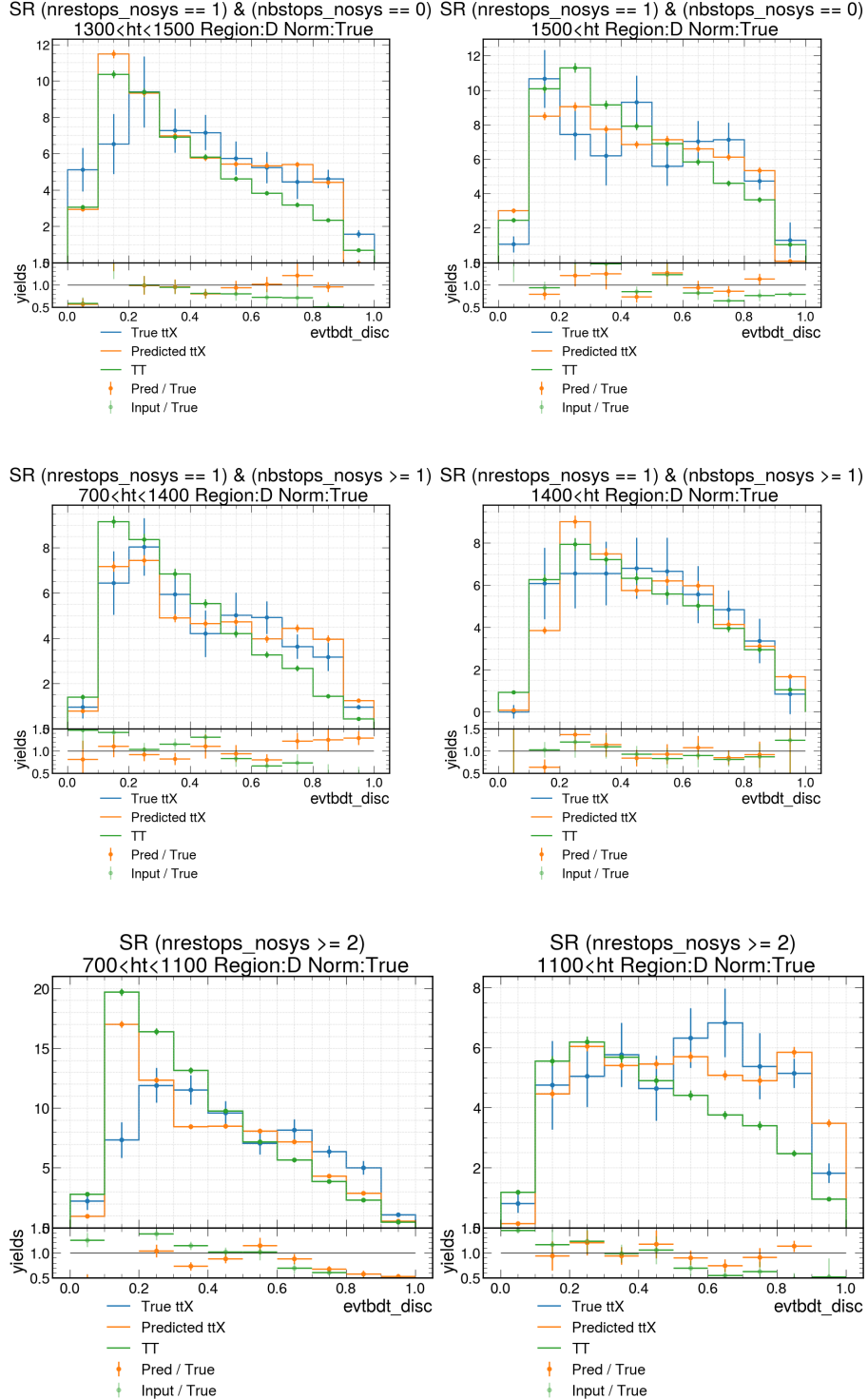


Figure 44: Results of morphing MC TT to ttX with 2016, 2017 and 2018 combined ultra-legacy dataset for the closure test of ABCDnn.

<sup>526</sup> **G Impact Plots**

<sup>527</sup> **G.1 2016**

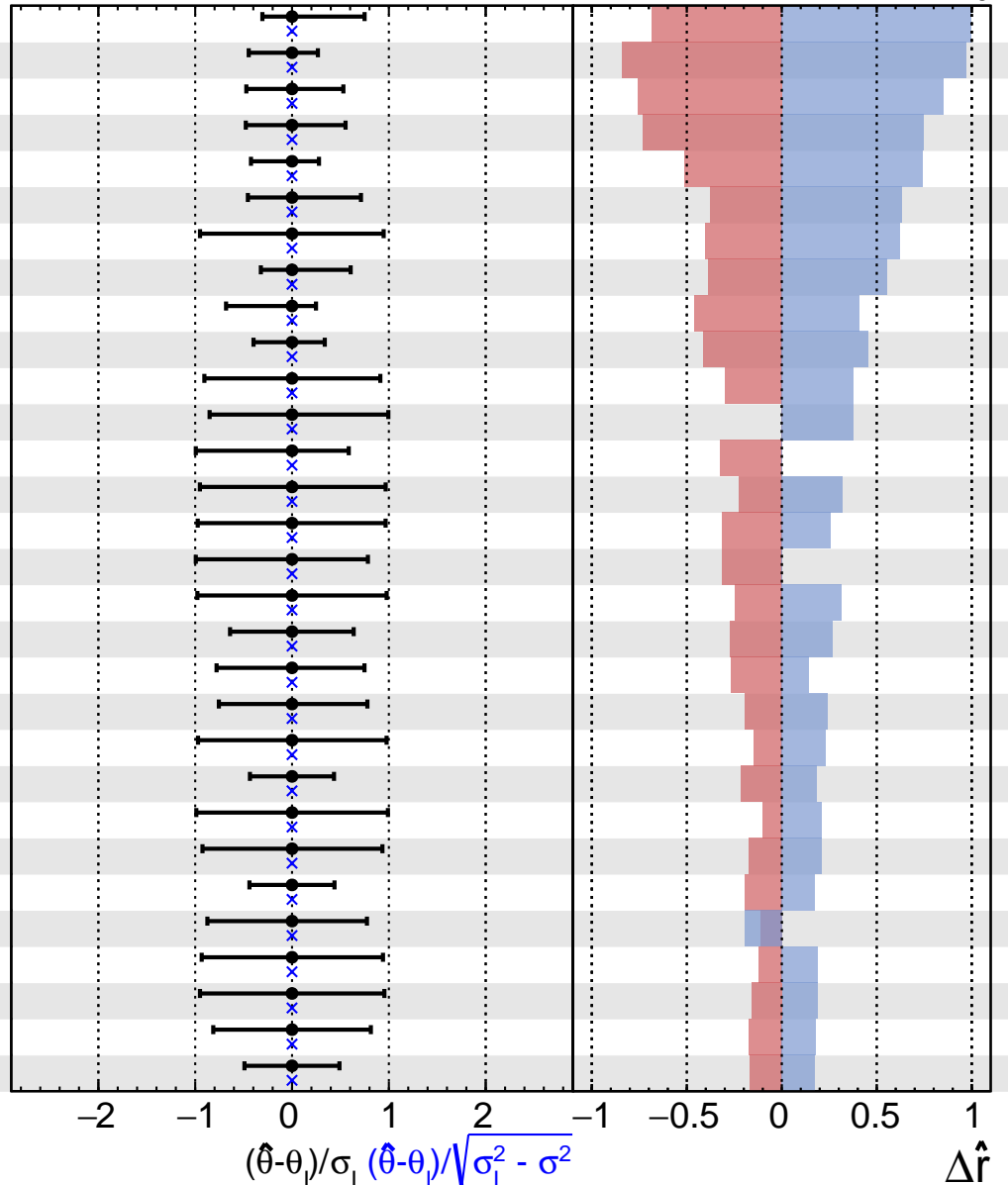
**CMS Internal**

$$\hat{r} = 1.0^{+1.0}_{-2.0}$$

```

1   data_pred_shape_disagreement_RT2BTALLhtbin1_2016merged
2   data_pred_shape_disagreement_RT2BTALLhtbin0_2016merged
3   data_pred_shape_disagreement_RT1BT1htbin0_2016merged
4   data_pred_shape_disagreement_RT1BT1htbin1_2016merged
5   data_pred_shape_disagreement_RT1BT0htbin3_2016merged
6   data_pred_shape_disagreement_RT1BT0htbin4_2016merged
7   btagCFerr1
8   data_pred_shape_disagreement_RT1BT0htbin6_2016merged
9   data_pred_shape_disagreement_RT1BT0htbin0_2016merged
10  data_pred_shape_disagreement_RT1BT0htbin5_2016merged
11  prop_binRT1BT1htbin1_2016merged_datacard9_bin7
12  data_pred_shape_disagreement_RT1BT0htbin1_2016merged
13  data_pred_shape_disagreement_RT1BT0htbin7_2016merged
14  PNetWSF_2016merged
15  cross_section
16  data_pred_shape_disagreement_RT1BT0htbin2_2016merged
17  btagCFerr2
18  data_pred_norm_disagreement_RT2BTALLhtbin1_2016merged
19  jes_2016merged
20  prop_binRT1BT0htbin3_2016merged_datacard3_bin7
21  prop_binRT1BT0htbin1_2016merged_datacard1_bin8
22  data_pred_norm_disagreement_RT2BTALLhtbin0_2016merged
23  btagLF
24  prop_binRT1BT0htbin2_2016merged_datacard2_bin8
25  data_pred_norm_disagreement_RT1BT1htbin0_2016merged
26  jer_2016merged
27  prop_binRT2BTALLhtbin1_2016merged_datacard11_bin6
28  prop_binRT2BTALLhtbin0_2016merged_datacard10_bin7
29  RT2BTALLhtbin1_2016merged_DDBKG_stat
30  data_pred_norm_disagreement_RT1BT1htbin1_2016merged

```

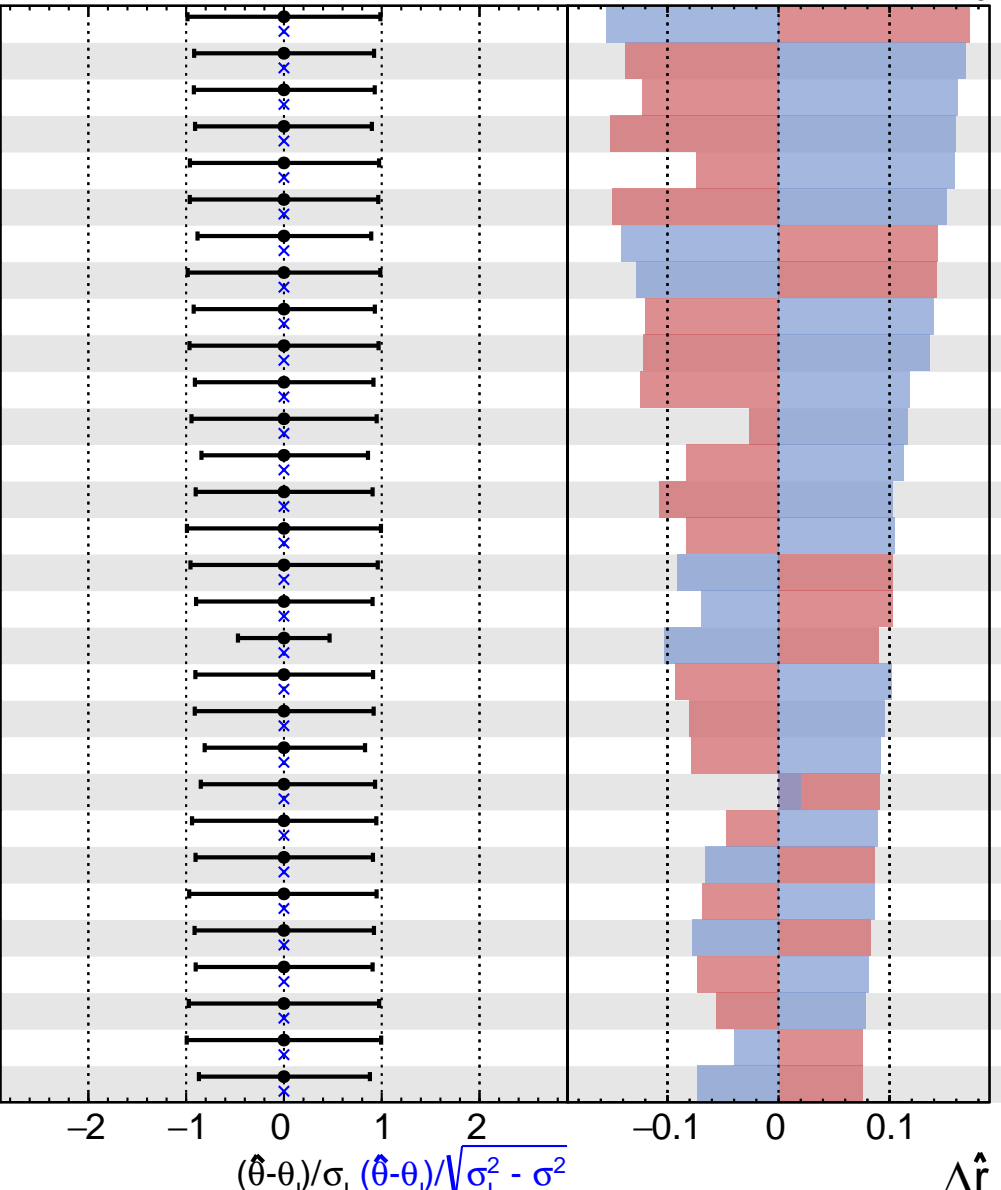


**CMS Internal**

$$\hat{r} = 1.0^{+1.0}_{-2.0}$$

31	btagLFstats1_2016merged
32	prop_binRT1BT1htbin0_2016merged_datacard8_bin4
33	prop_binRT1BT0htbin1_2016merged_datacard1_bin7
34	prop_binRT1BT0htbin7_2016merged_datacard7_bin8
35	prop_binRT1BT0htbin0_2016merged_datacard0_bin8
36	prop_binRT1BT1htbin0_2016merged_datacard8_bin8
37	prop_binRT1BT1htbin1_2016merged_datacard9_bin3
38	btagLFstats2_2016merged
39	prop_binRT1BT0htbin4_2016merged_datacard4_bin7
40	prop_binRT2BTALLhtbin1_2016merged_datacard11_bin7
41	prop_binRT1BT1htbin1_2016merged_datacard9_bin6
42	prop_binRT2BTALLhtbin1_2016merged_datacard11_bin0
43	prop_binRT1BT0htbin7_2016merged_datacard7_bin7
44	prop_binRT1BT0htbin2_2016merged_datacard2_bin7
45	ResTopMiss_2016merged
46	prop_binRT2BTALLhtbin1_2016merged_datacard11_bin4
47	prop_binRT1BT1htbin1_2016merged_datacard9_bin0
48	data_pred_norm_disagreement_RT1BT0htbin7_2016merged
49	prop_binRT1BT0htbin2_2016merged_datacard2_bin6
50	prop_binRT1BT0htbin3_2016merged_datacard3_bin6
51	prop_binRT1BT0htbin5_2016merged_datacard5_bin6
52	btagHF
53	prop_binRT1BT1htbin0_2016merged_datacard8_bin7
54	prop_binRT1BT1htbin1_2016merged_datacard9_bin1
55	PNetTopSF_2016merged
56	prop_binRT1BT1htbin0_2016merged_datacard8_bin1
57	prop_binRT1BT0htbin2_2016merged_datacard2_bin5
58	prop_binRT2BTALLhtbin1_2016merged_datacard11_bin8
59	btagHFstats1_2016merged
60	prop_binRT1BT0htbin7_2016merged_datacard7_bin3

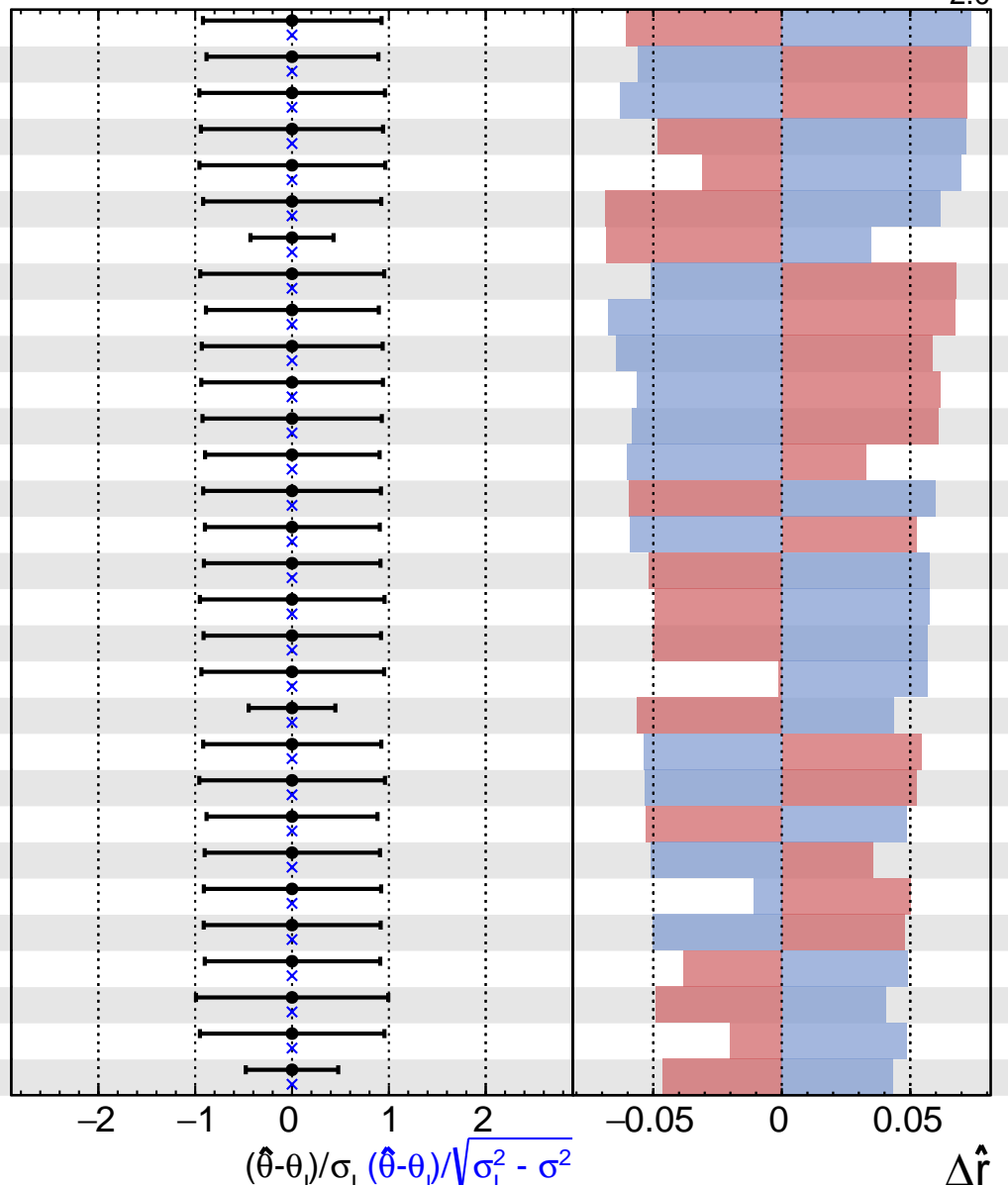
● Fit      +1 $\sigma$  Impact  
 ✕ Pull      -1 $\sigma$  Impact



**CMS Internal**

$$\hat{r} = 1.0^{+1.0}_{-2.0}$$

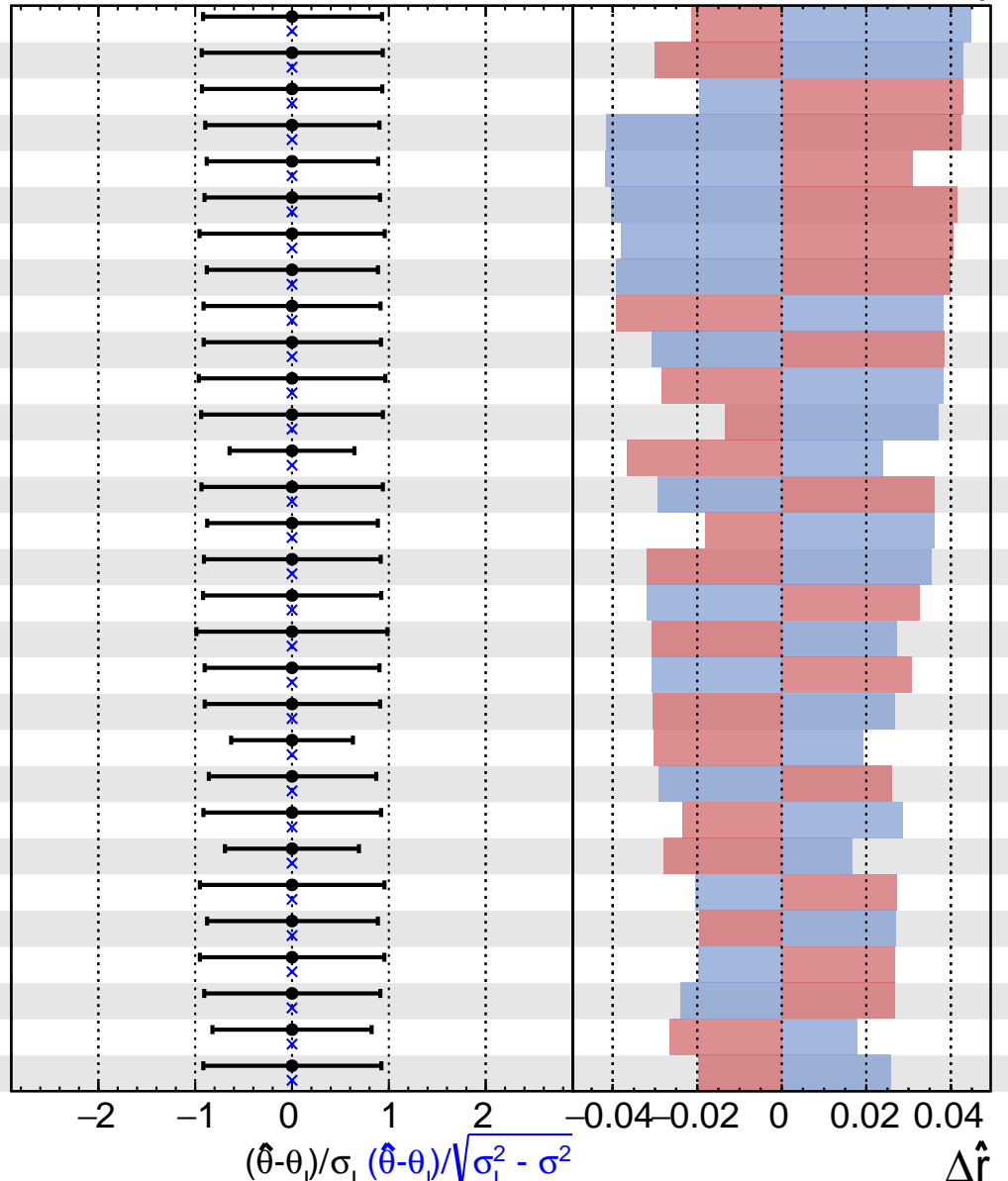
61	prop_binRT1BT0htbin1_2016merged_datacard1_bin6
62	prop_binRT1BT1htbin1_2016merged_datacard9_bin2
63	prop_binRT2BTALLhtbin1_2016merged_datacard11_bin1
64	prop_binRT1BT0htbin6_2016merged_datacard6_bin8
65	prop_binRT1BT0htbin4_2016merged_datacard4_bin8
66	prop_binRT1BT0htbin5_2016merged_datacard5_bin7
67	data_pred_norm_disagreement_RT1BT0htbin2_2016merged
68	prop_binRT2BTALLhtbin1_2016merged_datacard11_bin2
69	prop_binRT1BT0htbin5_2016merged_datacard5_bin2
70	prop_binRT1BT0htbin2_2016merged_datacard2_bin0
71	prop_binRT1BT0htbin1_2016merged_datacard1_bin0
72	prop_binRT1BT0htbin1_2016merged_datacard1_bin1
73	prop_binRT1BT0htbin4_2016merged_datacard4_bin3
74	RT2BTALLhtbin0_2016merged_DDBKG_stat
75	prop_binRT1BT0htbin7_2016merged_datacard7_bin1
76	prop_binRT1BT0htbin0_2016merged_datacard0_bin4
77	prop_binRT2BTALLhtbin0_2016merged_datacard10_bin4
78	prop_binRT1BT0htbin1_2016merged_datacard1_bin5
79	prop_binRT1BT1htbin1_2016merged_datacard9_bin8
80	data_pred_norm_disagreement_RT1BT0htbin1_2016merged
81	prop_binRT1BT0htbin3_2016merged_datacard3_bin2
82	prop_binRT2BTALLhtbin0_2016merged_datacard10_bin1
83	RT1BT1htbin1_2016merged_DDBKG_stat
84	prop_binRT1BT0htbin6_2016merged_datacard6_bin1
85	prop_binRT1BT1htbin0_2016merged_datacard8_bin6
86	prop_binRT1BT0htbin2_2016merged_datacard2_bin1
87	prop_binRT1BT0htbin6_2016merged_datacard6_bin6
88	trigger_2016merged
89	prop_binRT2BTALLhtbin1_2016merged_datacard11_bin3
90	data_pred_norm_disagreement_RT1BT0htbin0_2016merged



**CMS Internal**

$$\hat{r} = 1.0^{+1.0}_{-2.0}$$

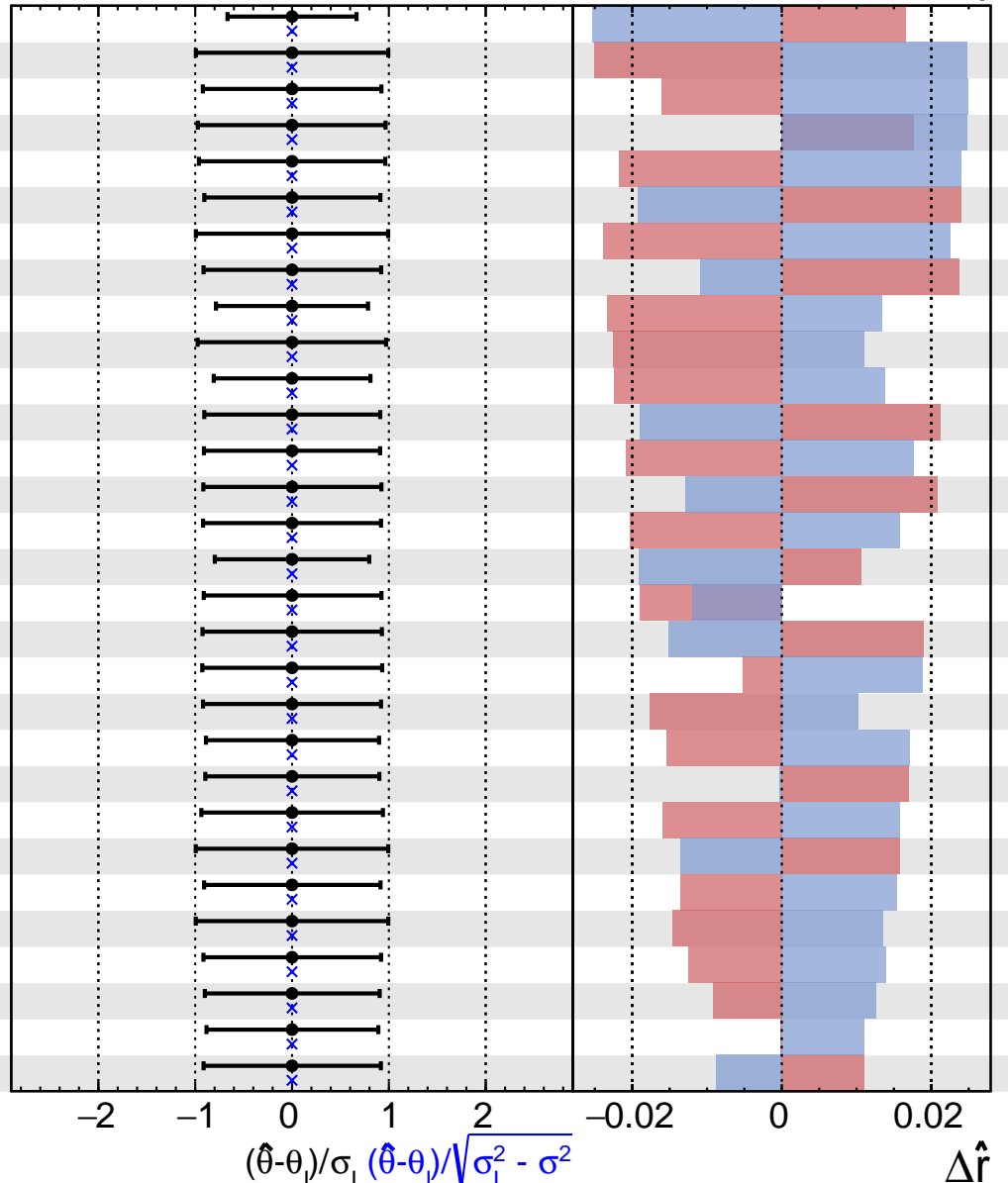
91	prop_binRT1BT0htbin6_2016merged_datacard6_bin7
92	prop_binRT1BT0htbin5_2016merged_datacard5_bin8
93	prop_binRT1BT0htbin4_2016merged_datacard4_bin0
94	prop_binRT1BT0htbin6_2016merged_datacard6_bin2
95	prop_binRT1BT0htbin6_2016merged_datacard6_bin3
96	prop_binRT1BT0htbin2_2016merged_datacard2_bin2
97	prop_binRT2BTALLhtbin0_2016merged_datacard10_bin2
98	prop_binRT1BT0htbin5_2016merged_datacard5_bin1
99	RT1BT1htbin0_2016merged_DDBKG_stat
100	prop_binRT1BT1htbin0_2016merged_datacard8_bin3
101	prop_binRT2BTALLhtbin0_2016merged_datacard10_bin0
102	prop_binRT1BT0htbin6_2016merged_datacard6_bin0
103	data_pred_norm_disagreement_RT1BT0htbin3_2016merged
104	prop_binRT1BT0htbin3_2016merged_datacard3_bin0
105	prop_binRT1BT1htbin1_2016merged_datacard9_bin5
106	prop_binRT1BT0htbin3_2016merged_datacard3_bin5
107	prop_binRT1BT0htbin0_2016merged_datacard0_bin1
108	prop_binRT1BT0htbin3_2016merged_datacard3_bin8
109	RT1BT0htbin7_2016merged_DDBKG_stat
110	prop_binRT1BT0htbin7_2016merged_datacard7_bin6
111	data_pred_norm_disagreement_RT1BT0htbin5_2016merged
112	prop_binRT1BT0htbin7_2016merged_datacard7_bin5
113	prop_binRT1BT0htbin1_2016merged_datacard1_bin4
114	data_pred_norm_disagreement_RT1BT0htbin4_2016merged
115	prop_binRT2BTALLhtbin0_2016merged_datacard10_bin3
116	prop_binRT1BT0htbin7_2016merged_datacard7_bin4
117	prop_binRT2BTALLhtbin0_2016merged_datacard10_bin5
118	prop_binRT1BT0htbin4_2016merged_datacard4_bin1
119	RT1BT0htbin3_2016merged_DDBKG_stat
120	prop_binRT1BT0htbin4_2016merged_datacard4_bin6



**CMS Internal**

$$\hat{r} = 1.0^{+1.0}_{-2.0}$$

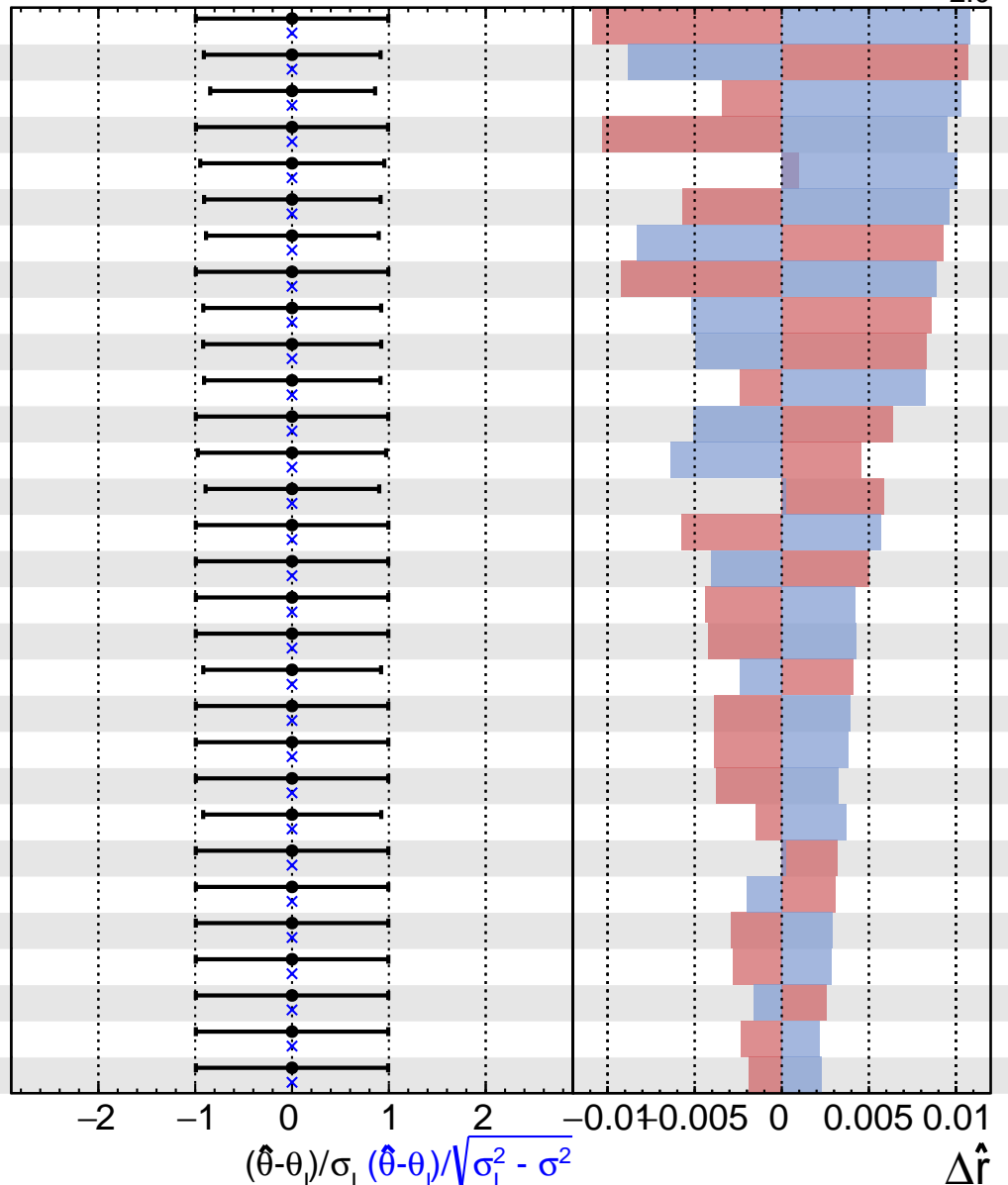
121	data_pred_norm_disagreement_RT1BT0htbin6_2016merged
122	ResTopEff_2016merged
123	prop_binRT1BT0htbin5_2016merged_datacard5_bin0
124	pileup_2016merged
125	prop_binRT2BTALLhtbin0_2016merged_datacard10_bin6
126	prop_binRT1BT0htbin6_2016merged_datacard6_bin5
127	RT2BTALLhtbin1_2016merged_TTX_stat
128	prop_binRT1BT1htbin0_2016merged_datacard8_bin5
129	RT1BT0htbin4_2016merged_DDBKG_stat
130	prop_binRT1BT0htbin0_2016merged_datacard0_bin7
131	RT1BT0htbin5_2016merged_DDBKG_stat
132	prop_binRT1BT0htbin2_2016merged_datacard2_bin3
133	RT1BT0htbin0_2016merged_DDBKG_stat
134	prop_binRT1BT1htbin0_2016merged_datacard8_bin2
135	RT1BT0htbin2_2016merged_DDBKG_stat
136	RT1BT0htbin6_2016merged_DDBKG_stat
137	prop_binRT1BT0htbin7_2016merged_datacard7_bin0
138	prop_binRT1BT0htbin3_2016merged_datacard3_bin1
139	prop_binRT1BT1htbin0_2016merged_datacard8_bin0
140	RT1BT0htbin1_2016merged_DDBKG_stat
141	prop_binRT1BT0htbin5_2016merged_datacard5_bin5
142	prop_binRT1BT1htbin1_2016merged_datacard9_bin4
143	prop_binRT1BT0htbin0_2016merged_datacard0_bin0
144	btagHFstats2_2016merged
145	prop_binRT1BT0htbin4_2016merged_datacard4_bin4
146	RT1BT1htbin0_2016merged_TTX_stat
147	prop_binRT1BT0htbin0_2016merged_datacard0_bin6
148	prop_binRT1BT0htbin2_2016merged_datacard2_bin4
149	prop_binRT1BT0htbin3_2016merged_datacard3_bin4
150	prop_binRT1BT0htbin3_2016merged_datacard3_bin3



**CMS Internal**

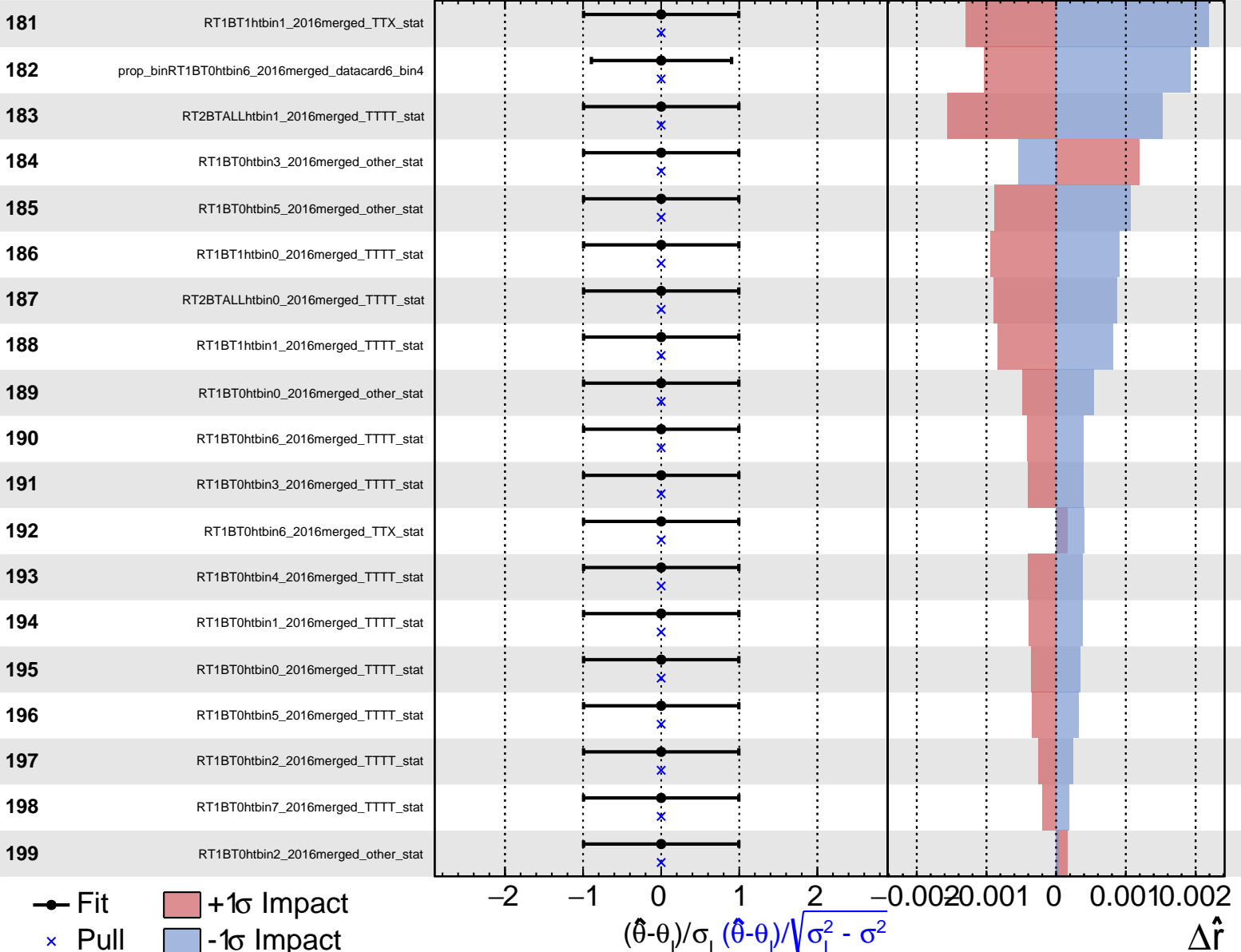
$$\hat{r} = 1.0^{+1.0}_{-2.0}$$

151	lumi_uncorr_2016merged
152	prop_binRT1BT0htbin0_2016merged_datacard0_bin3
153	prop_binRT1BT0htbin5_2016merged_datacard5_bin4
154	RT2BTALLhtbin1_2016merged_other_stat
155	prop_binRT2BTALLhtbin1_2016merged_datacard11_bin5
156	prop_binRT1BT0htbin4_2016merged_datacard4_bin5
157	prop_binRT1BT0htbin5_2016merged_datacard5_bin3
158	RT2BTALLhtbin0_2016merged_TTX_stat
159	prop_binRT1BT0htbin0_2016merged_datacard0_bin5
160	prop_binRT1BT0htbin1_2016merged_datacard1_bin2
161	prop_binRT1BT0htbin4_2016merged_datacard4_bin2
162	RT1BT0htbin7_2016merged_TTX_stat
163	prop_binRT2BTALLhtbin0_2016merged_datacard10_bin8
164	prop_binRT1BT0htbin7_2016merged_datacard7_bin2
165	lumi_corr16_17_18
166	RT1BT0htbin7_2016merged_other_stat
167	RT1BT0htbin5_2016merged_TTX_stat
168	RT1BT0htbin0_2016merged_TTX_stat
169	prop_binRT1BT0htbin0_2016merged_datacard0_bin2
170	RT1BT0htbin4_2016merged_TTX_stat
171	RT1BT0htbin2_2016merged_TTX_stat
172	RT2BTALLhtbin0_2016merged_other_stat
173	prop_binRT1BT0htbin1_2016merged_datacard1_bin3
174	RT1BT0htbin1_2016merged_other_stat
175	RT1BT0htbin6_2016merged_other_stat
176	RT1BT0htbin1_2016merged_TTX_stat
177	RT1BT0htbin3_2016merged_TTX_stat
178	RT1BT0htbin4_2016merged_other_stat
179	RT1BT1htbin0_2016merged_other_stat
180	RT1BT1htbin1_2016merged_other_stat



**CMS Internal**

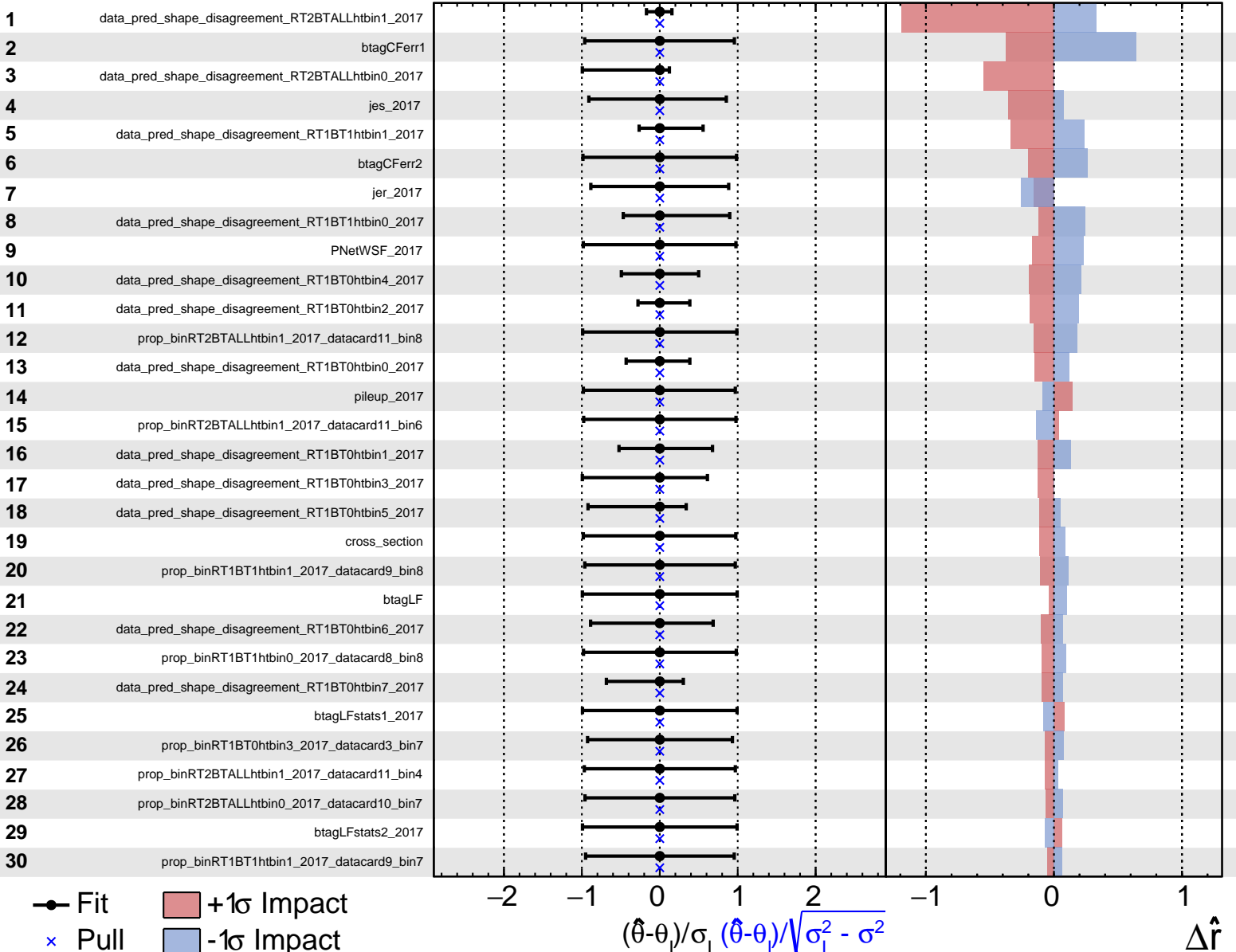
$$\hat{r} = 1.0^{+1.0}_{-2.0}$$



<sup>535</sup> **G.2 2017**

**CMS Internal**

$$\hat{r} = 1.0^{+1.0}_{-1.7}$$

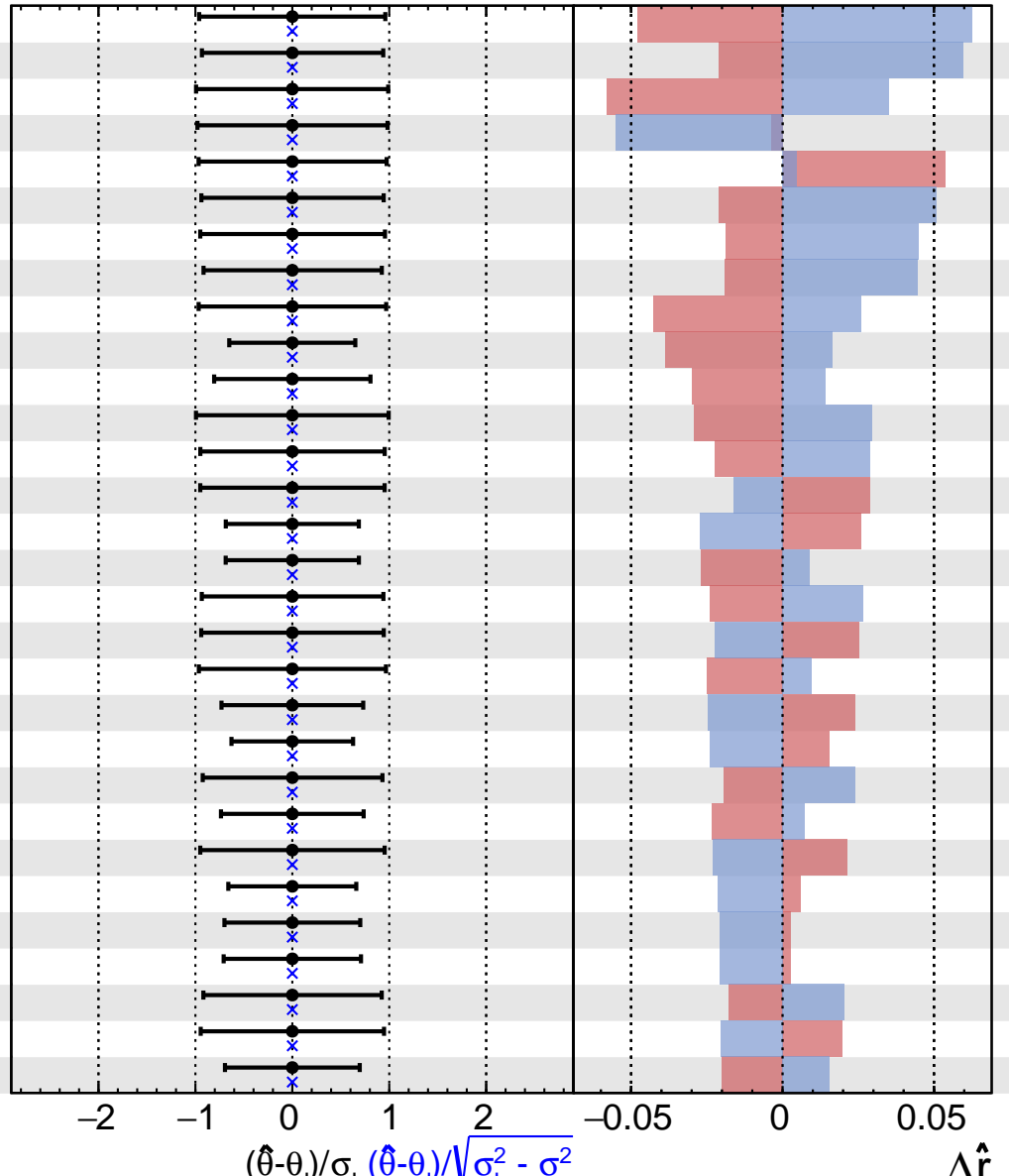


**CMS Internal**

$$\hat{r} = 1.0^{+1.0}_{-1.7}$$

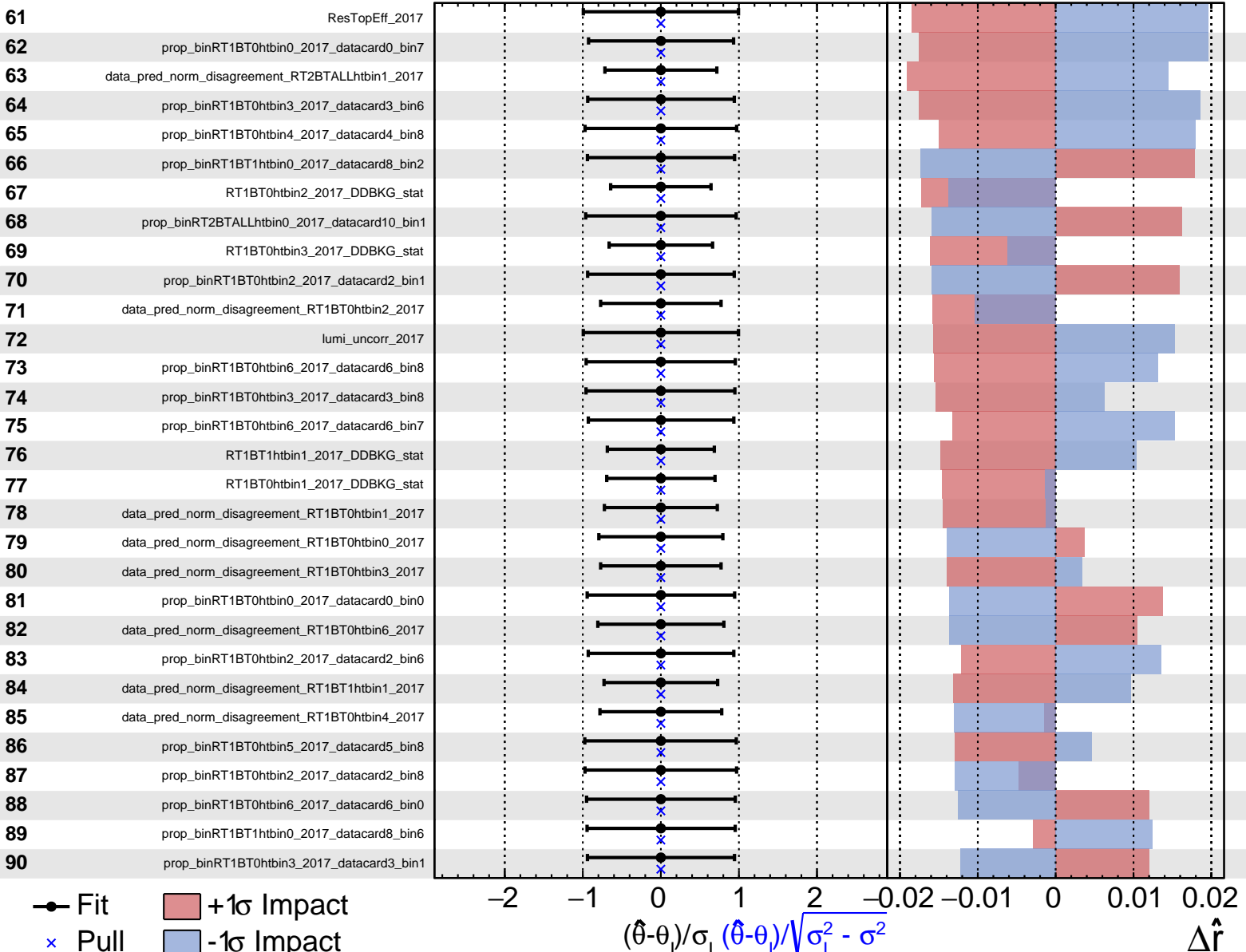
31	prop_binRT1BT1htbin1_2017_datacard9_bin3
32	prop_binRT1BT0htbin4_2017_datacard4_bin7
33	PNetTopSF_2017
34	prop_binRT2BTALLhtbin1_2017_datacard11_bin7
35	btagHF
36	prop_binRT1BT0htbin2_2017_datacard2_bin7
37	prop_binRT1BT1htbin0_2017_datacard8_bin7
38	prop_binRT1BT0htbin5_2017_datacard5_bin7
39	prop_binRT2BTALLhtbin1_2017_datacard11_bin2
40	RT1BT1htbin0_2017_DDBKG_stat
41	data_pred_norm_disagreement_RT1BT1htbin0_2017
42	ResTopMiss_2017
43	prop_binRT2BTALLhtbin0_2017_datacard10_bin6
44	prop_binRT1BT0htbin3_2017_datacard3_bin0
45	RT1BT0htbin7_2017_DDBKG_stat
46	RT2BTALLhtbin0_2017_DDBKG_stat
47	prop_binRT1BT0htbin6_2017_datacard6_bin6
48	prop_binRT1BT1htbin1_2017_datacard9_bin5
49	prop_binRT2BTALLhtbin1_2017_datacard11_bin3
50	data_pred_norm_disagreement_RT1BT0htbin7_2017
51	RT1BT0htbin6_2017_DDBKG_stat
52	prop_binRT1BT0htbin1_2017_datacard1_bin7
53	data_pred_norm_disagreement_RT2BTALLhtbin0_2017
54	prop_binRT1BT1htbin1_2017_datacard9_bin6
55	RT1BT0htbin0_2017_DDBKG_stat
56	RT1BT0htbin5_2017_DDBKG_stat
57	data_pred_norm_disagreement_RT1BT0htbin5_2017
58	prop_binRT1BT0htbin1_2017_datacard1_bin6
59	prop_binRT1BT0htbin1_2017_datacard1_bin0
60	RT2BTALLhtbin1_2017_DDBKG_stat

● Fit      +1σ Impact  
  × Pull    -1σ Impact



**CMS Internal**

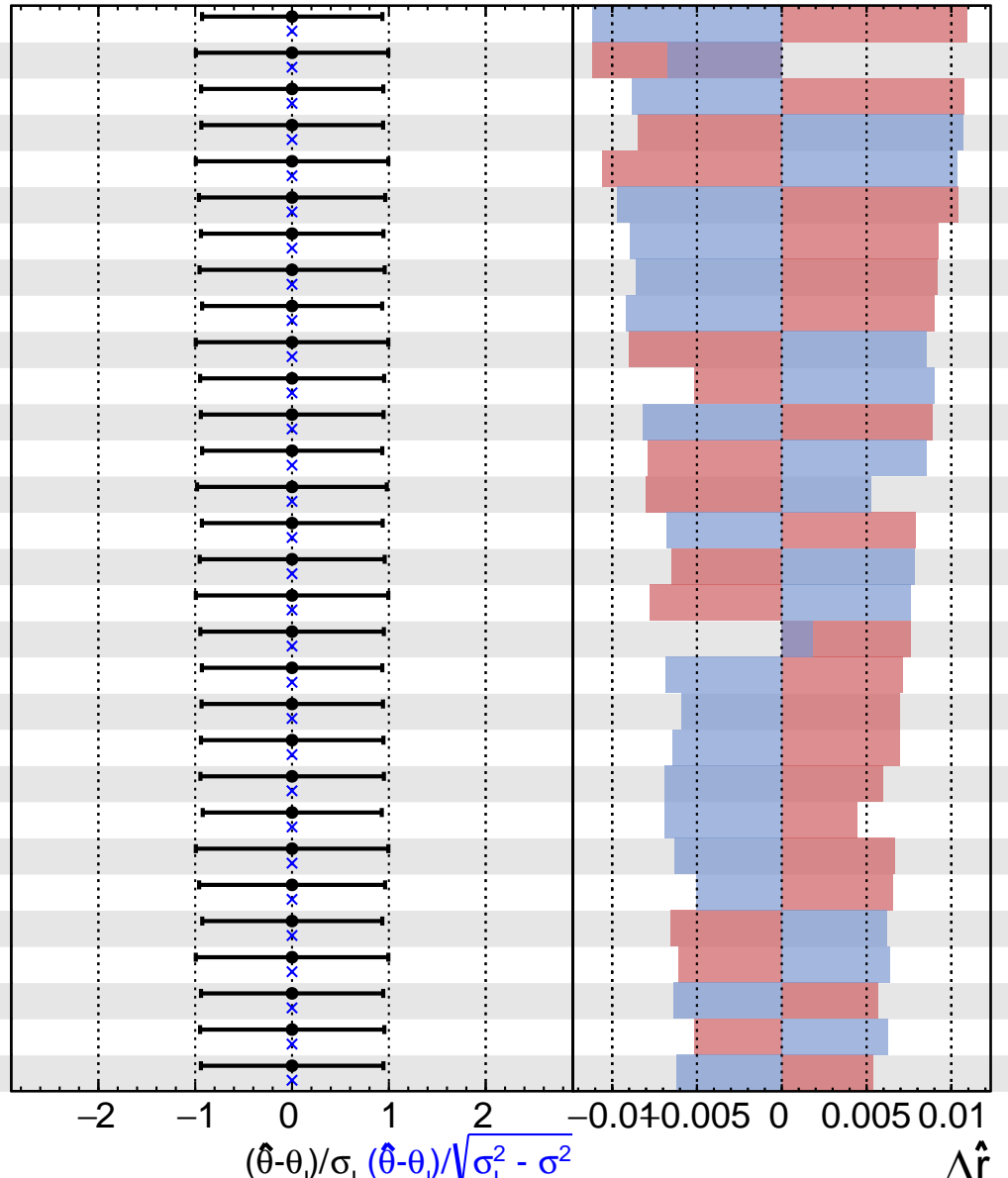
$$\hat{r} = 1.0^{+1.0}_{-1.7}$$



**CMS Internal**

$$\hat{r} = 1.0^{+1.0}_{-1.7}$$

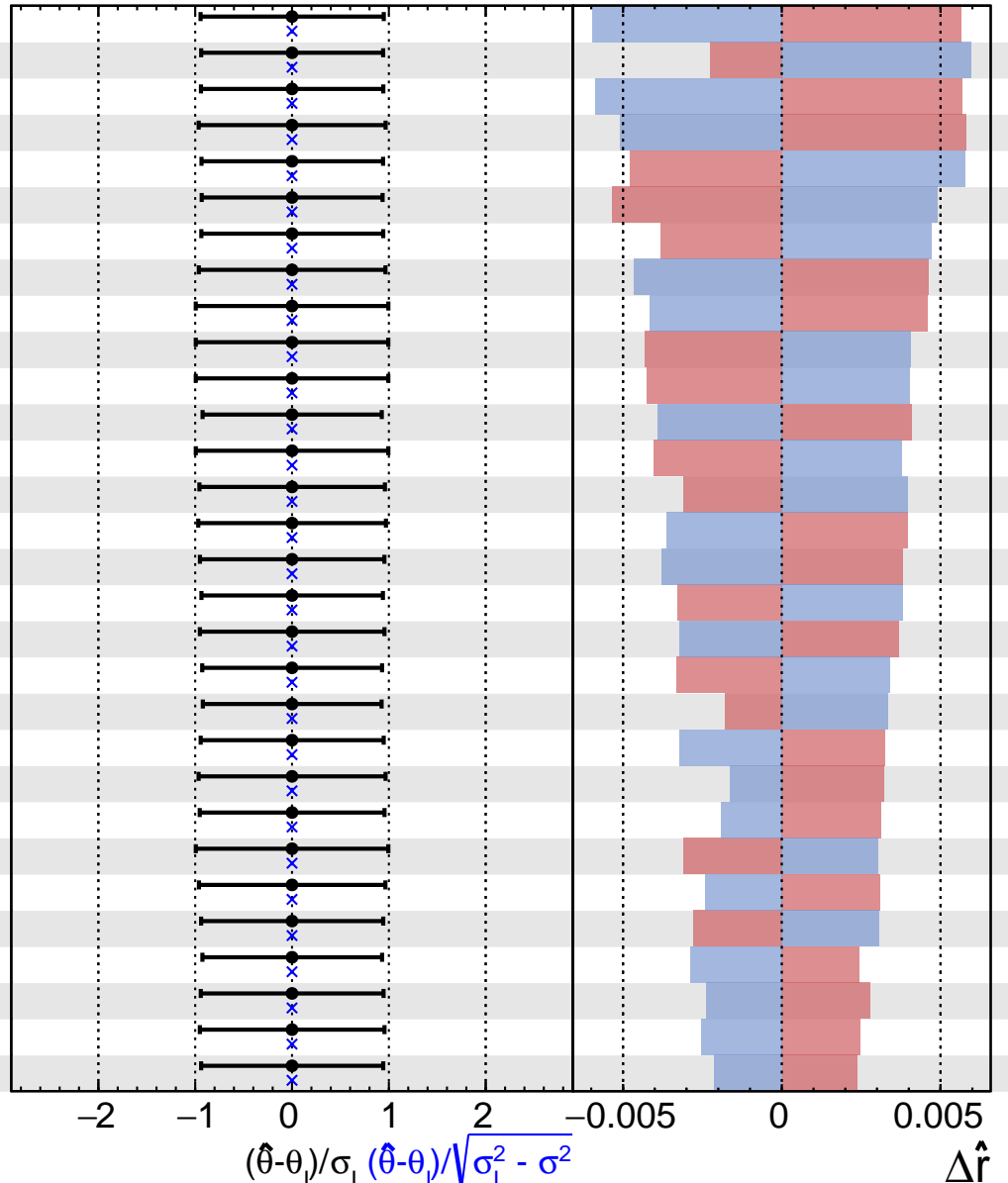
91	prop_binRT1BT0htbin5_2017_datacard5_bin1
92	prop_binRT2BTALLhtbin0_2017_datacard10_bin8
93	prop_binRT1BT1htbin1_2017_datacard9_bin0
94	prop_binRT1BT0htbin4_2017_datacard4_bin6
95	trigger_2017
96	prop_binRT2BTALLhtbin0_2017_datacard10_bin2
97	prop_binRT1BT0htbin4_2017_datacard4_bin2
98	prop_binRT1BT0htbin4_2017_datacard4_bin0
99	prop_binRT1BT0htbin1_2017_datacard1_bin1
100	RT2BTALLhtbin1_2017_TTX_stat
101	prop_binRT1BT0htbin1_2017_datacard1_bin8
102	prop_binRT1BT1htbin1_2017_datacard9_bin4
103	prop_binRT1BT0htbin0_2017_datacard0_bin6
104	prop_binRT1BT0htbin7_2017_datacard7_bin8
105	prop_binRT1BT1htbin1_2017_datacard9_bin1
106	prop_binRT2BTALLhtbin0_2017_datacard10_bin5
107	RT2BTALLhtbin0_2017_TTX_stat
108	prop_binRT1BT1htbin0_2017_datacard8_bin0
109	prop_binRT1BT0htbin0_2017_datacard0_bin1
110	prop_binRT1BT1htbin1_2017_datacard9_bin2
111	prop_binRT1BT1htbin0_2017_datacard8_bin1
112	prop_binRT1BT0htbin5_2017_datacard5_bin0
113	prop_binRT1BT0htbin5_2017_datacard5_bin2
114	btagHFstats2_2017
115	prop_binRT2BTALLhtbin0_2017_datacard10_bin3
116	prop_binRT1BT0htbin5_2017_datacard5_bin6
117	lumi_corr16_17_18
118	prop_binRT1BT0htbin2_2017_datacard2_bin2
119	prop_binRT1BT0htbin7_2017_datacard7_bin7
120	prop_binRT1BT0htbin4_2017_datacard4_bin4



**CMS Internal**

$$\hat{r} = 1.0^{+1.0}_{-1.7}$$

121	prop_binRT1BT0htbin4_2017_datacard4_bin1
122	prop_binRT1BT0htbin3_2017_datacard3_bin5
123	prop_binRT1BT0htbin3_2017_datacard3_bin2
124	prop_binRT2BTALLhtbin1_2017_datacard11_bin5
125	prop_binRT1BT1htbin0_2017_datacard8_bin5
126	prop_binRT1BT0htbin0_2017_datacard0_bin5
127	prop_binRT1BT1htbin0_2017_datacard8_bin4
128	prop_binRT1BT0htbin7_2017_datacard7_bin0
129	btagHFstats1_2017
130	RT1BT1htbin0_2017_TTX_stat
131	RT1BT1htbin1_2017_TTX_stat
132	prop_binRT1BT0htbin1_2017_datacard1_bin2
133	lumi_corr17_18
134	prop_binRT2BTALLhtbin0_2017_datacard10_bin4
135	prop_binRT2BTALLhtbin1_2017_datacard11_bin0
136	prop_binRT1BT0htbin7_2017_datacard7_bin3
137	prop_binRT1BT0htbin2_2017_datacard2_bin5
138	prop_binRT1BT0htbin7_2017_datacard7_bin6
139	prop_binRT1BT0htbin1_2017_datacard1_bin4
140	prop_binRT1BT0htbin1_2017_datacard1_bin5
141	prop_binRT1BT0htbin6_2017_datacard6_bin2
142	prop_binRT2BTALLhtbin0_2017_datacard10_bin0
143	prop_binRT1BT0htbin7_2017_datacard7_bin2
144	RT2BTALLhtbin1_2017_TTTT_stat
145	prop_binRT2BTALLhtbin1_2017_datacard11_bin1
146	prop_binRT1BT0htbin3_2017_datacard3_bin4
147	prop_binRT1BT0htbin5_2017_datacard5_bin3
148	prop_binRT1BT0htbin6_2017_datacard6_bin1
149	prop_binRT1BT0htbin7_2017_datacard7_bin4
150	prop_binRT1BT0htbin6_2017_datacard6_bin4

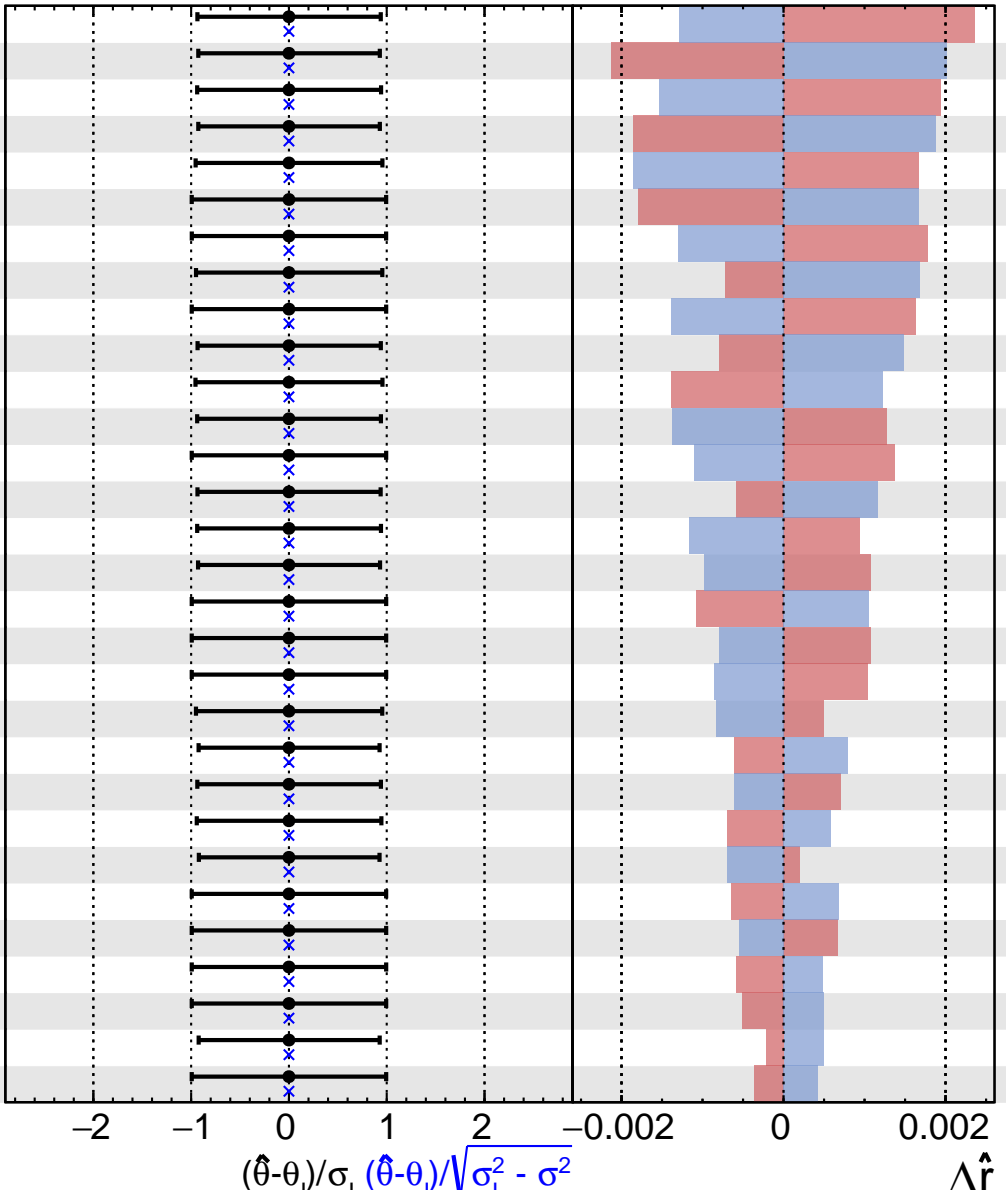


**CMS Internal**

$$\hat{r} = 1.0^{+1.0}_{-1.7}$$

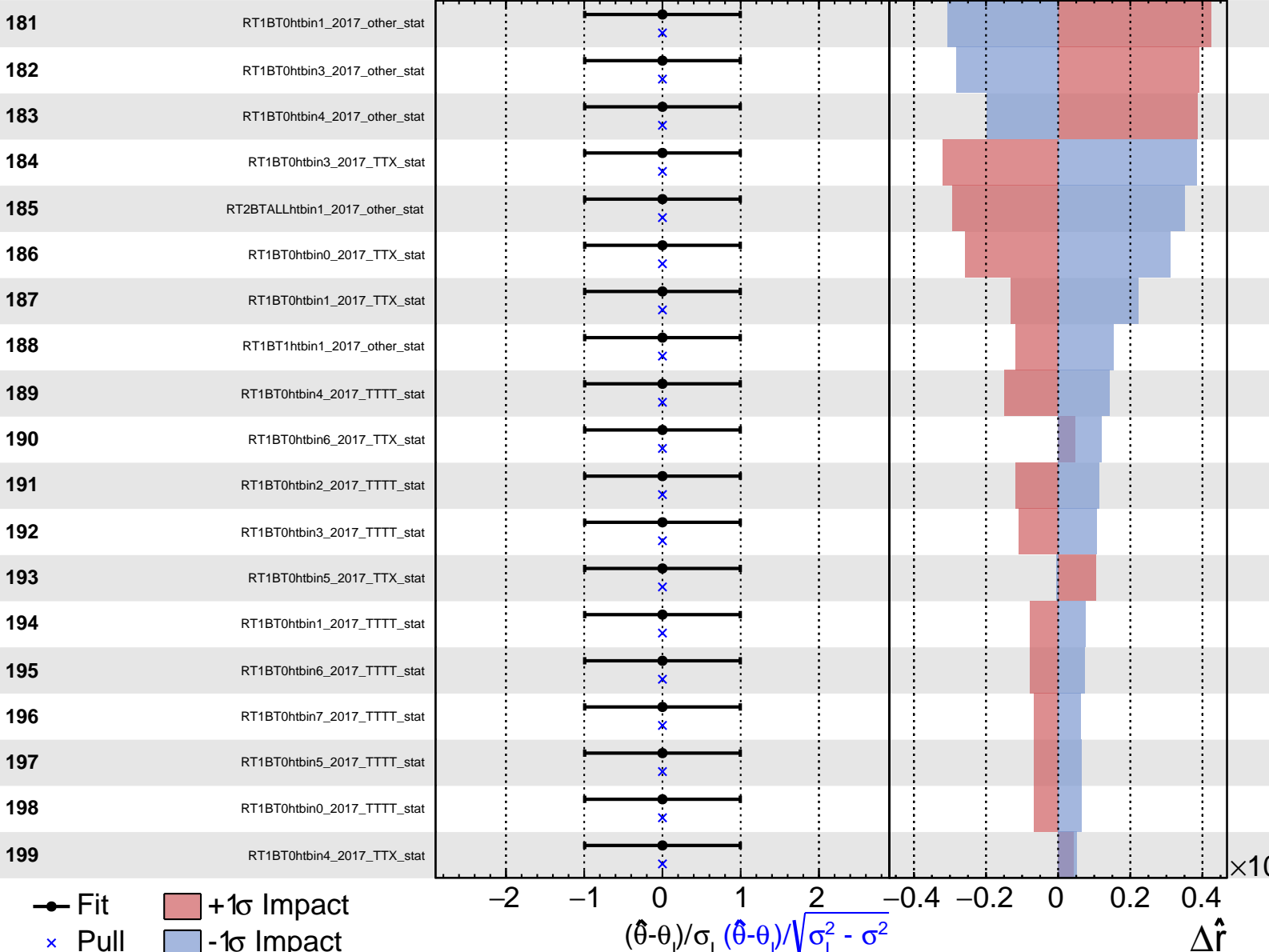
151	prop_binRT1BT0htbin2_2017_datacard2_bin3
152	prop_binRT1BT0htbin0_2017_datacard0_bin2
153	prop_binRT1BT0htbin6_2017_datacard6_bin5
154	prop_binRT1BT0htbin0_2017_datacard0_bin4
155	prop_binRT1BT0htbin7_2017_datacard7_bin1
156	RT2BTALLhtbin0_2017_other_stat
157	RT1BT0htbin0_2017_other_stat
158	prop_binRT1BT0htbin0_2017_datacard0_bin8
159	RT1BT0htbin7_2017_other_stat
160	prop_binRT1BT1htbin0_2017_datacard8_bin3
161	prop_binRT1BT0htbin2_2017_datacard2_bin0
162	prop_binRT1BT0htbin3_2017_datacard3_bin3
163	RT1BT0htbin5_2017_other_stat
164	prop_binRT1BT0htbin2_2017_datacard2_bin4
165	prop_binRT1BT0htbin6_2017_datacard6_bin3
166	prop_binRT1BT0htbin0_2017_datacard0_bin3
167	RT2BTALLhtbin0_2017_TTTT_stat
168	RT1BT0htbin7_2017_TTX_stat
169	RT1BT0htbin6_2017_other_stat
170	prop_binRT1BT0htbin7_2017_datacard7_bin5
171	prop_binRT1BT0htbin1_2017_datacard1_bin3
172	prop_binRT1BT0htbin4_2017_datacard4_bin5
173	prop_binRT1BT0htbin4_2017_datacard4_bin3
174	prop_binRT1BT0htbin5_2017_datacard5_bin4
175	RT1BT1htbin0_2017_other_stat
176	RT1BT0htbin2_2017_other_stat
177	RT1BT1htbin0_2017_TTTT_stat
178	RT1BT1htbin1_2017_TTTT_stat
179	prop_binRT1BT0htbin5_2017_datacard5_bin5
180	RT1BT0htbin2_2017_TTX_stat

● Fit      +1σ Impact  
  × Pull      -1σ Impact



**CMS Internal**

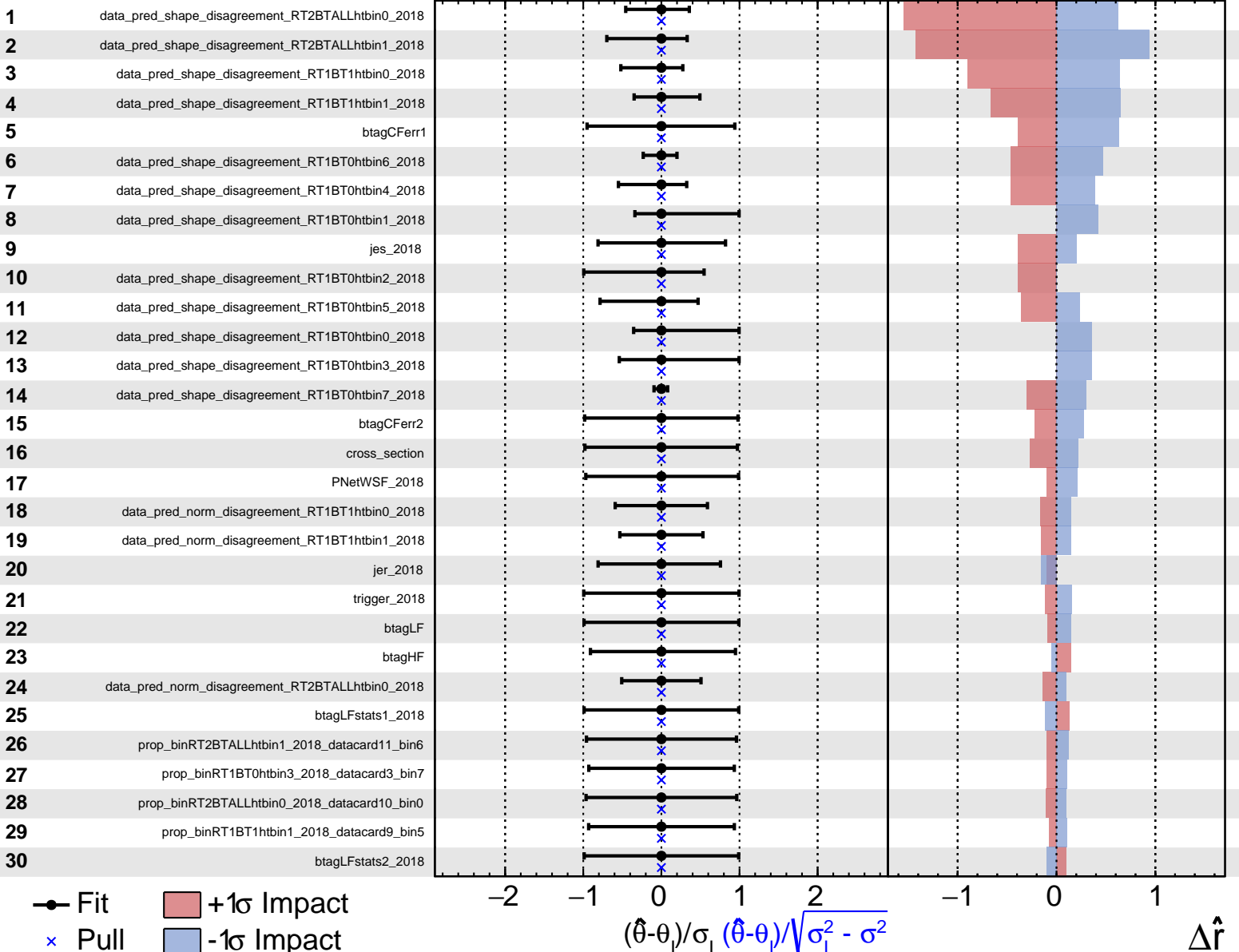
$$\hat{r} = 1.0^{+1.0}_{-1.7}$$



<sup>543</sup> **G.3 2018**

**CMS Internal**

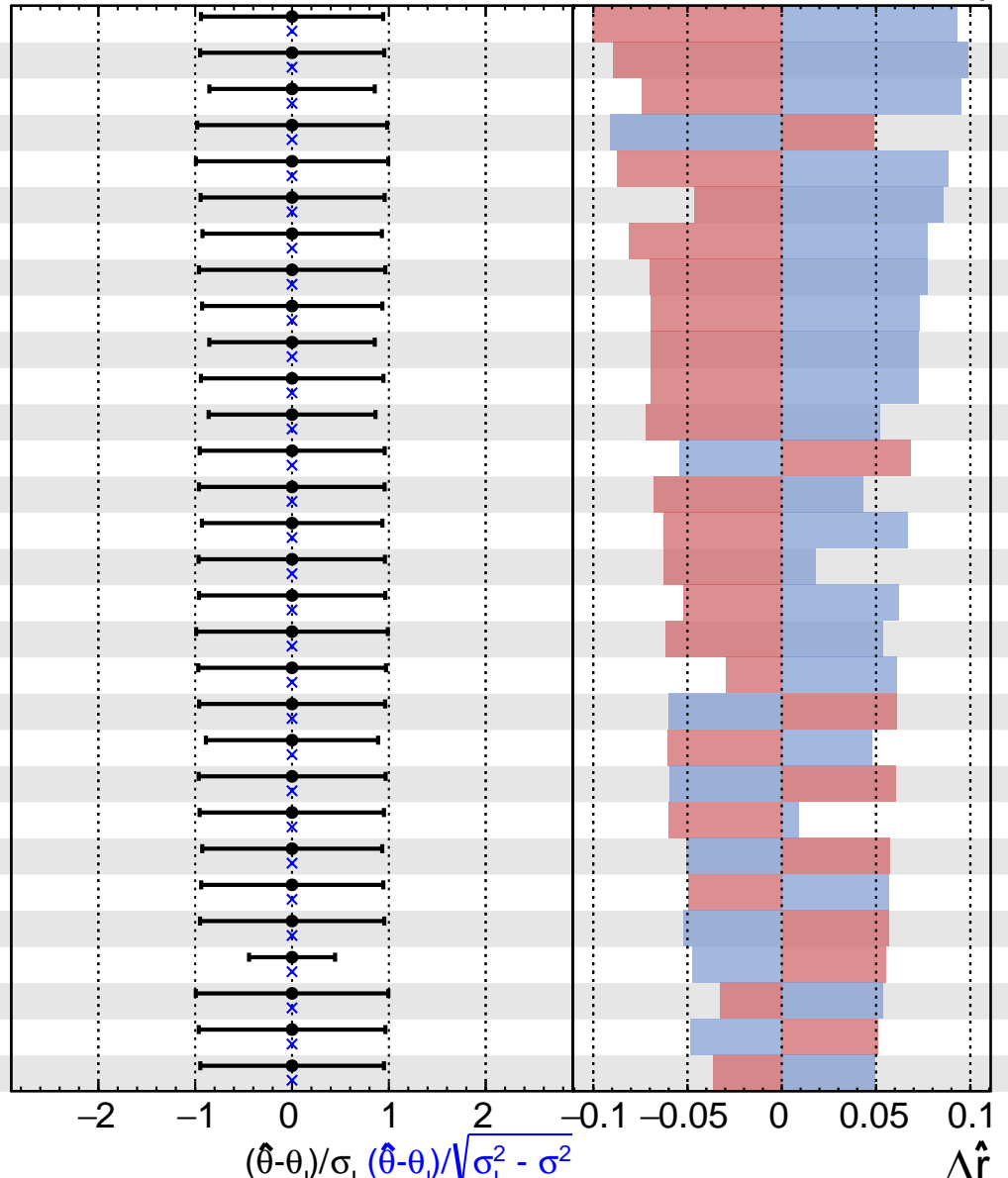
$$\hat{r} = 1.0^{+1.0}_{-2.0}$$



**CMS Internal**

$$\hat{r} = 1.0^{+1.0}_{-2.0}$$

31	prop_binRT1BT0htbin2_2018_datacard2_bin7
32	prop_binRT1BT1htbin0_2018_datacard8_bin6
33	RT2BTALLhtbin1_2018_DDBKG_stat
34	prop_binRT2BTALLhtbin0_2018_datacard10_bin7
35	prop_binRT2BTALLhtbin0_2018_datacard10_bin8
36	prop_binRT1BT0htbin3_2018_datacard3_bin8
37	prop_binRT1BT0htbin2_2018_datacard2_bin6
38	prop_binRT2BTALLhtbin0_2018_datacard10_bin6
39	prop_binRT1BT0htbin3_2018_datacard3_bin6
40	RT1BT1htbin0_2018_DDBKG_stat
41	prop_binRT1BT0htbin4_2018_datacard4_bin7
42	RT1BT1htbin1_2018_DDBKG_stat
43	prop_binRT2BTALLhtbin1_2018_datacard11_bin3
44	prop_binRT1BT1htbin1_2018_datacard9_bin8
45	prop_binRT1BT0htbin1_2018_datacard1_bin6
46	prop_binRT1BT0htbin5_2018_datacard5_bin8
47	prop_binRT2BTALLhtbin1_2018_datacard11_bin5
48	prop_binRT2BTALLhtbin1_2018_datacard11_bin8
49	prop_binRT2BTALLhtbin1_2018_datacard11_bin7
50	prop_binRT2BTALLhtbin0_2018_datacard10_bin2
51	RT2BTALLhtbin0_2018_DDBKG_stat
52	prop_binRT2BTALLhtbin1_2018_datacard11_bin2
53	prop_binRT1BT0htbin2_2018_datacard2_bin8
54	prop_binRT1BT1htbin1_2018_datacard9_bin1
55	prop_binRT1BT0htbin6_2018_datacard6_bin7
56	prop_binRT1BT1htbin0_2018_datacard8_bin1
57	data_pred_norm_disagreement_RT1BT0htbin7_2018
58	ResTopMiss_2018
59	prop_binRT2BTALLhtbin0_2018_datacard10_bin1
60	prop_binRT1BT1htbin0_2018_datacard8_bin3

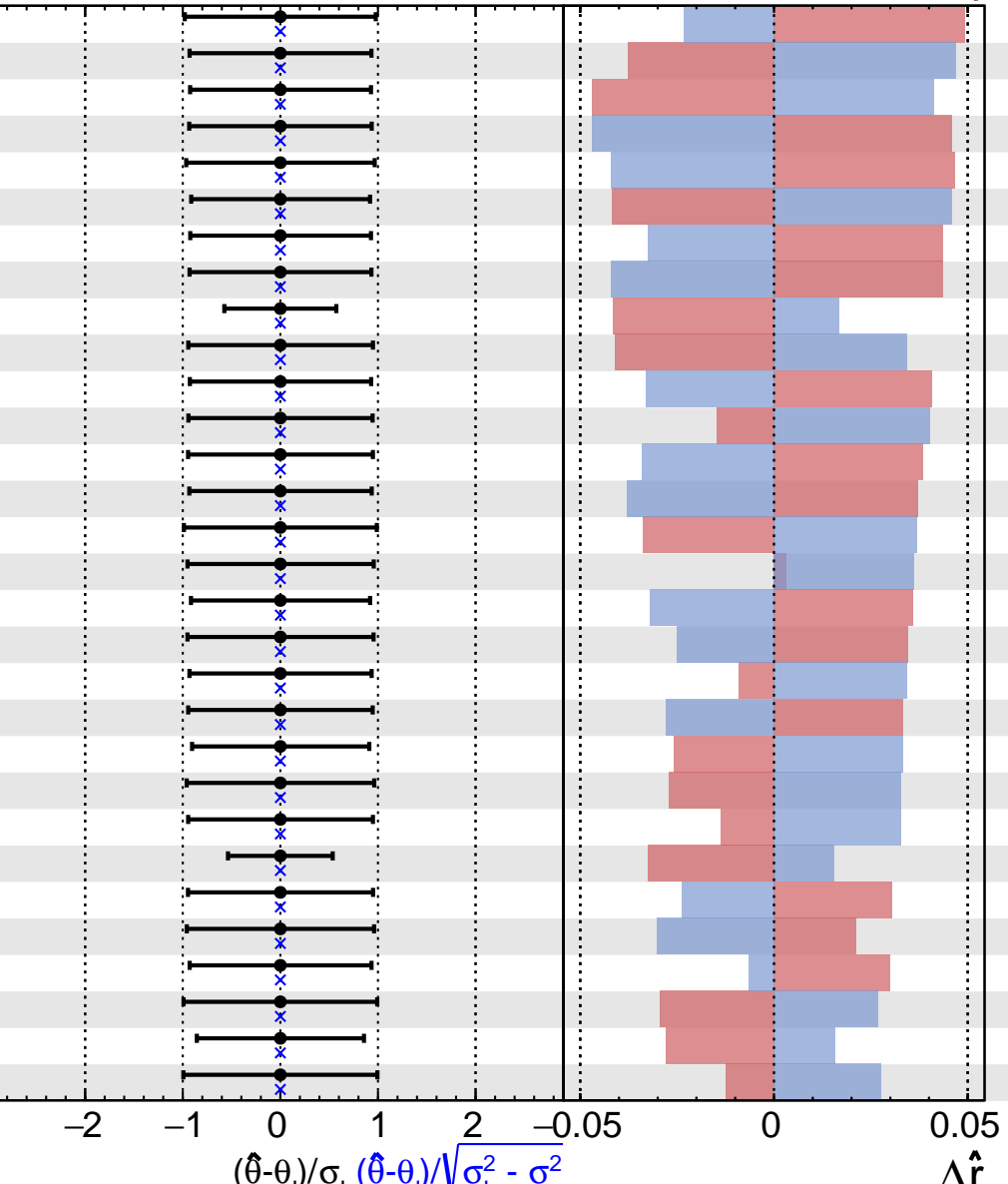


**CMS Internal**

$$\hat{r} = 1.0^{+1.0}_{-2.0}$$

61	pileup_2018
62	prop_binRT1BT0htbin3_2018_datacard3_bin4
63	prop_binRT1BT0htbin5_2018_datacard5_bin7
64	prop_binRT1BT0htbin2_2018_datacard2_bin1
65	prop_binRT2BTALLhtbin1_2018_datacard11_bin1
66	prop_binRT1BT0htbin5_2018_datacard5_bin5
67	prop_binRT1BT1htbin1_2018_datacard9_bin0
68	prop_binRT1BT0htbin3_2018_datacard3_bin1
69	data_pred_norm_disagreement_RT1BT0htbin2_2018
70	prop_binRT1BT0htbin0_2018_datacard0_bin7
71	prop_binRT1BT0htbin1_2018_datacard1_bin1
72	prop_binRT1BT1htbin0_2018_datacard8_bin0
73	prop_binRT1BT0htbin2_2018_datacard2_bin0
74	prop_binRT1BT0htbin4_2018_datacard4_bin1
75	prop_binRT1BT1htbin0_2018_datacard8_bin8
76	prop_binRT1BT1htbin1_2018_datacard9_bin7
77	prop_binRT1BT0htbin5_2018_datacard5_bin2
78	prop_binRT1BT1htbin0_2018_datacard8_bin5
79	prop_binRT1BT0htbin0_2018_datacard0_bin6
80	prop_binRT1BT0htbin3_2018_datacard3_bin0
81	prop_binRT1BT0htbin5_2018_datacard5_bin6
82	prop_binRT2BTALLhtbin0_2018_datacard10_bin3
83	prop_binRT1BT0htbin1_2018_datacard1_bin7
84	data_pred_norm_disagreement_RT1BT0htbin1_2018
85	prop_binRT1BT1htbin0_2018_datacard8_bin4
86	prop_binRT2BTALLhtbin0_2018_datacard10_bin4
87	prop_binRT1BT1htbin1_2018_datacard9_bin2
88	PNetTopSF_2018
89	RT1BT0htbin2_2018_DDBKG_stat
90	lumi_uncorr_2018

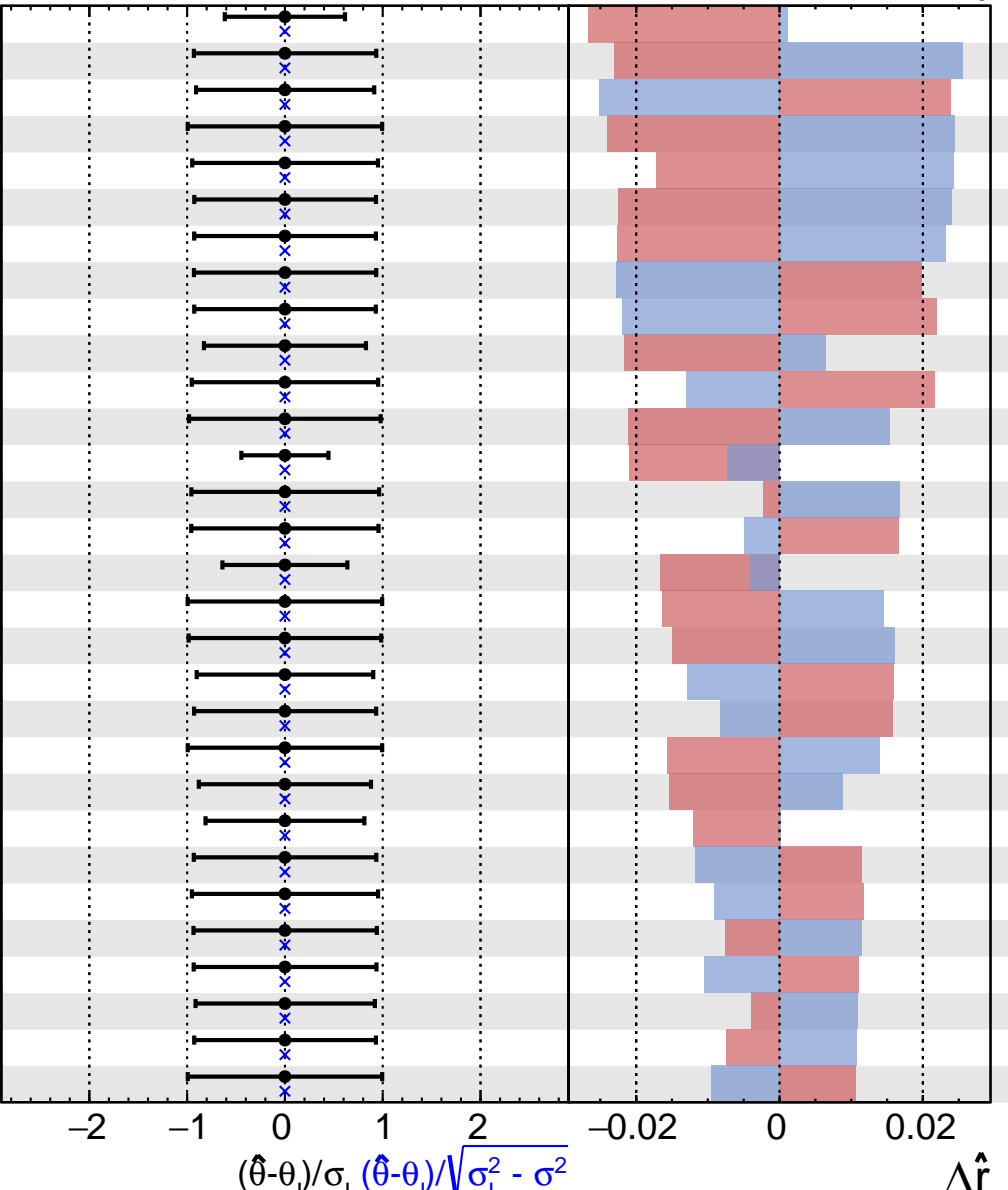
- Fit
- +1σ Impact
- ✖ Pull
- ▢ -1σ Impact



**CMS Internal**

$$\hat{r} = 1.0^{+1.0}_{-2.0}$$

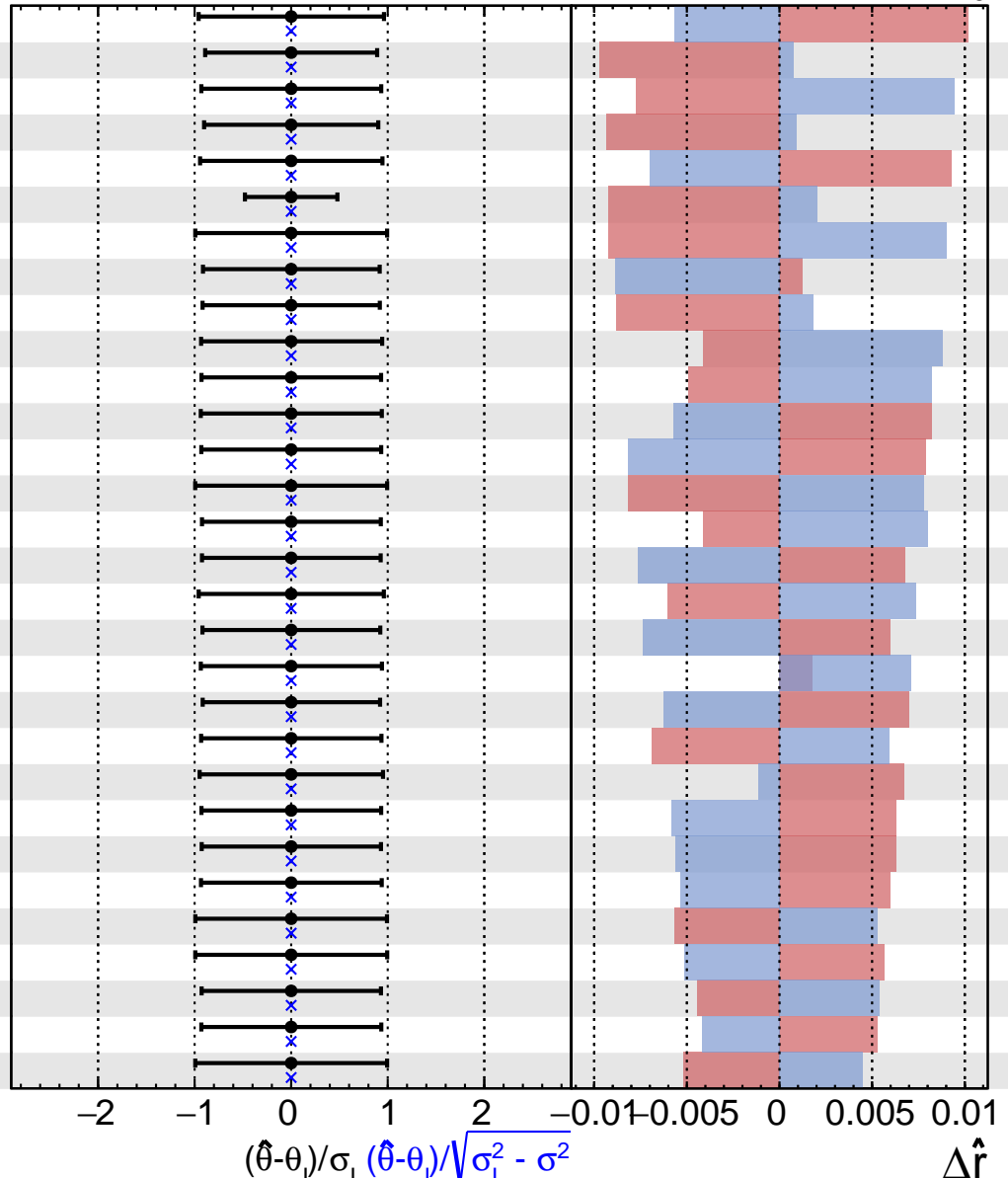
91	data_pred_norm_disagreement_RT1BT0htbin3_2018
92	prop_binRT1BT0htbin4_2018_datacard4_bin3
93	prop_binRT1BT0htbin5_2018_datacard5_bin1
94	lumi_corr16_17_18
95	prop_binRT1BT1htbin0_2018_datacard8_bin7
96	prop_binRT1BT0htbin7_2018_datacard7_bin7
97	prop_binRT1BT0htbin0_2018_datacard0_bin3
98	prop_binRT1BT0htbin5_2018_datacard5_bin0
99	prop_binRT1BT0htbin0_2018_datacard0_bin2
100	RT1BT0htbin3_2018_DDBKG_stat
101	prop_binRT1BT0htbin1_2018_datacard1_bin0
102	prop_binRT1BT0htbin4_2018_datacard4_bin8
103	data_pred_norm_disagreement_RT1BT0htbin0_2018
104	prop_binRT1BT0htbin1_2018_datacard1_bin8
105	prop_binRT1BT0htbin0_2018_datacard0_bin0
106	data_pred_norm_disagreement_RT1BT0htbin4_2018
107	RT2BTALLhtbin0_2018_TTX_stat
108	prop_binRT1BT0htbin6_2018_datacard6_bin8
109	RT1BT0htbin7_2018_DDBKG_stat
110	prop_binRT1BT1htbin1_2018_datacard9_bin4
111	ResTopEff_2018
112	RT1BT0htbin1_2018_DDBKG_stat
113	RT1BT0htbin4_2018_DDBKG_stat
114	prop_binRT1BT0htbin0_2018_datacard0_bin1
115	prop_binRT1BT0htbin6_2018_datacard6_bin0
116	prop_binRT1BT1htbin1_2018_datacard9_bin6
117	prop_binRT1BT0htbin6_2018_datacard6_bin4
118	prop_binRT1BT0htbin4_2018_datacard4_bin6
119	prop_binRT1BT0htbin1_2018_datacard1_bin5
120	btagHFstats1_2018



**CMS Internal**

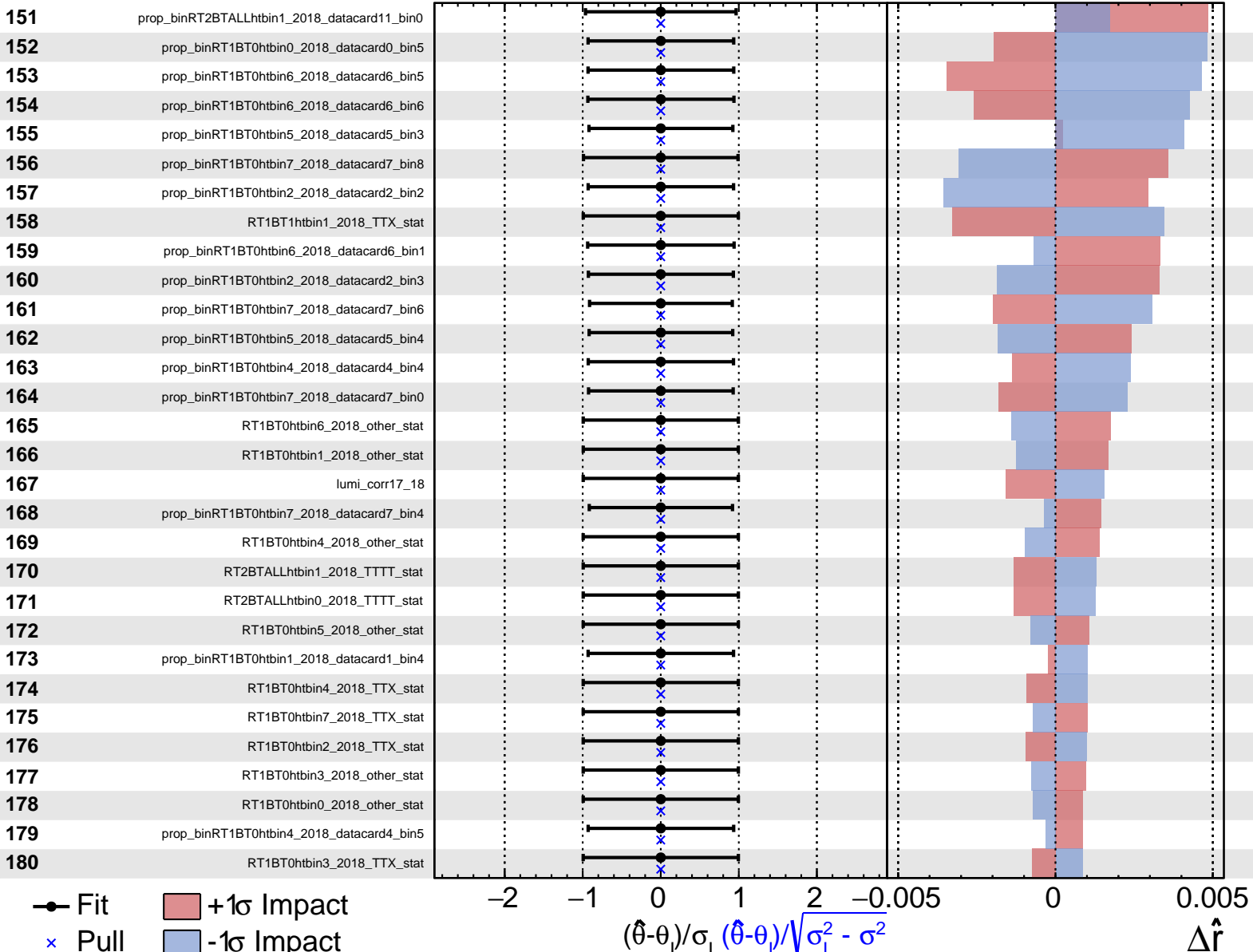
$$\hat{r} = 1.0^{+1.0}_{-2.0}$$

121	prop_binRT2BTALLhtbin1_2018_datacard11_bin4
122	RT1BT0htbin5_2018_DDBKG_stat
123	prop_binRT1BT0htbin1_2018_datacard1_bin3
124	RT1BT0htbin6_2018_DDBKG_stat
125	prop_binRT1BT0htbin4_2018_datacard4_bin0
126	data_pred_norm_disagreement_RT1BT0htbin5_2018
127	RT2BTALLhtbin1_2018_TTX_stat
128	prop_binRT1BT0htbin7_2018_datacard7_bin2
129	RT1BT0htbin0_2018_DDBKG_stat
130	prop_binRT1BT0htbin0_2018_datacard0_bin8
131	prop_binRT1BT0htbin0_2018_datacard0_bin4
132	prop_binRT1BT0htbin6_2018_datacard6_bin2
133	prop_binRT1BT0htbin1_2018_datacard1_bin2
134	RT1BT1htbin0_2018_TTX_stat
135	prop_binRT1BT0htbin3_2018_datacard3_bin5
136	prop_binRT1BT0htbin7_2018_datacard7_bin1
137	prop_binRT2BTALLhtbin0_2018_datacard10_bin5
138	prop_binRT1BT0htbin7_2018_datacard7_bin3
139	prop_binRT1BT1htbin1_2018_datacard9_bin3
140	prop_binRT1BT0htbin7_2018_datacard7_bin5
141	prop_binRT1BT0htbin2_2018_datacard2_bin5
142	prop_binRT1BT1htbin0_2018_datacard8_bin2
143	prop_binRT1BT0htbin3_2018_datacard3_bin2
144	prop_binRT1BT0htbin3_2018_datacard3_bin3
145	prop_binRT1BT0htbin6_2018_datacard6_bin3
146	RT1BT1htbin0_2018_other_stat
147	btagHFstats2_2018
148	prop_binRT1BT0htbin2_2018_datacard2_bin4
149	prop_binRT1BT0htbin4_2018_datacard4_bin2
150	RT2BTALLhtbin1_2018_other_stat



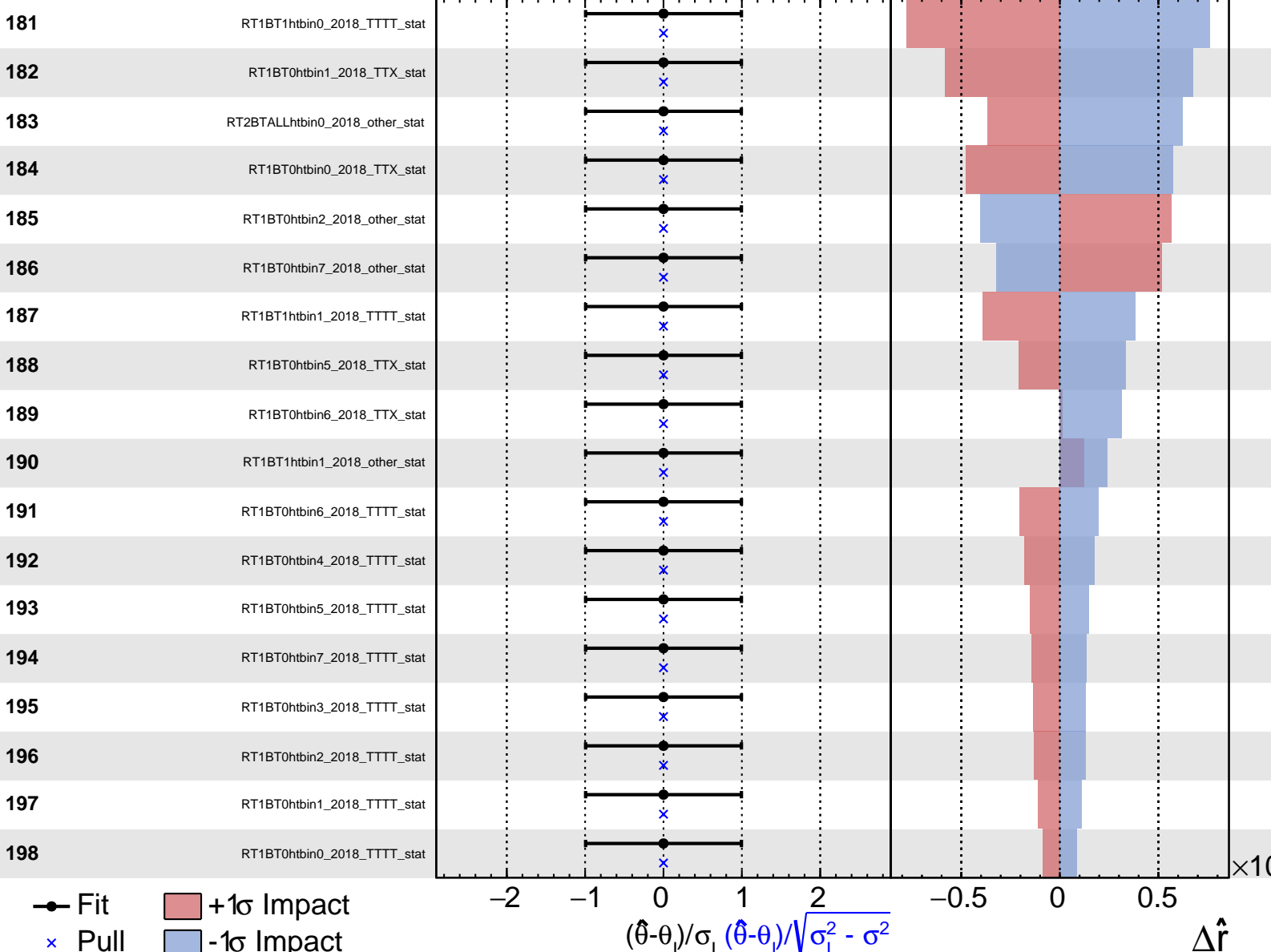
**CMS Internal**

$$\hat{r} = 1.0^{+1.0}_{-2.0}$$



**CMS Internal**

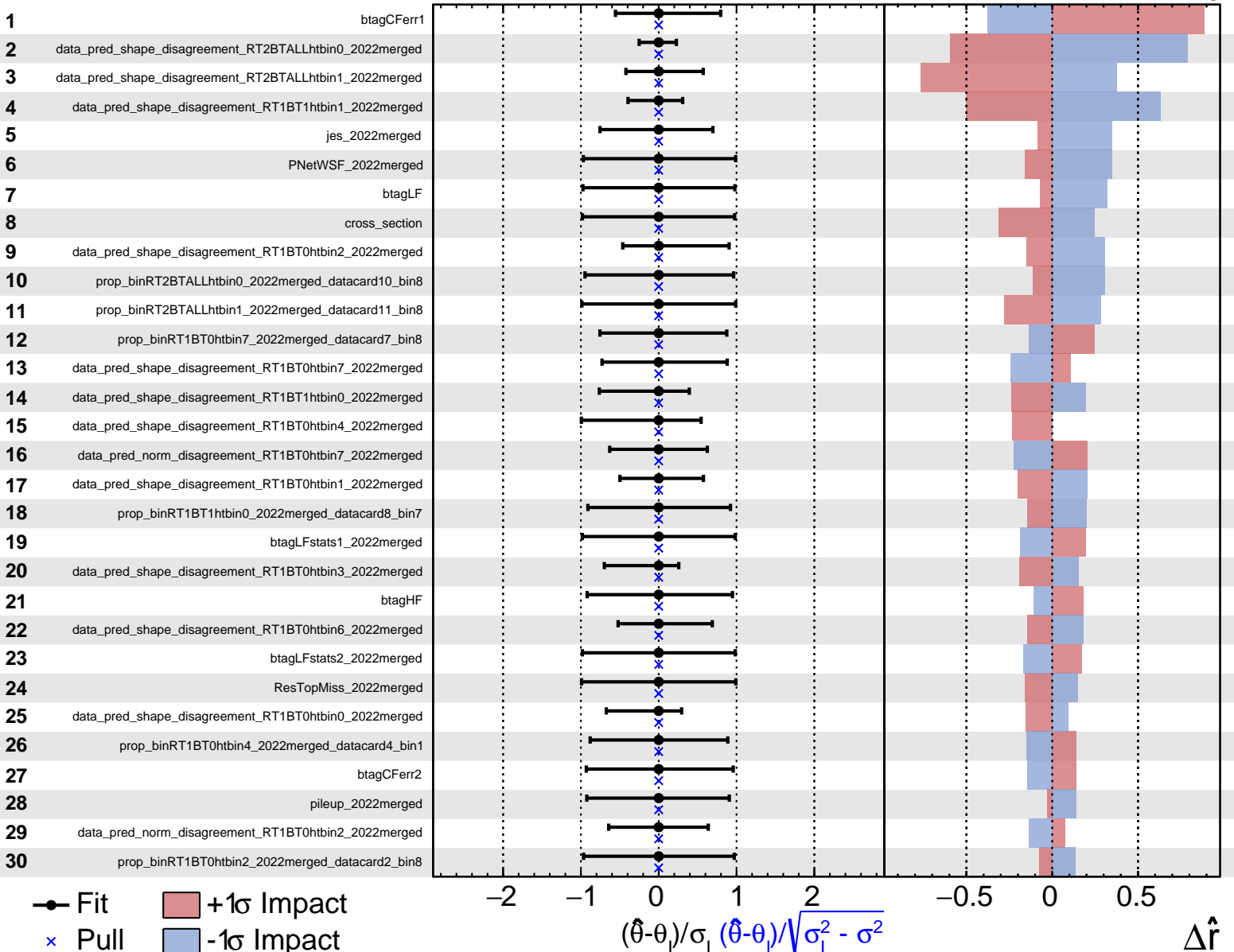
$$\hat{r} = 1.0^{+1.0}_{-2.0}$$



<sub>551</sub> G.4 2022

**CMS Internal**

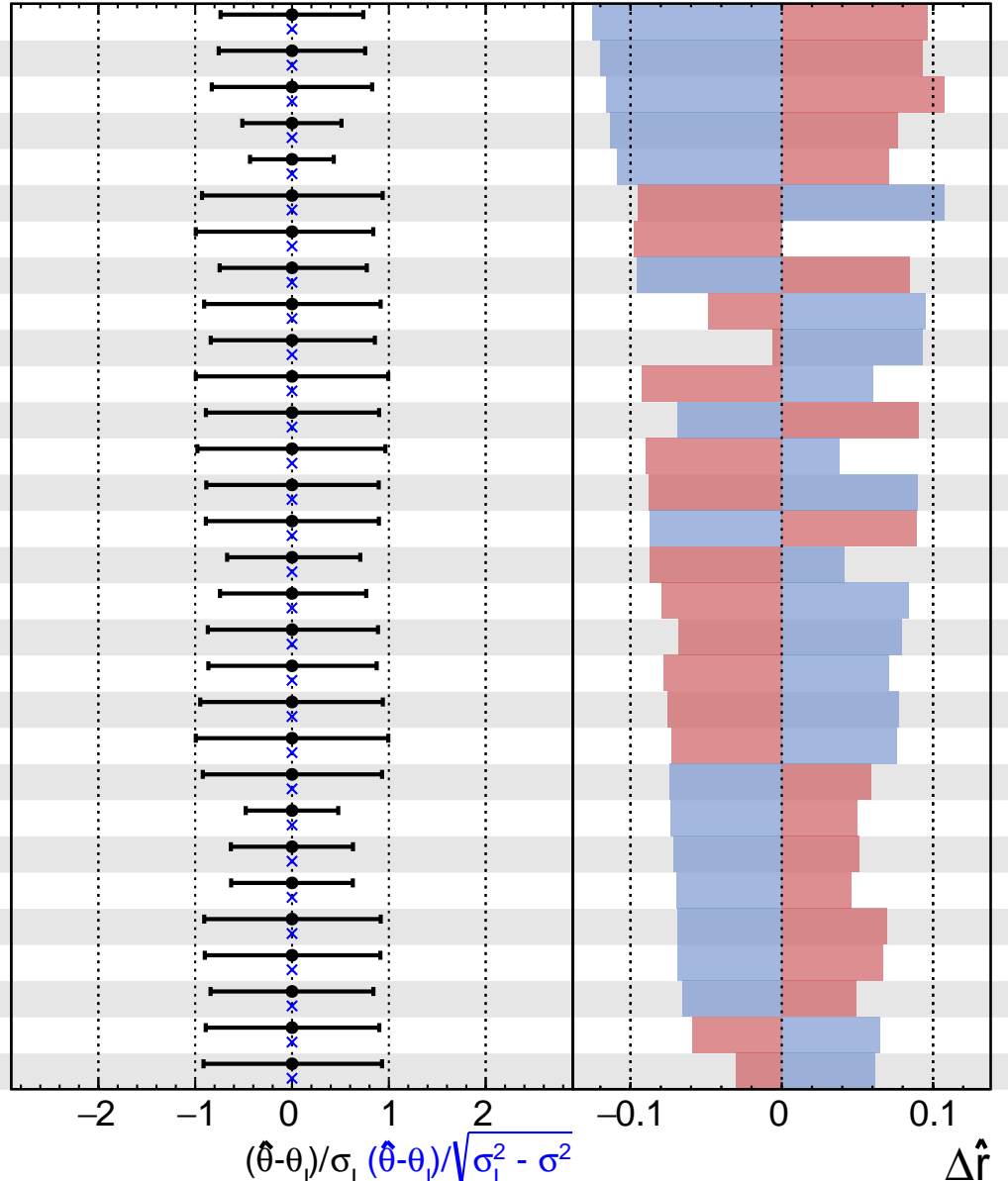
$$\hat{r} = 1.0^{+1.0}_{-1.8}$$



**CMS Internal**

$$\hat{r} = 1.0^{+1.0}_{-1.8}$$

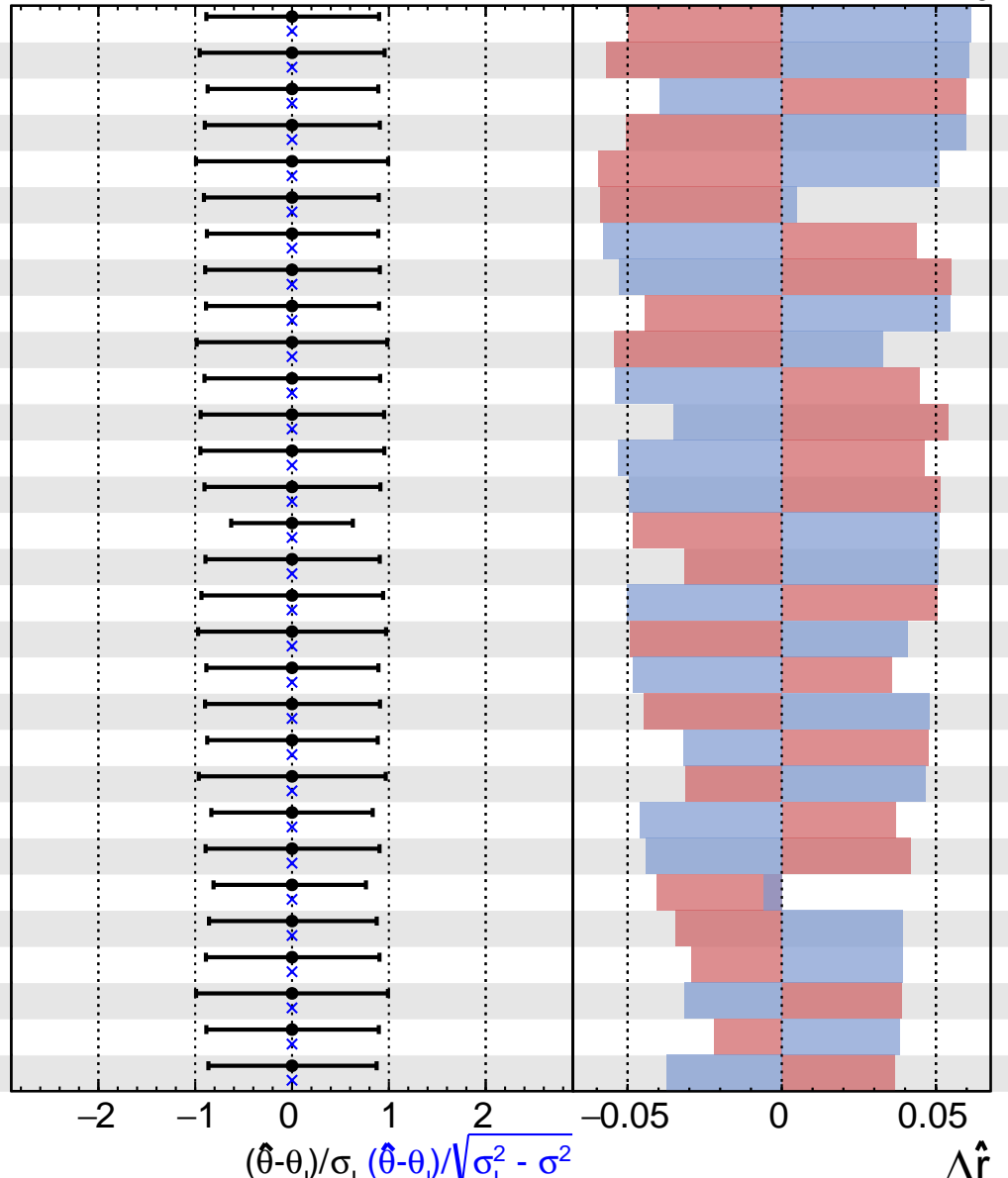
31	data_pred_norm_disagreement_RT1BT0htbin6_2022merged
32	RT1BT0htbin6_2022merged_DDBKG_stat
33	RT1BT0htbin7_2022merged_DDBKG_stat
34	data_pred_norm_disagreement_RT1BT0htbin5_2022merged
35	data_pred_norm_disagreement_RT1BT0htbin0_2022merged
36	prop_binRT2BTALLhtbin1_2022merged_datacard11_bin5
37	data_pred_shape_disagreement_RT1BT0htbin5_2022merged
38	prop_binRT1BT0htbin5_2022merged_datacard5_bin0
39	prop_binRT1BT1htbin1_2022merged_datacard9_bin1
40	prop_binRT1BT0htbin3_2022merged_datacard3_bin7
41	RT2BTALLhtbin1_2022merged_TTX_stat
42	prop_binRT1BT0htbin7_2022merged_datacard7_bin0
43	prop_binRT1BT1htbin1_2022merged_datacard9_bin8
44	prop_binRT1BT0htbin4_2022merged_datacard4_bin5
45	prop_binRT1BT0htbin2_2022merged_datacard2_bin2
46	prop_binRT1BT0htbin7_2022merged_datacard7_bin2
47	prop_binRT1BT0htbin1_2022merged_datacard1_bin7
48	prop_binRT1BT0htbin6_2022merged_datacard6_bin7
49	prop_binRT1BT0htbin5_2022merged_datacard5_bin8
50	prop_binRT1BT1htbin0_2022merged_datacard8_bin8
51	ResTopEff_2022merged
52	prop_binRT2BTALLhtbin1_2022merged_datacard11_bin1
53	data_pred_norm_disagreement_RT1BT0htbin4_2022merged
54	data_pred_norm_disagreement_RT1BT0htbin1_2022merged
55	data_pred_norm_disagreement_RT1BT0htbin3_2022merged
56	prop_binRT1BT1htbin0_2022merged_datacard8_bin2
57	prop_binRT1BT1htbin1_2022merged_datacard9_bin2
58	RT1BT0htbin2_2022merged_DDBKG_stat
59	prop_binRT1BT0htbin4_2022merged_datacard4_bin6
60	prop_binRT1BT0htbin2_2022merged_datacard2_bin7



**CMS Internal**

$$\hat{r} = 1.0^{+1.0}_{-1.8}$$

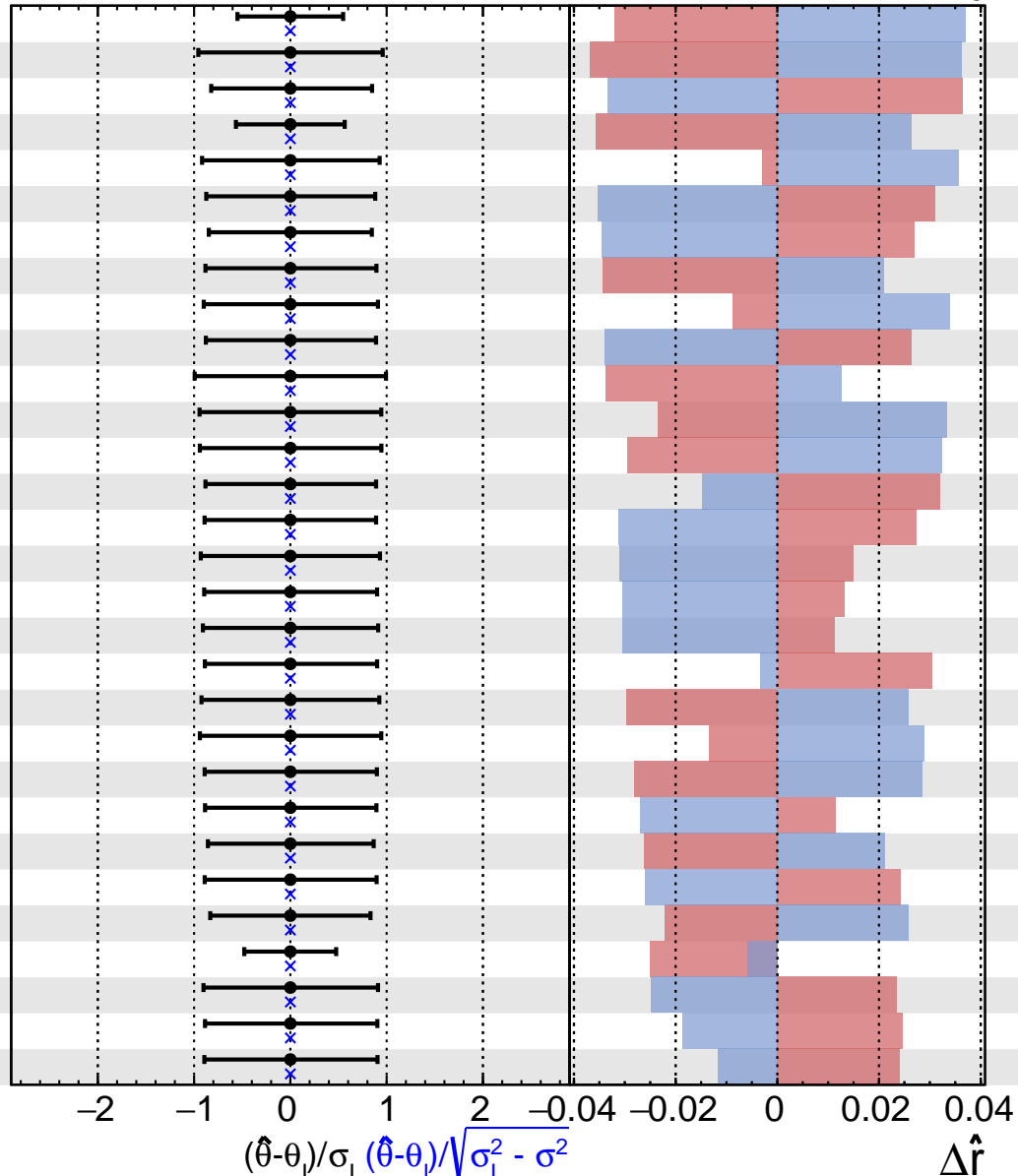
61	prop_binRT1BT0htbin5_2022merged_datacard5_bin7
62	prop_binRT2BTALLhtbin0_2022merged_datacard10_bin0
63	prop_binRT1BT1htbin1_2022merged_datacard9_bin0
64	prop_binRT1BT0htbin2_2022merged_datacard2_bin5
65	PNetTopSF_2022merged
66	prop_binRT1BT0htbin4_2022merged_datacard4_bin7
67	prop_binRT1BT0htbin5_2022merged_datacard5_bin1
68	prop_binRT1BT1htbin0_2022merged_datacard8_bin1
69	prop_binRT1BT0htbin3_2022merged_datacard3_bin6
70	prop_binRT2BTALLhtbin0_2022merged_datacard10_bin7
71	prop_binRT1BT0htbin3_2022merged_datacard3_bin1
72	prop_binRT2BTALLhtbin0_2022merged_datacard10_bin6
73	prop_binRT2BTALLhtbin1_2022merged_datacard11_bin6
74	prop_binRT1BT0htbin6_2022merged_datacard6_bin3
75	data_pred_norm_disagreement_RT1BT1htbin0_2022merged
76	prop_binRT1BT1htbin1_2022merged_datacard9_bin5
77	prop_binRT2BTALLhtbin0_2022merged_datacard10_bin1
78	prop_binRT2BTALLhtbin1_2022merged_datacard11_bin7
79	prop_binRT1BT0htbin1_2022merged_datacard1_bin2
80	prop_binRT1BT0htbin5_2022merged_datacard5_bin6
81	prop_binRT1BT0htbin1_2022merged_datacard1_bin5
82	prop_binRT1BT0htbin1_2022merged_datacard1_bin8
83	RT1BT0htbin3_2022merged_DDBKG_stat
84	prop_binRT1BT0htbin5_2022merged_datacard5_bin3
85	jer_2022merged
86	prop_binRT1BT0htbin7_2022merged_datacard7_bin7
87	prop_binRT1BT1htbin0_2022merged_datacard8_bin6
88	RT1BT0htbin7_2022merged_other_stat
89	prop_binRT1BT0htbin2_2022merged_datacard2_bin6
90	prop_binRT1BT0htbin3_2022merged_datacard3_bin2



**CMS Internal**

$$\hat{r} = 1.0^{+1.0}_{-1.8}$$

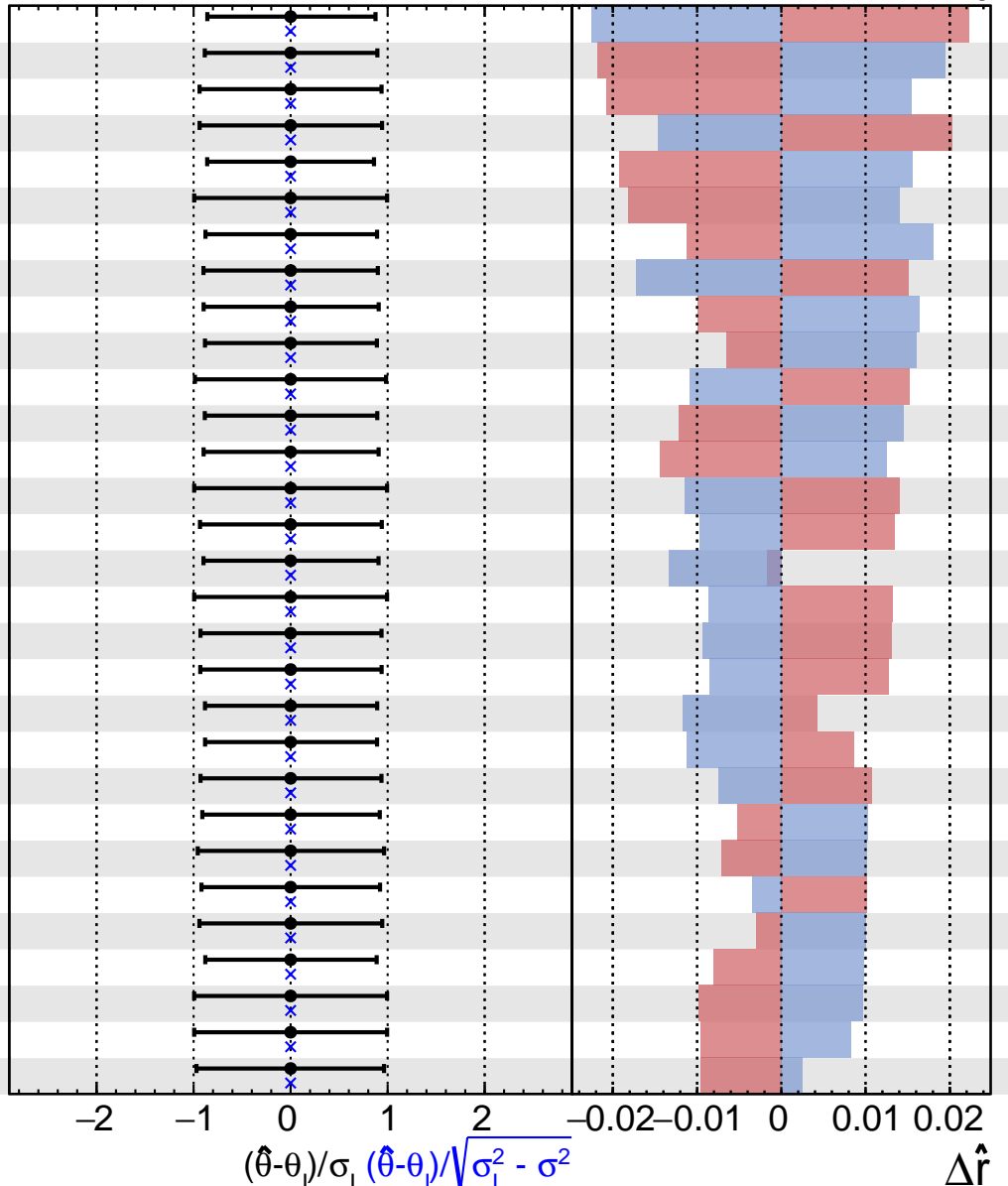
91	data_pred_norm_disagreement_RT1BT1htbin1_2022merged
92	prop_binRT1BT0htbin4_2022merged_datacard4_bin8
93	prop_binRT1BT0htbin1_2022merged_datacard1_bin1
94	data_pred_norm_disagreement_RT2BTALLhtbin1_2022merged
95	prop_binRT1BT1htbin1_2022merged_datacard9_bin7
96	prop_binRT1BT0htbin0_2022merged_datacard0_bin3
97	RT1BT0htbin1_2022merged_DDBKG_stat
98	prop_binRT1BT0htbin7_2022merged_datacard7_bin4
99	prop_binRT1BT1htbin1_2022merged_datacard9_bin3
100	prop_binRT1BT0htbin6_2022merged_datacard6_bin4
101	RT2BTALLhtbin0_2022merged_TTX_stat
102	prop_binRT1BT0htbin6_2022merged_datacard6_bin8
103	prop_binRT2BTALLhtbin0_2022merged_datacard10_bin5
104	prop_binRT1BT0htbin7_2022merged_datacard7_bin3
105	RT1BT0htbin5_2022merged_DDBKG_stat
106	RT1BT0htbin0_2022merged_DDBKG_stat
107	prop_binRT1BT0htbin2_2022merged_datacard2_bin3
108	prop_binRT1BT0htbin2_2022merged_datacard2_bin1
109	prop_binRT1BT1htbin1_2022merged_datacard9_bin6
110	prop_binRT1BT0htbin1_2022merged_datacard1_bin0
111	prop_binRT2BTALLhtbin1_2022merged_datacard11_bin2
112	prop_binRT1BT0htbin3_2022merged_datacard3_bin3
113	prop_binRT1BT0htbin4_2022merged_datacard4_bin0
114	prop_binRT1BT0htbin1_2022merged_datacard1_bin4
115	prop_binRT1BT0htbin0_2022merged_datacard0_bin1
116	RT1BT1htbin0_2022merged_DDBKG_stat
117	data_pred_norm_disagreement_RT2BTALLhtbin0_2022merged
118	prop_binRT1BT0htbin6_2022merged_datacard6_bin1
119	prop_binRT1BT0htbin1_2022merged_datacard1_bin6
120	prop_binRT1BT1htbin1_2022merged_datacard9_bin4



**CMS Internal**

$$\hat{r} = 1.0^{+1.0}_{-1.8}$$

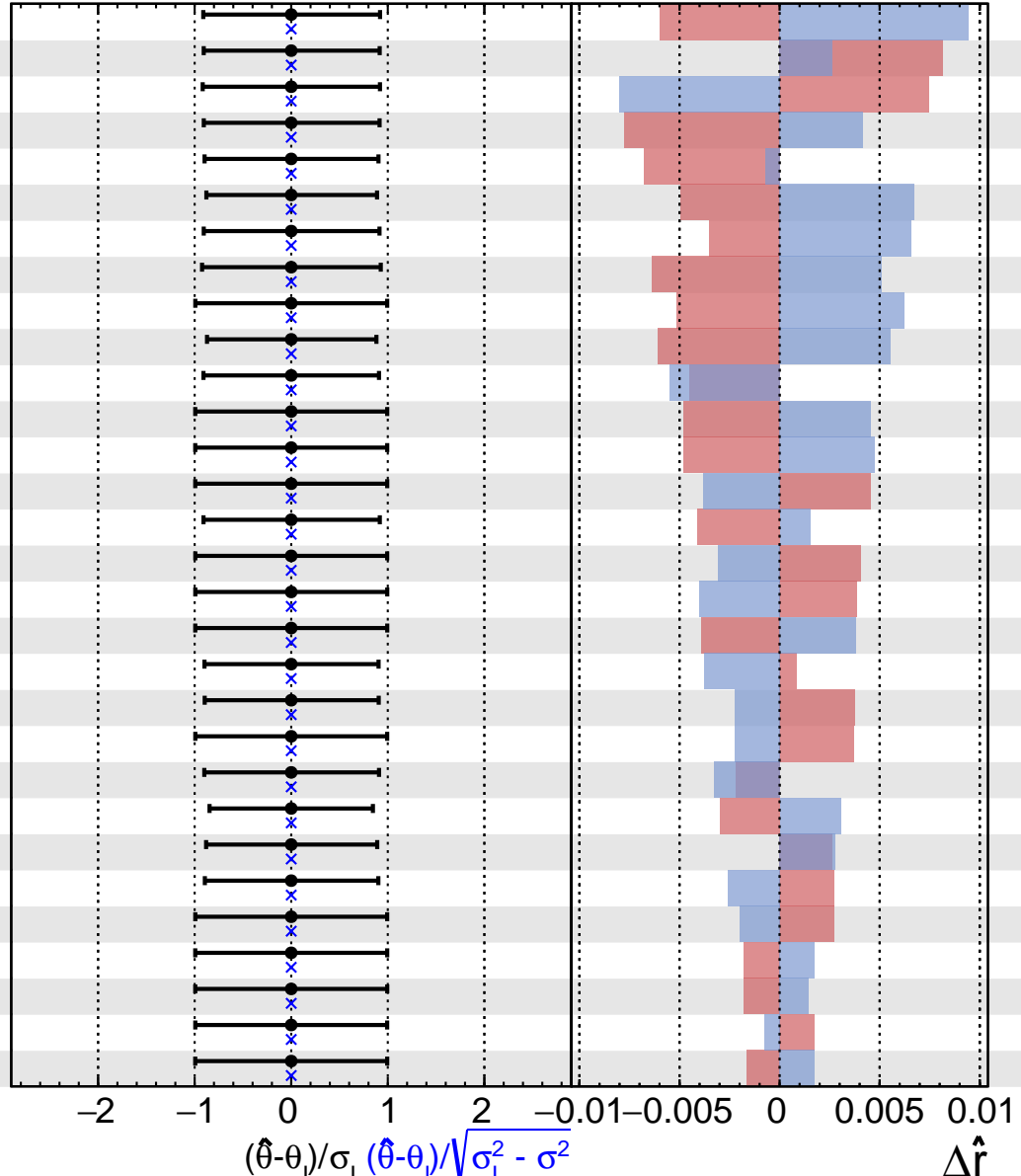
121	prop_binRT1BT1htbin0_2022merged_datacard8_bin3
122	prop_binRT1BT0htbin0_2022merged_datacard0_bin6
123	prop_binRT1BT0htbin0_2022merged_datacard0_bin7
124	prop_binRT2BTALLhtbin0_2022merged_datacard10_bin2
125	RT1BT1htbin1_2022merged_DDBKG_stat
126	lumi_uncorr_2022merged
127	prop_binRT1BT1htbin0_2022merged_datacard8_bin0
128	RT1BT0htbin4_2022merged_DDBKG_stat
129	prop_binRT1BT1htbin0_2022merged_datacard8_bin4
130	prop_binRT1BT0htbin1_2022merged_datacard1_bin3
131	RT1BT0htbin1_2022merged_other_stat
132	prop_binRT1BT0htbin4_2022merged_datacard4_bin2
133	prop_binRT1BT0htbin5_2022merged_datacard5_bin4
134	btagHFstats2_2022merged
135	prop_binRT2BTALLhtbin0_2022merged_datacard10_bin4
136	prop_binRT1BT0htbin7_2022merged_datacard7_bin1
137	btagHFstats1_2022merged
138	prop_binRT2BTALLhtbin1_2022merged_datacard11_bin4
139	prop_binRT2BTALLhtbin1_2022merged_datacard11_bin0
140	prop_binRT1BT0htbin4_2022merged_datacard4_bin4
141	prop_binRT1BT0htbin4_2022merged_datacard4_bin3
142	prop_binRT2BTALLhtbin1_2022merged_datacard11_bin3
143	prop_binRT1BT1htbin0_2022merged_datacard8_bin5
144	prop_binRT1BT0htbin0_2022merged_datacard0_bin8
145	prop_binRT1BT0htbin2_2022merged_datacard2_bin0
146	prop_binRT2BTALLhtbin0_2022merged_datacard10_bin3
147	prop_binRT1BT0htbin0_2022merged_datacard0_bin2
148	RT1BT1htbin1_2022merged_TTX_stat
149	RT2BTALLhtbin1_2022merged_other_stat
150	prop_binRT1BT0htbin3_2022merged_datacard3_bin8



**CMS Internal**

$$\hat{r} = 1.0^{+1.0}_{-1.8}$$

151	prop_binRT1BT0htbin7_2022merged_datacard7_bin6
152	prop_binRT1BT0htbin6_2022merged_datacard6_bin6
153	prop_binRT1BT0htbin6_2022merged_datacard6_bin0
154	prop_binRT1BT0htbin5_2022merged_datacard5_bin5
155	prop_binRT1BT0htbin0_2022merged_datacard0_bin4
156	prop_binRT1BT0htbin3_2022merged_datacard3_bin5
157	prop_binRT1BT0htbin6_2022merged_datacard6_bin2
158	prop_binRT1BT0htbin0_2022merged_datacard0_bin0
159	RT1BT0htbin2_2022merged_TTX_stat
160	prop_binRT1BT0htbin0_2022merged_datacard0_bin5
161	RT2BTALLhtbin0_2022merged_DDBKG_stat
162	RT1BT1htbin1_2022merged_other_stat
163	RT1BT1htbin0_2022merged_TTX_stat
164	RT1BT0htbin7_2022merged_TTX_stat
165	prop_binRT1BT0htbin6_2022merged_datacard6_bin5
166	RT1BT0htbin6_2022merged_other_stat
167	trigger_2022merged
168	RT2BTALLhtbin1_2022merged_TTTT_stat
169	prop_binRT1BT0htbin3_2022merged_datacard3_bin0
170	prop_binRT1BT0htbin7_2022merged_datacard7_bin5
171	RT1BT0htbin5_2022merged_other_stat
172	prop_binRT1BT0htbin5_2022merged_datacard5_bin2
173	RT2BTALLhtbin1_2022merged_DDBKG_stat
174	prop_binRT1BT0htbin2_2022merged_datacard2_bin4
175	prop_binRT1BT0htbin3_2022merged_datacard3_bin4
176	RT1BT0htbin2_2022merged_other_stat
177	RT1BT1htbin0_2022merged_other_stat
178	RT2BTALLhtbin0_2022merged_TTTT_stat
179	RT1BT0htbin4_2022merged_other_stat
180	RT1BT0htbin4_2022merged_TTX_stat

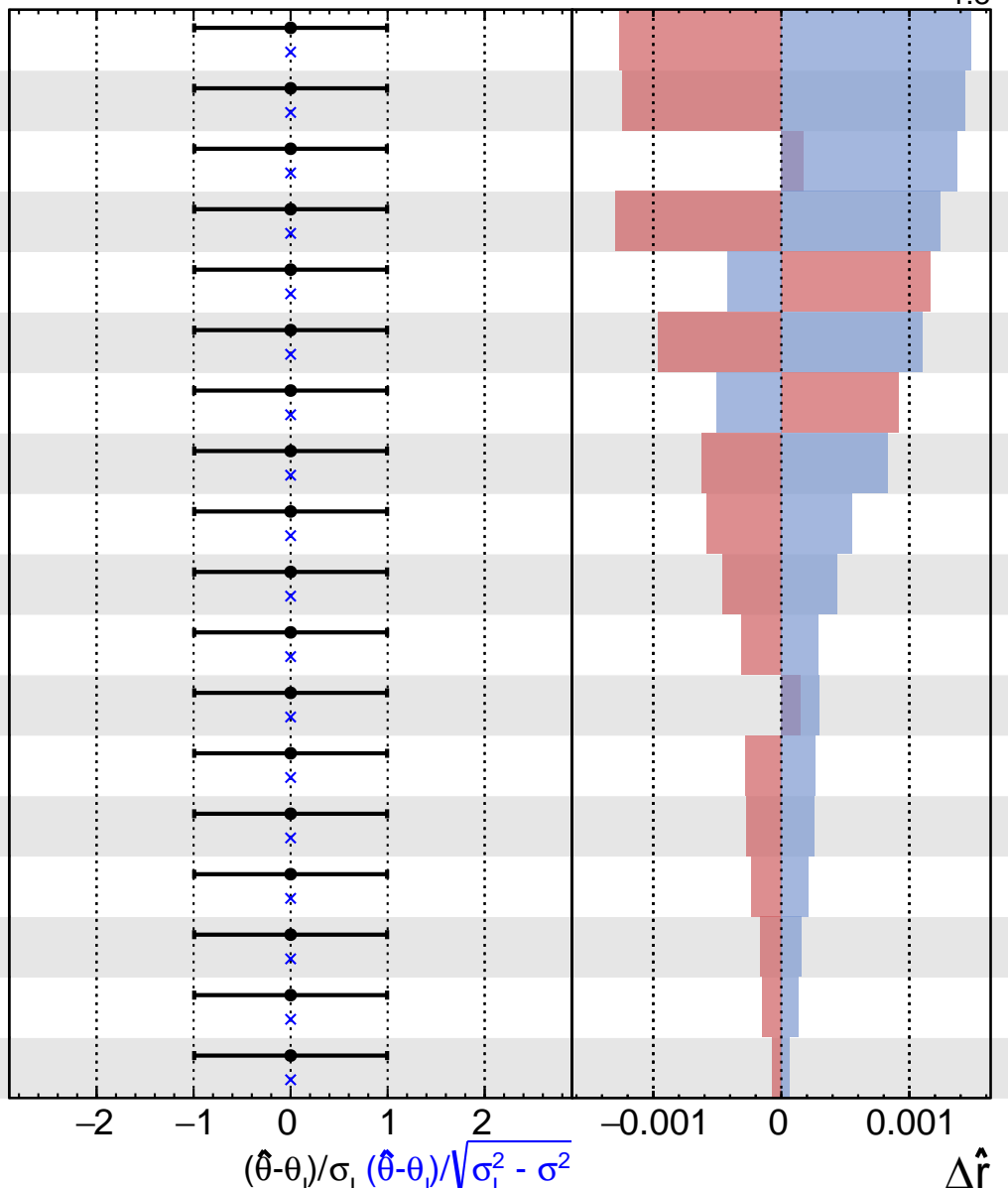


**CMS Internal**

$$\hat{r} = 1.0^{+1.0}_{-1.8}$$

181	RT1BT0htbin3_2022merged_TTX_stat
182	RT1BT0htbin0_2022merged_TTX_stat
183	RT1BT0htbin3_2022merged_other_stat
184	RT1BT1htbin1_2022merged_TTTT_stat
185	RT1BT0htbin6_2022merged_TTX_stat
186	RT1BT0htbin1_2022merged_TTX_stat
187	RT1BT0htbin0_2022merged_other_stat
188	RT2BTALLhtbin0_2022merged_other_stat
189	RT1BT1htbin0_2022merged_TTTT_stat
190	RT1BT0htbin2_2022merged_TTTT_stat
191	RT1BT0htbin4_2022merged_TTTT_stat
192	RT1BT0htbin5_2022merged_TTX_stat
193	RT1BT0htbin1_2022merged_TTTT_stat
194	RT1BT0htbin3_2022merged_TTTT_stat
195	RT1BT0htbin6_2022merged_TTTT_stat
196	RT1BT0htbin0_2022merged_TTTT_stat
197	RT1BT0htbin5_2022merged_TTTT_stat
198	RT1BT0htbin7_2022merged_TTTT_stat

- Fit
- +1 $\sigma$  Impact
- ✖ Pull
- ▢ -1 $\sigma$  Impact



**559 References**

- 560 [1] Suyong Choi, Jaehoon Lim, and Hayoung Oh. Data-driven estimation of background distribution  
561 through neural autoregressive flows, 2020.
- 562 [2] CMS Collaboration. Observation of  $t\bar{t}$  production. *Physical Review Letters*, 120(23), June  
563 2018.
- 564 [3] CMS Collaboration. Evidence for four-top quark production in proton-proton collisions at  
565  $\sqrt{s} = 13$  tev. *Physics Letters B*, 844:138076, September 2023.
- 566 [4] Jeong Han Kim, Kyoungchul Kong, Seung J. Lee, and Gopolang Mohlabeng. Probing tev scale  
567 topophilic resonances with boosted top-tagging at the high luminosity lhc. *Physical Review D*,  
568 94(3), August 2016.
- 569 [5] Melissa van Beekveld, Anna Kulesza, and Laura Moreno Valero. Threshold resummation for  
570 the production of four top quarks at the lhc, 2022.